CORE ENGINE NOISE CONTROL PROGRAM. VOLUME III. PREDICTION METHODS

S. B. Kazin, et al

General Electric Company

Prepared for:

Federal Aviation Administration

August 1974

REPORT No. FAA-RD-74-125, III

CORE ENGINE NOISE CONTROL PROGRAM

Volume III - PREDICTION METHODS

K.R. BILWAKESH
J.J. EMMERLING
S.B. KAZIN
D. LATHAM
R.K. MATTA
H. MOROZUMI

AIRCRAFT ENGINE GROUP
GENERAL ELECTRIC COMPANY
CINCINNATI, OHIO 45215

AUGUST 1974

FINAL REPORT

Prepared for

U.S. DEPARTMENT OF TRANSPORTATION
FEDERAL AVIATION ADMINISTRATION
Systems Research & Development Service
Washington, D.C. 20590

1. Report No.	2. Government Accession No.	3. Recipient's Catalog No.
FAA-RD-74-125, III		

4. Title and Subtitle	5. Report Date
Core Engine Noise Control Program Volume III - Prediction Methods	August 1974 6. Performing Organization Code

7. Author(s)	8. Performing Organization Report No.
S.B. Kazin (Prog. Tech. Dir.), R.K. Matta (Ed.), K.R. Bilwakesh, J.J. Eberling, D. Latham, H. Morozumi	

9. Performing Organization Name and Address	10. Work Unit No.
General Electric Company Aircraft Engine Group Evendale, Ohio 45215	36310 11. Contract or Grant No. DOT-FA72WA-3023

12. Sponsoring Agency Name and Address	13. Type of Report and Period Covered
U.S. Department of Transportation Federal Aviation Administration Systems Research and Development Service Washington, D.C. 20590	Final July 1972 - April 1974 14. Sponsoring Agency Code

15. Supplementary Notes

Volume I - Identification of Component Noise Sources, FAA-RD-74-125, I

Volume II - Identification of Noise Generation and Suppression Mechanisms, FAA-RD-74-125, II

16. Abstract

Prediction methods for core engine noise were reviewed and either updated or new noise evaluation techniques formulated for low velocity coannular jets, combustors ("core" noise), low pressure turbines, interaction between turbine tones and fan/core jet streams, obstructions in the flow passages and casing radiation. The development was based, to a large extent, on the analytical investigation and the model, component and engine tests evaluated during Phases II and III of this program.

The results were cast in a general form, so as to be applicable to a wide variety of cycles, including present and future turbofan engines. The prediction methods were validated with measured acoustic data wherever possible.

17. Key Words (Suggested by Author(s))	18. Distribution Statement
Core Engine Noise, Turbofan Engine Noise, Aircraft Noise Control, Low Noise Technology, Jet Noise, Combustor Noise, Core Noise, Turbine Noise, Tone/Jet Stream Interaction, Obstruction Noise, Casing Radiation, Compressor Noise.	Document is available to the public through the National Technical Information Service, Springfield, Virginia 22151

19. Security Classif. (of this report)	20. Security Classif. (of this page)	21. No. of Pages	22. Price*
Unclassified	Unclassified	179	7.00

PREFACE

This report describes the work performed under the DOT/FAA Core Engine Noise Control Program (Contract DOT-FA72WA-3023). The objectives of the program were:

- Identification of component noise sources of core engine noise
- Identification of mechanisms associated with core engine noise generation and noise reduction
- Development of techniques for predicting core engine noise in advanced systems for future technology aircraft

The objectives were accomplished in four phases as follows:

- Phase I - Analysis of engine and component acoustic data to identify potential sources of core engine noise and classification of the sources into major and minor categories.
- Phase II - Identification of the noise generating mechanisms associated with each source through a balanced program of:
  - Analytical studies
  - Component and model tests
  - Acoustic evaluation of data from existing and advanced engine systems.
- Phase III - Identification of noise reduction mechanisms for each source through a program with elements similar to Phase II.
- Phase IV - Development of improved prediction techniques incorporating the results obtained during the preceding two phases.

The work accomplished is reported in three volumes corresponding respectively to the three objectives stated above.

- Volume I - Identification of Component Noise Sources.
- Volume II - Identification of Noise Generation and Suppression Mechanisms.
- Volume III- Prediction Methods.

A visual representation of the overall program and report organization is shown on page v.

This volume documents the results of the Phase IV activity which consisted of updating and validating existing prediction techniques and evolving new prediction methods through data correlation or analysis. The work accomplished in Phases II and III (reported in Volume II) provided the basis for this above effort. In turn, the new prediction methods were used to reevaluate the preliminary ranking of the core engine noise sources obtaine in the initial stages of the program. The final ranking is reported in Volume I.

CORE ENGINE NOISE CONTROL PROGRAM
OVERALL REPORT ORGANIZATION

Contract Phase		Contract Documentation
Phase I	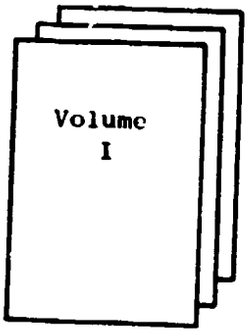	Identification of Component Noise Sources
Phase II and Phase III	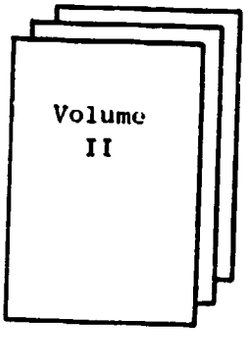	Definition of Mechanisms of Noise Generation Definition of Mechanisms of Noise Reduction
Phase IV	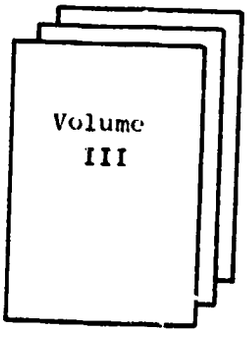	Development of Prediction Techniques

SUMMARY AND CONCLUSIONS

Prediction methods are presented for the following component sources of core engine noise:

- Low velocity, coannular flow, jet noise
- Combustor ("core") noise
- Low pressure (fan) turbine noise
- Interaction of turbine tones with fan/core jet streams
- Obstruction noise
- Casing radiation

The prediction methods were developed, with one exception, from correlations during the Core Engine Noise Control Program. The exception, analytical prediction of turbine discrete frequency noise, consists of a variation of an existing General Electric method for fan noise prediction, the two sources being very similar. The rationale behind each prediction method and the salient features of the component sources are briefly described below.

Jet Noise

The prediction procedure is based on the detailed acoustic testing of statically operated single and coannular flow nozzle configurations. The resulting correlations are applicable for a range of bypass ratios from 4.5 to 14.0, area ratios (fan/core) from 2 to 8 and velocity ratios (fan/core) from 0.6 to 1.0.

The method first makes a prediction of the noise generated by the core flow alone, using the core jet velocity, and corrected for the core jet temperature through a velocity-dependent function of the jet density. The effect of shrouding the core flow with the secondary fan flow is entered as a function of the velocity ratio and area ratio. Generally speaking, the combined noise level is lower than that for the primary jet alone for velocity ratios lower than 0.7 and higher for velocity ratios above 0.7.

A simplified prediction technique was also developed to account for the suppression achieved using a multilobe daisy type core nozzle. The data used were from an 18-lobe suppressor, with annulus/core flow area of 2, installed in a coannular flow system with area ratio (fan/core) of 3 and a core velocity of 1600 ft/sec (488 m/sec). Further parametric studies are required if the prediction method is to be generalized.

Combustor Core Noise

The noise generated by the combustion process is attributed to mass and momentum fluctuations resulting from unsteady burning. It consists of broadband noise arising from a statistical distribution of monopole sources scattered throughout the reaction zone. It generally occurs in the low frequency range, peaks at about 400 Hz (for engines), and at about 150° from the inlet.

Combustor noise in an engine has been found to vary in direct proportion to the airflow rate, to the temperature rise across the combustor, and to the density at the inlet to the combustor. When these parameters are input, the prediction method provides a spectrum at each angle. There is a systematic difference in the noise levels for turbojet, turboshaft and turbofan engines. The turbojet data correlate highest and the turbofan data correlate lowest.

Turbine Noise

Noise is generated in a turbine primarily by viscous wake interaction between adjacent blade rows and by the impact of turbulence on the rotating blade rows. The former is responsible for discrete frequency noise generation at the blade passing frequency (BPF) and the latter for broadband noise generation centered at the BPF. A typical turbine noise spectrum, therefore, consists of a high frequency broadband signal with superimposed discrete frequency spikes.

The turbine noise peaks at 120° and 110° from the inlet for high bypass engines and turbojet engines, respectively. Turbine noise is most discernible at low power settings and can be the dominant noise source at approach power.

The controlling variables include the ideal work extraction (pressure ratio) and blade tip speed or relative velocity. The noise increases with pressure ratio for constant speed and decreases with blade tip speed at constant pressure ratio. The latter also corresponds to increasing noise with blade relative velocity at constant pressure ratio.

Three separate prediction procedures have been outlined to suit varied requirements:

(A) Preliminary prediction method - provides quick approximate estimates of perceived noise levels at the max angle. Required as input are the turbine pressure ratio, blade tip speed and the core nozzle exit area.

(B) Detailed prediction method - provides a complete turbine noise spectrum at each angle for each stage. The stage pressure ratio, blade tip speed, blade inlet relative velocity and stage exit area must be input.

(C) Analytical prediction of discrete frequency noise - capable of evaluating effects of aeromechanical configuration variations on the noise generation. A source power level is provided. A complete description of the stage is required, including the physical dimensions and velocity triangles.

Methods (A) and (B) are based on correlations of available acoustic data from high bypass turbofan engines, and Method (C) is based on an analytical description of viscous wake interaction between adjoining blade rows.

Turbine Tone/Jet Stream Interaction

Turbine tones are modulated in frequency and amplitude due to turbulence scattering while propagating through the jet mixing regions. The tone SPL drops and the energy is redistributed into sidebands. Energy is apparently conserved during this process and there is no evidence of amplifications.

While this interaction is observed for both turbojet and turbofan engines, the effect is enhanced by the coannular flow arrangement of the turbofan. The modulated tone appears as a "haystack" in the farfield narrowband spectrum centered at the BPF at the peak aft angle (120°). The haystack possesses all the properties of turbine discrete noise and is thus most visible at 120° and at low power settings.

The controlling variables (and the input required for the prediction method) are the fan jet velocity and the relative distance between the fan and core nozzle exhaust planes. The output consists of the tone amplitude reduction and the frequency spread. A coplanar exhaust arrangement greatly minimizes the tone modulation.

Obstruction Noise

Flow over obstructions such as struts and pylons results in noise generation due to interaction of the obstruction body with the inflow turbulence, the boundary layer on the surface, and the trailing edge vortex. The latter two mechanisms appear to be dominant. The vortex shedding may be periodic, leading to discrete frequency noise, or it may be random, producing broadband noise. For the Reynolds number range encountered in aircraft engines, the shedding is normally random. Since both of the other mechanisms also result in broadband noise only, the obstruction noise is normally encountered as a broadband peak in the spectrum. The peak frequency demonstrates a Strouhal number dependency; that is, it tracks with the stream velocity.

Data show that the peak occurs near 120° from the engine inlet. The noise would be expected to be most noticeable at the lower power settings because it varies with the fifth power of the velocity (jet noise varies with the eighth power).

Flow velocity is the prime controlling variable, however, the profile drag coefficient and the physical dimensions of the obstructions also influence the noise.

The prediction method presented supplies the overall acoustic power and the one-third octave band power level spectrum for acoustic radiation from struts placed in a smooth uniform flow. The formulation is valid for angles of attack in the range 0 to 15° and Reynolds numbers in the range 3×10^5 to 1×10^6 (based on the chord).

Casing Radiation

Noise generated by the engine internal components may be radiated either through the inlet or exhaust or transmitted directly through the engine casing. The casing radiation is actually determined by evaluating the noise generation by the component sources and applying the casing transmission characteristics contained in Section 7.3 of Volume II. Volume III contains a less detailed casing radiation noise procedure which may be used for quick, preliminary purposes, as in the early stages of engine design.

This prediction method was developed by evaluation of acoustic data from the J79 test mentioned in Volume II. The correlating parameter is the compressor tip speed. The radiated spectrum is fairly flat with a slight peak near 500 Hz. The peak radiation angle is assumed to be normal to the jet axis.

The prediction methods contained in this volume are cast in a general form so as to be applicable to a wide variety of cycles, including current and envisaged future technology aircraft engines. The methods were validated with measured acoustic data wherever possible.

TABLE OF CONTENTS

TABLE OF CONTENTS (concluded)

NOMENCLATURE

A	-	area
A_o	-	incident wave amplitude
A_w	-	axial chord
AR	-	exhaust nozzle area ratio (fan/core)
BPF	-	blade passing frequency
BPR	-	bypass ratio (fan/core)
b	-	distance between centers of adjacent blade rows (Section 4); also, distance propagated through turbulence region (Section 5)
C_D	-	profile drag coefficient
C_p	-	coefficient of specific heat at constant pressure
c	-	acoustic velocity; also, semichord (Section 4)
D	-	diameter, normally fan jet diameter
DI	-	directivity index
d	-	diameter, normally core jet diameter
dB	-	decibel
EGA	-	extra ground attenuation
EPNL	-	effective perceived noise level
e	-	2.71828
F	-	fan tone
f	-	frequency
f_c	-	1/3 octave band center frequency
f_{peak}	-	spectrum peak frequency
f^*	-	modified Strouhal frequency
G_m	-	coefficient of unsteady upwash
grad	-	gradient, ∇ operator
H	-	blade height
Hz	-	Hertz, cycles/second
HP	-	horsepower
h	-	span
I	-	acoustic intensity
J	-	Bessel Function of first kind
K	-	modified Bessel Function; also, constant (Sections 3,4)

NOMENCLATURE (Continued)

k	-	wave number, $2\pi/\lambda = \omega/c$
kHz	-	kilo-Hertz
k_o	-	wave number of the incident wave
L	-	distance between fan and core nozzle exhaust planes (Section 5); also, sideline distance (Appendix A)
ℓ	-	chord; also, characteristic length (Section 5)
M	-	Mach number, V/c
M_R	-	relative Mach number, V_{rel}/c
M_t	-	turbulence Mach number
m	-	slope
N	-	rpm
N_f	-	design fan rpm
NPSL	-	nondimensional power spectrum level
NPWL	-	normalized measured OAPWL
n	-	harmonic number
OAPWL	-	overall power level (acoustic), dB re 10^{-3} watt
OASPL	-	overall sound pressure level, dB re .0002 d/cm^2
P	-	total pressure; also, acoustic power in watts (Section 2)
P_R	-	pressure ratio
PWL	-	acoustic power level, dB re 10^{-3} watt
PWL_N	-	normalized 1/3 octave band PWL
p	-	acoustic pressure or static pressure
q	-	dynamic pressure
R	-	turbulence region (Section 5); also, arc radius (Appendix A)
R_e	-	Reynolds number
R_{nm}	-	cylinder function
r	-	position vector; also, radial coordinate in a polar system (Section 4)
S	-	Sears Function
S_n	-	Strouhal number, $\frac{\text{frequency x length}}{\text{velocity}}$
SPL	-	sound pressure level, dB re .0002 d/cm^2
s	-	axial spacing between blade rows

NOMENCLATURE (Continued)

T	-	total temperature; also, turbine tone (Section 4)
TL	-	transmission loss
t	-	static temperature; pitch (Section 4); thickness (Section 6); also, time (Section 5)
t_e	-	trailing edge thickness of turbine blade
U	-	flow velocity
U_T	-	blade tip speed
U_o	-	free stream velocity
U_1	-	primary (core) jet parameter
U_2	-	secondary (fan) jet parameter
u_c	-	maximum velocity defect in viscous wake
V	-	velocity; also, volume (Section 5)
V_a	-	velocity of ambient atmosphere relative to the jet nozzle
V_m	-	expanded mean jet velocity
V_{rel}	-	relative velocity
VR	-	exhaust velocity ratio (fan/core)
$\dot{W}$	-	airflow rate
x	-	axial coordinate
x'	-	$\left[c_2 \frac{b}{c_2 \cos \alpha_1} + \frac{x_2}{c_2} \frac{V_1}{V_2} \right] - 0.6$, Equation (4.2.1-5)
Y	-	wake half width (Section 4); also, Bessel Function of the second kind
y	-	normal coordinate
α	-	air angle; also, air attenuation (Appendix A)
α_m	-	mean angle
α°	-	angle of attack
α_1	-	stagger angle of blades
β	-	air angle between rotor and stator blades
Γ	-	unsteady circulation
γ	-	ratio of specific heats
Δ	-	difference
ΔA	-	incremental area
Δt	-	incremental time

NOMENCLATURE (Continued)

Δ	-	drop in tone SPL due to "haystacking" (Section 5); also, maximum thickness (Section 6)
ζ_p	-	pressure loss coefficient
η	-	norm, $\int_0^1 r R^2_{nm}(\lambda_{nm} r)\, dr$
θ	-	angle
κ	-	compressibility, $\frac{1}{\rho}\left(\frac{\partial \rho}{\partial p}\right)$
π	-	3.14159
ρ	-	density
ρ_c	-	acoustic impedance
ρ_{core}	-	expanded jet density
ρ_{isa}	-	density at international standard atmospheric conditions
σ	-	blade row solidity, ℓ/t
ϕ	-	angle
ω	-	circular frequency, $2\pi f$
ω_w	-	jet density exponent for sound power correlation
ω_o	-	circular frequency of incident tone
$\omega 2$	-	reduced frequency, $\frac{\pi c_2 U \sigma_1}{c_1 V_1}$ (Section 4)
$(\ )_c$	-	correlation value
$(\ )_{coann}$	-	value for coannular configuration
$(\ )_{core}$	-	primary (core) nozzle or jet parameter
$(\ )_{fan}$	-	secondary (fan) nozzle or jet parameter
$(\ )_i$	-	incident wave
$(\ )_{max}$	-	maximum value
$(\ )_{mean}$	-	mean value
$(\ )_{Ref}$	-	value at reference conditions, reference parameter
$(\ )_s$	-	static conditions
$(\ )_T$	-	total conditions
$(\ )_{Tone}$	-	value for tone
$(\ )_x$	-	component in x-direction
$(\ )_y$	-	component in y-direction

NOMENCLATURE (Concluded)

$( )_\omega$	-	simple harmonic component
$( )_\infty$	-	freestream condition
$( )_{1/3OB}$	-	1/3 octave band value
$( )_0$	-	reference conditions
$( )_1$	-	upstream conditions; also, distance along an upstream blade (Section 4)
$( )_2$	-	downstream conditions; also, distance along a downstream blade (Section 4)
$( )_{28}$	-	conditions at fan nozzle exit plane
$( )_3$	-	conditions entering a combustor
$( )_4$	-	conditions at combustor exit
$( )_5$	-	conditions at turbine exit
$( )_8$	-	conditions at core nozzle exit plane
$\hat{( )}$	-	space-averaged value over an arc
$\overline{( )}$	-	mean, time-averaged value
$( )'$	-	derivative
$( )^*$	-	normalized quantity
$\langle\ \rangle$	-	time and space-average of mean square quantity
$\lvert\ \rvert$	-	magnitude, absolute value

SECTION 1.0

INTRODUCTION

A great need exists for reliable prediction methods for core engine noise sources in view of present and expected future generations of high bypass turbofan engines which will incorporate quiet fan installations. When an engine system is in development, it is necessary to evaluate accurately the potential noise contribution from the various components so that source reduction techniques may be incorporated, if necessary, in order to meet community noise standards.

At the start of the Core Engine Noise Control Program, little was known about the basic mechanisms of core engine noise generation and transmission. Existing prediction techniques were largely based on observation and empiricism. Since the data on which the prediction methods were based were frequently restricted to a small operating range and/or to a specific type of engine, the range of application was limited. Extension of the results to other machines was not always possible, or was open to misinterpretation.

The objective of this program was to develop meaningful predictions for the significant sources of core engine noise, founded on an understanding of the noise generation and transmission mechanisms. During Phases II and III of this program, acoustic data were compiled from a large number of model, component and engine tests. This information, along with the analytical work performed earlier (Volume II), was used to develop new correlations for the following noise sources previously identified (Volume I) as potential contributors to the core engine noise levels:

- Low velocity, coannular jet noise
- Combustor or "core" noise
- Low pressure turbine noise
- Turbine tone interaction with fan/core jet streams
- Obstructions in the flowpaths
- Casing radiation

The compressor noise prediction method developed under previous FAA sponsorship (Reference 1-1) was found, in Volume II, to be adequate for present purposes and will not be repeated here.

References

1-1 "Fan/Compressor Noise Research, Volume I", Final Report under DOT/FAA Contract FA68WA-1960, General Electric Company, FAA Report No. FAA-RD-71-85, December 1971.

SECTION 2.0

LOW VELOCITY JET NOISE

2.1 OBJECTIVES

The objective of this work effort was to develop a jet noise prediction procedure based on detailed acoustic experiments on statically operated single and coannular jets. The nozzles, both unsuppressed and suppressed, were examined in terms of OAPWL, PWL spectra and directivities.

2.2 UNSUPPRESSED COANNULAR PREDICTION

2.2.1 Introduction

The experimental work described in Volume II provides an excellent data bank from which to formulate an empirical coannular jet noise procedure. The configurations and the test matrices were chosen to encompass the performance cycles of turbofan engines with bypass ratios from 4.5 to 14.0. This range is representative of engines used on current commercial aircraft as well as advanced STOL and VTOL engines. The data from the JENOTS jet facility, with relatively large model sizes and a hot primary jet, can be scaled up to provide full-scale data for the prediction method. Such information is a useful addition to previous investigations in this field (References 2.2.1-1 to 2.2.1-4).

The prediction procedure presented herein considers the overall sound power level produced by the core nozzle alone, related to core jet velocity. The variation in core jet temperature (and hence jet density) is provided for by normalizing the power level using a velocity-dependent function of the jet density as determined in Reference 2.2.1-5.

To derive the overall sound power level of a coannular system, the method corrects the single jet levels by a factor determined from the experimental program. This correction factor is dependent upon the area ratio of the system and the velocity ratio of the cycle.

The spectral characteristics of the system are introduced in terms of power spectrum level related to a modified Strouhal number. Each expression is normalized to account for the coannular configuration by means of the modification suggested in Reference 2.2.1-4.

The final stage in describing the noise characteristics of the coannular jet is to relate the directivity index of each configuration to the modified Strouhal number. For a specific distance at a given temperature, the prediction method computes the one-third octave band sound pressure levels of a coannular jet noise system over the range of the experimental test matrices.

The development of the semiempirical coannular jet noise prediction program is summarized as follows:

1. The correlations were based on core jet sound power levels which can be related to parallel analytical techniques.

2. The sound power levels were normalized to account for jet temperature by means of a density ratio raised to an experimentally determined exponent.

3. The relationship between power spectrum level and Strouhal number for coannular jets was found valid if a modification was made to each parameter.

4. The directivity indices were also related to the same modified Strouhal number.

The prediction procedure is defined in five steps, as shown in Figure 2.2.1-1.

Step 1 determines the overall sound power level of the core nozzle.

Step 2 enables the overall sound power level of coannular nozzles to be determined by applying a ΔOAPWL to the $OAPWL_{core}$. The correction is dependent on area ratio at a given velocity ratio.

Step 3. The nondimensional power spectrum level (NPSL) equals the power level spectrum PWL_f [where $PWL_f = PWL_{band} - 10 \log (\Delta f)$], normalized and related to the coannular PWL. Thus,

$$NPSL = PWL_{band} - 10 \log_{10} (\Delta f) - OAPWL_{coann} + 10 \log_{10} \left\{ \frac{V_m}{D} \left(\frac{V_{core}}{V_{fan}} \right) \right\}^{1/2} \qquad (2.2.1\text{-}1)$$

was determined from the experimental data for each value of the dimensionless frequency $(f_b/V_m)\ (V_{fan}/V_{core})^{1/2}$ for a specific area ratio and velocity ratio.

Step 4. The directivity index, DI_θ, is established (for a specific area ratio and angle) from experimental results at each value of the dimensionless frequency where $DI_\theta = SPL_\theta - SPL_{space\ average}$.

Step 5. The farfield noise spectra at any acoustic angle for any given arc or sideline are computed from:

$$SPL_{space\ average} = PWL_{band} - 20 \log_{10} R - 9.25 - EGA - \alpha \qquad (2.2.1\text{-}2)$$

1 RELATIONSHIP OF PRIMARY NOZZLE NORMALIZED OVERALL POWER LEVEL AND PRIMARY JET MACH NUMBER

$$OAPWL_{core} - 10 \text{ LOG } \left[A_{core} \left(\frac{\rho_{core}}{\rho_{isa}} \right)^{\omega_w} \right] \text{ VS } \text{LOG } \frac{V_{core}}{}$$

2 RELATIONSHIP OF DIFFERENCE BETWEEN OVERALL SOUND POWER LEVELS OF COANNULAR AND CORE JETS AND VELOCITY RATIO FOR AREA RATIOS OF 2 TO 8

$$OAPWL_{coannular} - OAPWL_{core} \text{ VS } \frac{V_{fan}}{V_{core}} \text{ FOR A GIVEN } \frac{A_{fan}}{A_{core}}$$

3 RELATIONSHIP OF NORMALIZED POWER SPECTRAL DENSITY AND MODIFIED STROUHAL NUMBER AT VARIOUS VELOCITY AND AREA RATIO COMBINATIONS

$$PWL_{coan} - OAPWL_{coan} + 10 \text{ LOG } \left[\frac{V_m}{D} \left(\frac{V_{core}}{V_{fan}} \right)^{1/2} \right] \text{ VS } \frac{fD}{V_m} \left(\frac{V_{fan}}{V_{core}} \right)^{1/2}$$

FOR A GIVEN $\frac{V_{fan}}{V_{core}} \frac{A_{fan}}{A_{core}}$

4 RELATIONSHIP OF DIRECTIVITY INDEX AND MODIFIED STROUHAL NUMBER AT ANY ANGLE FOR AREA RATIOS BETWEEN 2 AND 8

$$D I_{\theta} \text{ VS } \frac{fD}{V_m} \left(\frac{V_{fan}}{V_{core}} \right)^{1/2} \text{ FOR A GIVEN } \theta, \frac{A_{fan}}{A_{core}}$$

5 FARFIELD NOISE SPECTRA AT ANY ACOUSTIC ANGLE FOR ANY GIVEN ARC OR SIDELINE

FIGURE 2.2.1-1 OUTLINE OF PREDICTION PROCEDURE FOR COANNULAR JET NOISE

Therefore,

$$SPL_\theta = NPSL + OAPWL_{coann} + 10 \log_{10} (\Delta f) \left| \frac{D}{V_m} \left(\frac{V_{fan}}{V_{core}} \right)^{1/2} \right| \qquad (2.2.1\text{-}3)$$

$$- 20 \log_{10} R - 9.25 - EGA - \alpha + DI_\theta$$

e.g., at 250 ft (76.2 m) arc, 59° F and 70% RH 1/3 octave band SPL

$$SPL_\theta = NPSL + OAPWL_{coann} + 10 \log_{10} \left| .23 \times \frac{D}{V_m} \left(\frac{V_{fan}}{V_{core}} \right)^{1/2} \right| \qquad (2.2.1\text{-}4)$$

$$- 57.2 - EGA - \alpha + DI_\theta$$

2.2.2 Experimental Results

Confirmation of Density Exponent

An effect due to the temperature of the core jet was recognized which would have to be accounted for by a normalization parameter. It was decided to utilize the results from Reference 2.2.1-5 and to conduct a short test program to validate the Reference 2.2.1-5 data. The test was conducted at selected values of jet velocity and total temperature for a conical nozzle at the JENOTS facility. The results were correlated as shown in Figure 2.2.2-1, where the sound power level for unit jet area is plotted as a function of the jet velocity at various normalized values of the jet density (ρ_{core}/ρ_{sia}). The results illustrate the varying effect of the density on the sound power of the jet, depending on jet velocity. At high velocities a reduction in sound power was observed when the density was decreased at a given jet velocity and area. As the jet velocity is reduced, this effect becomes less marked.

The information indicates that if the sound power levels of jets are to be expressed by a unique curve over a wide range of operating conditions, then an exponent ω_w should be used for the jet density. The value of the density exponent ω_w at the given jet velocity corresponds to the slope of the mean line passing through the test points.

The values of the exponent determined from the available test data are shown in Figure 2.2.2-2. The actual values used in the prediction procedure (Reference 2.2.1-5) are shown as the solid line. The values recently proposed by the SAE Committee A21 are also shown for comparison. Acceptable agreement with the Reference 2.2.1-5 trend is demonstrated, which supports the use of the existing exponent.

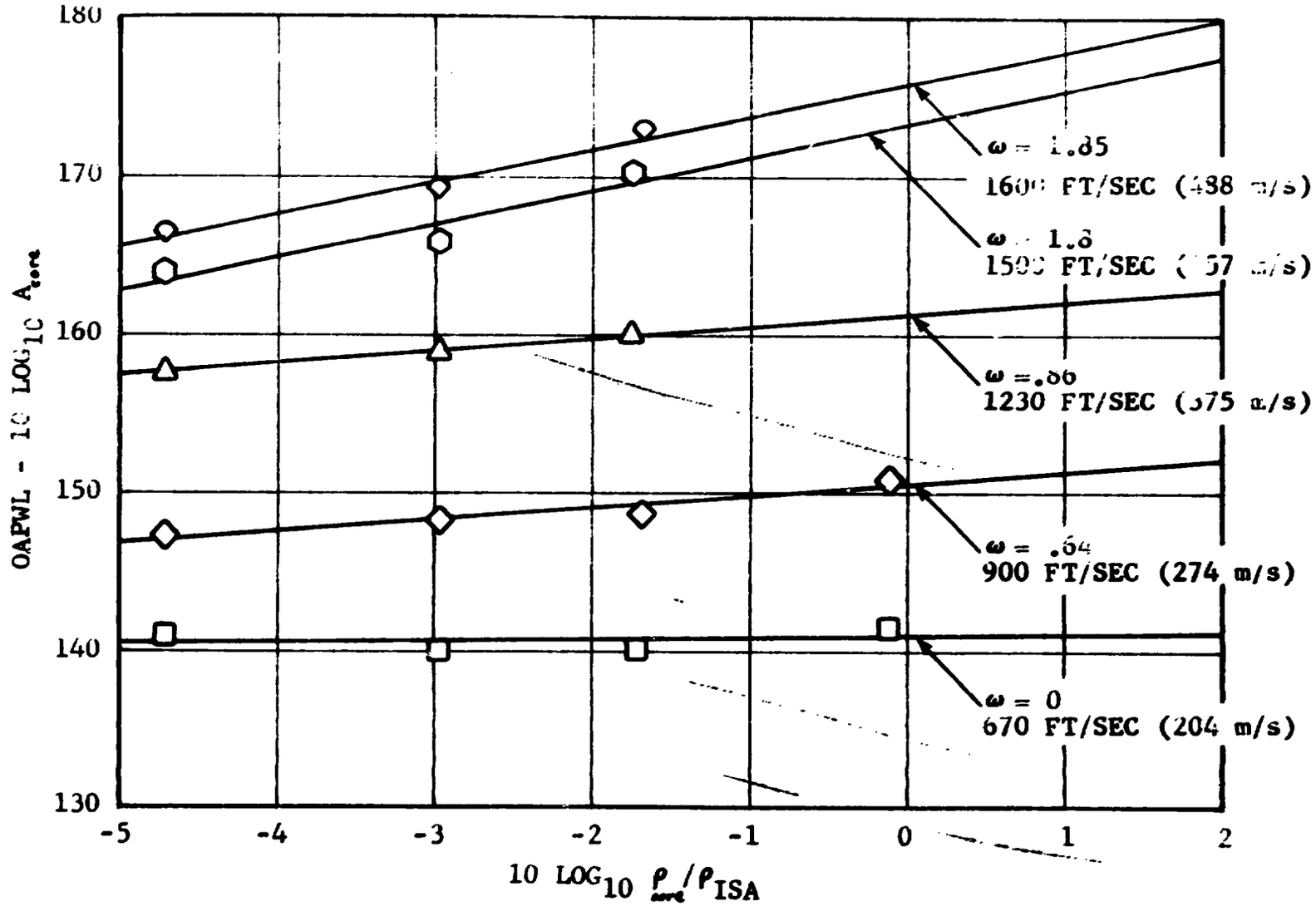

FIGURE 2.2.2-1 $OAPWL_{Conical}$ - 10 LOG_{10} A_{core} VS. 10 LOG_{10} ρ_{core}/ρ_{ISA}

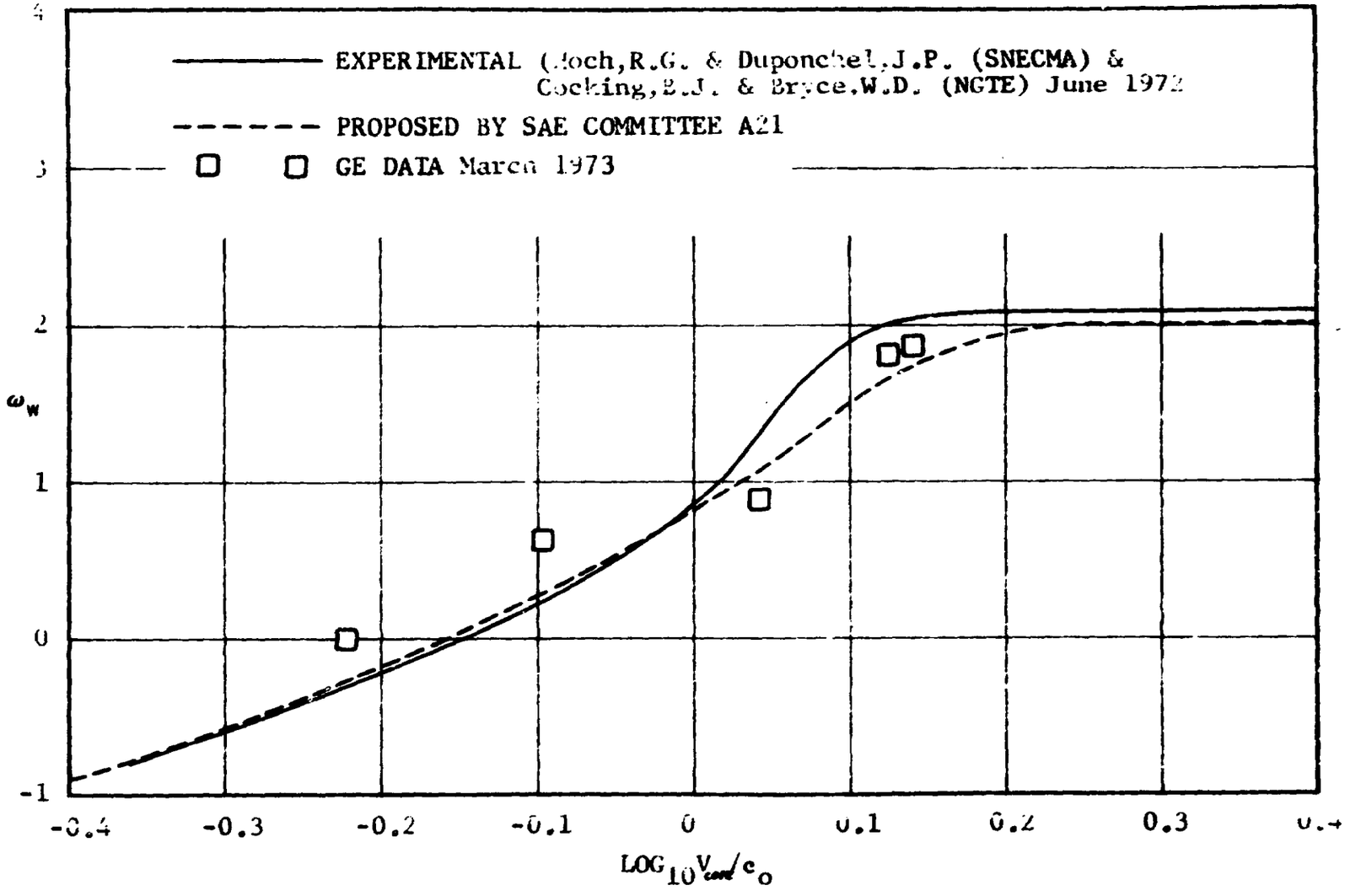

FIGURE 2.2.2-2 JET DENSITY EXPONENT VS JET VELOCITY

Core Nozzle Sound Power Correlation

The data from the model tests were scaled to full size which essentially produces spectra free from ground interference patterns. The overall sound power level of the core nozzle was normalized and plotted as a function of normalized core jet velocity, as shown in Figure 2.2.2-3. Since the facility was free from parasitic noise, the slope of the line obeys a V^8 law down to a core velocity of 500 ft/sec (152 m/sec). The temperature of the jet varied from 550° R (305° K) to 1660° R (520° K), but the chosen normalization parameter sensibly collapsed the data. Also shown in Figure 2.2.2-3 are the data from the fan nozzle (e.g., "annular conical") only tests. Agreement with the conventional conical results is quite good.

Calculation of Coannular Jet Overall Sound Power Level

The difference between the full-scale sound power levels of coannular jets and a single jet is plotted as a function of velocity ratio (V_{fan}/V_{core}) at each area ratio tested. These relationships are shown in Figure 2.2.2-4.

Power Spectrum Levels

In order to establish the distribution of the energy between the frequencies, the nondimensional acoustic power spectrum is plotted against nondimensional frequency. The mean lines through the data are indicated in Figures 2.2.2-5 to 2.2.2-8. It was observed that the spectrum levels at a specific area ratio can be more accurately related if separate plots are made at each velocity ratio, as demonstrated in the Figures. The coannular flow spectra peaks in the region of $f_o = 0.2\ (V_m/D)\ (V_{core}/V_{fan})^{1/2}$.

Directivity Indices

The polar directional characteristics of the noise from the jets are obtained for each configuration in Figures 2.2.2-9 to 2.2.2-12 where the difference in the sound pressure measured in the far field and the space-average sound pressure level is termed DI_θ. For the conical baseline nozzle the directivity of a given acoustic frequency is a function of the jet diameter and jet velocity; however, for the coannular nozzles the directivities are related to the modified Strouhal number $(f_D/V_m)\ (V_{fan}/V_{core})^{1/2}$. No appreciable difference was observed with respect to velocity ratio.

2.2.3 Application of Prediction Procedure

Upon completion of all the necessary correlations, the procedure was transformed into a computer program. The information flow for the program is outlined in Figure 2.2.3-1. This procedure is mathematically modeled utilizing the various functions which are calculated from the input parameters shown in Figure 2.2.3-2.

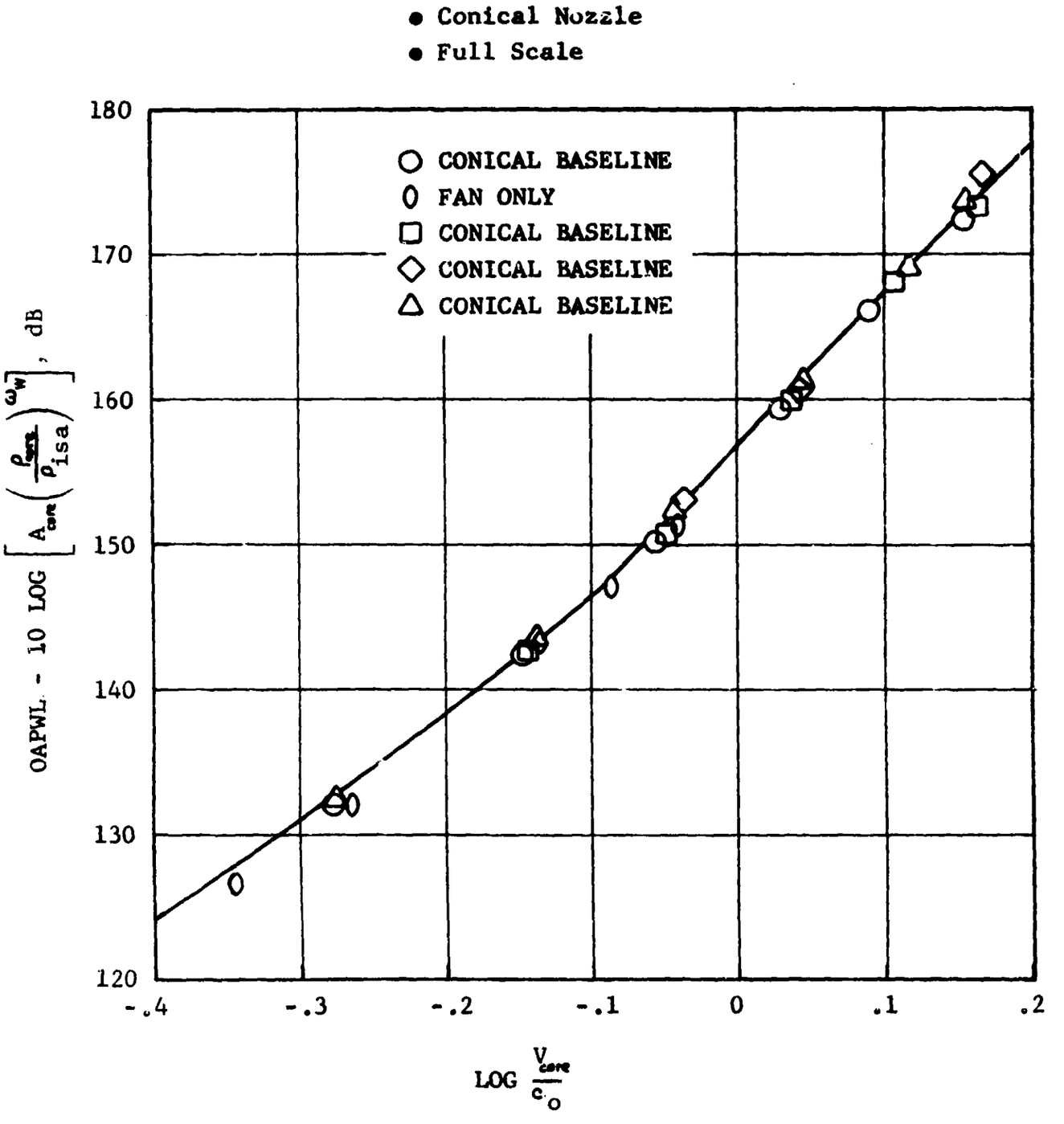

FIGURE 2.2.2-3 NORMALIZED OAPWL VS. LOG V_{core}/c_o

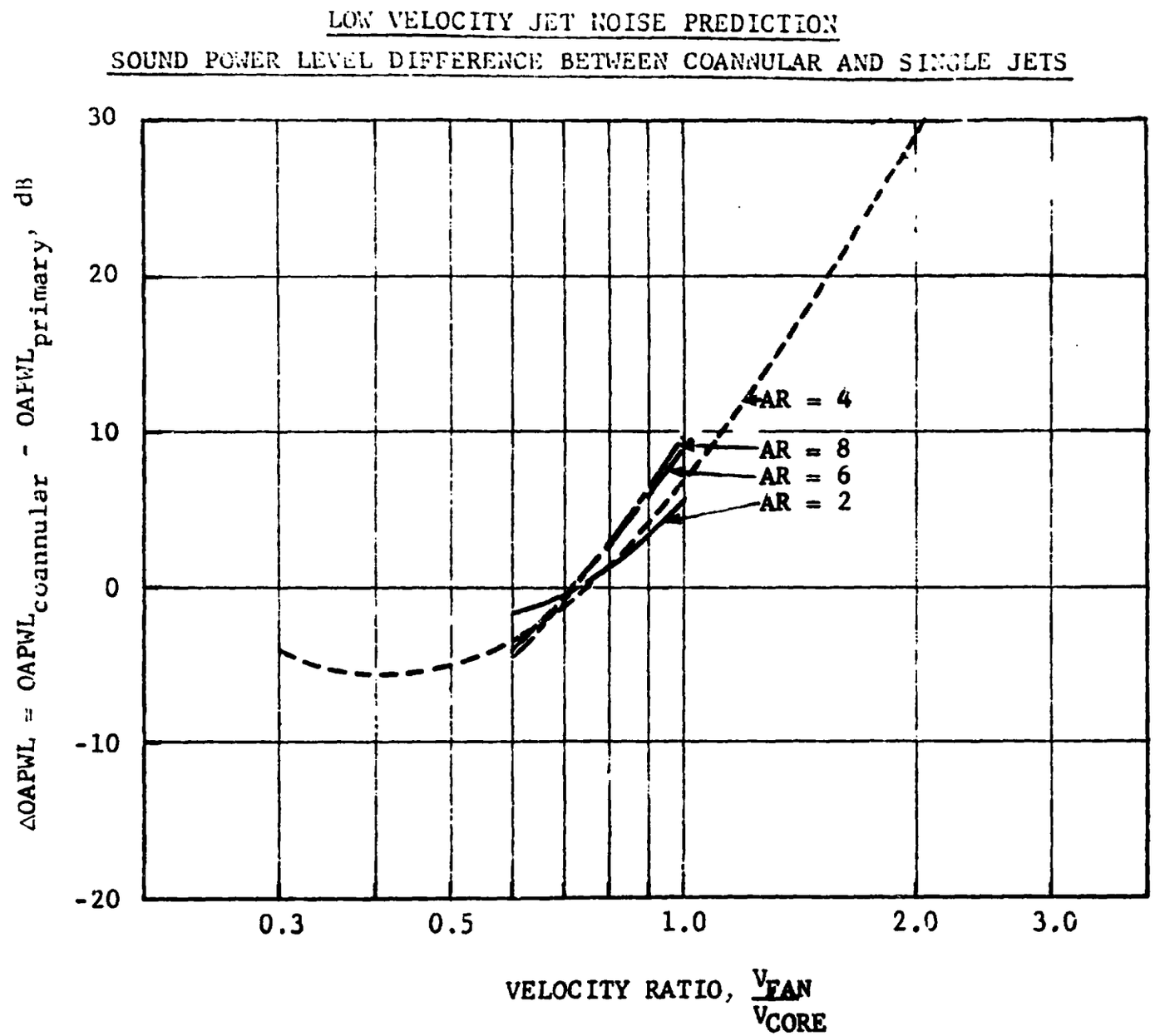

FIGURE 2.2.2-4 ΔOAPWL VS. VELOCITY RATIO

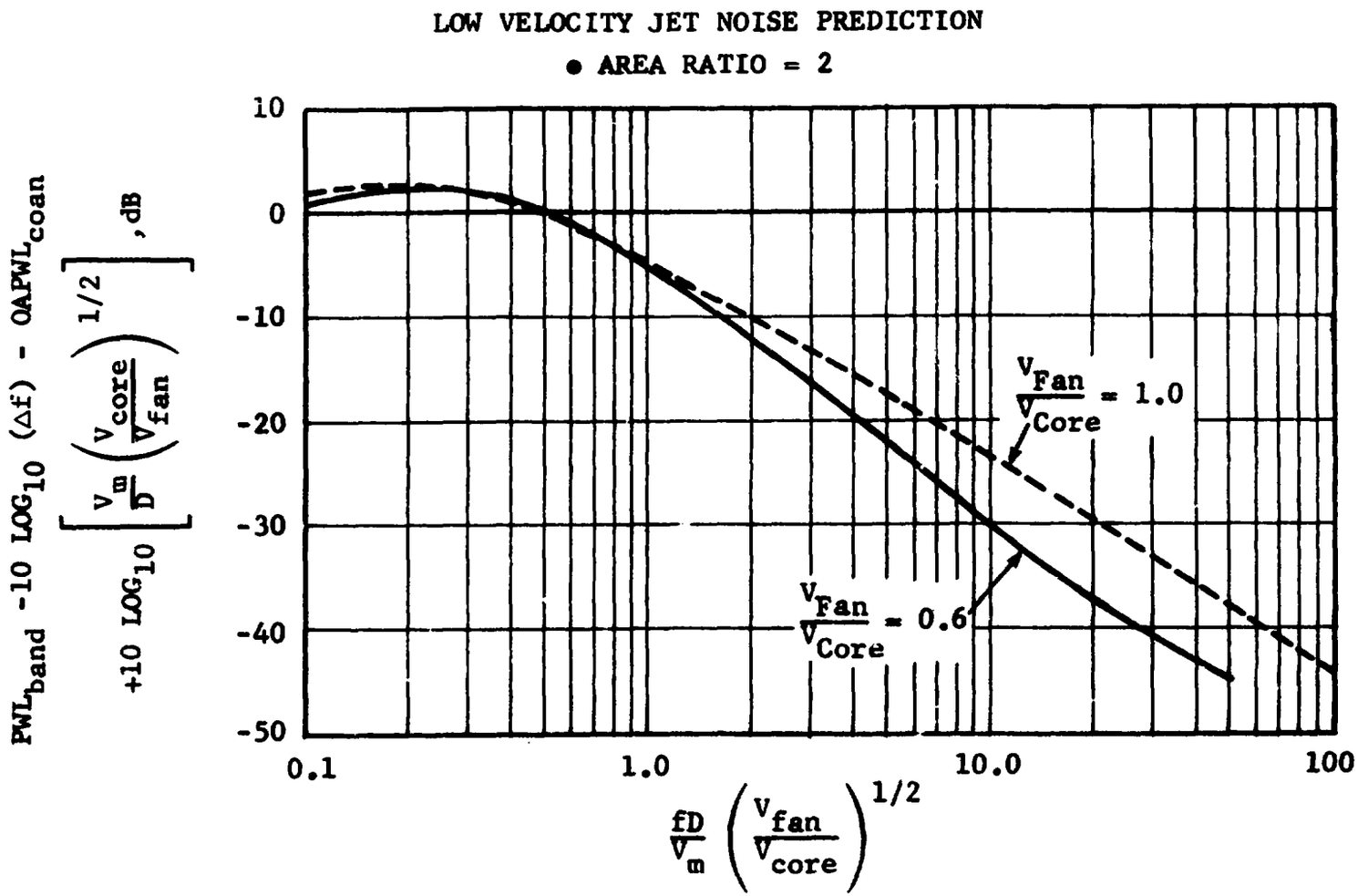

FIGURE 2.2.2-5. NORMALIZED POWER SPECTRUM LEVEL VERSUS MODIFIED STROUHAL NUMBER

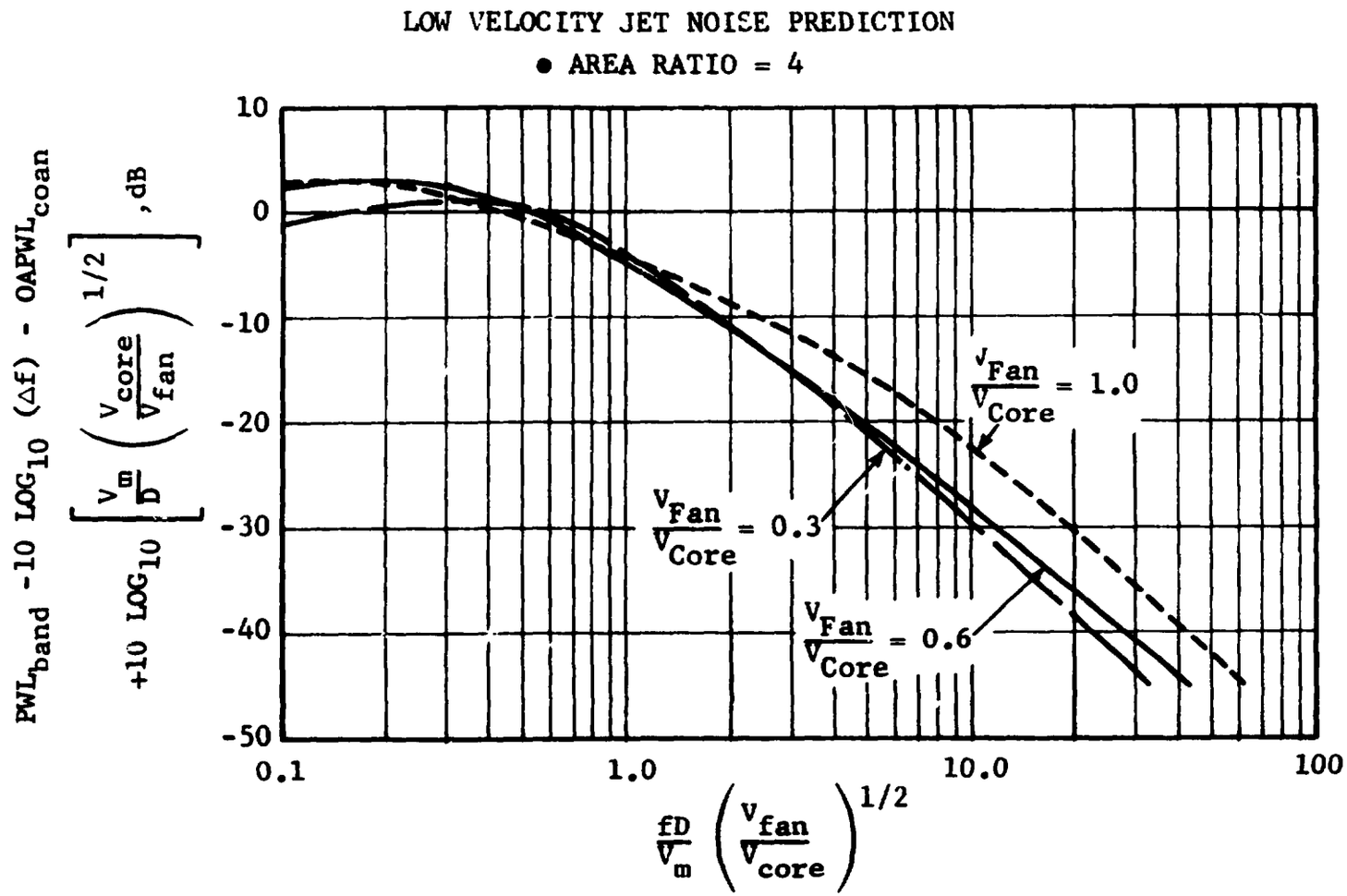

FIGURE 2.2.2-6. NORMALIZED POWER SPECTRUM LEVEL VERSUS MODIFIED STROUHAL NUMBER

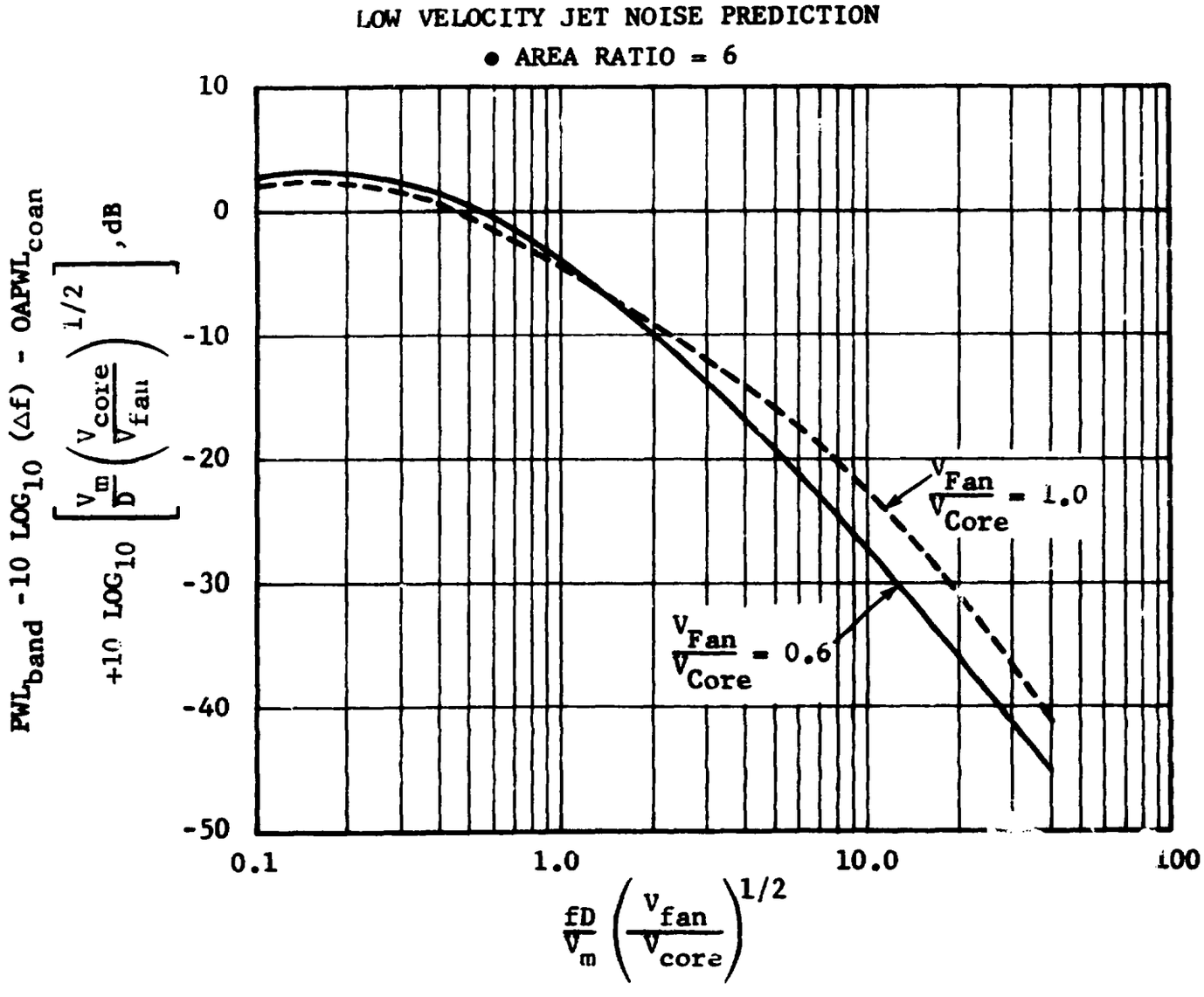

FIGURE 2.2.2-7. NORMALIZED POWER SPECTRUM LEVEL VERSUS MODIFIED STROUHAL NUMBER

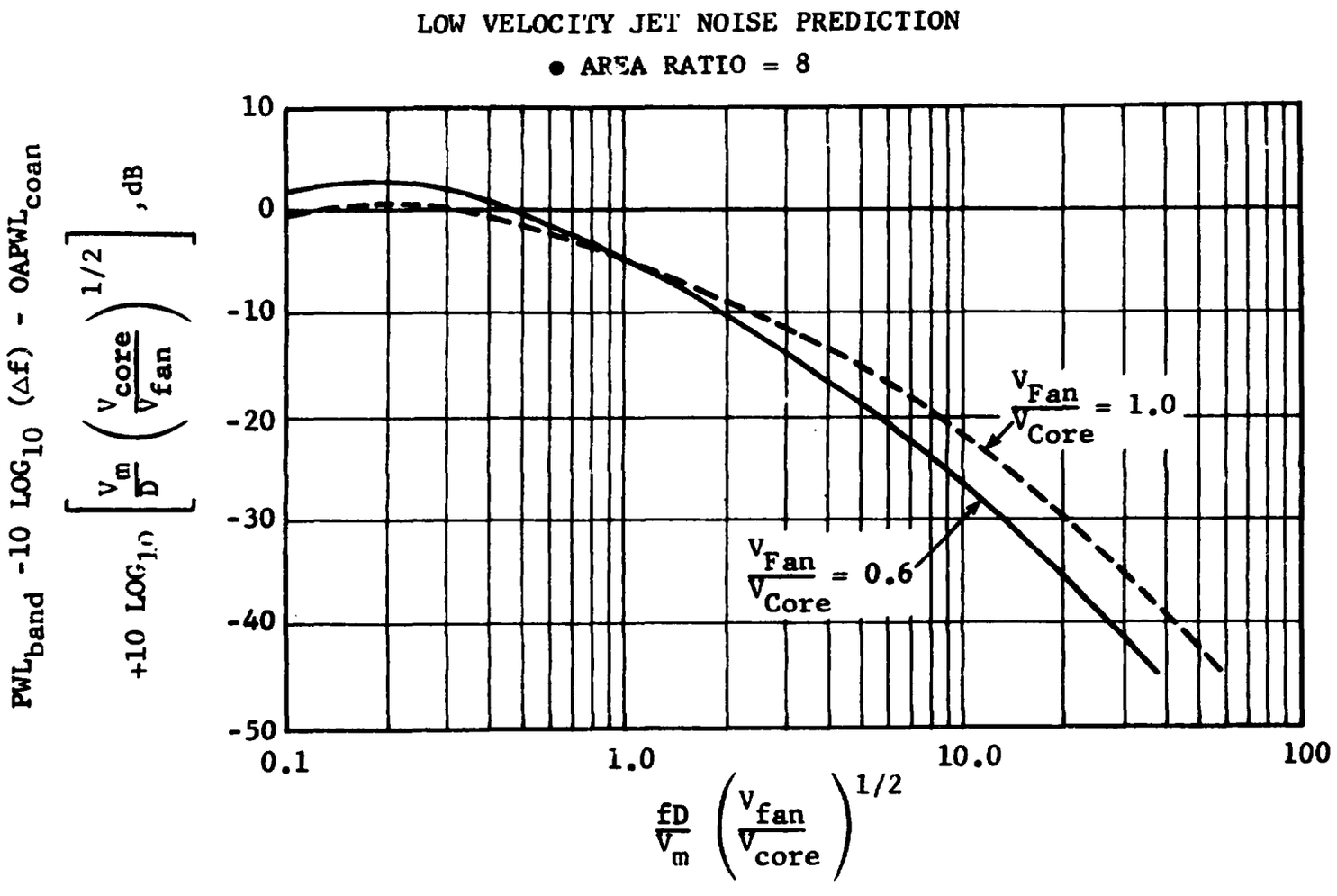

FIGURE 2.2.2-8. NORMALIZED POWER SPECTRUM LEVEL VERSUS MODIFIED STROUHAL NUMBER

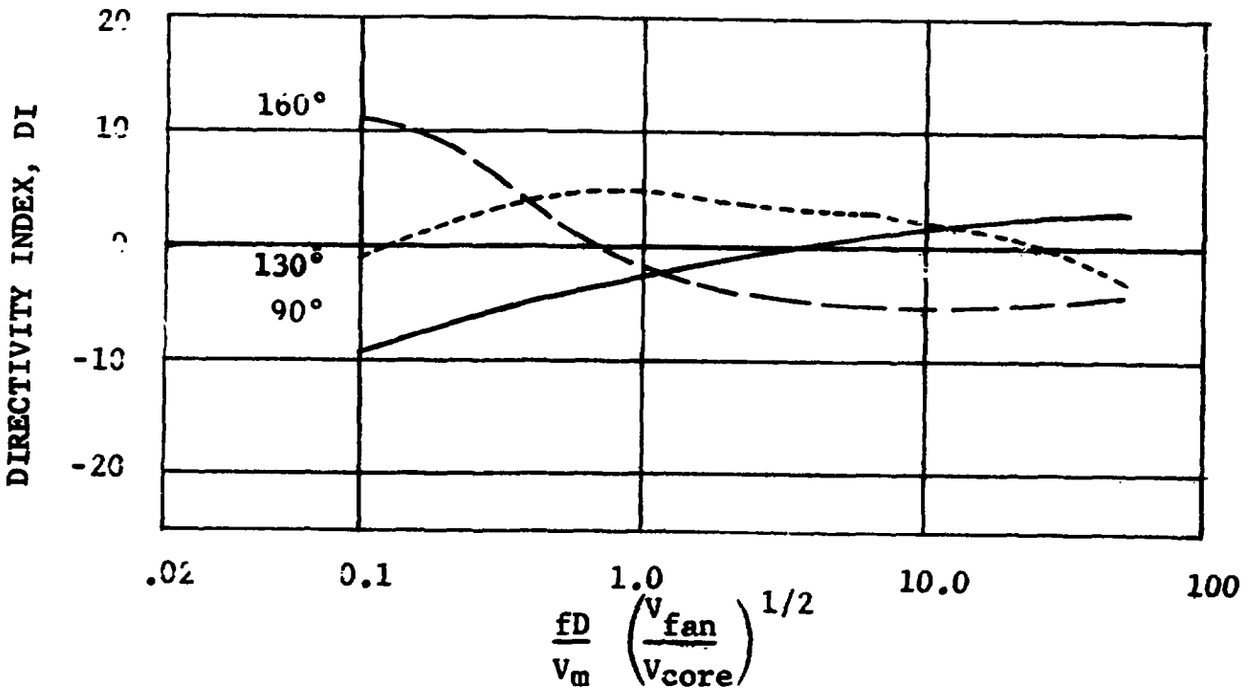

FIGURE 2.2.2-9. DIRECTIVITY INDEX VERSUS MODIFIED STROUHAL NUMBER, AREA RATIO = 2

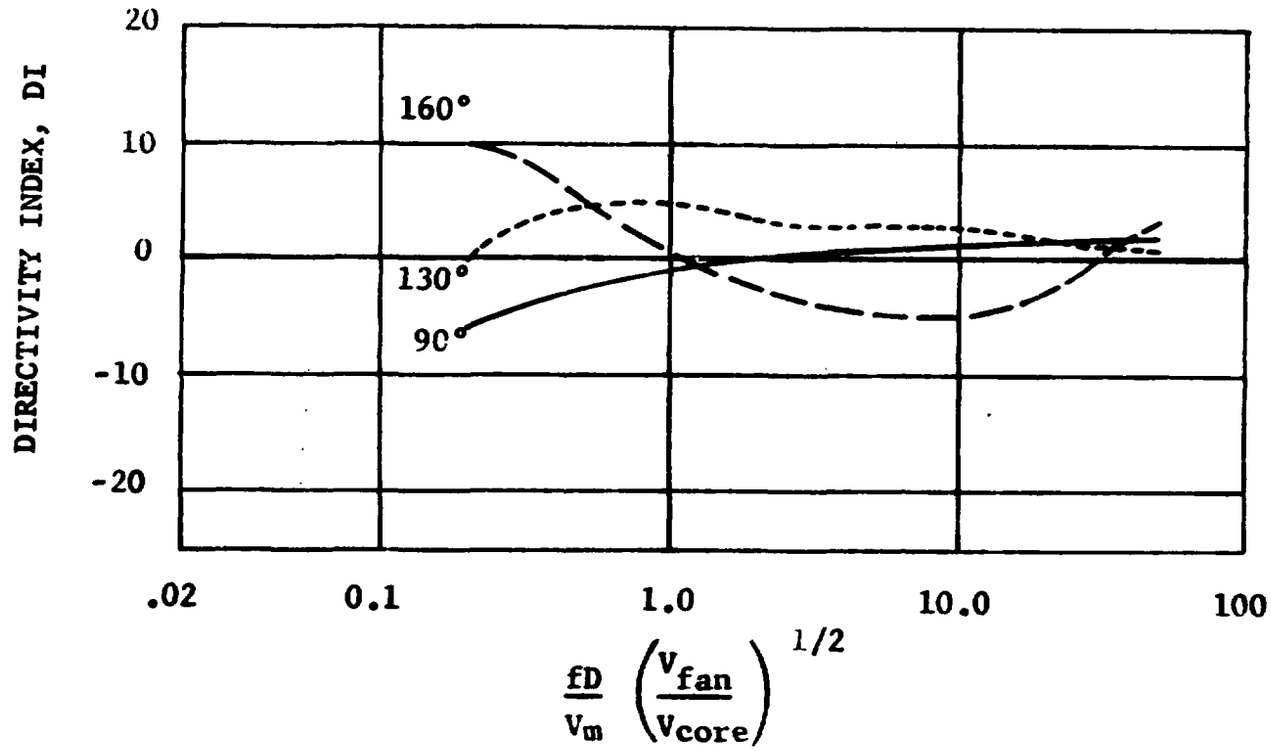

FIGURE 2.2.2-10. DIRECTIVITY INDEX VERSUS MODIFIED STROUHAL NUMBER, AREA RATIO = 4

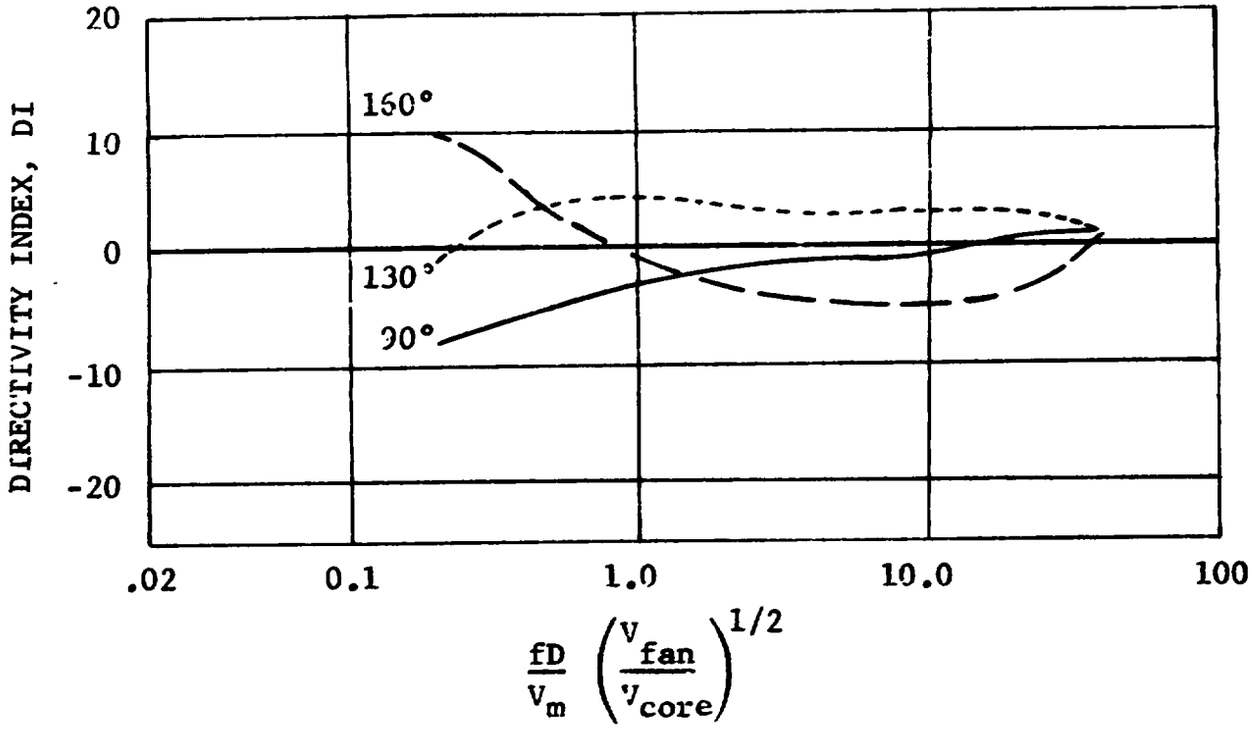

FIGURE 2.2.2-11. DIRECTIVITY INDEX VERSUS MODIFIED STROUHAL NUMBER, AREA RATIO = 6

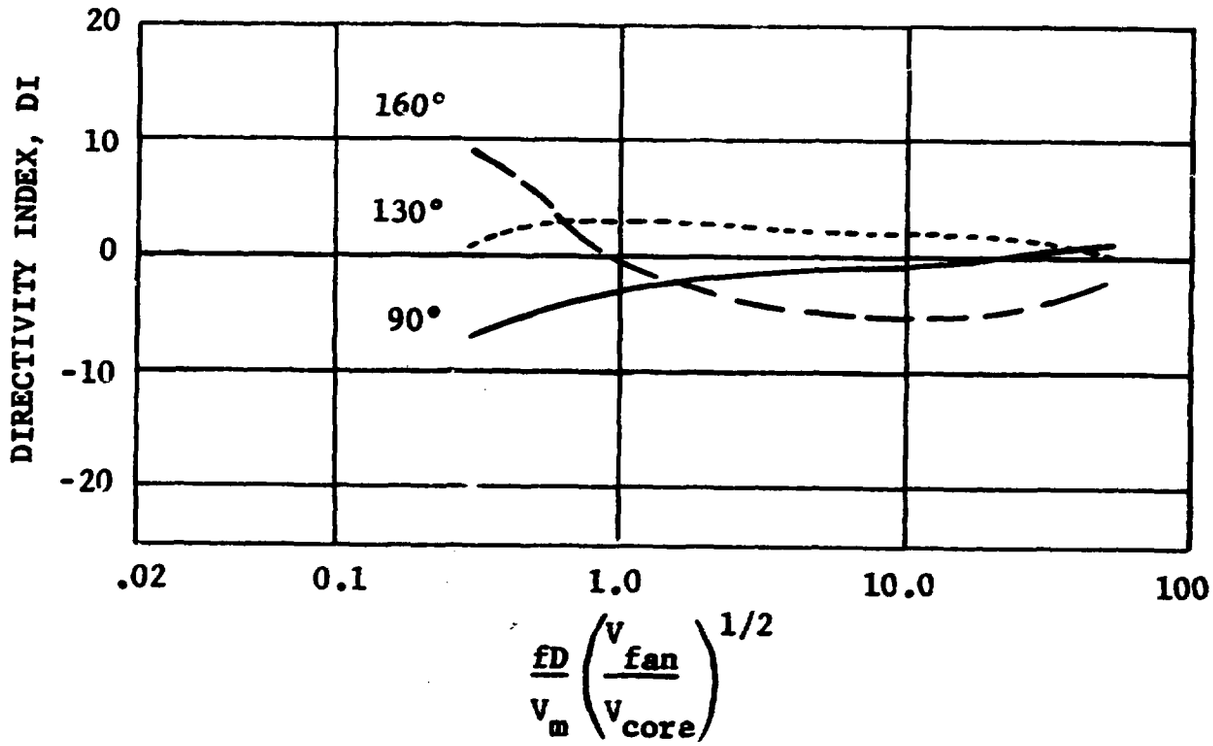

FIGURE 2.2.2-12. DIRECTIVITY INDEX VERSUS MODIFIED STROUHAL NUMBER, AREA RATIO = 8

COANNULAR JET PREDICTION MODEL

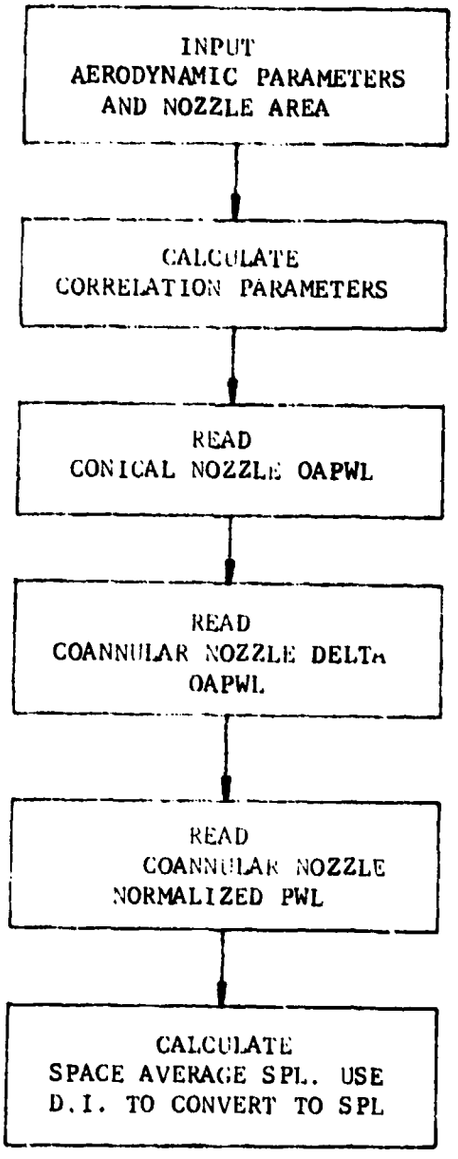

FIGURE 2.2.3-1 INFORMATION FLOW

COANNULAR JET NOISE PREDICTION INFORMATION

OUTPUT: COANNULAR OR SINGLE JET FARFIELD NOISE SPECTRA AT ANY ACOUSTIC ANGLE FOR ANY ARC OR SIDELINE

INPUT:

CORE DATA		FAN DATA	
MASS FLOW	W_8, LBM/SEC	MASS FLOW	W_{28}, LBM/SEC
NOZZLE AREA	A_8, FT^2	NOZZLE AREA	A_{28}, FT^2
JET VELOCITY	V_8, FT/SEC	JET VELOCITY	V_{28}, FT/SEC
TEMPERATURE	T_8, $^\circ R$		
PRESSURE RATIO	P_{T8}/P_o		
	SIDELINE OR ARC DISTANCE		

CALCULATES: CORRELATION PARAMETERS FROM -

AREA RATIO	A_{28}/A_8
VELOCITY RATIO	V_{28}/V_8
MEAN VELOCITY	V_m
FAN DIAMETER	D
CORE JET DENSITY	ρ_j

FIGURE 4.2.3-2 AERODYNAMIC INPUT PARAMETERS

Computations were made with the prediction model to illustrate the model characteristics. An initial comparison was made with the overall power levels derived in Reference 2.2.1-5 from an anechoic chamber. Figure 2.2.3-3 illustrates the comparison between the normalized overall power level used in the prediction and values independently determined by researchers at NGTE and SNECMA. The agreement is good at values corresponding to velocities between 600 ft/sec (183 m/sec) and 1800 ft/sec (548 m/sec).

Power level spectral comparisons were made with the anechoic chamber data reported in Reference 2.2.1-3. The results are shown in Figures 2.2.3-4 to 2.2.3-6. At the low and high area ratios the present prediction underestimates the levels in the mid and high frequency ranges, whereas at an area ratio of 5 there is an overprediction at all frequencies of approximately 3 to 4 dB. The directivity characteristics of the same configurations are shown in Figures 2.2.3-7 to 2.2.3-9. Although absolute levels between predicted and anechoic results differ, angle of peak noise and OASPL trends are in reasonable agreement.

The purpose of the jet noise prediction model is to allow the estimation of full-scale engine noise levels and to perform parametric studies to facilitate the selection of low noise performance cycles. On this basis a comparison between measured engine noise levels and predictions was performed to evaluate the trends in the predictions. A comparison was first made with noise levels of a model nozzle configuration geometrically identical to a large high bypass ratio engine; the model data were scaled to represent the full-scale engine. The results are shown in Figures 2.2.3-10 and 2.2.3-11 for low power and high power settings. The overprediction of the results at this area ratio is similar to the comparison with the anechoic chamber data (Figure 2.2.3-5).

A comparison between actual engine static data is shown in Figures 2.2.3-12 to 2.2.3-15. The predicted PWL spectra in Figure 2.2.3-12 is within 3 dB of measured values if ground reflection and absorption present in the measurements are smoothed out. The directional characteristics of predicted jet noise generally are higher than the measured data except for angles close to the jet axis (Figure 2.2.3-13). The SPL spectral comparisons at polar angles of 120° and 150° are shown in Figures 2.2.3-14 and 2.2.3-15. The predicted spectral shapes agree with the measurements if ground reflections are corrected. Generally, predicted levels are 3 dB higher at the peak frequency.

Comparisons were also made with highly suppressed engines. In Figure 2.2.3-16 measured static data from QEP Engine "C" appear to be approximately 3 dB lower after ground reflection effects have been removed. This engine contained turbine noise treatment as well as fan noise treatment. In Figure 2.2.3-17 the fully suppressed TF34 engine included core noise treatment. The predicted jet noise SPL spectral are approximately 3 dB below the measured data.

Thus, the differences between the prediction and other model data and engine data vary. Some of the difference is probably attributable to measuring field differences and other noise sources (particularly in engines).

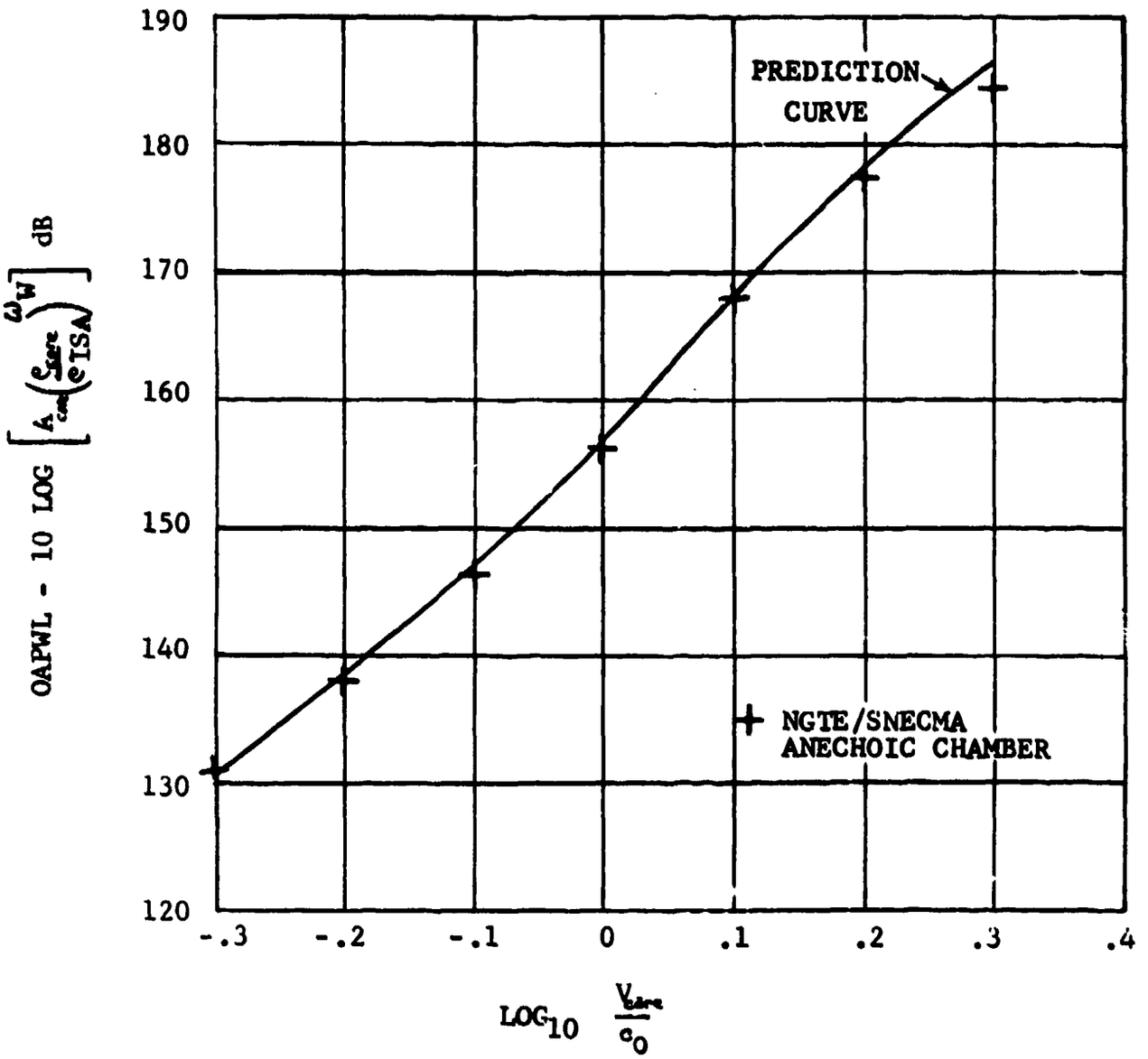

FIGURE 2.2.3-3 NORMALIZED OAPWL COMPARISON WITH ANECHOIC DATA

- CORE DIA. .75 IN (.019m)
- CORE VELOCITY 1360 FT/SEC (414.53m/s)
- CORE TEMP. 1215°R (675°K)
- VELOCITY RATIO .69

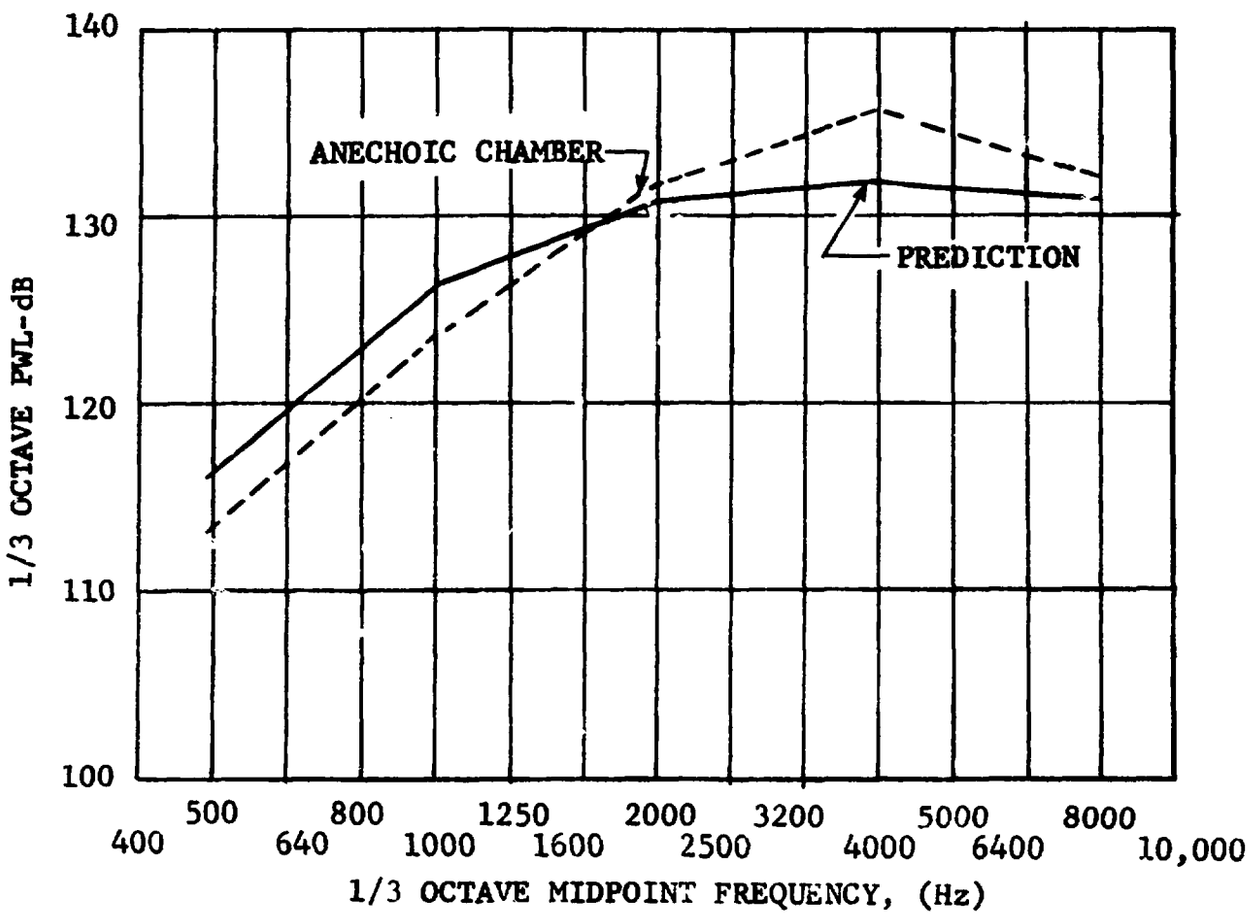

FIGURE 2.2.3-4 COMPARISON OF PREDICTED AND MEASURED PWL SPECTRA FOR COANNULAR/COPLANAR NOZZLE, AREA RATIO 2

- CORE DIA. .75 IN (.019m)
- CORE VELOCITY 1360 FT/SEC (414.53m/s)
- CORE TEMP. 1220°R (674.78°K)
- VELOCITY RATIO .69

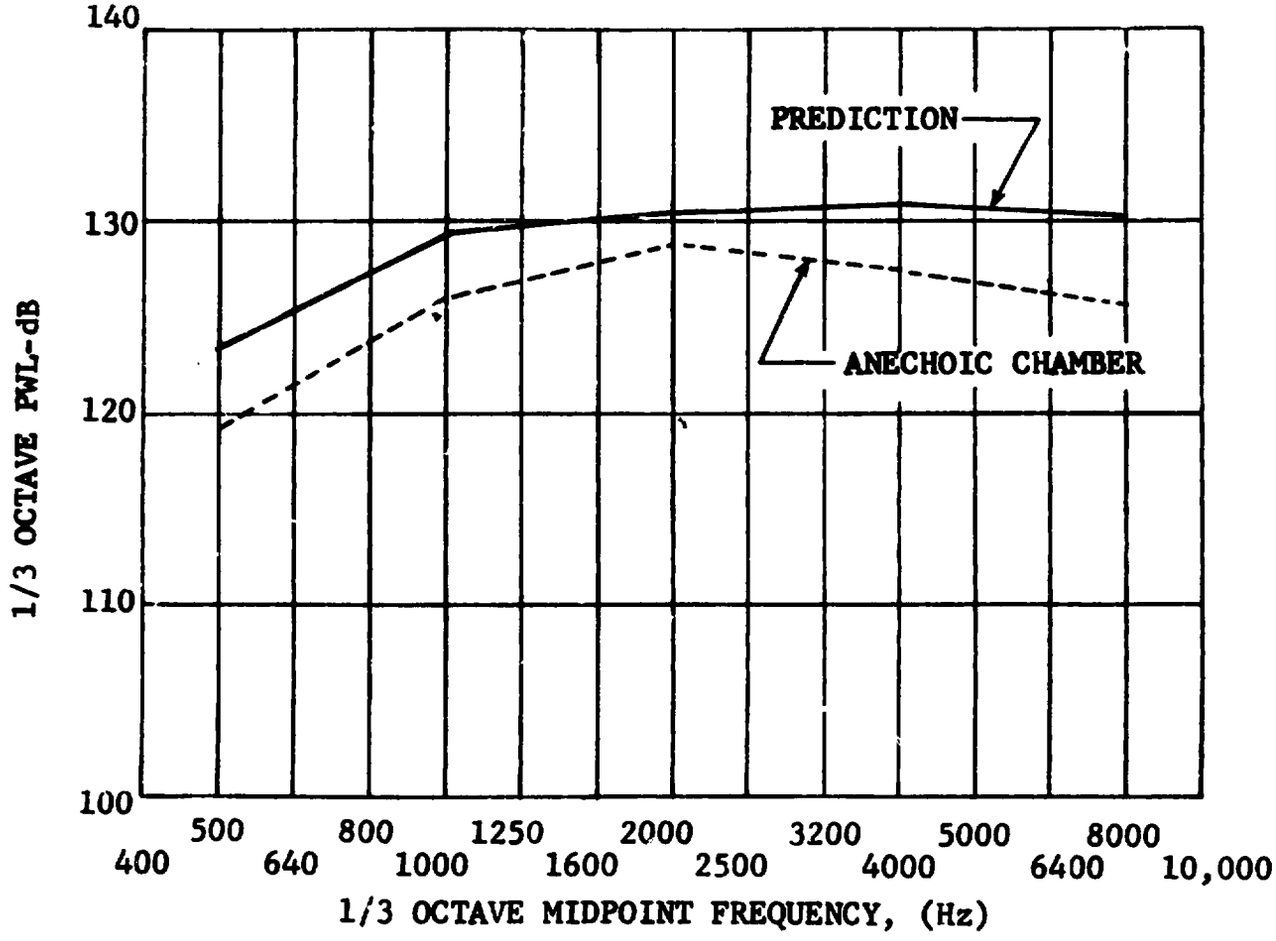

FIGURE 2.2.3-5 COMPARISON OF PREDICTED AND MEASURED PWL SPECTRA FOR COANNULAR/COPLANAR NOZZLE, AREA RATIO 5

- CORE DIA. .75 IN (.019m)
- CORE VELOCITY 1360 FT/SEC (414.53m/s)
- CORE TEMP. 1215°R (675°K)
- VELOCITY RATIO .69

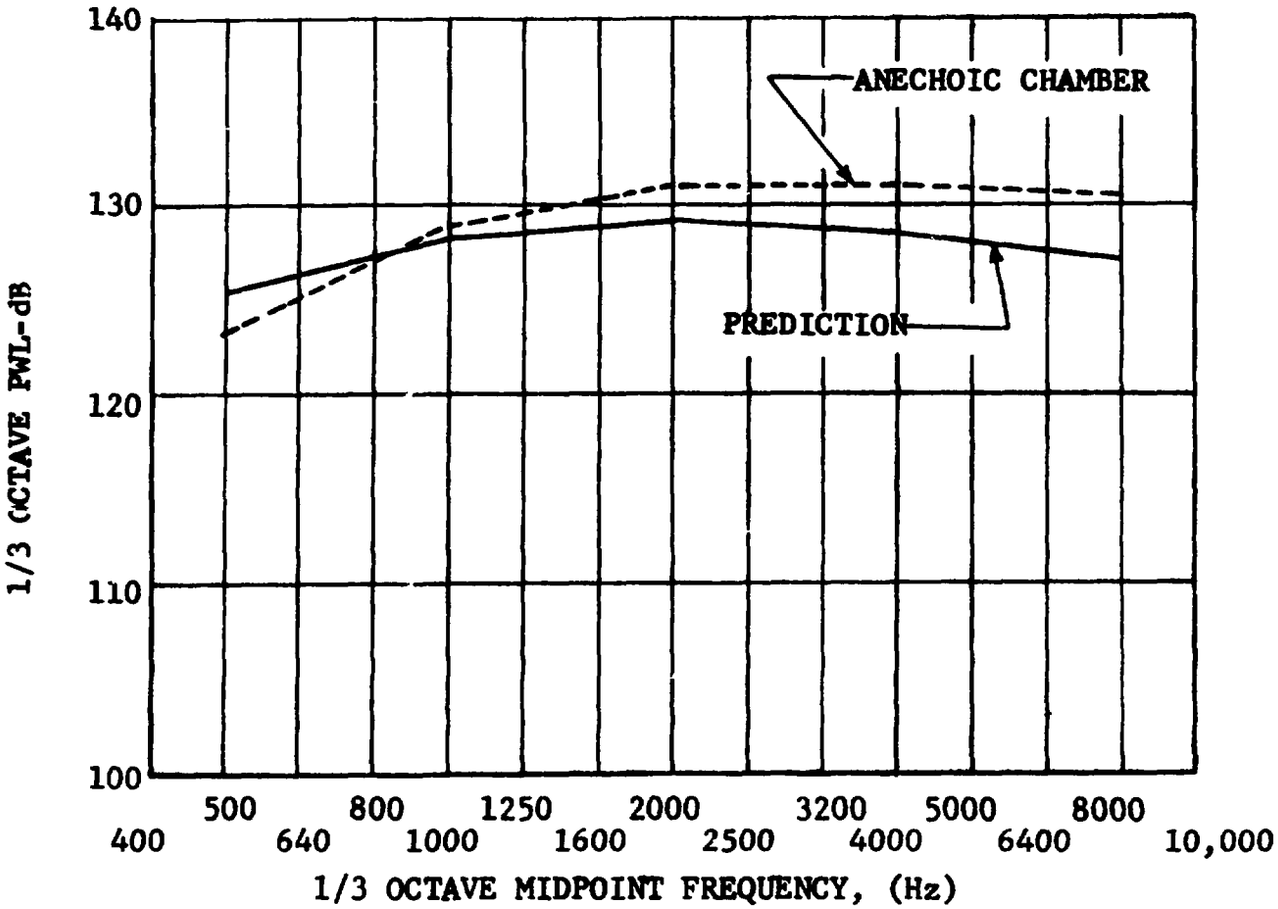

FIGURE 2.2.3-6 COMPARISON OF PREDICTED AND MEASURED PWL SPECTRA FOR COANNULAR/COPLANAR NOZZLE, AREA RATIO 10

- 10.67 FT (3.25m) RADIUS
- CORE DIA. .75 IN (.019m)
- CORE VELOCITY 1360 FT/SEC (414.53m/s)
- CORE TEMP. 1215°R (675°K)
- VELOCITY RATIO .69

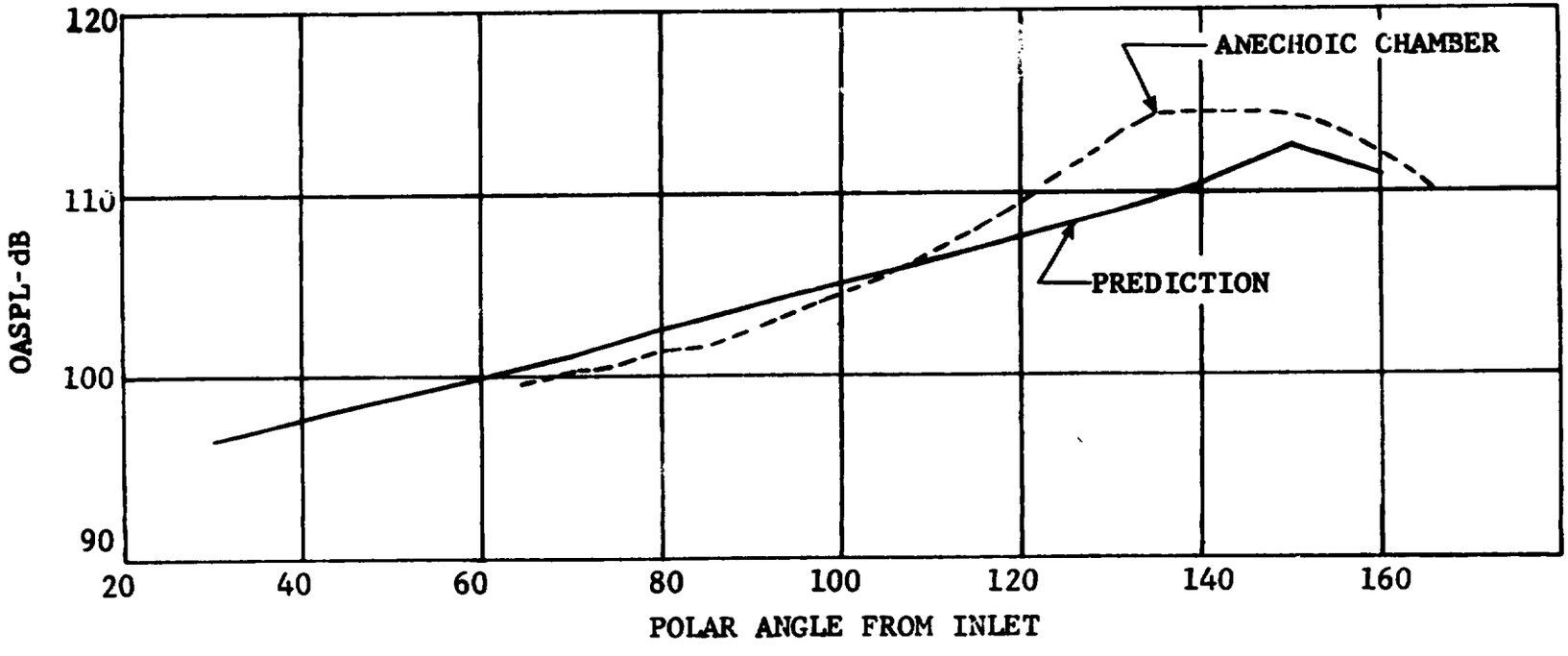

FIGURE 2.2.3-7 COMPARISON OF PREDICTED AND MEASURED OASPL DISTRIBUTIONS FOR COANNULAR/COPLANAR NOZZLE, AREA RATIO 2

- 10.67 FT (3.25m) RADIUS
- CORE DIA. .75 IN (.019m)
- CORE VELOCITY 1360 FT/SE. (414.53m/s)
- CORE TEMP. 1220°R (677.78°K)
- VELOCITY RATIO .69

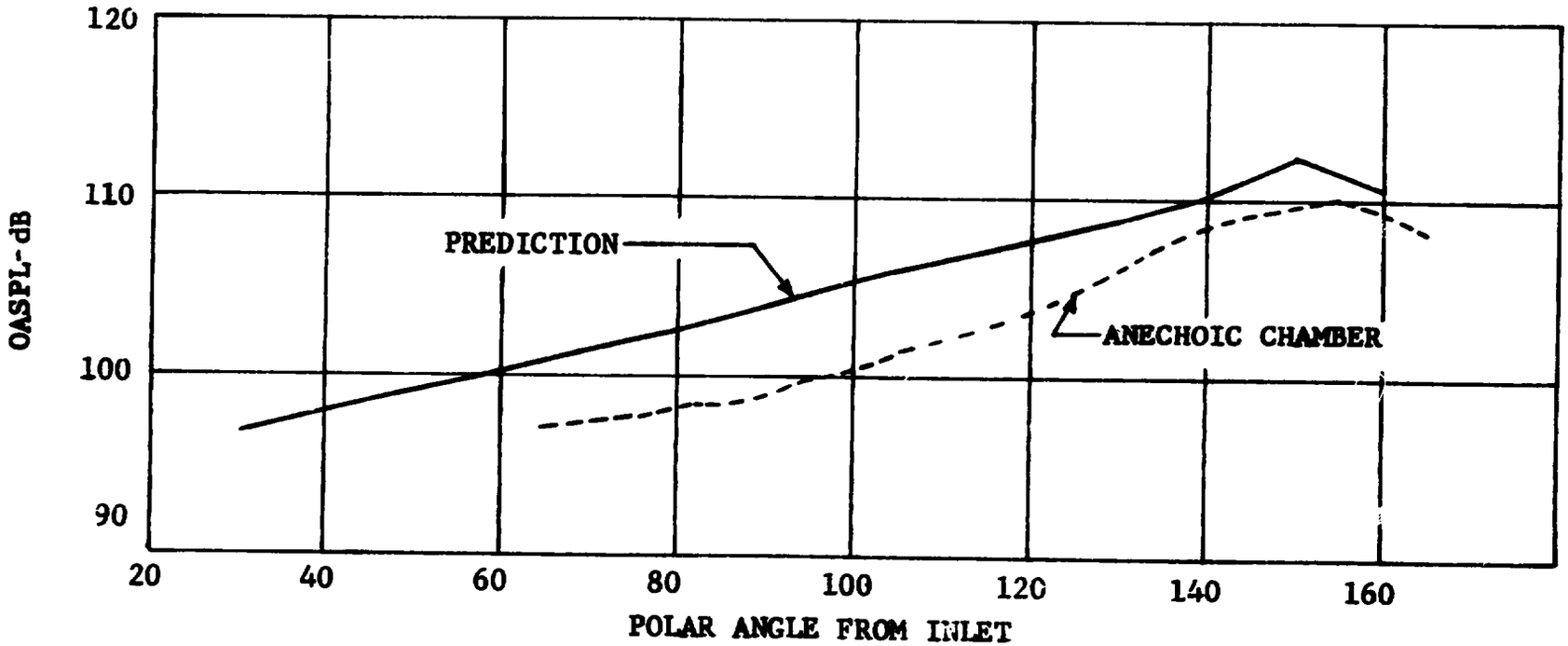

FIGURE 2.2.3-8 COMPARISONS OF PREDICTED AND MEASURED OASPL DISTRIBUTIONS FOR COANNULAR/COPLANAR NOZZLE, AREA RATIO 5

- 10.67 FT (3.25m) RADIUS
- CORE DIA. .75 IN (.019m)
- CORE VELOCITY 1360 FT/SEC (414.53m/s)
- CORE TEMP. 1215°R (675°K)
- VELOCITY RATIO .69

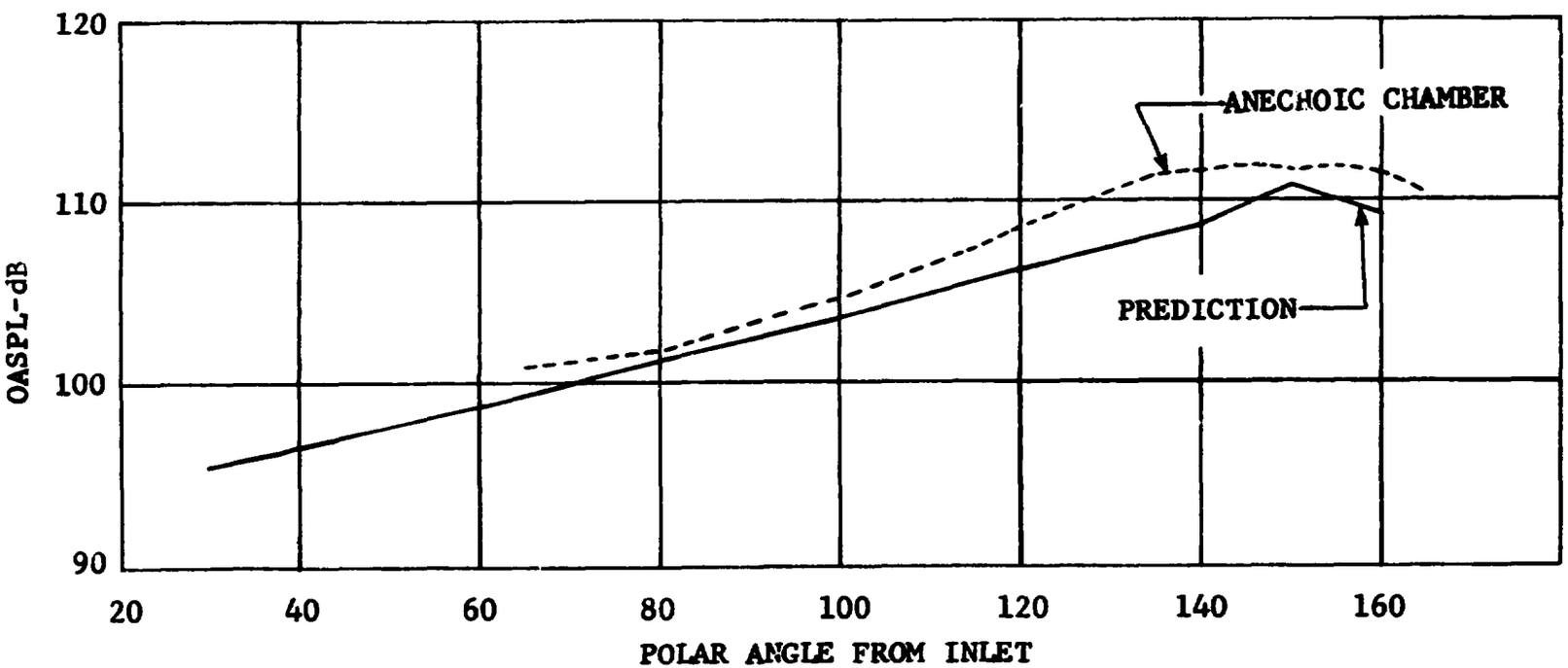

FIGURE 2.2.3-9 COMPARISON OF PREDICTED AND MEASURED OASPL DISTRIBUTIONS FOR COANNULAR/COPLANAR NOZZLE, AREA RATIO 10

- CORE AREA 5.66 FT^2 (.53m^2)
- AREA RATIO 3.13
- CORE VELOCITY 915 FT/SEC (278.89m/s)
- VELOCITY RATIO .84

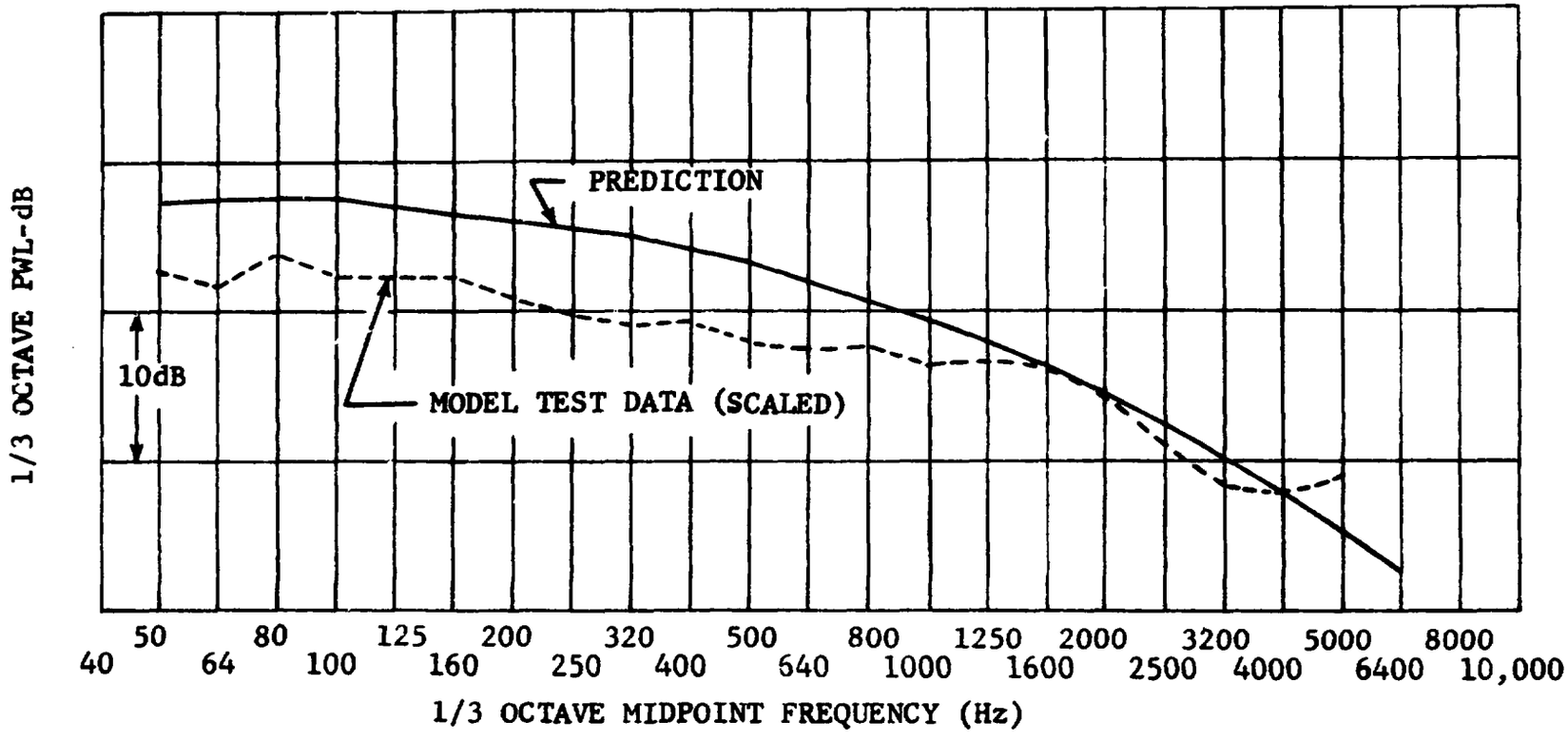

FIGURE 2.2.3-10 COMPARISON OF PREDICTED AND SCALED PWL SPECTRA FROM HIGH BYPASS TURBOFAN MODEL NOZZLE CONFIGURATION. LOW POWER SETTING.

- CORE AREA 5.66 FT^2 (.53m^2)
- AREA RATIO 3.13
- CORE VELOCITY 1230 FT/SEC (374.9m/s)
- VELOCITY RATIO .7

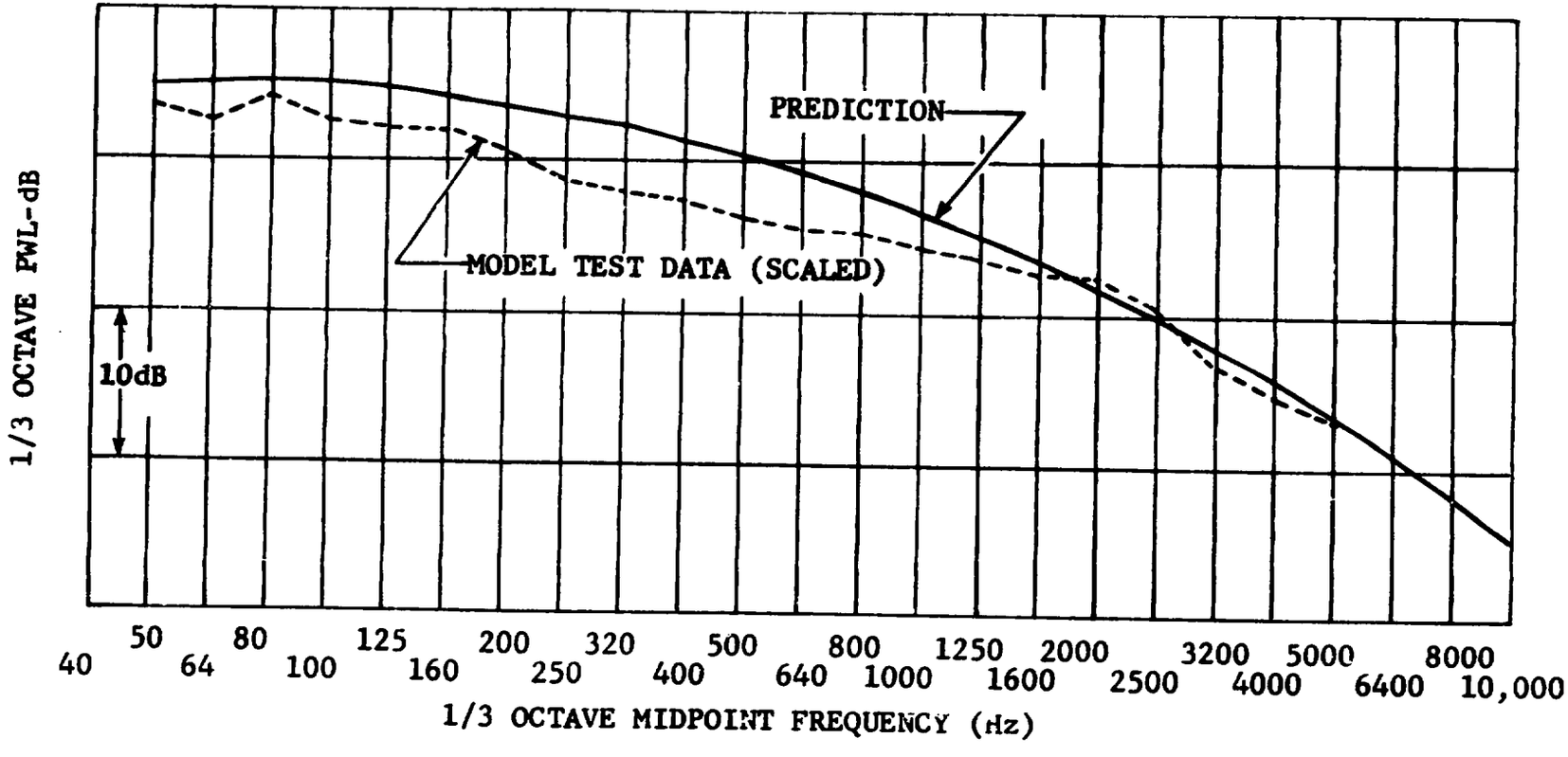

FIGURE 2.2.3-11 COMPARISON OF PREDICTED AND SCALED PWL SPECTRA FROM HIGH BYPASS TURBOFAN MODEL NOZZLE CONFIGURATION. HIGH POWER SETTING.

- CORE AREA 5.98 FT^2 (.56m^2)
- AREA RATIO 2.7
- CORE VELOCITY 1490 FT/SEC (454.15m/s)
- VELOCITY RATIO .68

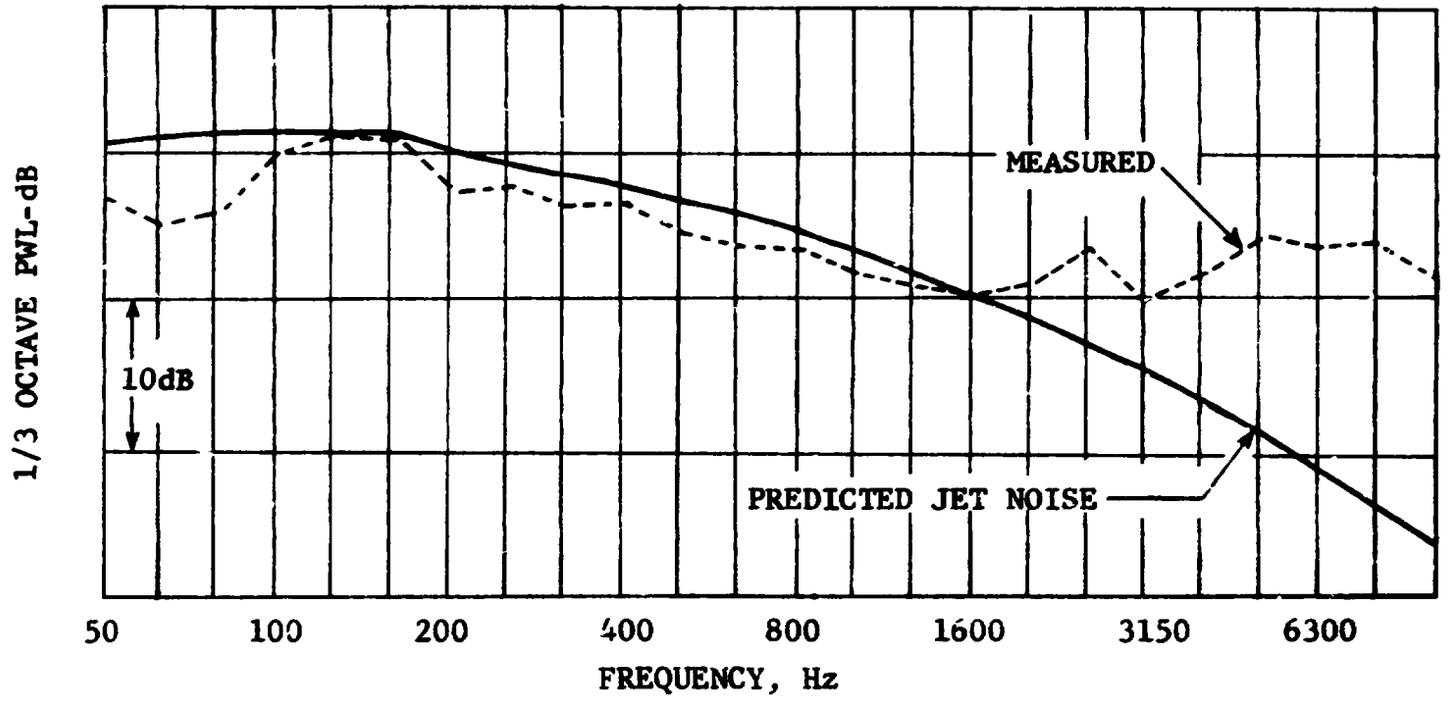

FIGURE 2.2.3-12 COMPARISON OF PREDICTED JET NOISE AND MEASURED PWL SPECTRA FOR STATIC CONDITIONS AT TAKEOFF POWER

- CORE AREA 5.08 FT^2 (.56m^2)
- AREA RATIO 2.7
- CORE VELOCITY 1490 FT/SEC (454.15m/s)
- VELOCITY RATIO .68

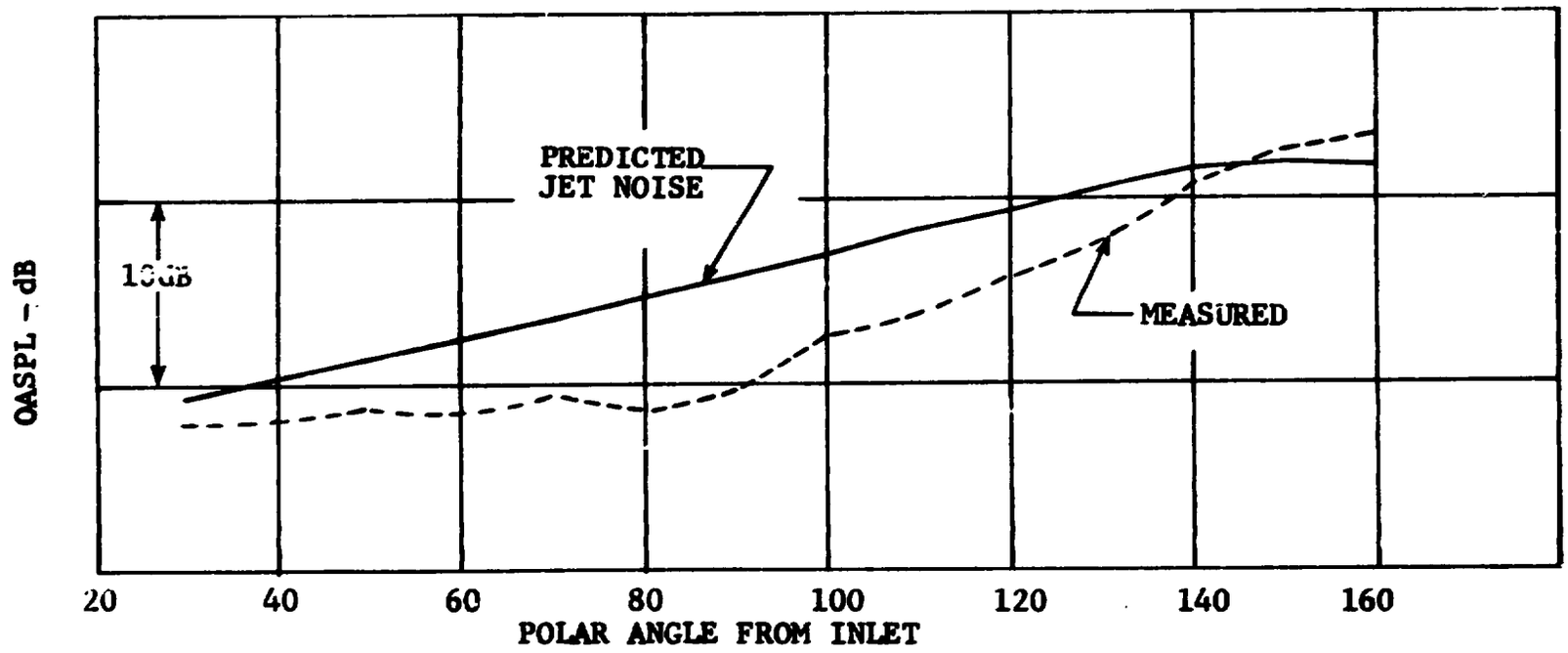

FIGURE 2.2.3-13 COMPARISON OF OASPL DIRECTIONAL CHARACTERISTICS FOR PREDICTED JET NOISE AND STATIC CONDITION MEASUREMENTS, TAKEOFF POWER

- CORE AREA 5.98 FT^2 (.56m^2)
- AREA RATIO 2.9
- CORE VELOCITY 1490 FT/SEC (454.15m/s)
- VELOCITY RATIO .68

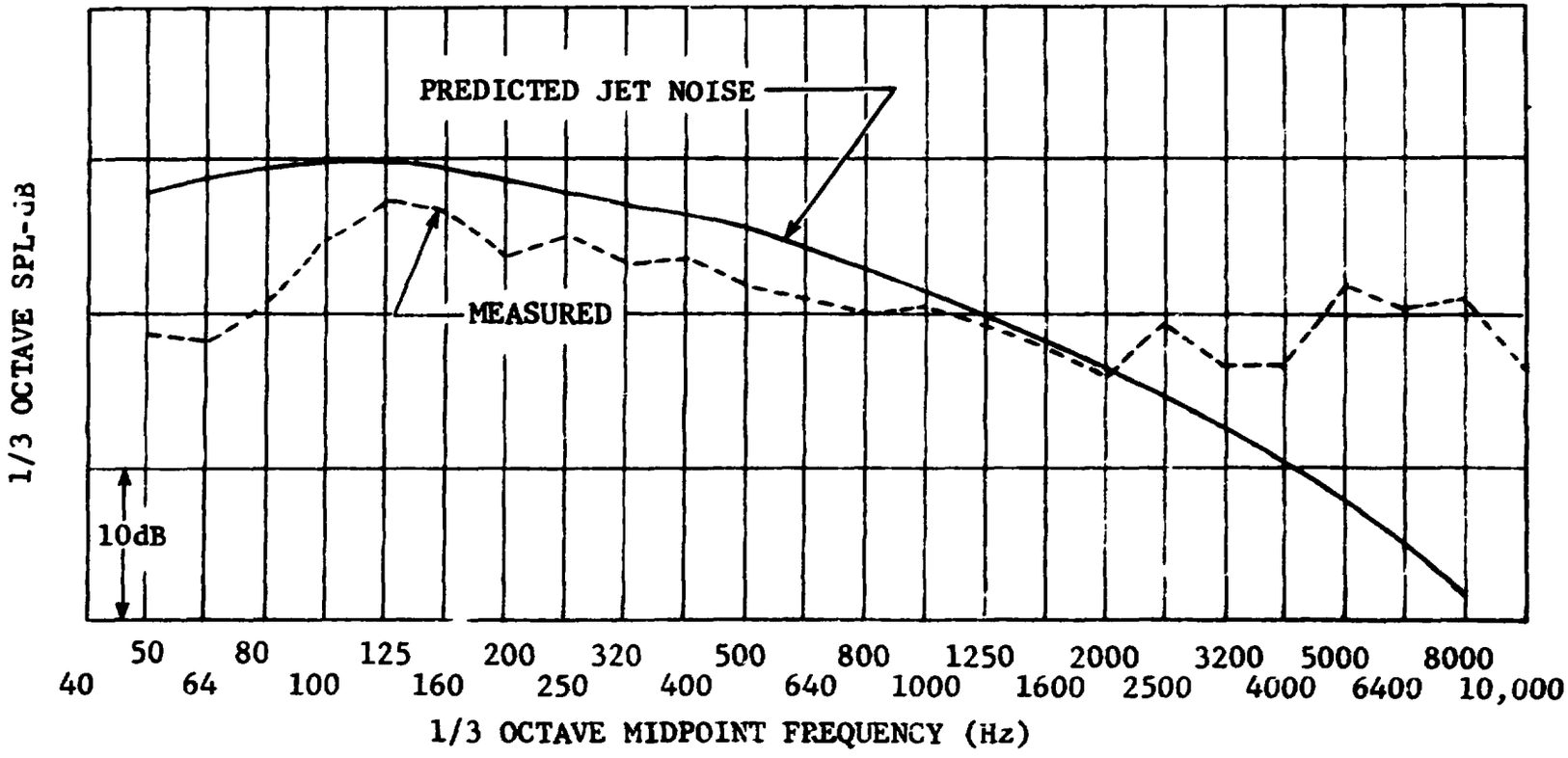

FIGURE 2.2.3-14 COMPARISON OF SPL SPECTRA FOR PREDICTED JET NOISE AND STATIC CONDITION MEASUREMENTS, TAKEOFF POWER, 120° POLAR ANGLE

- CORE AREA 5.98 FT^2 (.56m^2)
- AREA RATIO 2.7
- CORE VELOCITY 1490 FT/SEC (454.15m/s)
- VELOCITY RATIO .68

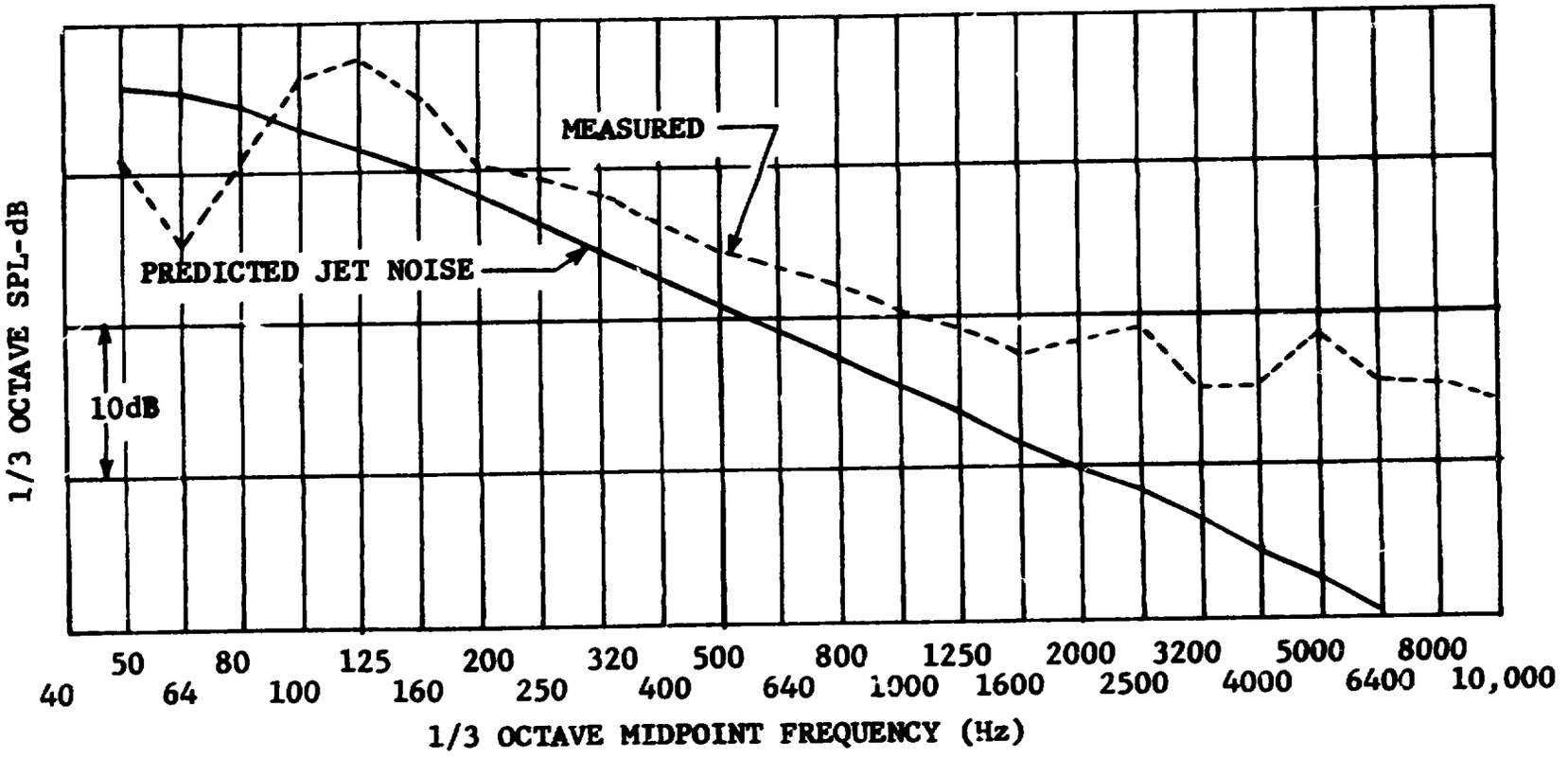

FIGURE 2.2.3-15 COMPARISON OF SPL SPECTRA FOR PREDICTED JET NOISE AND STATIC CONDITION MEASUREMENTS, TAKEOFF POWER, 150° POLAR ANGLE

- A_{CORE} 5.9 FT^2 (.55m^2)
- AREA RATIO 1.81
- V_{CORE} 860 FT/SEC (262.13m/s)
- VELOCITY RATIO 1.01

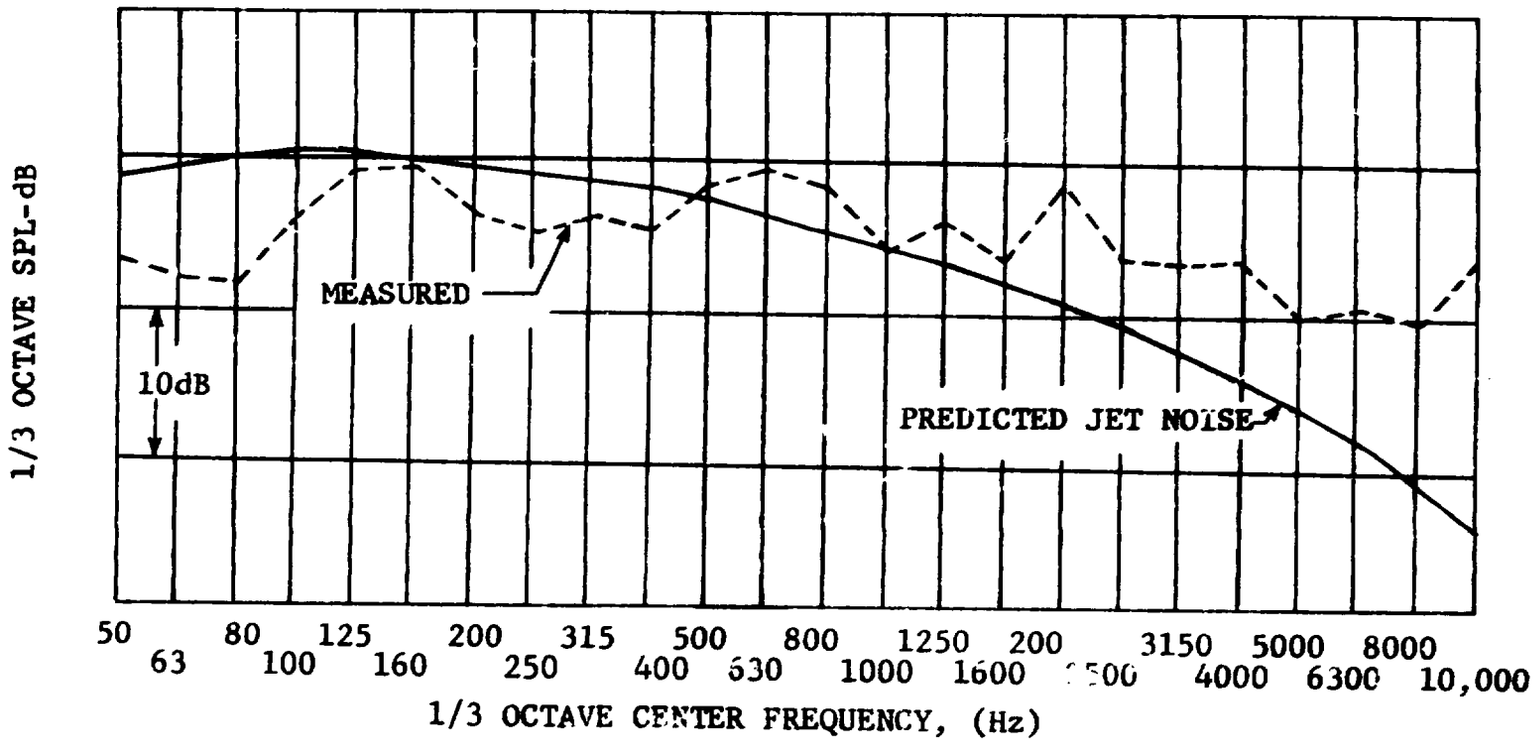

FIGURE 2.2.3-16 COMPARISON OF SPL SPECTRA FOR PREDICTED JET NOISE AND STATIC ENGINE C, HIGH POWER, 130° POLAR ANGLE

- A_{CORE} 1.95 FT^2 (.18m^2)
- AREA RATIO 2.81
- V_{CORE} 920 FT/SEC (280.42m/s)
- VELOCITY RATIO .81

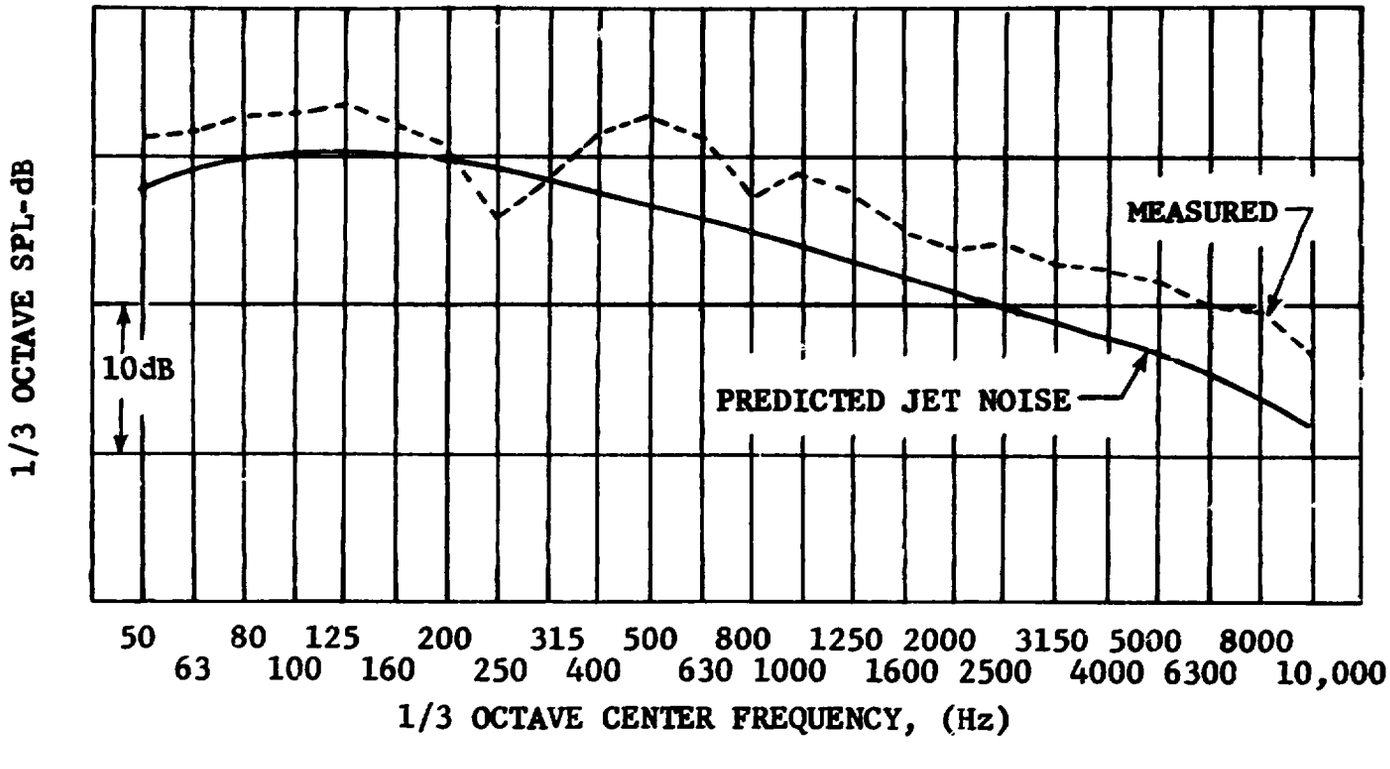

FIGURE 2.2.3-17 COMPARISON OF SPECTRA FOR PREDICTED JET NOISE AND STATIC TF34, FULLY SUPPRESSED, 110° POLAR ANGLE

It appears then that the prediction given here is accurate to within ±3 dB across the spectrum.

2.2.4 Prediction of Suppressor Effects

The acoustic tests conducted on several core suppressor configurations with dual flow operation showed that a multilobe design was the most promising suppressor configuration. A low area ratio (annulus area/flow area) nozzle was required to avoid the creation of an additional noise source as the fan flow passed over the lobes (see Volume II, Section 2.4). A suppressed prediction technique for dual flow jet noise is presented which provides incremental suppression from a baseline level.

In order to compare the suppressor characteristics with those of coplanar/coannular systems, the 18 capped lobe core suppressor was acoustically evaluated at a constant core jet velocity of 1600 ft/sec (488 m/sec) and with velocity ratios (V_{fan}/V_{core}) of 0.65, 0.58 and 0.48.

In Figure 2.2.4-1 the OASPL directivities demonstrate the overall interaction effect of the secondary flow. The mechanism causes a reduction in noise as the velocity ratio is reduced. Spectrally, the fan interaction effect with respect to the suppressed primary flow nozzle only is shown in Figure 2.2.4-2 for the peak angle. For primary flow only, the 18 capped lobe core suppressor successfully reduced low frequency noise but transferred the energy into the frequency band above 315 Hz. For dual flow operation, the effect was to substantially reduce the high frequency noise at the expense of increasing the low frequency content. The low frequency noise decreased, however, with decreasing velocity ratio. This demonstrates that the design was successful in allowing the low velocity fan flow to mix with an increased core jet periphery and reduce the turbulence intensity in the shear layer between them.

The secondary flow would be expected to reduce the high frequencies in preference to the low frequencies because the high frequency acoustic sources are located in the initial mixing region of the primary jet where the effect of the secondary flow is greatest. Lower frequencies, on the other hand, are produced downstream where the secondary flow has less effect. The mixing action of the 18-lobe core suppressor has already generated a spectrum which has dominant high frequency characteristics and a reduced potential core length. The interaction effect of the secondary flow thus enhances this system.

The acoustic relationships for the baseline (1) nozzle and the 18 capped lobe configuration are shown in Table 2.2.4-1. The value ΔOAPWL is the difference between the dual flow OAPWL and the single jet OAPWL. This same parameter was determined and used in the prediction procedure derived from tests on unsuppressed coplanar, coannular nozzles. The area ratio (A_{fan}/A_{core}) of both configurations is 3. The determined values are shown in Figure 2.2.4-3. The baseline data comply with the broken curve representing

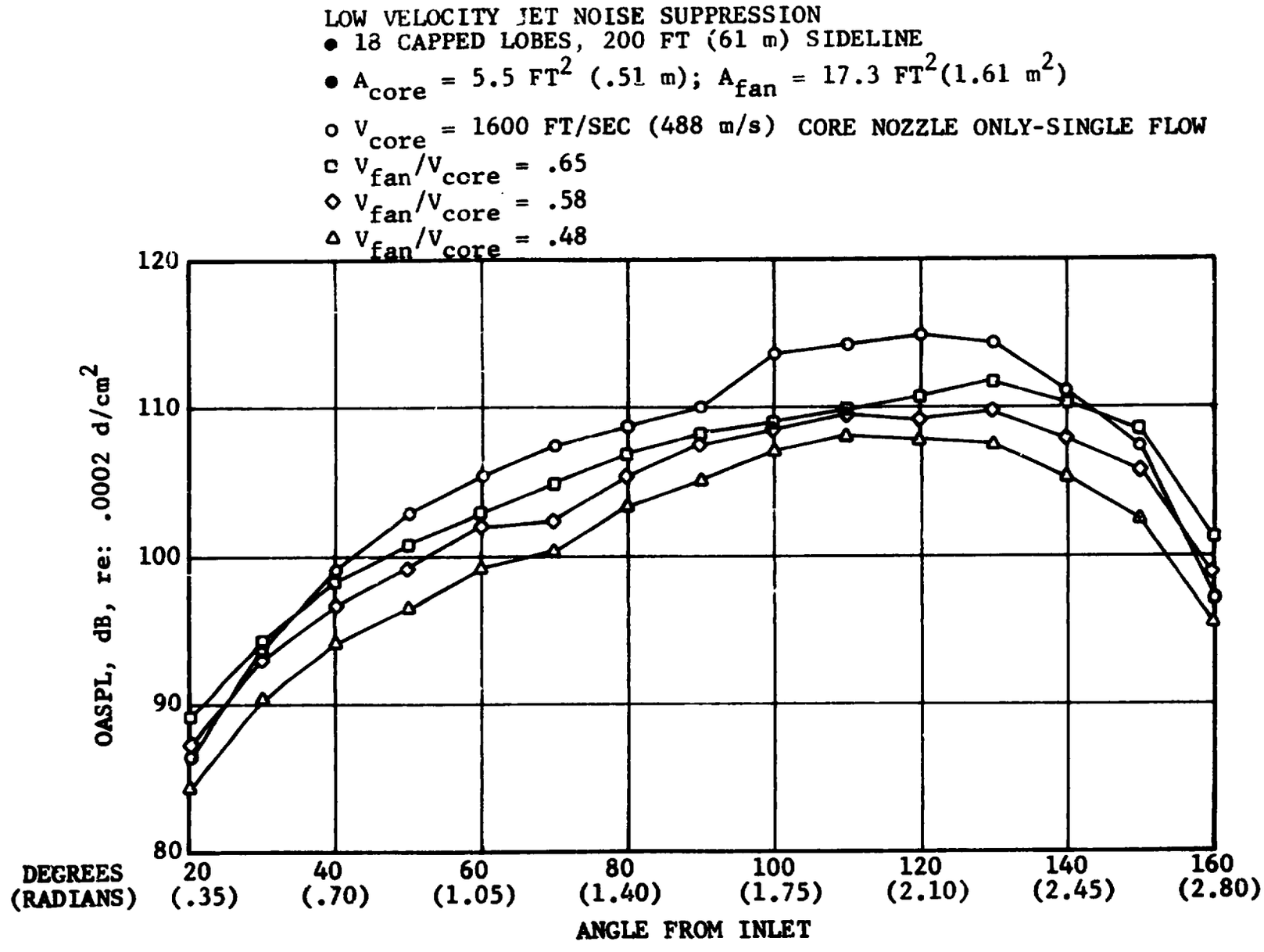

FIGURE 2.2.4-1 OASPL VS. ACOUSTIC ANGLE FOR RANGE OF VELOCITY RATIOS

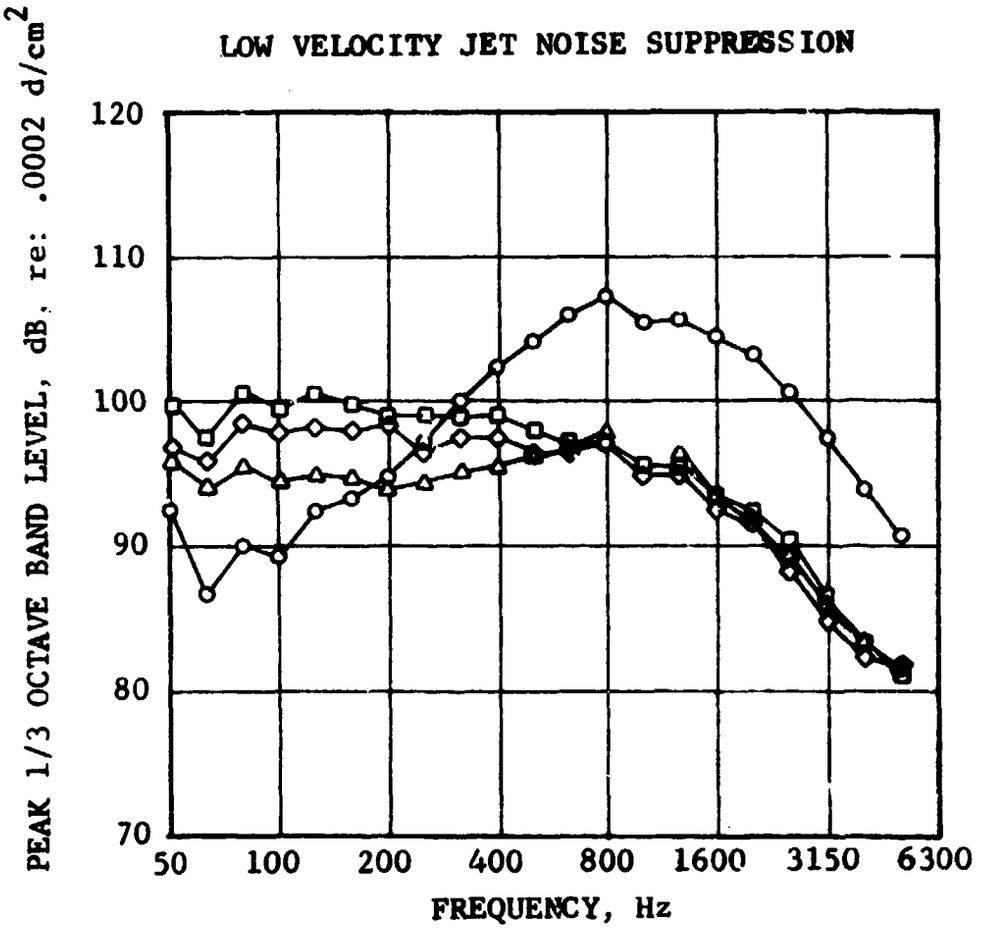

- 18 CAPPED LOBES
- 200 FT (61 m) SIDELINE
- A_{core} = 5.5 FT^2 (.51 m^2); A_{fan}= 17.3 FT^2(1.61m^2)

V_{core}=1600 FT/SEC(488m/s)

	OASPL	PNL
○ CORE NOZZLE ONLY- SINGLE FLOW	115	124
□ V_{fan}/V_{core} = .65	111	117
◇ V_{fan}/V_{core} = .58	109	116
△ V_{fan}/V_{core} = .48	108	115

FIGURE 2.2.4-2 PEAK ANGLE SPECTRA FOR RANGE OF VELOCITY RATIOS

TABLE 2.2.4-1 ACOUSTIC RELATIONSHIPS FOR COANNULAR FLOW JET NOISE

Baseline (I). unsuppressed. coannular separate flow. AR = 3

	Velocity Ratio	Peak Angle 200 Ft(61m) Sideline OASPL	PNL	OAPWL	ΔOAPWL
V_{core}=1600 Ft/Sec (488 m/s)	-	119.7	123.9	173.2	-
	.60	116.8	119.2	170.4	-2.8
	.50	116.1	118.4	169.5	-3.7
	.40	116.4	118.8	169.8	-3.4

18 Capped lobe core suppressor, coannular separate flow. AR = 3

	Velocity Ratio	Peak Angle 200 Ft(61m) Sideline OASPL	PNL	OAPWL	ΔOAPWL
V_{core}=1600 Ft/Sec (488 m/s)	-	115	124	170	-
	.65	111	117	166.5	-3.5
	.58	109	116	165	-5.0
	.48	108	115	163	-7.0

where $\Delta OAPWL = OAPWL_{coannular} - OAPWL_{core}$.

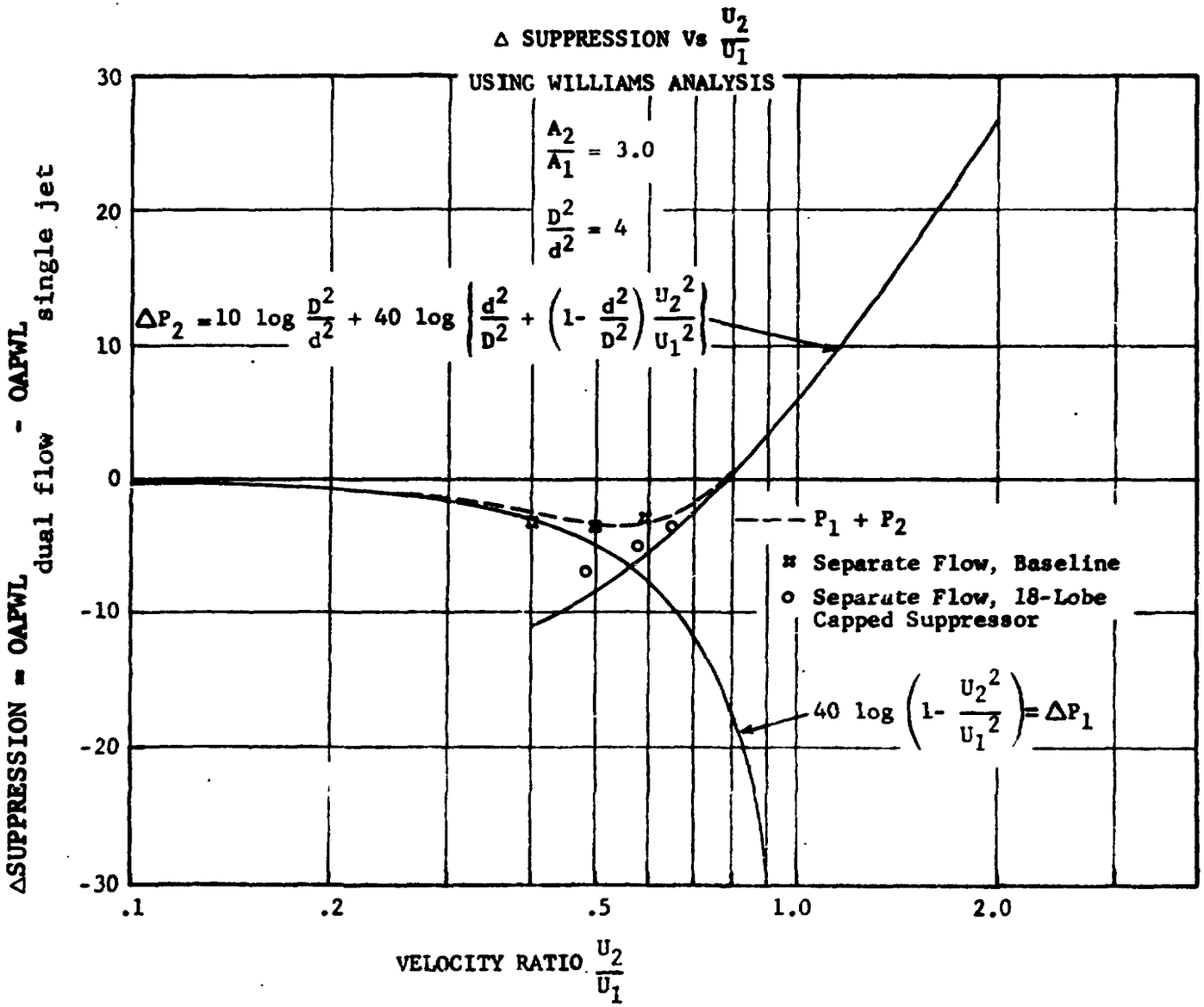

FIGURE 2.2.4-3 COMPARISON BETWEEN PREDICTED CURVES OF THE NOISE OUTPUT OF EXTERNALLY MIXED COAXIAL JETS AND MEASURED DATA - UNSUPPRESSED AND SUPPRESSED

the logarithmic sum of the two noise contributors. The suppressor data are shown as the difference in power levels of a coannular system with suppressed core and the suppressed core alone.

The noise reduction provided by the 18-lobe suppressor could be referred to either Baseline I or Baseline II as the two configurations were very similar. While the spectra and the levels associated with the two baselines were similar, there was sufficient difference in the mid frequency range, particularly for the aft angles, to result in perceptibly higher PNL reduction using Baseline II. However, if a conservative estimate is required, it is suggested that the ΔSPL's resulting from a Baseline I comparison be used.

The prediction technique is applicable to static jet noise only, since inflight effects have not been established for dual flow systems. The empirically determined suppression values are considered valid for coaxial configurations of area ratios (A_{fan}/A_{core}) between 2 and 4. The SPL differences between unsuppressed and suppressed coaxial systems are tabulated in Appendix B (for both baseline nozzles) in lieu of further refinements which can only be made following a more extensive study of this successful technique. These data applies for a core velocity of 1600 ft/sec (488 m/sec), but the values can be extrapolated to lower core jet velocities by means of the plot presented in Figure 2.3.2-1, where the peak OASPL of the baseline and suppressed configurations is compared for core jet velocities down to 800 ft/sec (244m/sec).

A flow chart of the suppression method is outlined in Figure 2.2.4-4. The unsuppressed noise levels of the coannular configuration should be obtained at a 320 ft (97.5 m) arc before the corrections are applied at the appropriate velocity ratio and core velocity. The suppressed values may now be extrapolated to the required sideline distance, as shown in the examples of Figures 2.2.4-5 and 2.2.4-6, where suppressed single and dual flow perceived noise levels are presented relative to the acoustic angle at a measurement location of 1500 ft (458 m) sideline.

2.2.5 Conclusions

A procedure to evaluate the acoustic effect due to the interaction between the core and fan streams was developed and applied to predict coannular flow jet noise for configurations of area ratios (A_{fan}/A_{core}) from 2 to 8 and velocity ratios (V_{fan}/V_{core}) from 0.6 to 1.0.

The predicted coannular flow SPL's are within 3 dB of actual measured engine data over the frequency range associated with jet noise. Some differences may be attributed to a lack of conformity in the measurement terrain causing differences in ground reflection effects. The structure of the prediction technique was devised to enable direct correlation with parallel analysis efforts and also to enable computerization of the method with the minimum of difficulty.

Area Ratio of Coaxial System 2 to 4

Velocity Ratio Range $\frac{V_{core}}{V_{fan}} \sim .45$ to $.75$

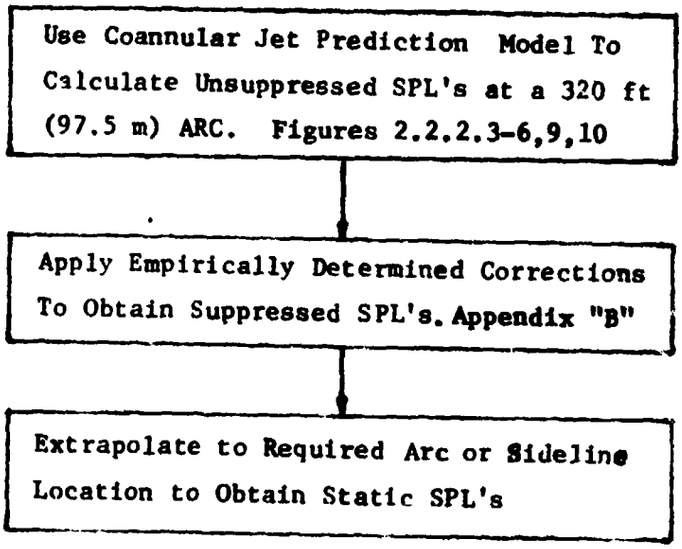

Figure 2.2.4-4 Suppressed Coannular Jet Procedure.

LOW VELOCITY JET NOISE SUPPRESSION

APPLICABLE FOR:

- 18-LOBE CORE SUPPRESSOR AR = 2
- $V_{core} \approx 1600$ FT/SEC (488 m/s)

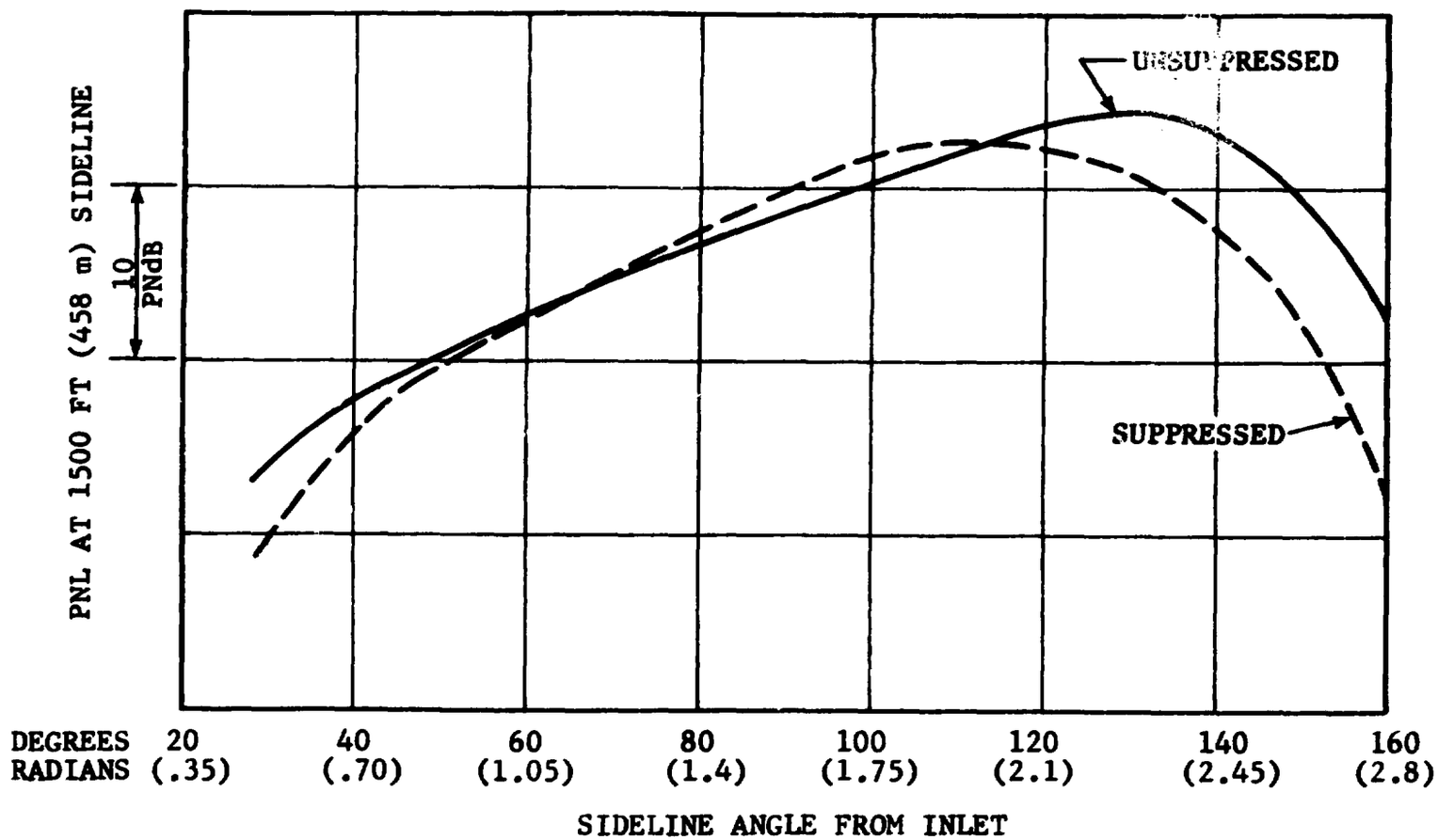

FIGURE 2.2.4-5 EFFECT OF MULTI-LOBE CORE SUPPRESSOR ON PNL OF SINGLE JET

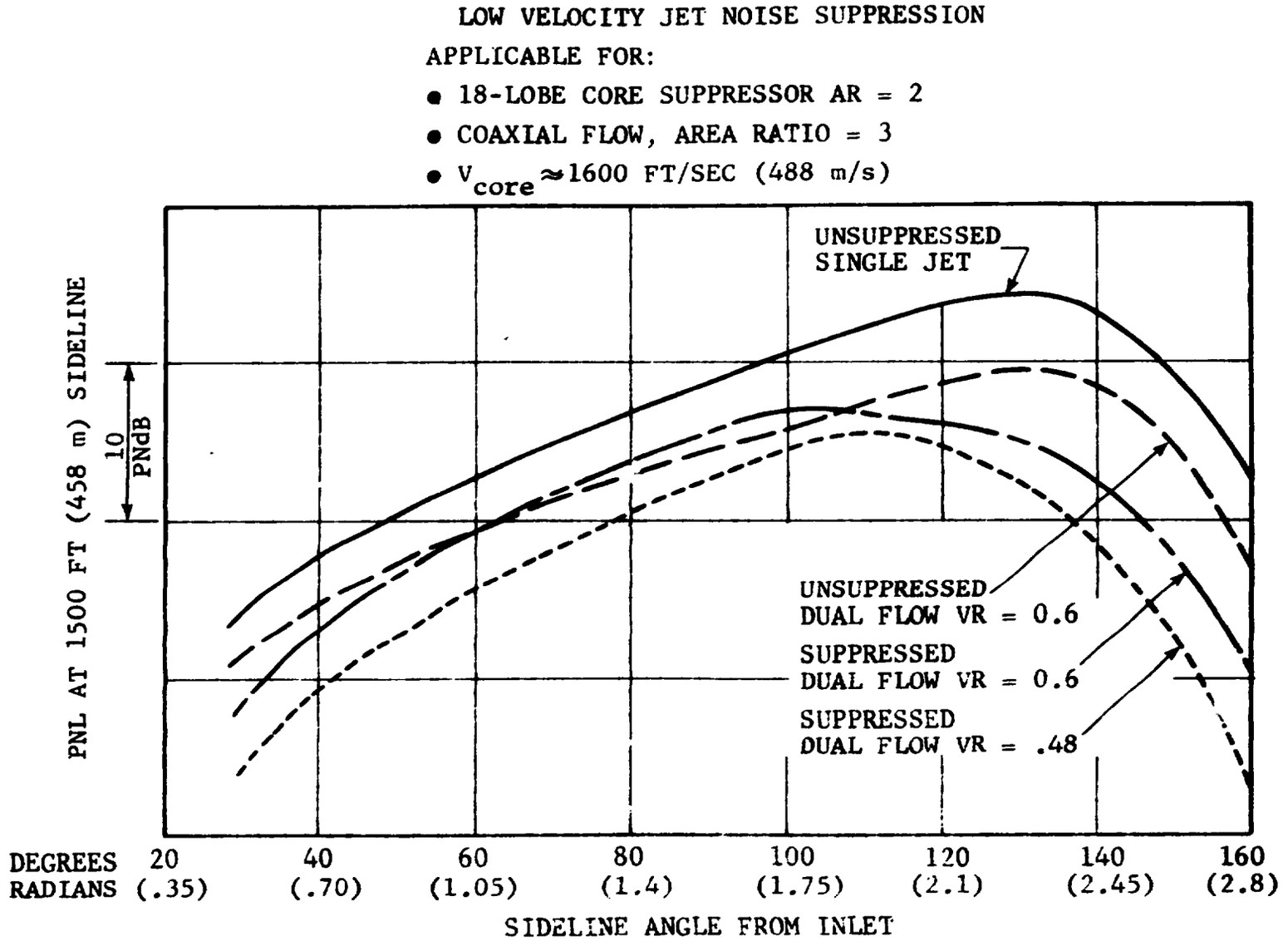

FIGURE 2.2.4-6 EFFECT OF MULTI-LOBE CORE SUPPRESSOR ON PNL OF COAXIAL JET

A simplified technique was developed to account for the case where the coannular jet noise was suppressed by means of a multilobe daisy-type nozzle. Further parametric studies are required if the prediction for suppressed nozzles is to become more generalized.

2.3 SUMMARY - FLOW CHARTS

2.3.1 Summary - Unsuppressed Coannular Prediction

The prediction procedure is valid for coannular nozzle configurations of area ratios (A_{fan}/A_{core}) between 2 and 8, operating at velocity ratios (V_{fan}/V_{core}) between 0.6 and 1.0.

The method provides a complete coaxial jet noise spectrum at each far-field location.

A flow chart for the implementation of a typical calculation is shown in Figure 2.2.3-1.

From a knowledge of the core and fan aerodynamic parameters described in Figure 2.2.3-2 a typical calculation would proceed in steps outlined in Figure 2.2.1-1.

For example, the following formulae are used in Step 1:

$$\rho_{core} = \frac{39.65}{T_{T_{core}}} \left(\frac{P_{T_{core}}}{P_o}\right)^{\frac{\gamma-1}{\gamma}} \qquad (2.3.1\text{-}1)$$

$$\frac{\rho_{core}}{\rho_{isa}} = \frac{\rho_{core}}{.076475} \qquad (2.3.1\text{-}2)$$

$$\frac{V_{core}}{C_o} = \frac{V_{core}}{116.89} \qquad (2.3.1\text{-}3)$$

The density exponent ω_w is obtained from the relationship shown in Figure 2.2.2-2 and the normalization factor for the power level of the core nozzle is thus calculated:

$$\text{OAPWL normalizer} = 10 \log_{10} \left[A_{core} \left(\frac{\rho_{core}}{\rho_o}\right)^{\omega_w}\right] \qquad (2.3.1\text{-}4)$$

There is now sufficient information to enter Figure 2.2.2-3 and calculate the OAPWL of the core nozzle alone.

The second power level of the required coannular nozzle system is determined in Step 2 by entering Figure 2.2.2-4 with a prior knowledge of velocity ratio (V_{fan}/V_{core}) and area ratio (A_{fan}/A_{core}). The relationship supplies a correction (ΔOAPWL) which is added to the overall power level of the core nozzle.

Processing to Step 3, the power level spectral characteristics can be determined by referring to Figures 2.2.2-6 to 2.2.2-9. The formulae used are as follows:

$$D = \left[\frac{4\ A_{core} + A_{fan}}{\pi}\right]^{1/2} \qquad (2.3.1\text{-}5)$$

$$V_m = \frac{\left(V_{core}\ W_{core} + V_{fan}\ W_{fan}\right)}{W_{core} + W_{fan}} \qquad (2.3.1\text{-}6)$$

Modified Strouhal Number (Dimensionless Frequency) = $(f*D/V_m)\ (V_{fan}/V_{core})^{1/2}$

The PWL spectra normalizer = $10 \log_{10} \left[(V_m/D)\ (V_{core}\ V_{fan})\right]^{1/2}$

The power level spectrum PWL_f is obtained from the curves over the frequency range of interest, where $PWL_f = PWL_{band} - 10 \log_{10} (\Delta f)$.

For 1/3 octave band width $\Delta f = 23\%$, and the PWL_{band} at each center frequency can be determined.

The conversion from sound power level to space-average mean square sound pressure level determined over a three/fourths sphere of area $3\pi R^2$ (where R = 250 ft) surrounding the source is given by,

$$SPL_{space\ average} = PWL_{band} - 20 \log_{10} R - 9.25 \qquad (2.3.1\text{-}7)$$

$$\text{Thus, } SPL_{space\ average} = PWL_{band} - 57.2. \qquad (2.3.1\text{-}8)$$

The directivity of the sound source is considered by progressing to Step 4. Experimentally determined directivity indexes which are related to the dimensionless frequency for specific area ratios are presented in Figures 2.2.2-11 to 2.2.2-14.

The determination of DI_θ enables the sound pressure level measured at 250 ft and angle θ° from the noise source to be calculated since,

$$SPL_\theta = SPL_{space\ average} + DI_\theta \quad (2.3.1\text{-}9)$$

$$\text{Thus,}\quad SPL_\theta = PWL_{band} - 57.2 + DI_\theta \quad (2.3.1\text{-}10)$$

at 250 ft (76.2m) arc

59° F (15° C), 70% RH

The above relationship is for the ideal case; for the actual case atmospheric absorption (α) and extra ground attenuation (EGA) corrections must be applied (subtracted from PWL).

Finally, in Step 5, the farfield noise spectra at any acoustic angle for any arc or sideline may be obtained by utilizing standard acoustic extrapolation techniques.

2.3.2 Summary - Suppressed Coannular Prediction

The suppressed prediction procedure is valid for coannular nozzle configurations of area ratios (A_{fan}/A_{core}) between 2 and 4, operating at velocity ratios (V_{fan}/V_{core}) from 0.45 to 0.6.

A table of suppression values is used based on a core velocity of 1600 ft/sec (488 m/sec). Values at core velocities down to 800 ft/sec (244 m/sec) are extrapolated by means of a relationship between the OASPL's of the baseline and suppressed configurations over the velocity range.

The procedure follows the flow chart outlined in Figure 2.2.4-4.

The first step is to obtain an unsuppressed noise level for the coannular configuration. The unsuppressed SPL's are required on a 320 ft (97.5 m) arc.

The second step is to determine the correct table of suppression values to use from Appendix B. This is done by matching velocity ratio requirements as closely as possible with those provided.

Step 3 is to extrapolate the suppression values in the Appendix B tables [valid for V_{core} = 1600 ft/sec (488 m/sec)] to values applicable to the core jet velocity in question. For example, in Figure 2.3.2-1 the OASPL suppression obtained at V_{core} = 1600 ft/sec was 7 dB, and the suppression for V_{core} = 1200 ft/sec was 4 dB. Thus, the values given in the tables should be adjusted by a factor of 4/7.

The final step in the suppression process is to use standard acoustic extrapolation techniques to produce a farfield suppressed spectrum.

COANNULAR JET NOISE SUPPRESSION

NOISE REDUCTION FROM
MODIFIED MULTI-LOBE NOZZLE

- 1500 FT (457m) ALTITUDE
- PEAK ANGLE
- COANNULAR FLOW

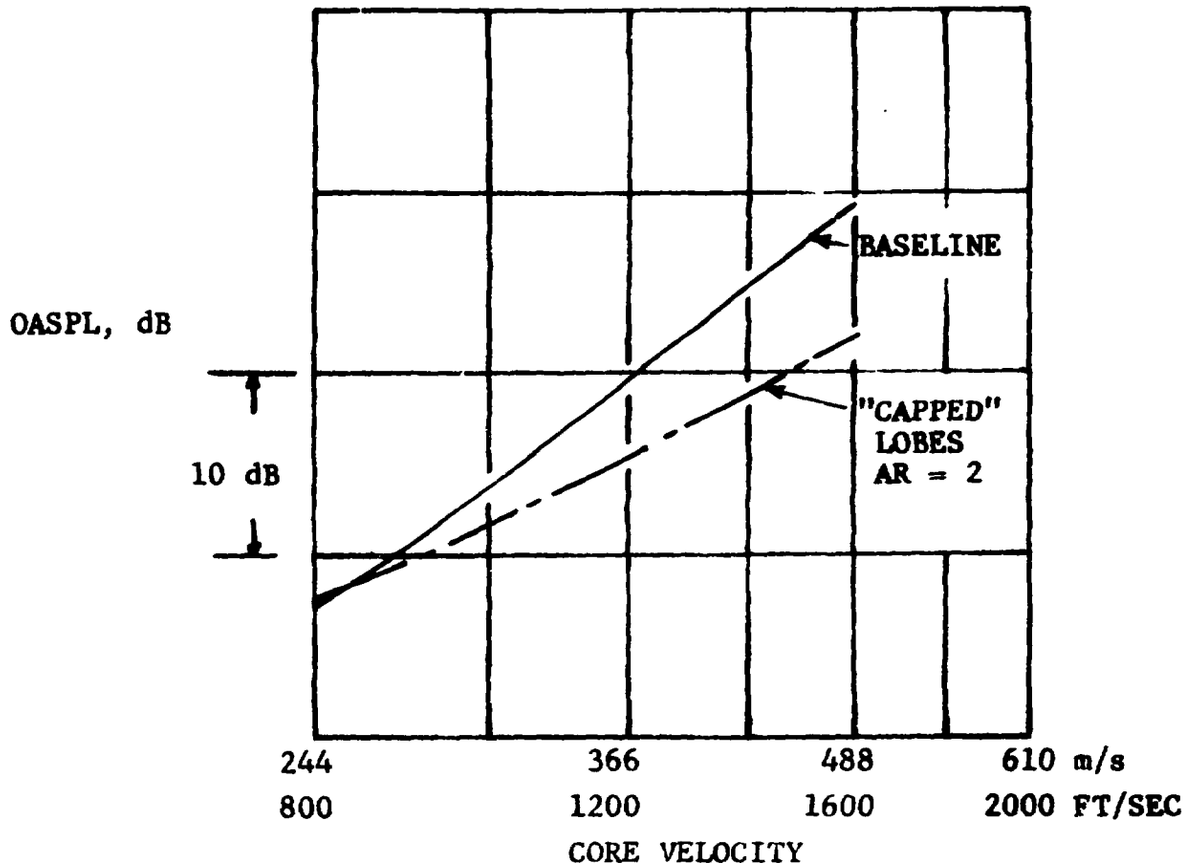

FIGURE 2.3.2-1 JET NOISE SUPPRESSION WITH MULTI-LOBE NOZZLES

Appendix B provides tables based on both Baselines (I and II). It is suggested that Baseline I estimates (Tables B-1 and -2) be used if conservative values are desired. Table B-3 provides the suppression indicated by a Baseline II comparison.

References

2.2.1-1 Olsen, W. and Friedman, R.; "Jet Noise from Co-axial Nozzles over a Wide Range of Geometric and Flow Parameters," NASA TM-X-71503, February 1974, Lewis Research Center, Cleveland, Ohio 44135.

2.2.1-2 Bielak, G.W.; "Coaxial Flow Jet Noise, DGE-10041-1, 1972, Boeing/ Aeritalia Company, Seattle, Washington.

2.2.1-3 Eldred, K.; "Far Field Noise Generation by Coaxial Flow Jet Exhausts. Volume I: Detailed Discussion," FAA-RD-71-101-Volume I, 1971, Wyle Laboratories, Inc., El Segundo, California.

2.2.1-4 Williams, T.J., Ali, M.R.M., and Anderson, J.S.; "Noise and Flow Characteristics of Coaxial Jets," Journal of Mechanical Engineering Science, Volume II, No. 2, April 1969, pp. 133-142.

2.2.1-5 Hoch, R.G., DuPonchel, J.P., Cocking, J.J., and Bryce, W.D.; "Studies of the Influence of Density on Jet Noise," presented at the First International Symposium on Air Breathing Engines, Marseille, 19-23 June 1972.

SECTION 3.0

COMBUSTOR NOISE PREDICTION

3.1 INTRODUCTION

Combustion noise is attributed to mass density and momentum fluctuations in the gas due to unsteady burning. It consists of a broadband noise arising from a statistical distribution of monopole sources scattered throughout the combustion reaction zone.

A number of experimental studies in component test rigs (References listed in Volume II) have shown that the level of noise generated depends on the airflow rate, fuel mass flow and the temperature rise resulting from the combustion. These tests showed that the peak frequency was relatively constant over a wide range of operating conditions. The peak frequency was also found to fall within a narrow low frequency range for a variety of combustors. The combustor (core) noise prediction technique was developed with these component results as background.

3.2 POWER LEVEL CORRELATION

The level of combustor noise from engines has been found to correlate with the total flow rate, the fuel mass flux and the density at the inlet to the combustor. Based on Knott's work (Reference 3.2-1) which showed the combustion thermoacoustic efficiency depended on the fuel mass flux (Figure 3.2-1), Motsinger (Reference 3.2-2) determined that the thermoacoustic efficiency was dependent on the air temperature rise and, based on measured pressure fluctuations in a combustor on an engine (Figure 3.2-2), postulated that the noise level should be dependent upon the air density into the combustor. The correlation, obtained with combustor noise from a T64 turboshaft engine, is shown in Figure 3.2-3 The combustor noise power level has been found to correlate with the following parameter:

$$20 \log_{10} \left[\sqrt{\dot{W}} \, (T_4 - T_3)(\rho_3/\rho_o) \right] \qquad (3\text{-}1)$$

where, $\dot{W}$ - air weight flow
T_4 - exit temperature
T_3 - inlet temperature
ρ_3 - inlet density
ρ_o - reference density

This parameter showed good agreement with the measured power level over a wide range of engine speeds.

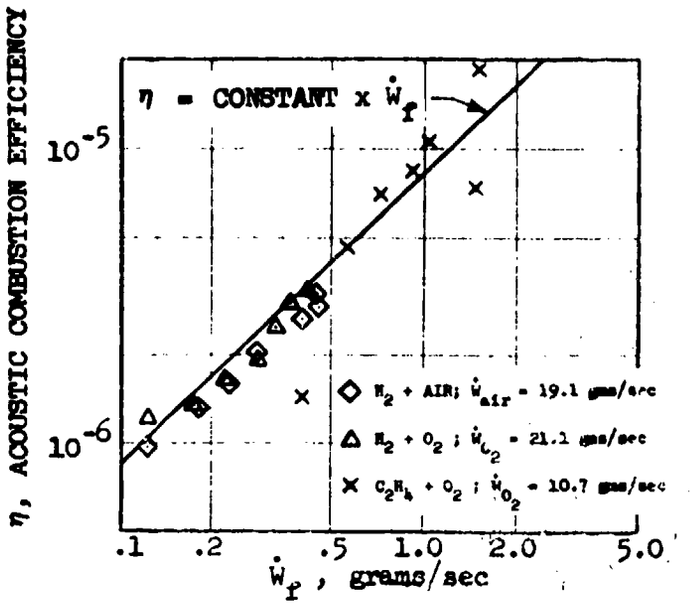

FIGURE 3.2-1 ACOUSTIC COMBUSTION EFFICIENCY vs. FUEL MASS FLOW RATE FOR NON PRE-MIXED CO-FLOWING FLAMES

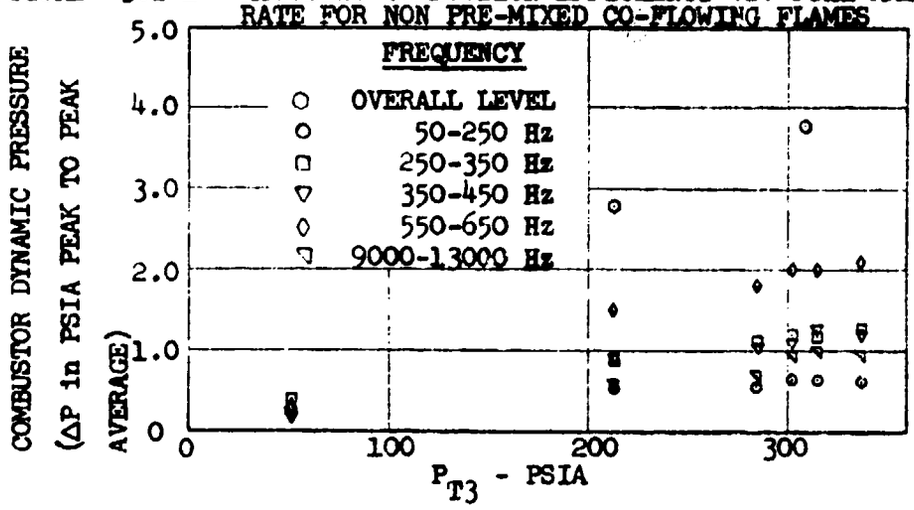

FIGURE 3.2-2 TF39 COMBUSTOR DYNAMIC PRESSURES

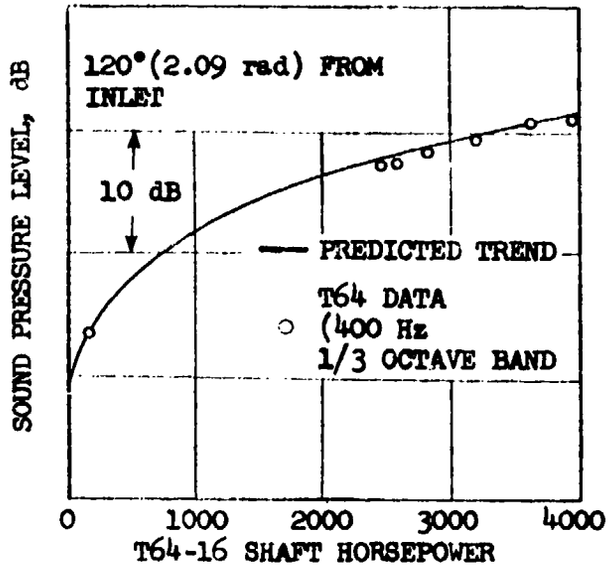

FIGURE 3.2-3 COMBUSTION NOISE - T64-16 ENGINE

Data from many different engines were examined for combustor, jet and fan noise. Three turbojet, two turboshaft and two turbofan engines had what is believed to be combustor noise in their spectra. These low frequency levels cannot be attributed to either jet or fan noise. Engine overall power levels were calculated by fitting the T64 engine spectrum to each of the engine power level spectra. The T64 spectrum shape was chosen because it closely agrees with the combustor component data shapes. The overall power level is 6.8 dB above the peak 1/3 octave band power level for this spectrum, and the combustor overall power level therefore was determined by adding 6.8 to the maximum low frequency (≤1000 Hz) 1/3 octave band power spectrum peak for each engine. Data from the seven engines are shown correlated in Figure 3.2-4. The power levels fall into three classes. For the same prediction parameters the turbojets had the highest combustor noise levels; the turbofans had the lowest levels; and the turboshaft engines made up a class in between the two. This indicates that different constants are necessary for the prediction depending on the engine type. The overall power level is defined as:

$$OAPWL = 20 \log_{10} \left[\sqrt{\dot{w}} \, (T_4 - T_3)(\rho_3/\rho_o) \right] + K \qquad (3\text{-}2)$$

where the constant K is,

K = 64 turbojet
K = 56 turboshaft
K = 48 turbofan

3.3 SPECTRUM SHAPE

Data from turbojet, turboshaft and turbofan engines were compared in the low frequency range. The spectra were corrected for ground effects and were found to have similar shapes (Figure 3.3-1). The turboshaft engine spectra are believed to be due almost entirely to combustor noise because the jet noise associated with the low exhaust velocities is not a factor. The spectra fall within an envelope which is defined by the SAE flight spectrum for jet noise. This envelope was found to fit the data best when peaked at 400 Hz plus or minus a 1/3 octave band.

The normalized spectrum shapes on a 1/3 octave band basis for turbojet and turbofan low speeds can be seen in Figure 3.3-2. Typical spectra fall under the same spectrum envelope peaked at 400 Hz as the turboshaft data. The peak frequency shown at 400 Hz could be plus or minus a 1/3 octave band due to the broad peak.

The spectra obtained from the combustor component tests were not as broad as the SAE jet noise envelope. However, the T64 spectrum closely approximates the spectrum from combustor component tests, and it is believed to be an accurate representation of the combustor noise spectrum. The broader spectra

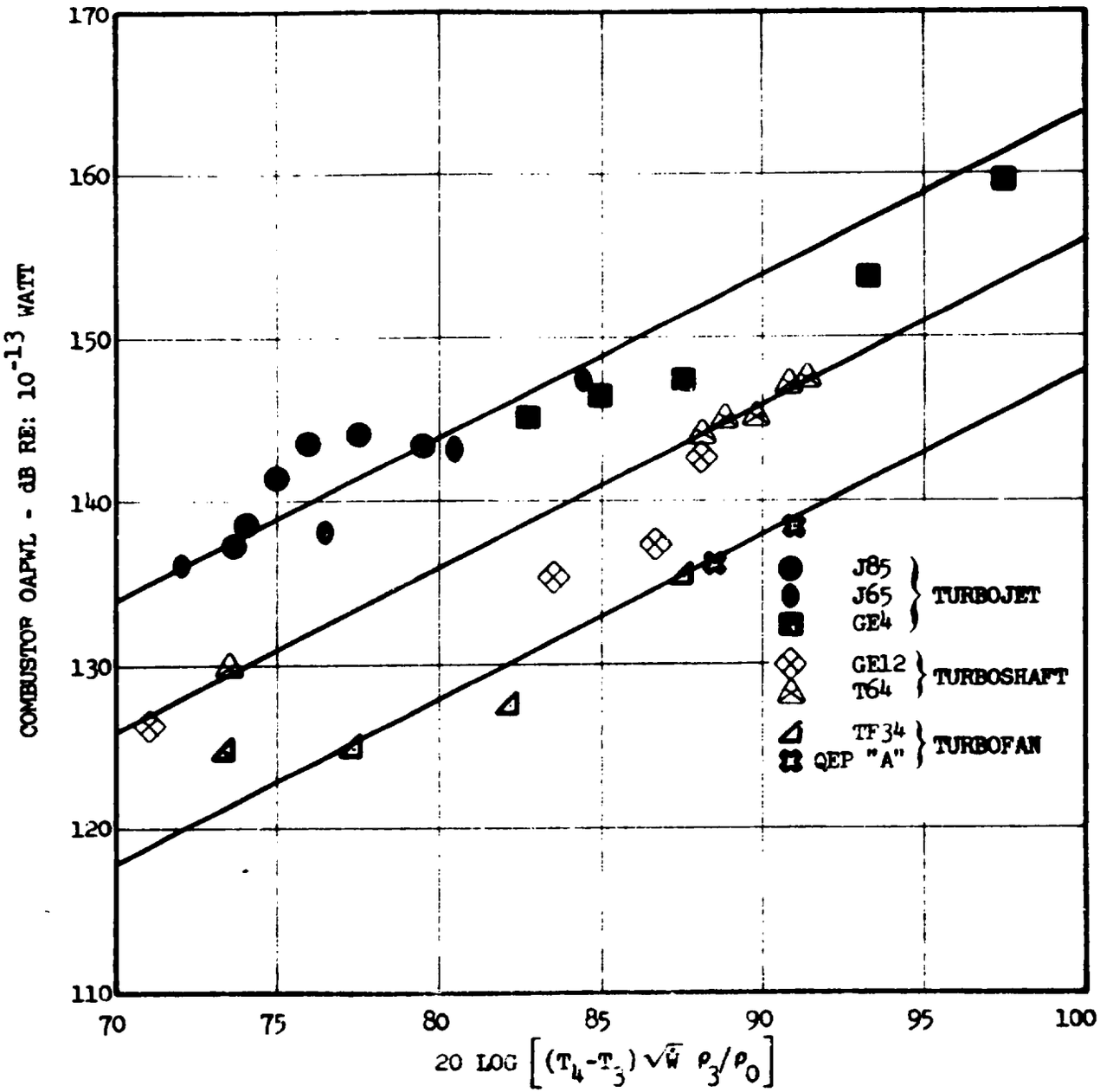

FIGURE 3.2-4 POWER LEVEL CORRELATION

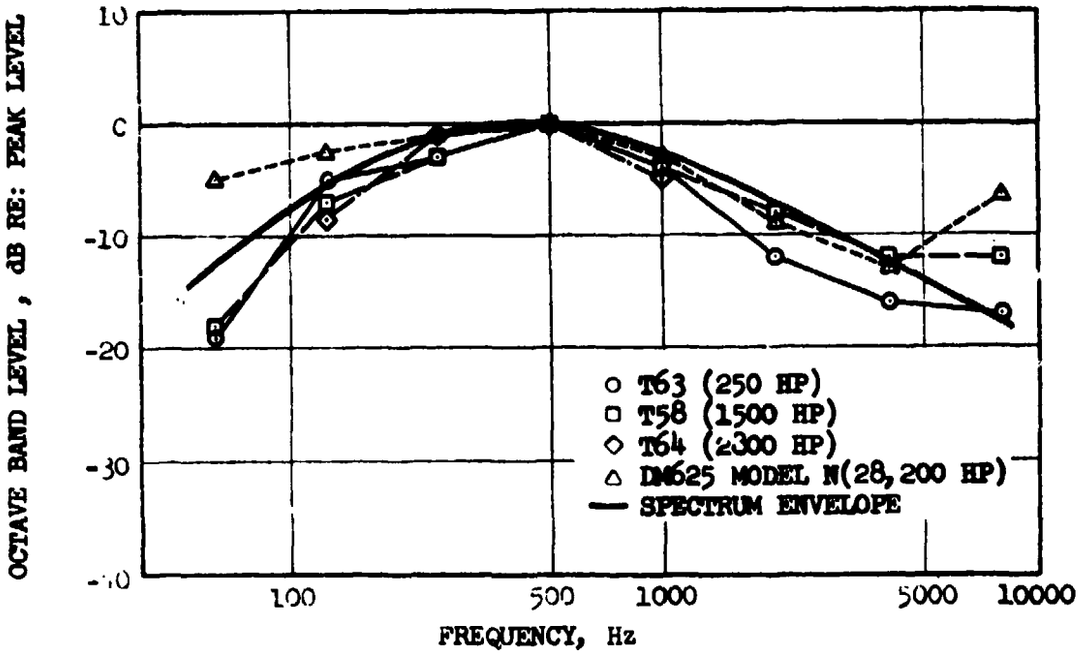

FIGURE 3.3-1 COMBUSTOR NOISE SPECTRA FOR TURBOSHAFT ENGINES

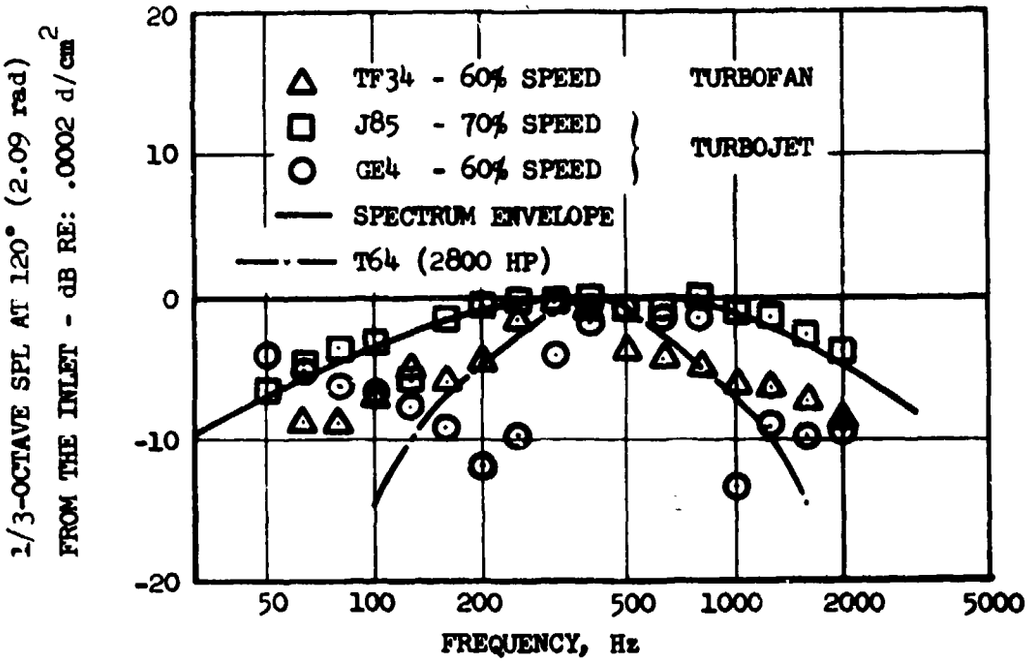

FIGURE 3.3-2 COMBUSTOR NOISE SPECTRA FOR TURBOFAN AND TURBOJET ENGINES

obtained from the other engine data are believed to be a consequence of flow noise in these engines. Use of the spectrum envelope shown in Figure 3.3-2 (solid line) to define the predicted power level spectrum will give a more conservative prediction than using the T64.

3.4 DIRECTIVITY

Data were examined from four engines, TF34, T64, J85, and GE4, identified as having combustor noise present at the lower power settings. The combustor noise radiation directivity pattern is shown in Figure 3.4-1. An average line is drawn through the data where two 1/3 octave bands on either side of the center frequency were used to define the average value at each angle. The peak SPL occurs at 120° from the inlet. The peak directivity is 5 dB above the spaced-average level. This directivity pattern is similar to the one seen in the component tests in Volume II of this report. The component CF6 and an advanced technology combustor directivities plotted in the Figure also fall within a narrow scatter band.

3.5 ANALYSIS

Typical low power setting high bypass turbofan engine spectra can be seen in Figures 3.5-1 and 3.5-2 for Quiet Engines "A" and "C". Figure 3.5-1 shows the fan alone spectrum (run at the NASA-Lewis Full-Scale Fan Acoustic Test Facility) as a dashed line, and the engine spectrum (run at the GE engine acoustic test facility) as a solid line, for both the frame treated and fully suppressed configurations. Figure 3.5-2 shows the same information for fan C except that the frame treated data are not available for the engine. The jet noise spectra are predicted by the method presented in Section 2, through the lowest frequencies of the data. In Figure 3.5-2, the fan and jet noise dominate the entire Engine "C" low frequency spectrum. However, in the Engine "A" spectrum there is a shaded region that cannot be identified as either jet or fan noise. This is suspected to be combustor noise because the noise level calculated by subtracting the fan and jet contribution in that frequency range agrees well with the correlation for turbofan engines shown on Figure 3.2-4. The combustor noise level for Engine "C" is not as easily identified in this frequency range due to the higher fan noise levels.

The overall power levels used in Figure 3.2-4 were computed as follows: 1) A typical TF34 spectrum is shown in Figure 3.5-3 as the circled data; 2) Correcting for ground effects by removal of the nulls and reinforcements results in the smooth spectrum shown by the solid line; and 3) The combustor noise spectrum from the T64 is fitted in (dashed line in the Figure) and the overall power level calculated.

3.6 SUMMARY - FLOW CHART

The prediction of combustor (core) noise is made by first calculating the overall power level from engine cycle data using Equation (3.2-1). The constant,

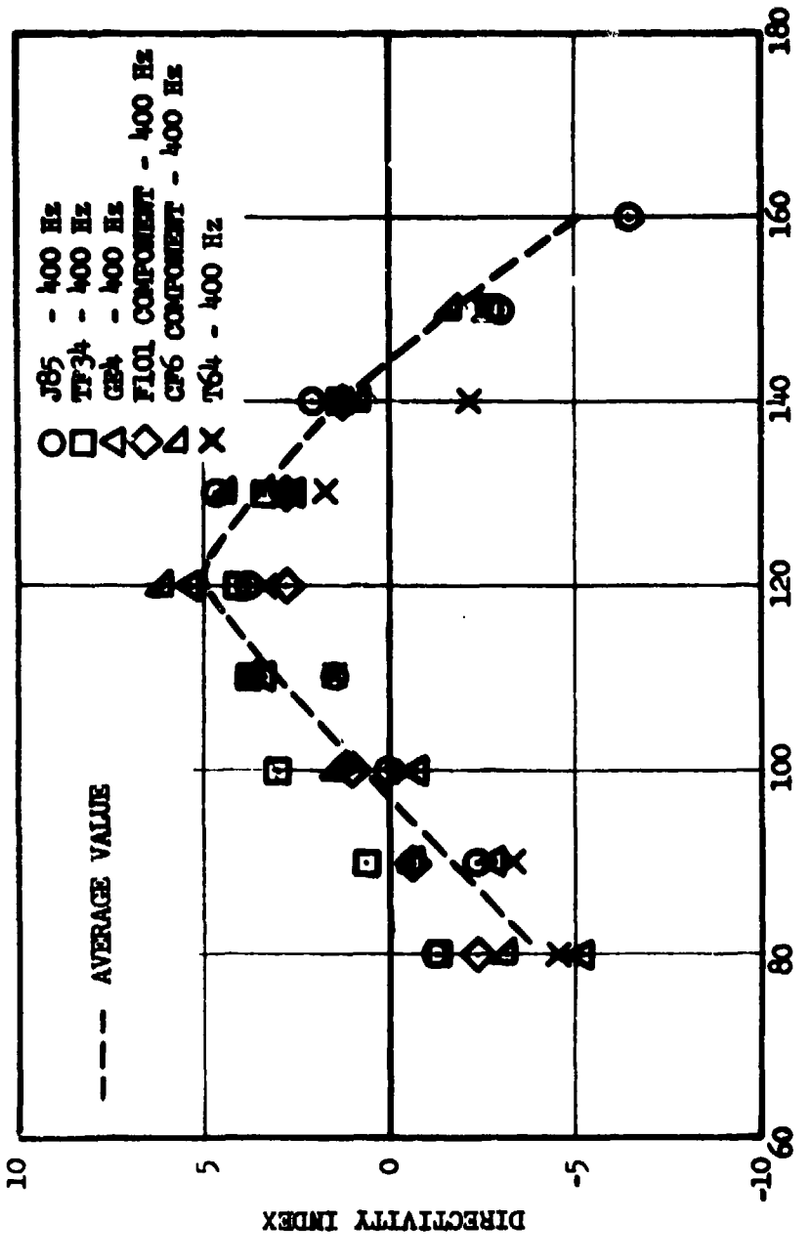

FIGURE 3.4-1 AVERAGE VALUE OF DIRECTIVITY

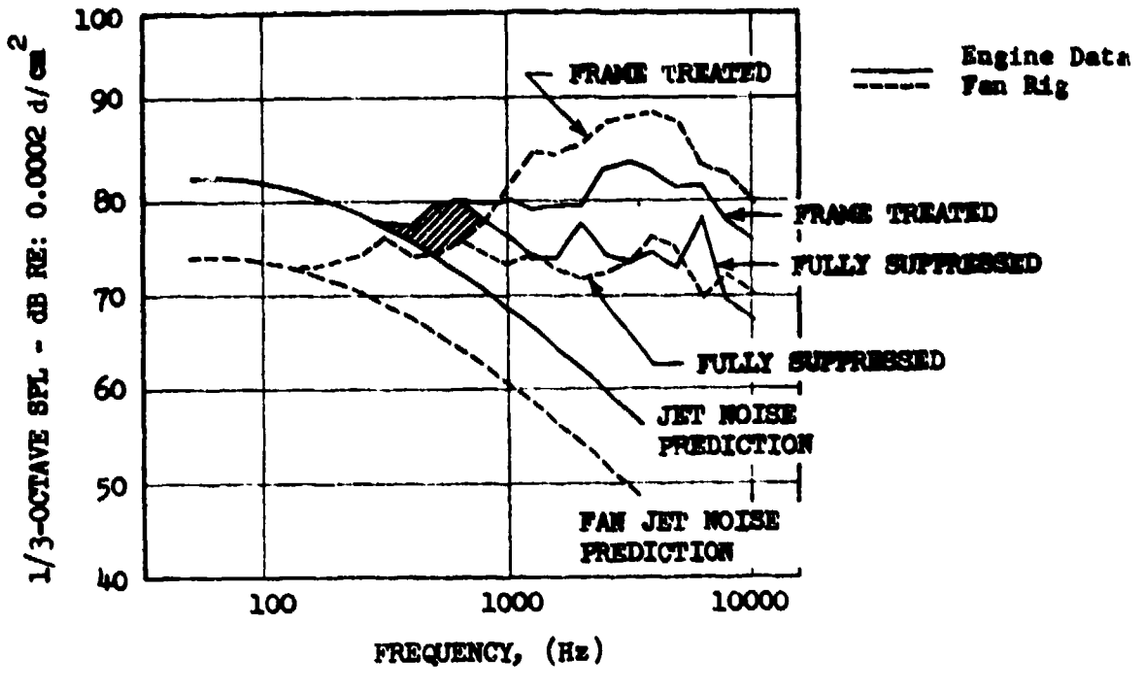

FIGURE 3.5-1 QEP "A" SPL SPECTRUMS AT 120° (2.09 rad) FROM THE INLET, 60% SPEED

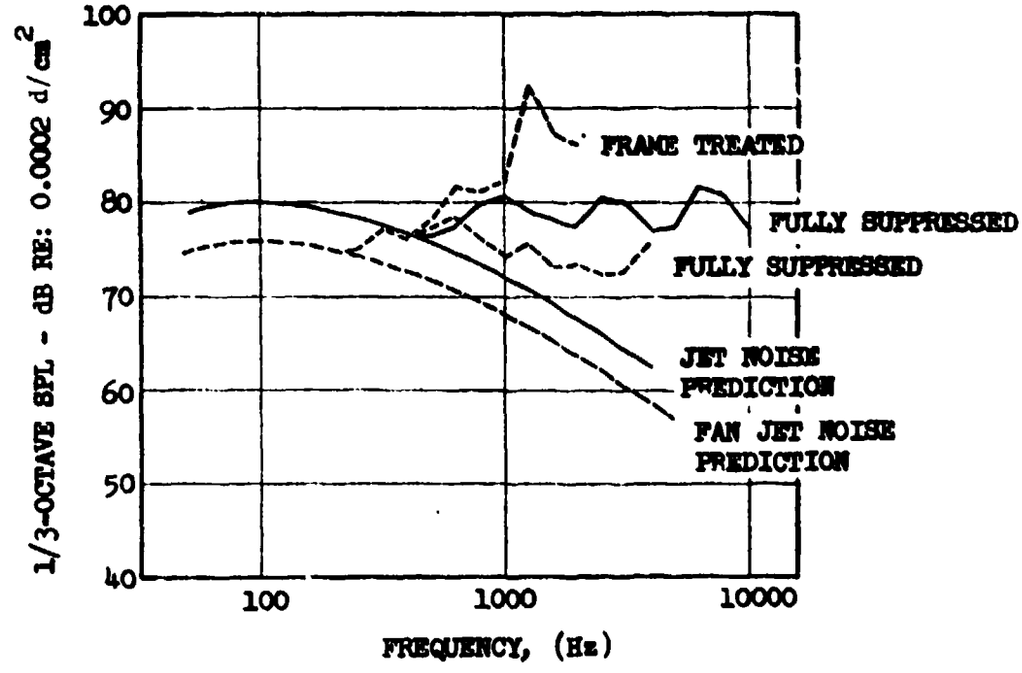

FIGURE 3.5-2 QEP "C" SPL SPECTRUMS AT 120° (2.09 rad) FROM THE INLET, 60% SPEED

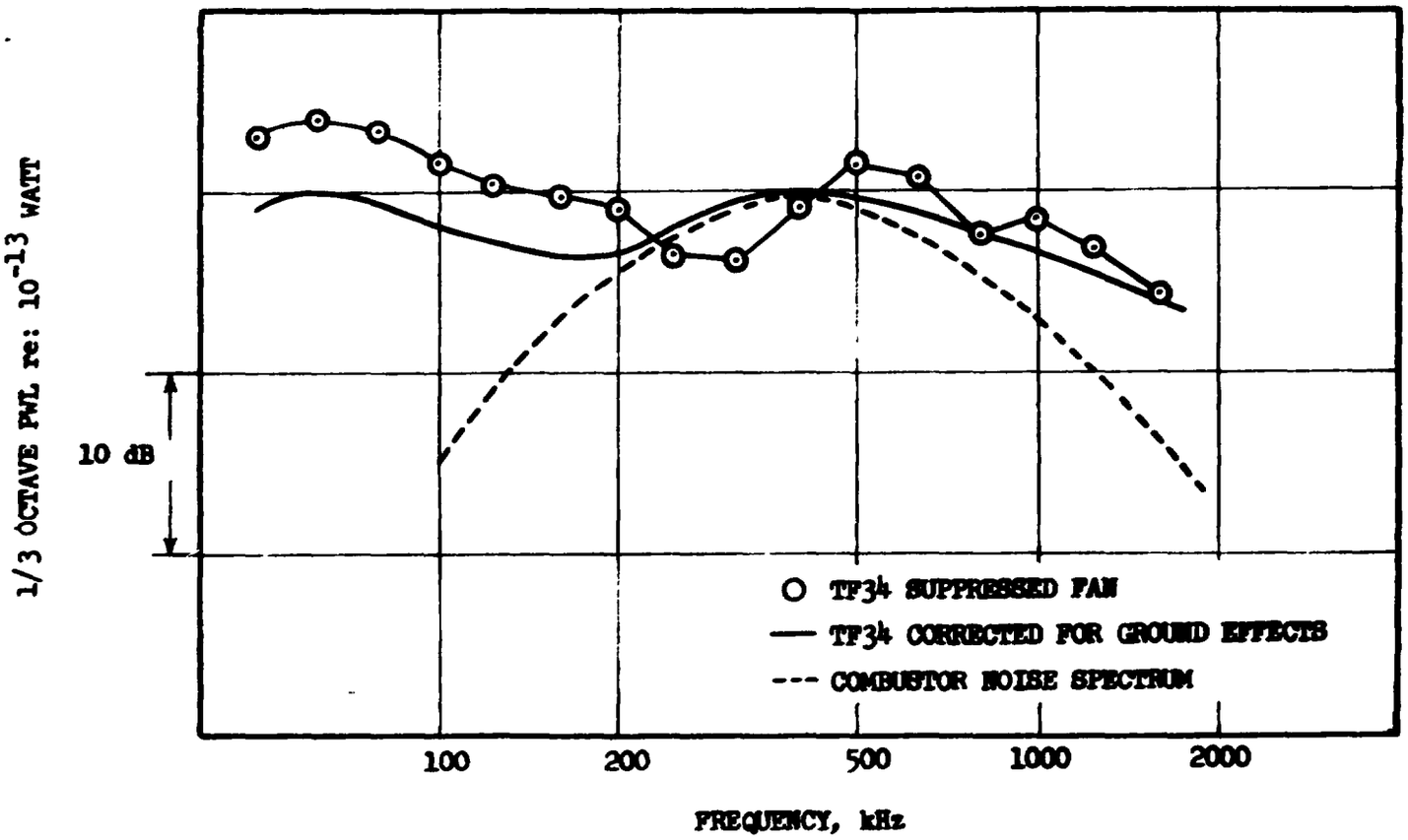

FIGURE 3.5-3 TYPICAL 1/3 OCTAVE BAND PWL SPECTRUM FOR THE TF34.

K, is selected based on the type of engine as discussed in Section 3.2. The power spectrum is then determined by superimposing the T64 spectrum. Here the peak frequency is placed at 400 Hz and the power level for this 1/3 octave band obtained by subtracting 6.8 dB from the OAPWL (a more conservative estimate will result if the spectrum envelope shown in Figure 3.3-2 is used instead of the T-64, with the same peak frequency of 400 Hz and the same peak PWL as above). From the 1/3 octave band power levels, a space-averaged sound pressure level is calculated for any arc of interest. The average value of directivity index (Figure 3.4-1) is then added to the space-averaged sound pressure level in order to arrive at a calculated value for the farfield sound pressure level. These levels must then be adjusted for air attenuation and ground effects for the given arc radius to arrive at the corrected farfield sound pressure levels.

A flow chart for implementing this prediction procedure is provided in Figure 3.6-1.

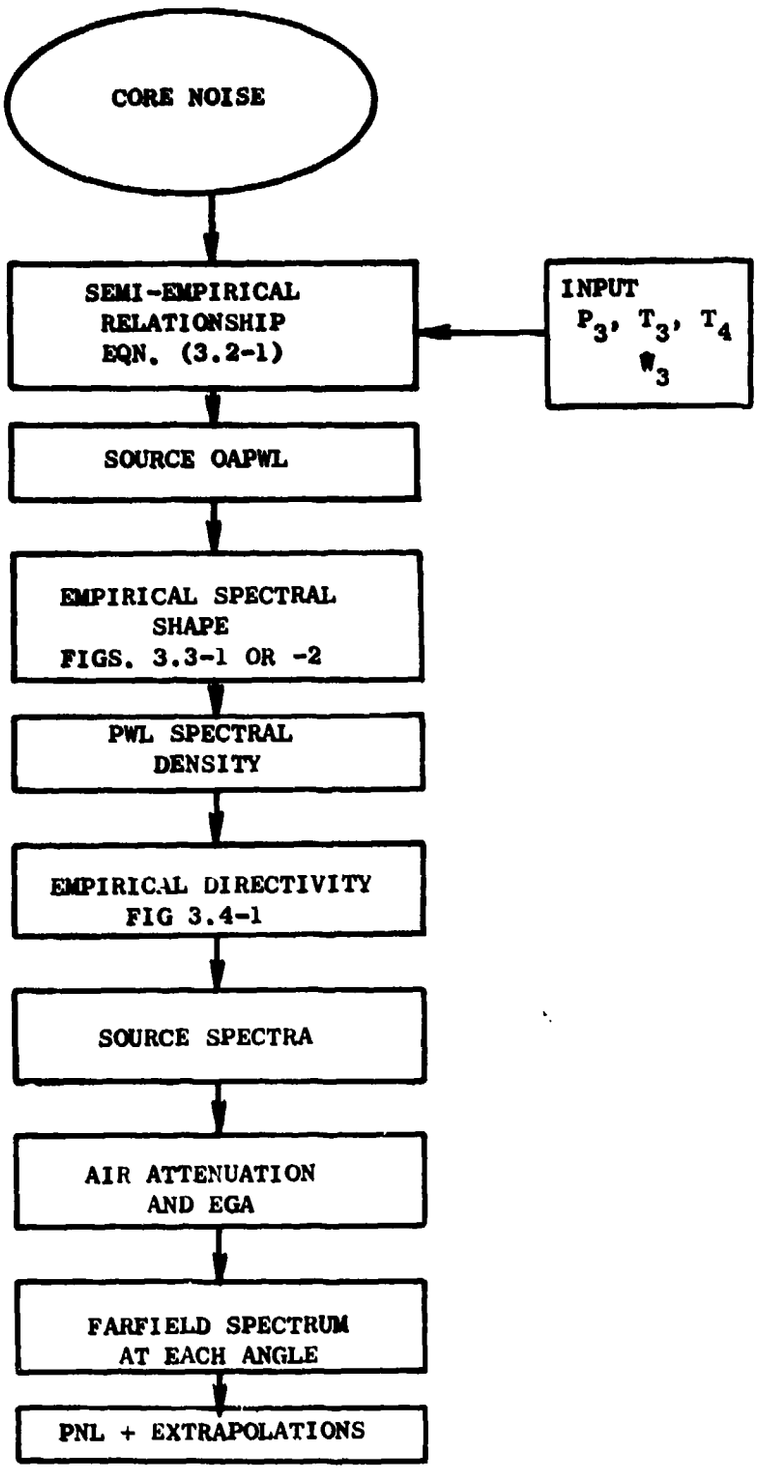

FIGURE 3.6-1 FLOW CHART FORCORE NOISE PREDICTION.

References

3.2-1 Knott, P.R.; "Noise Generated by Turbulent Non-Premixed Flames," AIAA paper No. 71-732.

3.2-2 Motsinger, R.; "Prediction of Engine Combustor Noise and Correlation with T64 Engine Low Frequency Noise," General Electric Report No. R72AEG313.

SECTION 4.0

TURBINE NOISE

4.1 BACKGROUND

A reliable turbine noise prediction procedure is necessary for the new generation of high bypass ratio engines where turbine noise is as high as fan noise at low power settings. The turbine noise levels must be known with a reasonable accuracy in the design stage so that acoustic treatment may be incorporated in the core nozzle when necessary in order to meet noise standards. The individual noise contribution of each core engine component must be predictable if overall noise levels are to be reduced on existing engines. A prediction method capable of assessing the effect of the design variables (solidity, blade and vane numbers, blade row spacing, and the work split between the stages) on the turbine noise generation would be valuable when designing a new turbine or when modifying the design of an existing one.

A single prediction method cannot meet all the above requirements. The need exists for a prediction method which can be exercised with gross overall parameters such as are available at the engine design stage. The need also exists for a method to predict the effect of internal configuration variations. The above requirements led to the development of three prediction methods:

(A) A Preliminary Design Method based on turbine parameters which are known early in the design stage. The prediction yields the PNL at maximum angle.

(B) A Comprehensive Method which uses the most pertinent noise generation parameters and is convenient to utilize. The output provides the complete high frequency turbine noise spectrum.

(C) A method which allows evaluation of the effects of aeromechanical configuration variations on the noise generation.

The analytical prediction technique described in Section 4.4 of Volume II for discrete frequency noise serves this requirement. The complexity of the noise generation mechanisms requires the first two correlations to be semiempirical.

Smith and Bushell (Reference 4.1-1) investigated turbine noise from two low bypass turbofan engines and the noise generated by a cold flow air turbine rig run as a single-stage and then as a two-stage machine. They developed a first approximation to a turbine noise prediction method based on these data. Separate correlations were derived for the broadband ("vortex") and discrete frequency components. Directivities for the noise from the engine tests were also shown. The correlations were based on earlier compressor noise correlations (Reference 4.1-2). Noise was assumed to be due to fluctuating lift

forces on the blades resulting from interaction with viscous wakes and flow turbulence. These two interactions were hypothesized to be responsible for discrete frequency and broadband noise generation, respectively. The fluctuating lift results in dipole noise radiation and therefore (from Lighthill's theory of aerodynamic sound) the acoustic power level (PWL) would theoretically display a sixth power dependence on the relative velocity (V_{rel}). If the PWL is normalized by the mass flow (size correction), the dependence drops to V^5_{rel}. Other parameters considered important were the fluid density, turbulence intensity, blade incidence, blade row solidity, axial spacing between blade rows, the convection velocity and the number of stages.

The desired end result was a correlation which included all of the above parameters, but the authors (Reference 4.1-2) made an initial correlation for broadband noise considering only the density effect and number of stages. The density correction was inserted to account for the different stream temperature between the model and engine tests. A blade row spacing correction was also used for the discrete frequency noise correlation. The broadband noise data were found to collapse reasonably well, and the correlating line could be expressed as:

$$SPL_{max} = 28.8 \log_{10} (V_{rel})_{max} + 10 \log_{10} \dot{W} + 30 \log_{10} \frac{1116}{C} + K \quad (4.1\text{-}1)$$

where SPL_{max} = SPL at the maximum angle (100° S.L.) for the band containing the BPF, dB re 0.0002 d/cm^2.

$(V_{rel})_{max}$ = maximum relative velocity at inlet to the final stage rotor, ft/sec.

$\dot{W}$ = weight flow, lb/sec.

C = mean acoustic velocity, ft/sec.

K = constant, and includes the effect of number of stages, i.e., $10 \log_{10} N$.

N = number of stages.

The engine directivity was shown as a function of the speed. A spectrum shape was provided with the noise peaking at the BPF. The spectrum shape was assumed to be the same for all angles.

The correlating efforts for the discrete frequency noise were less encouraging. The tone peak SPL was normalized for the weight flow and the density as in the case of the broadband noise, but the spacing correction was doubled. This normalized SPL was plotted against 10 log (V_{rel}). The results are shown in Figure 4.1-1. There is considerable data scatter for the model results, plus the engine data lie along the lower fringe of the model points. Vague trends can be discerned which show large differences between the model and engine data. The normalized tone SPL appears to vary as 10 log (V_{rel}) for the engines, as opposed to 30 log (V_{rel}) for the model.

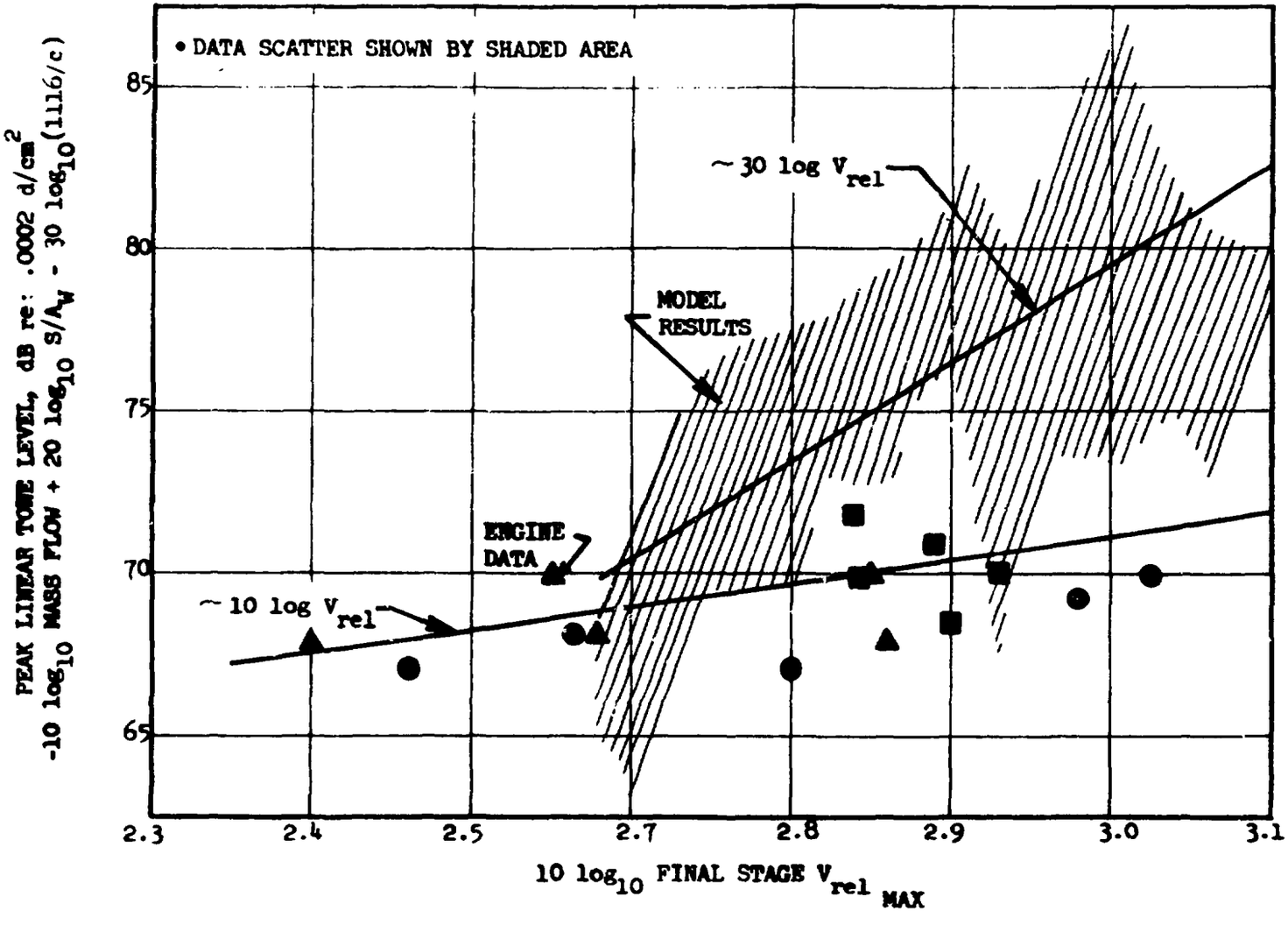

FIGURE 4.1-1 SMITH AND BUSHELL CORRELATION FOR TURBINE TONES (Ref.4.1-1).

The authors (Reference 4.1-2) caution that more work is necessary to resolve the differences between engine and component model results, and that this "... must be preceded by a fuller understanding of the basic mechanisms of (noise) generation and radiation."

Dunn and Peart (Reference 4.1-3) recently updated the Smith and Bushell work with data from several turbofan engines, but data scatter problems were still encountered.

The two papers discussed above (References 4.1-2 and 4.1-3) provide valuable insight into the extent of the turbine noise generation problem, and demonstrate that the relative velocity is an important parameter. The correlations presented are inadequate for present purposes, however, for the reasons outlined below.

The studies were based on the assumption that the relative velocity at the inlet to the rotor fully determined the noise generated, and that the other parameters (solidity, turbulence, etc.) merely serve to normalize the results. It is believed that the work extraction plays an essential role in the noise generation in addition to the relative velocity as assumed in the above studies. Consideration of the viscous wake interaction mechanism shows that the noise generated arises from fluctuations in the lift on the downstream blade row. While the relative velocity provides a measure of the wake velocity defect which is the cause of the fluctuating lift, the work extraction (or enthalpy drop) determines the circulation on the blades. Prediction methods must therefore include both a velocity and a work term.

The analysis of Section 4.4, Volume II, includes consideration of both effects and is shown to correctly predict the noise generation by various turbines over a range of operating conditions. The velocity plus work approach is further validated by the correlation derived in Section 4.3, Volume II, for the discrete frequency noise from the last stage of a three-stage turbine rig. The correlation is shown here in Figure 4.1-2 along with available data for the last stages of Quiet Engines "A" and "C". The data collapse is achieved by using the stage ideal work extraction, nondimensionalized by the inlet enthalpy ($\Delta T/T$), as the correlating parameter and the blade tip speed as a normalizer for the acoustic power level. A size correction is provided through use of a 10 log (exit area) factor.

$$\text{Here,} \qquad \left[\frac{\Delta T}{T}\right] = 1 - \left[\frac{1}{P_R}\right]^{\frac{\gamma-1}{\gamma}} \qquad (4.1\text{-}2)$$

where P_R = total-to-static pressure ratio
and γ = ratio of specific heats

An adjustment for blade row spacing was made in the Smith and Bushel work through a 20 log (spacing/chord) term for the discrete frequency noise levels. Data provided by the turbine rig tests (Sections 4.2, 4.3 of Volume II), however, indicate the compensation should be 3 dB per doubling, that is, 10 log (spacing/chord).

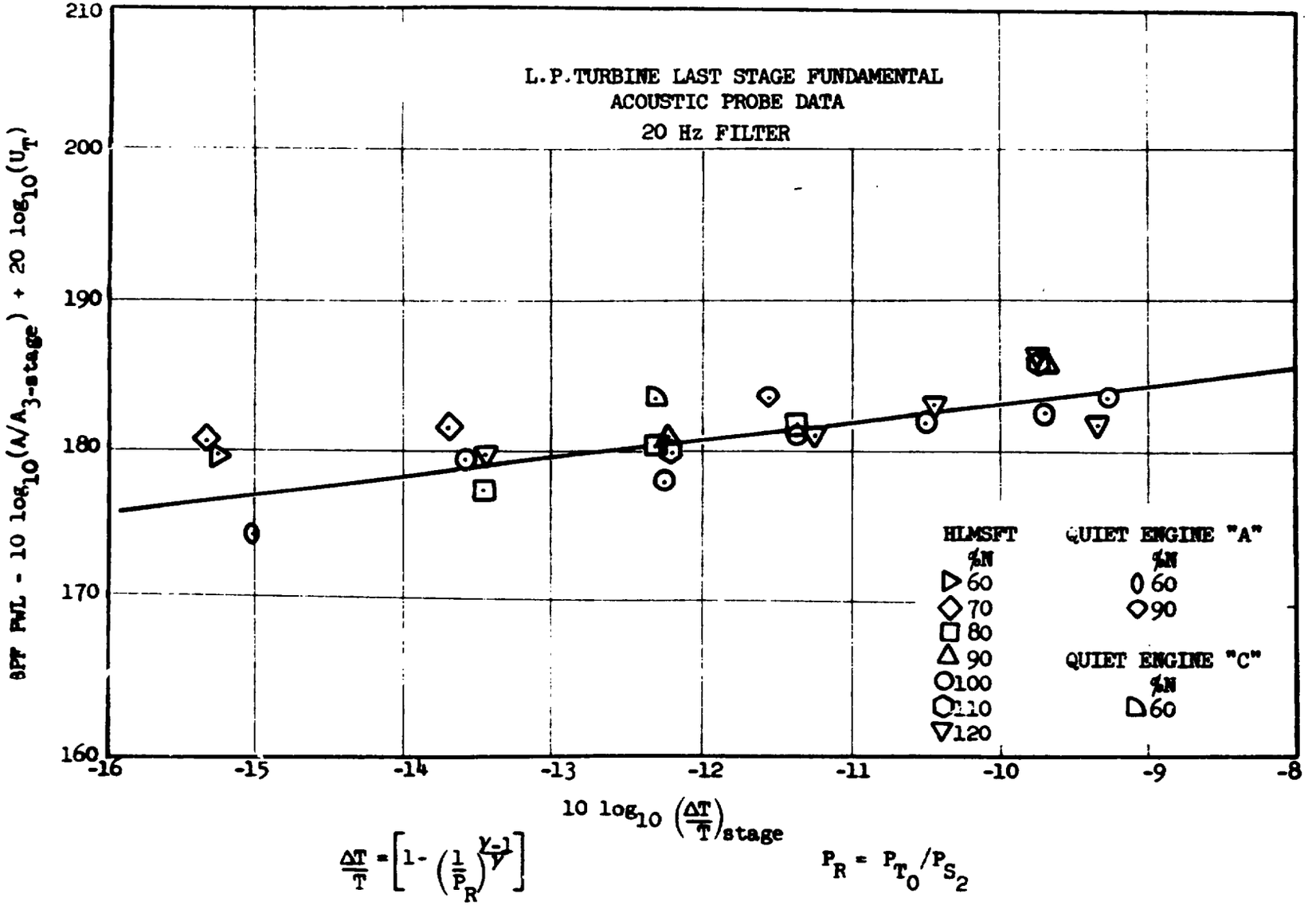

$$\frac{\Delta T}{T} = \left[1 - \left(\frac{1}{P_R}\right)^{\frac{\gamma-1}{\gamma}}\right] \qquad P_R = P_{T_0}/P_{S_2}$$

FIGURE 4.1-2 VARIATION OF NORMALIZED PWL WITH IDEAL WORK EXTRACTION FOR THE LAST STAGE FUNDAMENTAL.

The above authors (References 4.1-2 and 4.1-3) have also suggested adding 10 log (number of stages) to the noise levels to adjust for increased turbulence levels due to each extra stage in multistage turbines. Their suggestion is based on the observation that the data correlating lines for two, three and four-stage turbines fall on roughly parallel but separate lines which appear to be related by a 10 log N relationship (see Figure 4.1-3). The two-stage points are 10 to 15 dB higher than for the first stage of the rig run separately. This is attributed to the fact that in the single-stage configuration the flow supply to the rig was smooth and uninterrupted, while in the two-stage configuration the last stage receives a flow made turbulent by the upstream stage.

It is hypothesized that, once the flow has been "broken up" either by an upstream stage or by the combustion process or high pressure turbine in an engine, the turbulence attains a "saturation" level and no further correction is necessary for number of stages. This follows naturally from the assumption that the overall work extraction is the prime determinant of the noise generated. Increasing the number of stages at constant turbine work should (and has been been found to) decrease the noise generation because of the lower work load imposed on each stage. The decrease in levels is such that it cannot be compensated for by relative velocity considerations alone.

Turbine aerodynamic considerations show that if turbine work controls the noise level, the use of the relative velocity on the abscissa results in the delineation of the acoustic data from the two, three and four-stage machines.

The prediction method significantly underpredicts the measured engine levels, as can be seen for Quiet Engine "C" in Figures 4.1-4 and 4.1-5. Figure 4.1-4 provides a spectral comparison at 200 ft (60.1 m) sideline and 120° (2.1 rad) angle at approach power setting. The discrepancy between predicted and measured levels is about 10 dB. Figure 4.1-5 shows that a similar problem exists for the peak OASPL over the entire operating range.

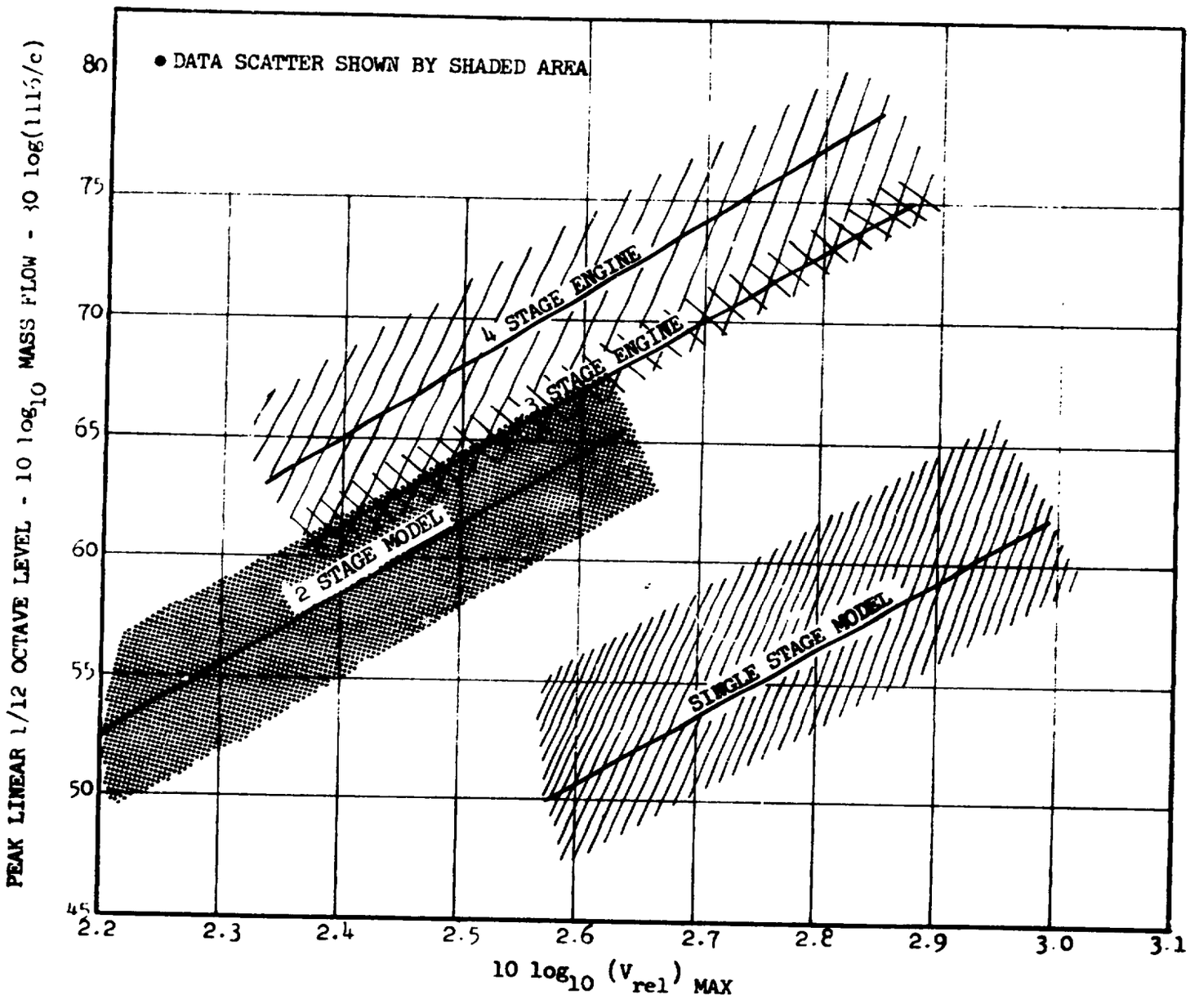

FIGURE 4.1-3 SMITH AND BUSHELL BROADBAND NOISE CORRELATION (Ref. 4.1-1).

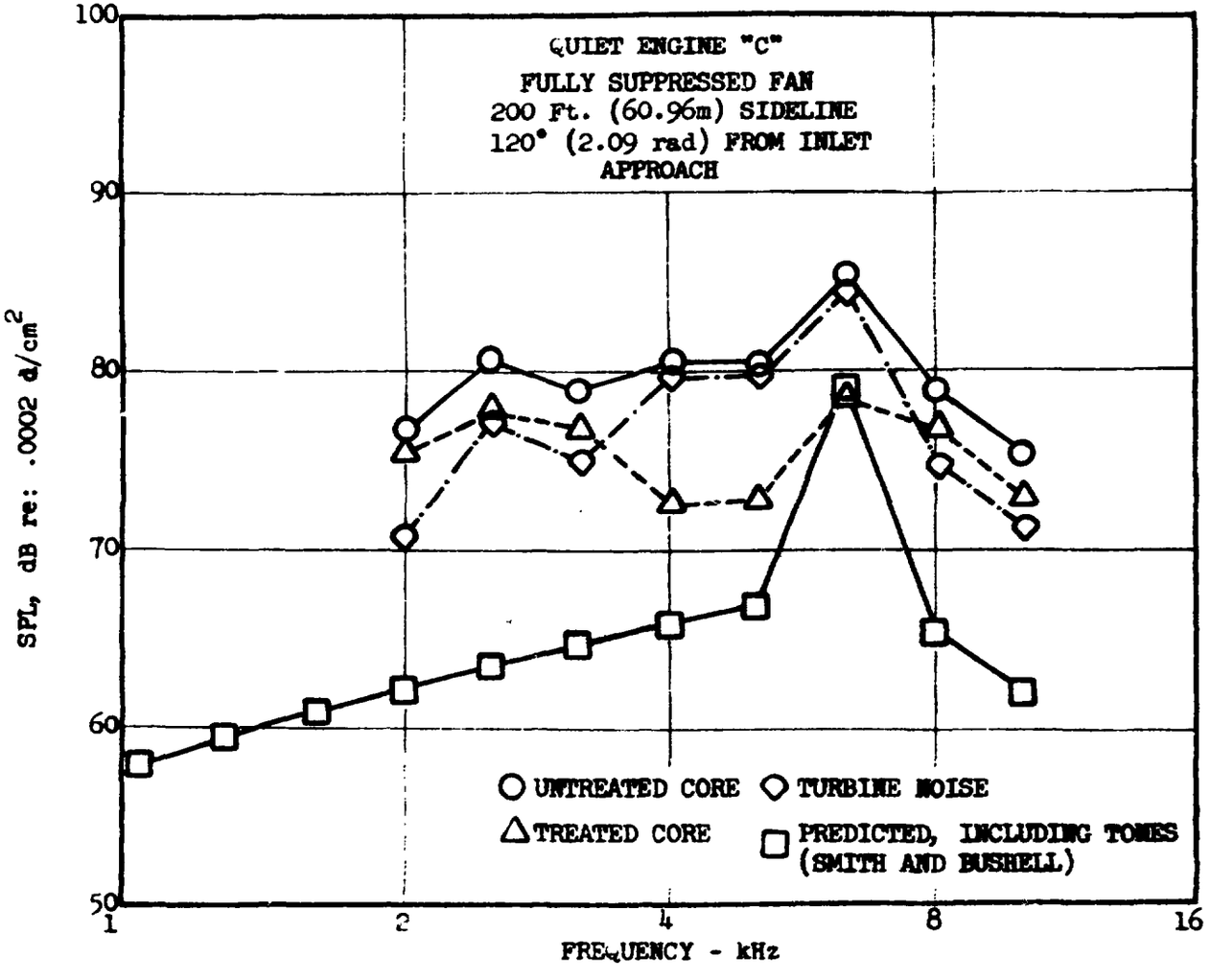

FIGURE 4.1-4 QUIET ENGINE "C" TURBINE NOISE SPECTRUM, COMPARISON WITH SMITH AND BUSHELL PREDICTION.

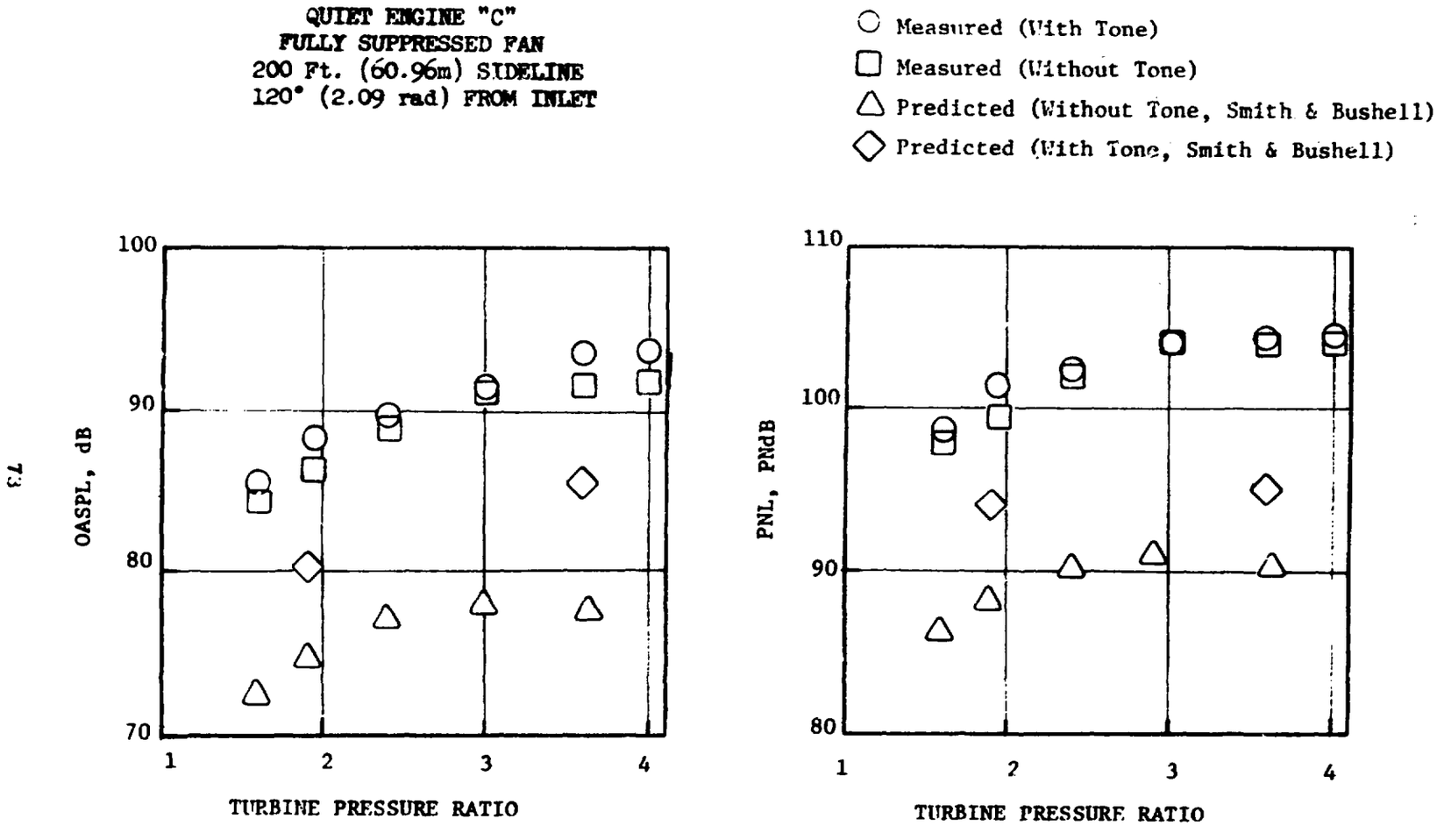

FIGURE 4.1-5 QUIET ENGINE "C" TURBINE NOISE OASPL AND PNL AS A FUNCTION OF TURBINE PRESSURE RATIO, COMPARISON WITH SMITH AND BUSHELL PREDICTION.

4.2 PREDICTION METHODS FOR TURBINE NOISE LEVELS

4.2.1 Analytical Prediction of Discrete Frequency Noise

The analytical method of finding turbine tone PWL described in Section 4.4 of Volume II is suitable as Prediction Method (C). The model computes the noise generated by viscous wakes from upstream blading impinging on a downstream blade row.

A semiempirical viscous wake model was developed for turbine blading in Section 4.4 of Volume II:

$$Y = 0.4\ell \left[\xi_p \, (t/\ell) \, (x/\ell + 0.2)\right]^{1/2} \qquad (4.2.1\text{-}1)$$

$$u_c/V = 0.615 \left[\xi_p \, (x/\ell)\right]^{1/2} \qquad (4.2.1\text{-}2)$$

$$\frac{u}{u_c} = \cos^2 \frac{\pi}{2} \frac{y}{Y} \qquad (4.2.1\text{-}3)$$

where: Y = wake half width

y = normal coordinate

x = axial distance downstream of the chord midpoint

ℓ = blade chord

t = pitch of blades in the cascade - or blade row

ξ_p = pressure loss coefficient

u = velocity defect in the wake

u_c = velocity defect at wake centerline

V = free stream velocity

The velocity defect in the wake results in the following unsteady circulation (Γ) being generated at the downstream blades:

$$|\Gamma| = c_2 \, V_2 \sum_{m=1}^{\infty} |G_m| \; |J_m(m\,\omega_2)| \; |S(m\,\omega_2)| \qquad (4.2.1\text{-}4)$$

where

$$J(m\,\omega_2) = \left|J_o^{\,2}\,(m\,\omega_2) + J_1^{\,2}\,(m\,\omega_2)\right|^{1/2}$$

$$S(m\omega_2) = \left|\{im\omega_2[K_o(im\omega_2) + K_1(im\omega_2]\}^{-1}\right|$$

J_0, J_1 are Bessel functions of zeroeth and first order and K_0, K_1 modified Bessell functions.

Referring to Figure 4.2.1-1, the reduced frequency ω_2 is given by:

$$\omega_2 = \pi \frac{c_2}{c_1} \frac{u}{V_2} \sigma_1$$

where c = semichord, $\ell/2$

σ = solidity = $2c/t = \ell/t$

the subscripts 1 and 2 refer to conditions at the upstream and downstream rows. G_m is the coefficient of the unsteady upwash and is given by:

$$G_m = 1.391\ \pi \frac{V_1}{V_2} \frac{\xi_{p1} \sin\beta}{(x^1/c_1 + 0.2)\cos\alpha_1} \left(\frac{x^1}{c_1}\right)^{1/2} \exp\left[-\pi m^2 \left(\frac{0.233}{\cos\alpha_1}\right)^2 \left(\xi_{p1}\, \sigma_1 \frac{x^1}{c_1}\right)\right]$$

where

$$\frac{x^1}{c_1} = \frac{c_2}{c_1}\left[\frac{b}{c_2 \cos\alpha_1} + \frac{x_2}{c_2}\frac{V_1}{V_2}\right] - 0.6 \qquad (4.2.1\text{-}5)$$

α_1 = stagger angle of blades

β = angle between stator and rotor blades

The center of pressure may normally be taken as the 1/4 chord point without incurring much error. Hence, $\chi_2/C_2 = 1/2$ in Equation (4.2.1-5).

This unsteady disturbance, consisting of rotating line sources, is then coupled into the duct acoustic modes (See Reference 5.2.1-1 for details):

$$p = \sum_{n=-\infty}^{\infty} \sum_{m=1}^{\infty} \rho c^2 n\omega A_{mn}\, e^{in(\theta-\omega t)}\, e^{iK_{nm}z}\, R_{nm}(\lambda_{nm} r) \qquad (4.2.1\text{-}6)$$

where

$$A_{nm} = \frac{M}{4\pi n R_o c \eta_{nm}} \int_h^1 r\Gamma(r) R_{nm}(\lambda_{nm} r)\, dr$$

and

n = number of circumferential modes (spinning lobes)
m = number of radial modes
M = number of rotating line sources

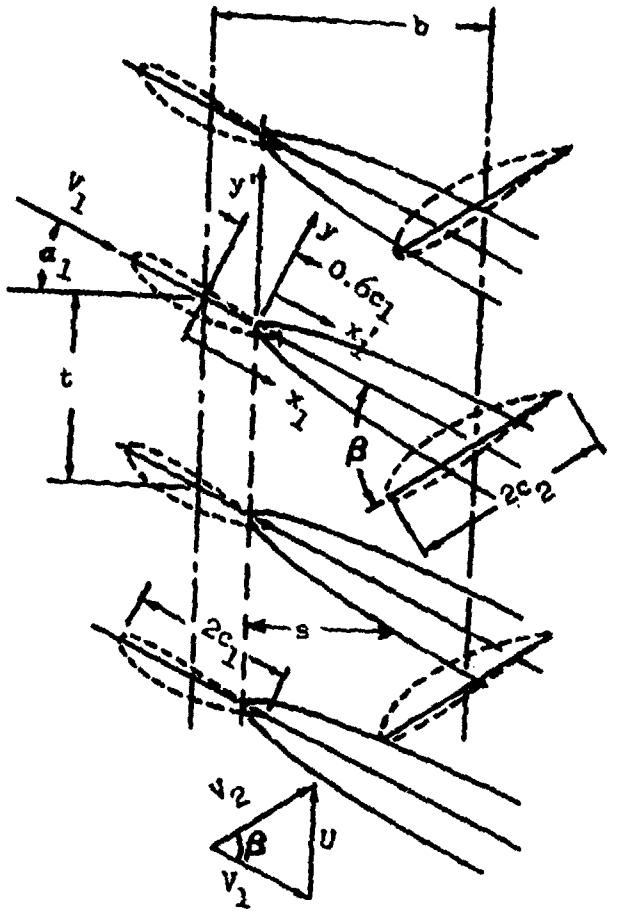

FIGURE 4.2 1-1 SCHEMATIC OF VISCOUS WAKE INTERACTION.

p = pressure perturbation
ρ = density
c = acoustic velocity

(r, θ, Z) = polar coordinate system

r and Z have been nondimensionalized using the tip radius, R.

h = nondimensionalized hub radius
$\Gamma(r)$ = circulation around the blade row

$$R_{nm}(\lambda_{nm}) = \{J_n(\lambda_{nm} r) - [J_n'(\lambda_{nm})/Y_n'(\lambda_{nm})]Y_n(\lambda_{nm} r)\}$$

Y_n are Bessel functions of the second kind and nth order

$(\ )'$ denotes a derivative with respect to the argument

λ_{nm} = eigenvalues satisfying the boundary conditions at the hub and tip

$$\eta_{nm} = \int_h^1 r R_{nm}^2(\lambda_{nm} r)dr \qquad (4.2.1\text{-}8)$$

$$= \frac{1}{2\lambda_{nm}^2}\left[(\lambda_{nm}^2 - n^2)R_{nm}^2(\lambda_{nm}) - (\lambda_{nm}^2 h^2 - n^2)R_{nm}^2(\lambda_{nm} h)\right]$$

The analysis includes the effect of the blade geometry and the turbine aerodynamics and provides a useful investigative tool for determination of the effect of various aerodynamic and mechanical configuration changes on the discrete frequency noise production. Further, by including the effects of incidence, Mach number and Reynolds number in the pressure loss coefficient, it is possible to predict the noise generation at off-design operating conditions.

This prediction method was exercised for several different low pressure turbines in Section 4.4 of Volume II, and good agreement was obtained with measured values.

A cut-off effect is implicit in this analysis as modes associated with imaginary wave-numbers will not propagate.

4.2.2 Correlations for Low Pressure Turbine Noise

Turbine noise was discernible for several turbofan engines. The cleanest acoustic data were obtained for the TF34 and Quiet Engine "C" in their fully suppressed fan configurations. Useable data from the CF6 were also available

for a limited number of low power settings. At higher power settings, fan and jet noise were found to overshadow turbine noise. The acoustic data from the fully suppressed configuration of Quiet Engine "A" could be used to qualitatively check the results derived, but was too contaminated by the high broadband noise floors (due to the fan and/or the jets) to provide reliable turbine noise estimates. The Engine "A" data could only be used with confidence in conjunction with the directional array (Reference 4.2.2-1). The directional array data were applied to determine a directivity for turbine discrete frequency noise (Section 4.3).

The turbine noise levels were extracted from the farfield data by comparison of two configurations which differed only in that one had a hardwall core and the other had acoustic treatment in the core nozzle designed to suppress the high frequency turbine noise. The core nozzle treatment as shown in Figure 4.2.2-1 for the TF34 and in Figure 4.2.2-2 for Quiet Engines "A" and "C". Representative spectra for the TF34 and Quiet Engine "C" are presented in Figures 4.2.2-3 and -4, respectively, for both hardwall and treated core nozzles. The turbine noise levels were determined by logarithmic subtraction of the two spectra. This procedure underestimates turbine noise levels when noise floors from other components dominate, as was true for Quiet Engine "A".

The ideal correlation would be in terms of the acoustic power level (PWL). The maximum angle (120° from inlet) sound pressure levels (SPL) are very convenient representations, however, since they are easily and accurately determined from farfield data, as contrasted to the PWL. A simple correction factor also provides the perceived noise level (PNL). If the directivity remains relatively unchanged, the maximum angle SPL's are as good as the PWL in any case, except for a constant.

Figure 4.2.2-5 shows a correlation derived using the turbine ideal work extraction normalized by the inlet enthalpy ($\Delta T/T$), as the correlating parameter. The peak angle overall sound pressure level (OASPL) has been normalized using 10 log (exit area) for the size and 20 log (tip speed), as indicated by the results of the three-stage low pressure turbine (HLMSFT) tests, Section 4.3 of Volume II. The correlating line may be expressed as:

$$\text{PEAK OASPL} = 40 \log_{10} \left(\frac{\Delta T}{T}\right)_{\text{turbine}} - 30 \log_{10} U_T + 10 \log_{10} A + 164 \qquad (4.2.2\text{-}1)$$

where PEAK OASPL = overall sound pressure level @ 120° and 200 ft (60.96 m) sideline, dB re 0.0002 d/cm^2 (corrected to standard day)

$$\left(\frac{\Delta T}{T}\right)_{\text{turbine}} = 1 - \left(\frac{1}{P_R}\right)^{\frac{\gamma-1}{\gamma}}$$

P_R = turbine total-to-static pressure ratio, P_{T_0}/P_{S_2}
U_T = blade tip speed of last stage, ft/sec
A = core nozzle exit area, ft^2
γ = ratio of specific heats $\sim$ 1.4

TF34 CORE TREATMENT

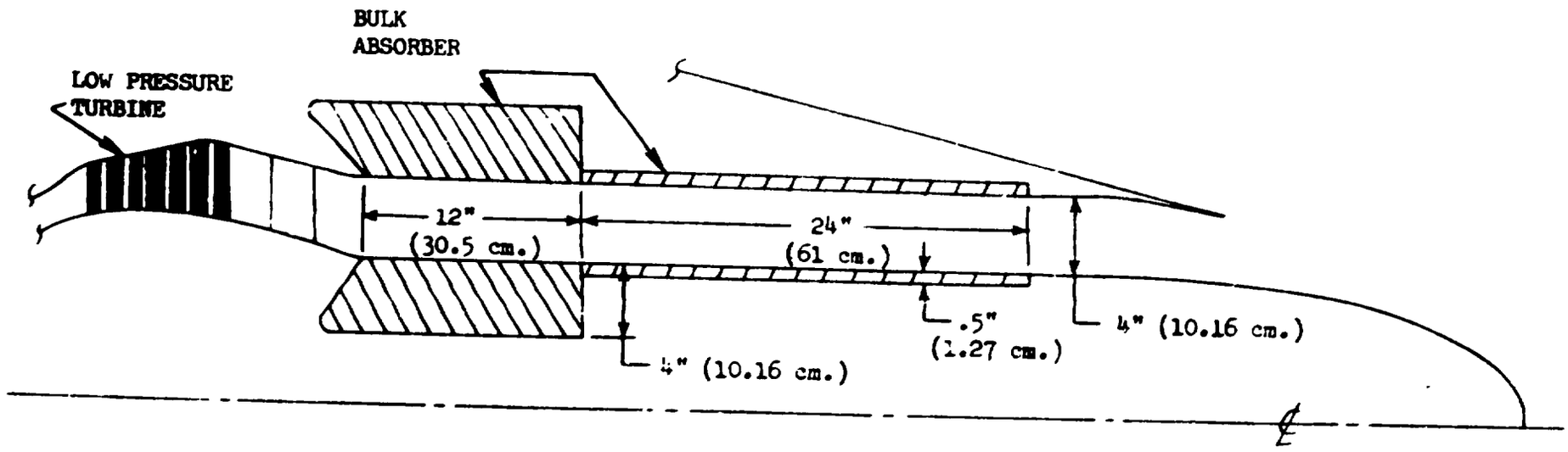

FIGURE 4.2.2-1 SUPPRESSED CORE CONFIGURATION FOR THE TF34.

QUIET ENGINE "A" ACOUSTICALLY TREATED EXHAUST NOZZLE
NOMINAL TREATED LENGTH = .711m (28")
AVERAGE DUCT HEIGHT = .241m (9.5")
APPROXIMATE LENGTH/HEIGHT = 3

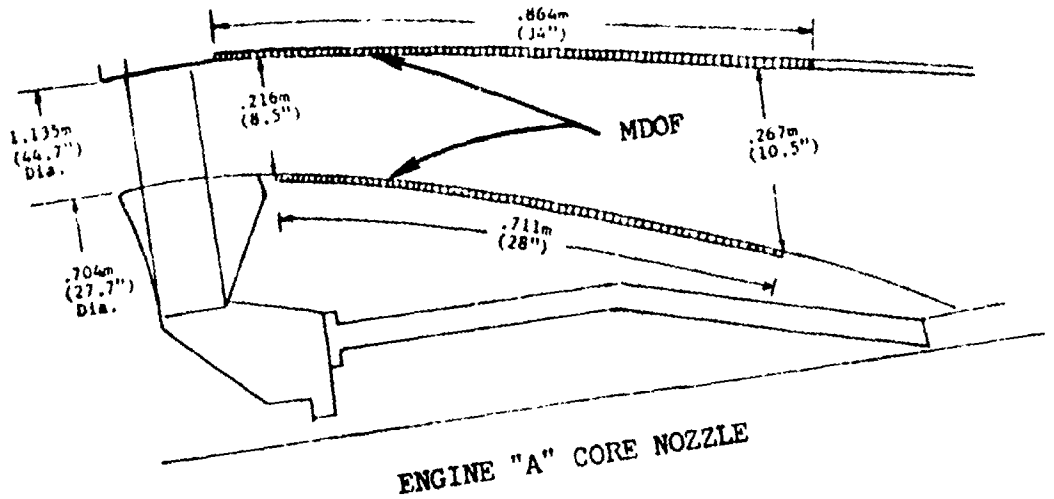

ENGINE "A" CORE NOZZLE

QUIET ENGINE "C" ACOUSTICALLY TREATED EXHAUST NOZZLE
NOMINAL TREATED LENGTH = .914m (36")
AVERAGE DUCT HEIGHT = .241m (9.5")
APPROXIMATE LENGTH/HEIGHT = 3.7

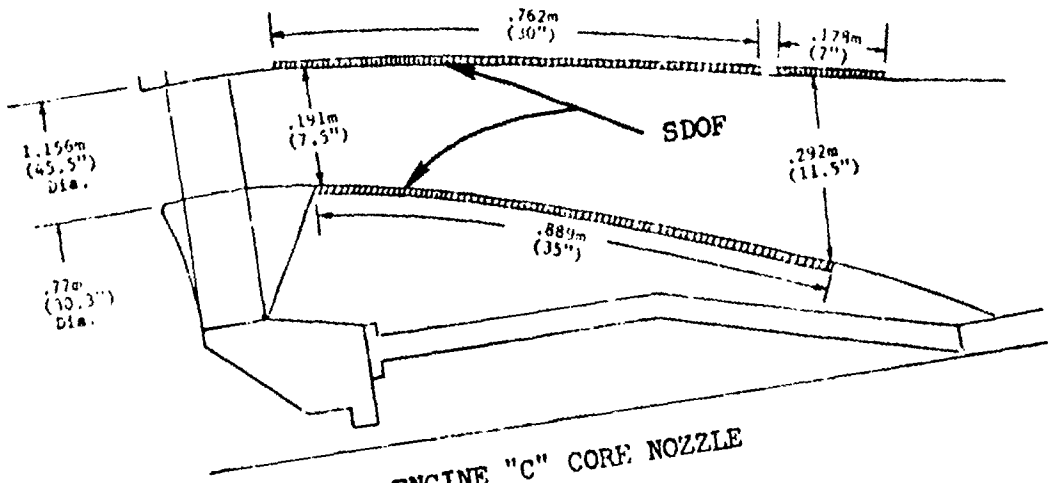

ENGINE "C" CORE NOZZLE

FIGURE 4.2.2-2 CORE TREATMENT FOR QUIET ENGINES "A" AND "C".

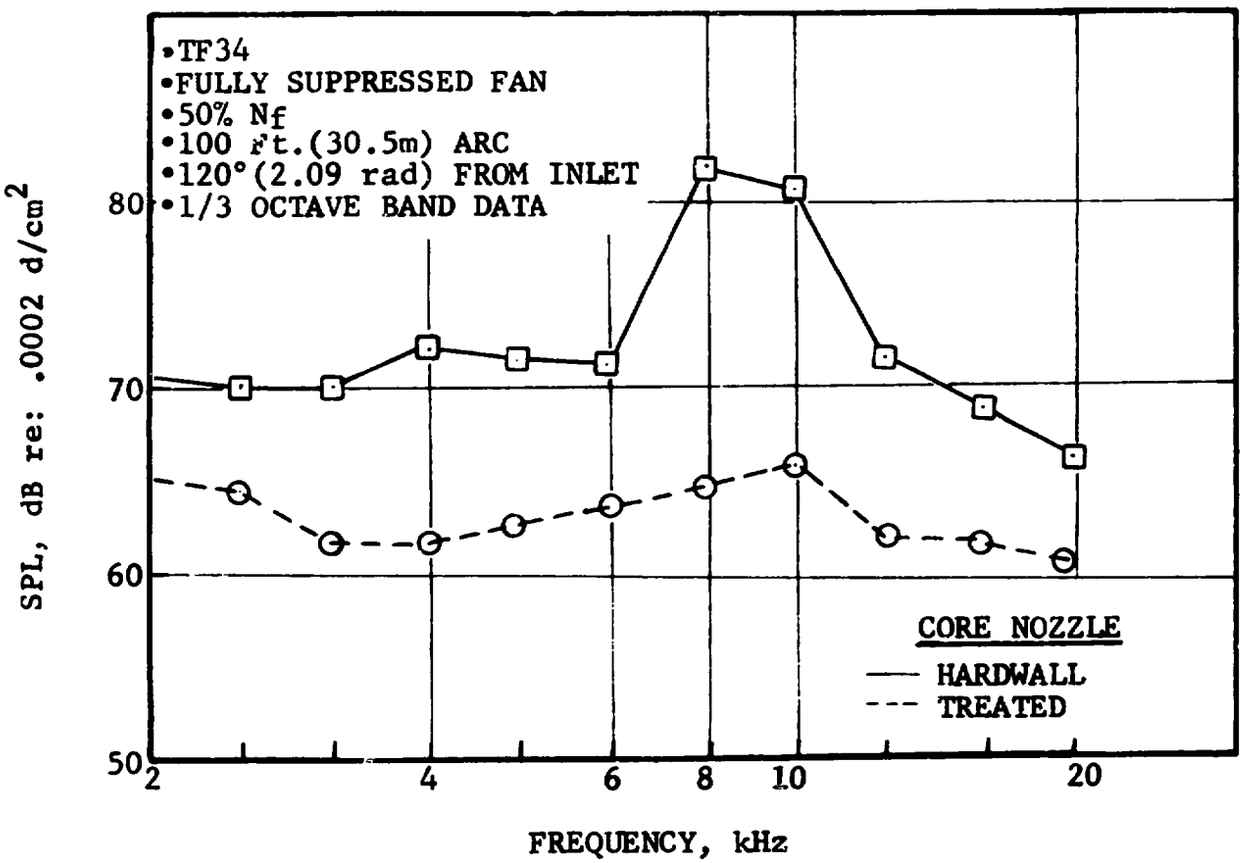

FIGURE 4.2.2-3 ENGINE NOISE SUPPRESSION ACHIEVED USING CORE TREATMENT FOR THE TF34.

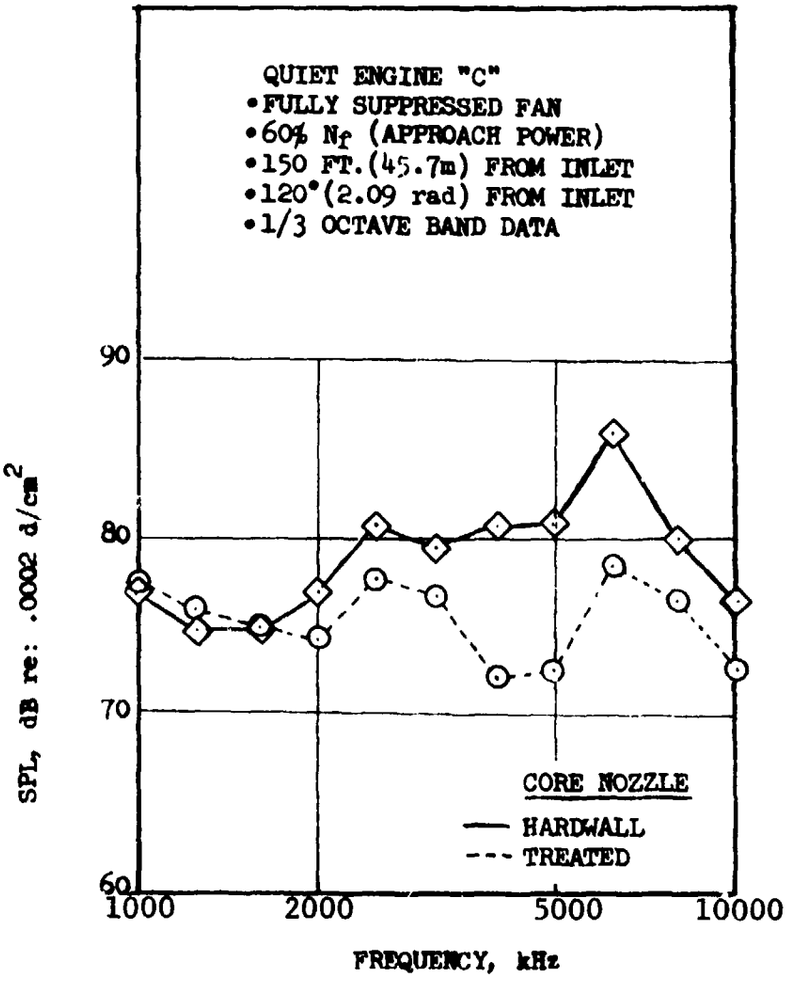

FIGURE 4.2.2-4 ENGINE SPECTRA SHOWING EFFECT OF CORE TREATMENT ON HIGH FREQUENCY NOISE.

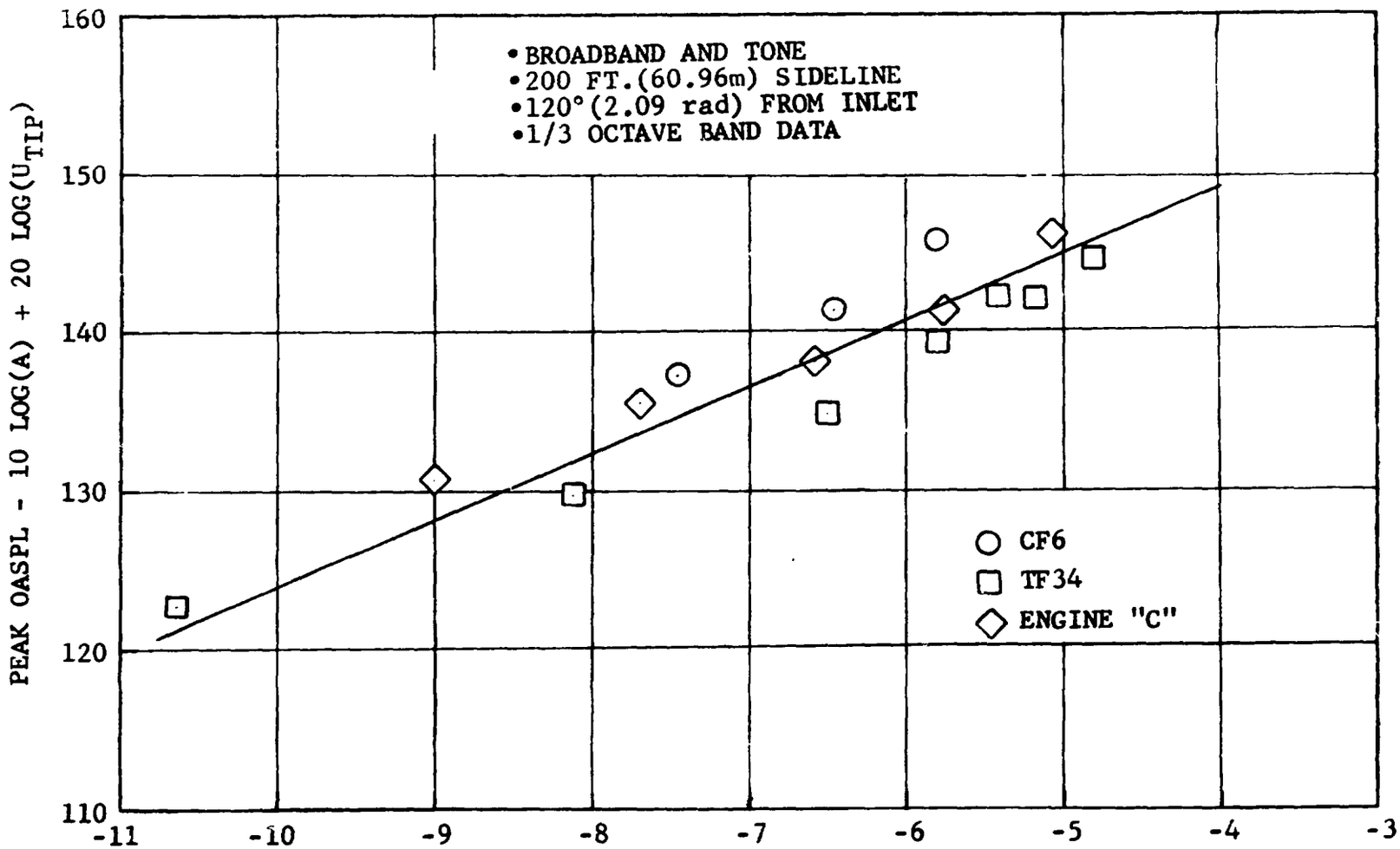

$$\frac{\Delta T}{T} = \left[1-\left(\frac{1}{P_R}\right)^{\frac{\gamma-1}{\gamma}}\right] \qquad P_R = \left(P_{T_0}/P_{S_2}\right)$$

FIGURE 4.2 2-5 TURBINE NOISE CORRELATION. THIS CORRELATION INCLUDES BOTH BROADBAND AND DISCRETE FREQUENCY NOISE. TO BE USED FOR QUICK(APPROXIMATE) ESTIMATES.

The data scatter would be reduced if air attenuation and EGA effects were included. The correlation uses data from Quiet Engine "C", the TF34 and the CF6. Quiet Engine "A" points have been omitted for the reason explained above, but fall a little below the correlating line as expected. The correlation satisfies the Prediction Method (A) requirement to provide quick, approximate predictions for turbine noise based on gross parameters available in the early stages of design.

The PNL is a function of the dominant tone location as the spectrum peaks at the tone frequency. Normally, the last or second-last stage will provide the dominant BPF, depending on the work split. The last stage appears to become dominant when the work split ratio (second-last stage/last stage) falls below 1.9, although this was not strictly true for Quiet Engine "C".

Once the dominant stage has been determined, the tone frequency can be computed and the OASPL converted to PNL by means of the adder (δ) from Figure 4.2.2-6:

$$PNL = OASPL + \delta \qquad (4.2.2\text{-}2)$$

Figure 4.2.2-6 was generated by shifting a typical turbine noise spectrum peak (See Figure 4.2.2-4) into different one-third octave bands and computing the PNL for each location.

The above correlation includes both discrete frequency and broadband noise. Figure 4.2.2-7 provides a correlation for the one-third octave band containing the dominant stage BPF, again as a function of the turbine pressure ratio:

$$\text{PEAK SPL} = 40 \log_{10} \left(\frac{\Delta T}{T}\right)_{\text{turbine}} - 20 \log_{10} U_T + 10 \log_{10} A + 165 \qquad (4.2.2\text{-}3)$$

where PEAK SPL = SPL of one-third octave band containing BPF @ 120° and 200 ft (60.96 m) sideline. The SPL does not include air of extra ground attenuation as these are strong functions of the tone frequency.

The most accurate representation of the noise generation results from consideration of each stage individually. The investigation of the three-stage turbine (HLMSFT) clearly indicated the importance of the stage pressure ratio and the blade tip speed in determining the discrete frequency noise generation by any stage (See Figure 4.1-2). The paper by Smith and Bushell (Reference 4.1-1) also shows the importance of the blade relative velocity in the broadband noise generation. Only two of the above three parameters (stage pressure ratio, blade tip speed and blade relative velocity), however, can be exercised independently at any time for constant mass flow. Figures 4.2.2-8 and -9 present correlations for the "composite" (broadband and discrete frequency) noise and turbine tone levels, respectively, using the above parameters for an individual stage. The "composite" noise correlation includes data from the TF34 and Quiet Engine "C", and the tone correlation also includes CF6 data.

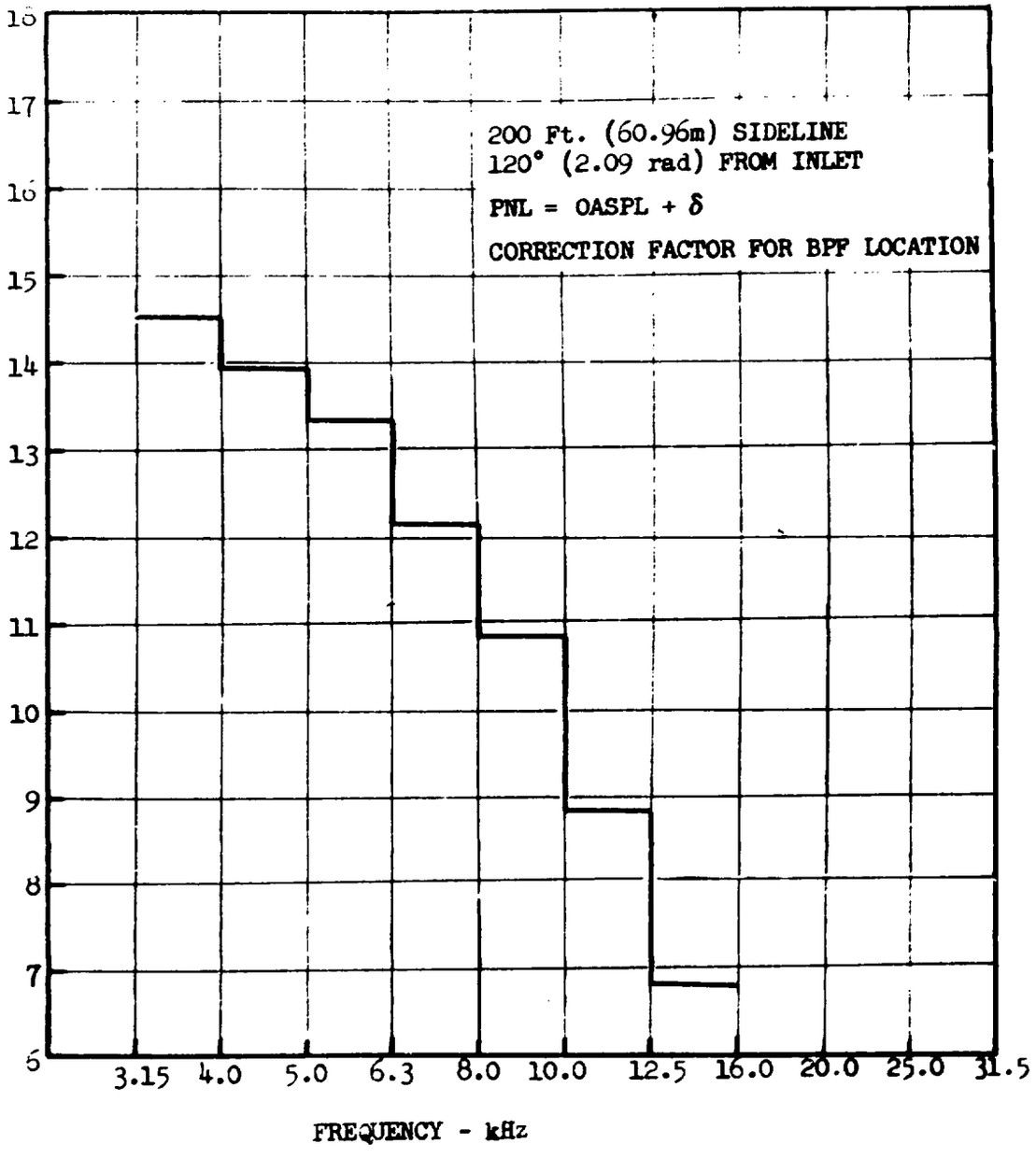

FIGURE 4.2.2-6 CORRECTION TO OASPL TO DETERMINE PNL

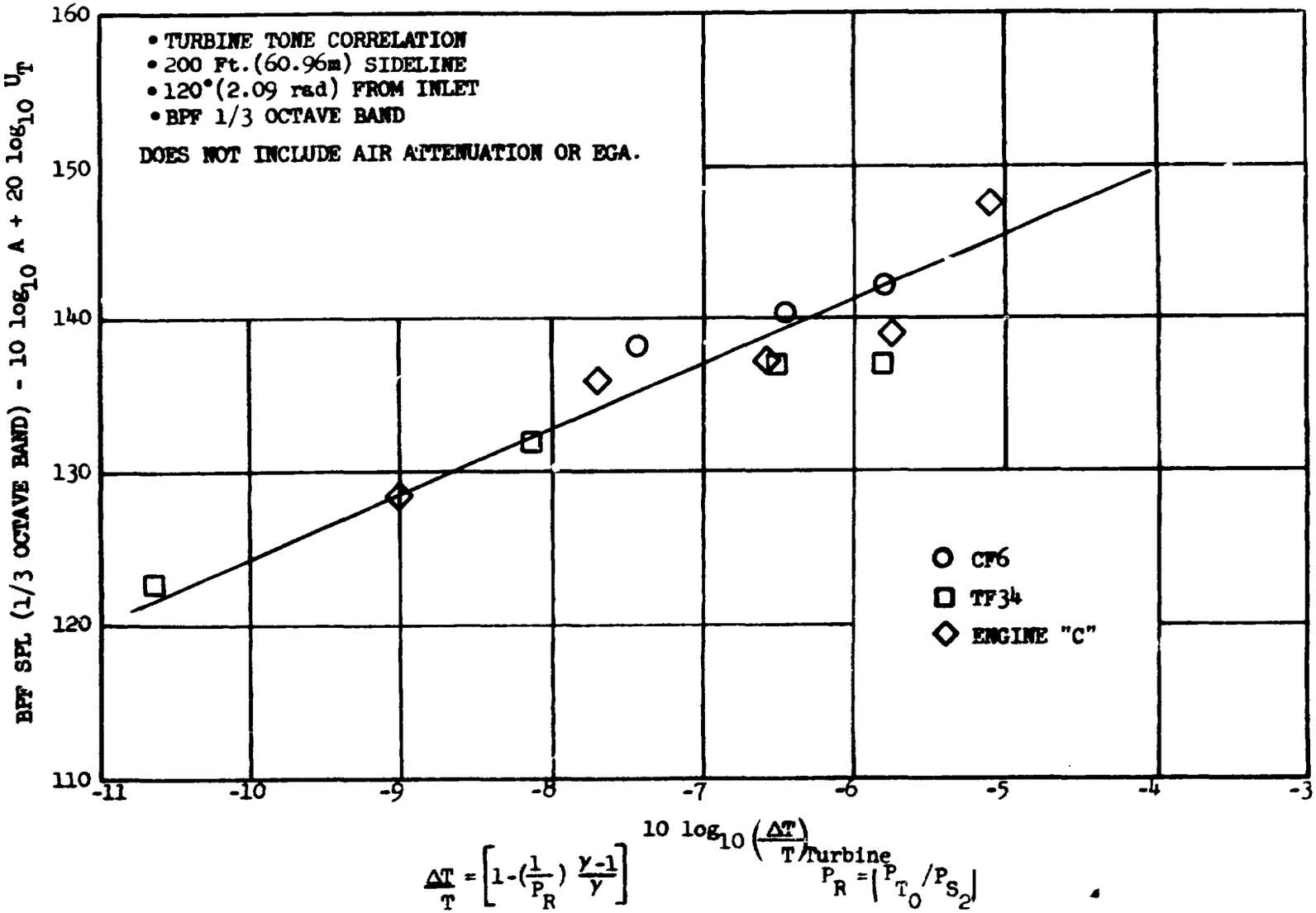

FIGURE 4.2.2-7 CORRELATION FOR TURBINE DISCRETE FREQUENCY NOISE - TO BE USED FOR QUICK (APPROXIMATE) ESTIMATES.

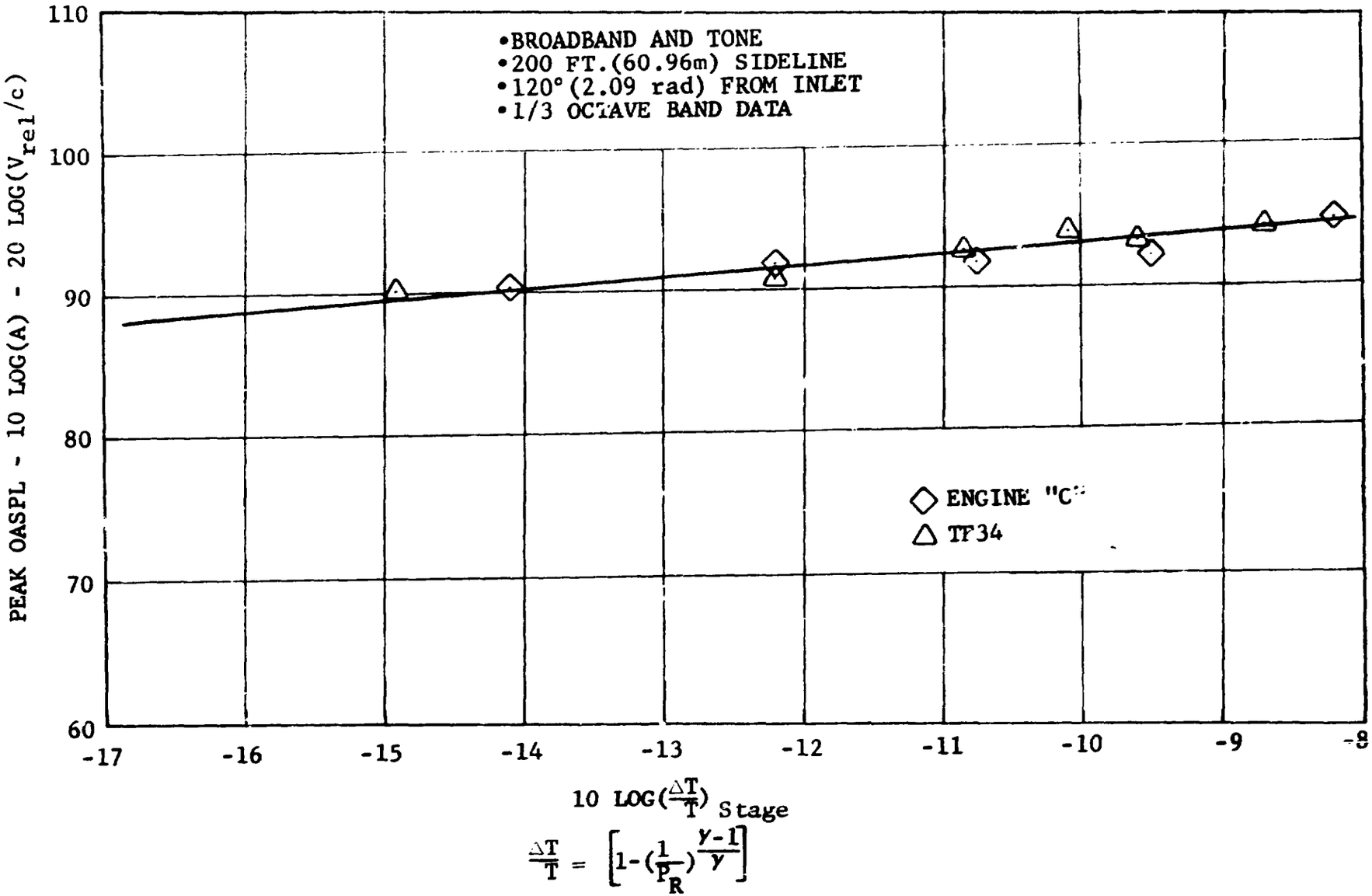

FIGURE 4.2.2-8 CORRELATION FOR TURBINE NOISE BASED ON STAGE PRESSURE RATIO.

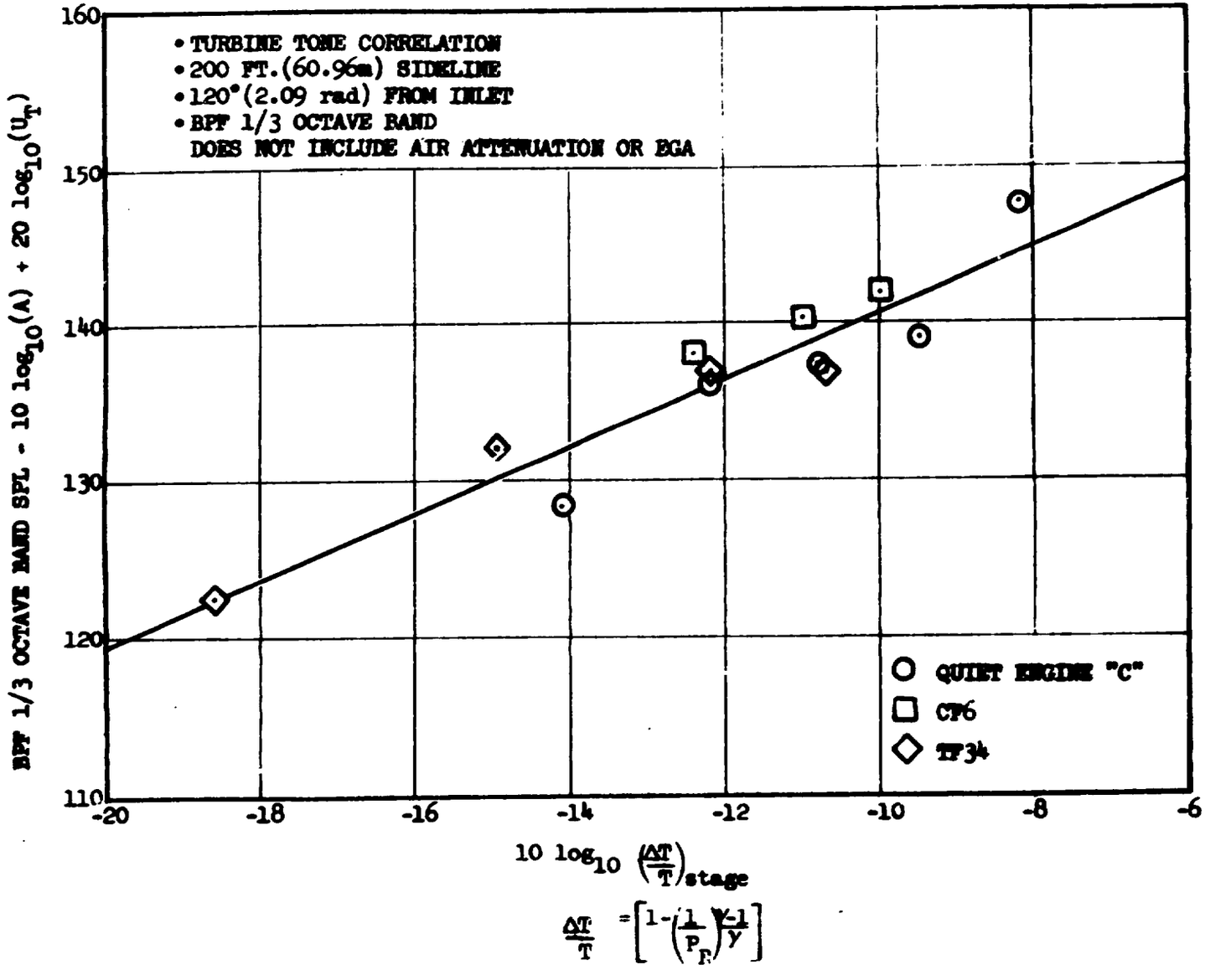

FIGURE 4.2.2-9 CORRELATION FOR TURBINE DISCRETE FREQUENCY NOISE BASED ON STAGE PRESSURE RATIO.

The relationships in Figures 4.2.2-8 and -9 can be expressed as:

$$\text{PEAK OASPL} = 8.75 \log_{10}\left(\frac{\Delta T}{T}\right)_{stage} + 20 \log_{10}\left(\frac{V_{rel}}{C}\right) + 10 \log_{10} A + 102.9 \quad (4.2.2\text{-}4)$$

$$\text{PEAK SPL} = 20 \log_{10}\left(\frac{\Delta T}{T}\right)_{stage} - 20 \log_{10}(U_T) + 10 \log_{10} A + 161.5 \quad (4.2.2\text{-}5)$$

where

PEAK OASPL = combined broadband and discrete frequency OASPL @ 120° and 200 ft (60.96 m) sideline in dB re 0.0002 d/cm^2 (standard day)

PEAK SPL = tone SPL @ 120° and 200 ft (60.96 m) sideline, without air attenuation and EGA, in dB re 0.0002 d/cm^2

$$\left(\frac{\Delta T}{T}\right)_{stage} = 1 - \left(\frac{1}{P_{R_{stg}}}\right)^{\frac{\gamma-1}{\gamma}} \quad (4.2.2\text{-}6)$$

$P_{R_{stg}}$ = dominant stage total-to-total pressure ratio

V_{rel} = tip blade relative velocity at inlet to the rotor, ft/sec

U_T = blade tip speed of dominant stage, ft/sec

C = mean acoustic velocity ft/sec

A = turbine exit area, ft^2

γ = ratio of specific heats, ≈1.4

It is interesting to observe that Equation (4.2.2-5) predicts the SPL accurately for both last and second-last stage tones, despite the blade row attenuation suffered by the second-last stage tones as they pass through the last stage. This may be a consequence of the fact that (1) the discrete frequency noise from the second-to-last stage consists of two blade row interactions, while the last stage tone is produced by only one such interaction and (2) the spacing-to-chord ratios for the second-to-last stage are much smaller than those for the last stage. The effects are apparently offsetting.

The effect of pressure ratio and velocity cannot be separated from engine data since the turbine is tied into an engine operating line and the parameters cannot be varied independently. It is found that the pressure ratio, blade relative velocity, thrust and other relevant parameters track with the engine speed (rpm), and the acoustic data can at times be correlated employing a single parameter. For example, the peak OASPL from the TF34 and Quiet Engine "C" can be collapsed using the blade tip relative velocity (V_{rel}) as the correlating parameter along with the area to normalize for size (Figure 4.2.2-10). However, the CF6 data are 7 to 8 dB above the correlating line

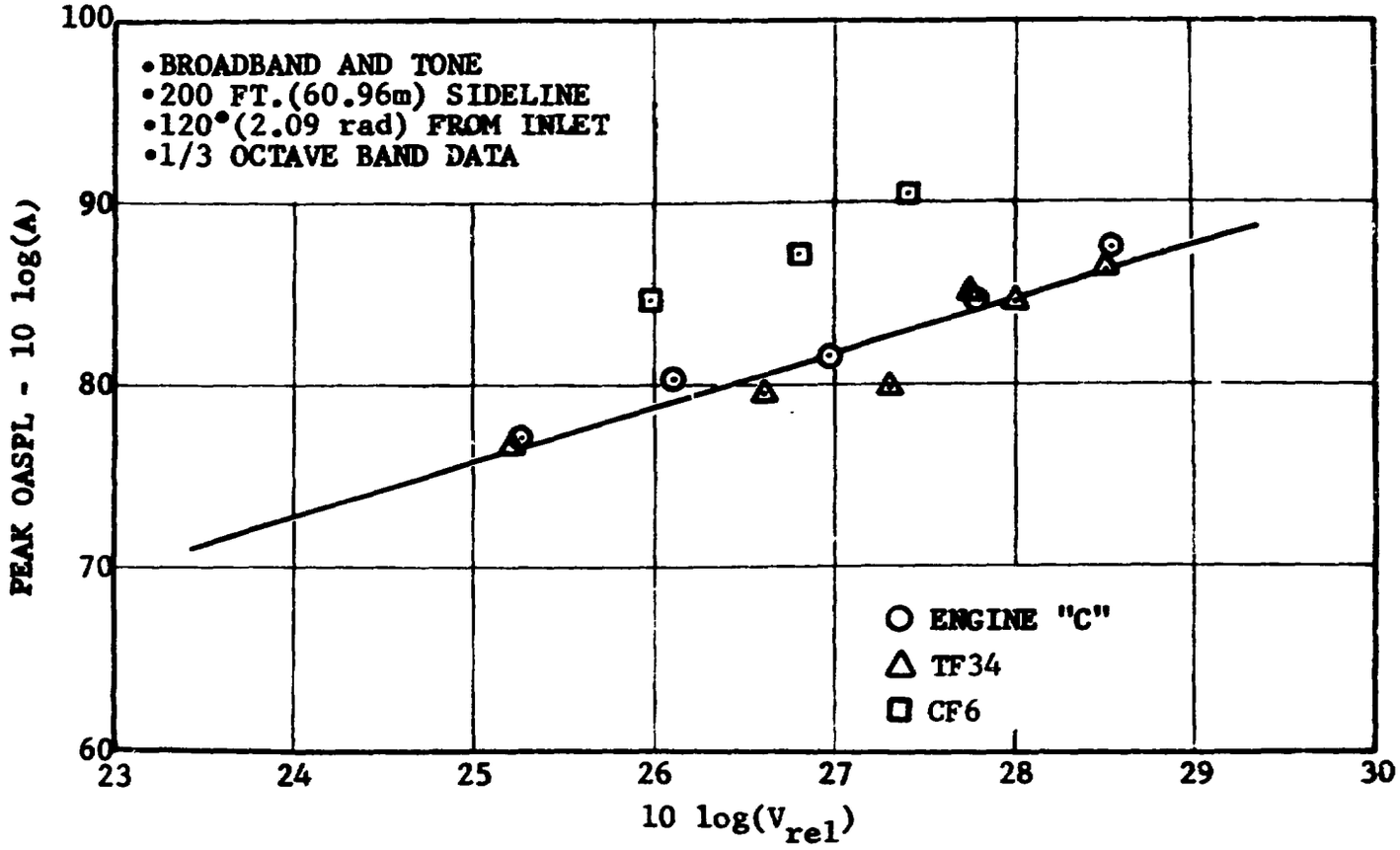

V_{rel} = TIP RELATIVE VELOCITY AT INLET TO THE LAST STAGE ROTOR

FIGURE 4.2.2-10 TURBINE NOISE CORRELATION WITH BLADE RELATIVE VELOCITY.

so obtained, indicating the need for a second independent parameter (pressure ratio).

In all of the above correlations, the exit area has been used to normalize for size. It is common to apply the weight flow as the size correction. This serves the same purpose as the area correlation, but it also introduces velocity and density effects which confuse the correlations.

4.3 TURBINE NOISE SPECTRUM

The study presented herein is for the peak angle along a 150 ft (30.48 m) arc, but may be exercised to define the spectrum at any other angle. The problem of a turbine noise spectrum was investigated using acoustic data from the TF34, CF6 and Quiet Engine "C". Using the 150 ft (30.4 m) arc data, it was found that the peak angle (120°) spectrum could be used without introducing too much error at other angles along the arc. A different spectrum would have to be defined for each angle if sideline data were to be employed because of air attenuation effects.

The turbine noise spectrum was extracted by logarithmic subtraction of the SPL's for two configurations which were identical except for acoustic treatment versus hardwalls in the core nozzle. This procedure results in sharp breaks in the extracted spectrum when the treated configuration levels either exceed or become equal to the hardwall configuration levels because of other noise sources (jet or core at the low frequency end) as a result of data scatter, or as the limits of the treatment effectiveness are reached.

Typical spectra at approach and take-off power settings are shown for Quiet Engine "C" in Figure 4.3-1. The noise peaks at the tone frequency (BPF) and falls off to either side with a distinctive spike at the BPF.

A broadband noise spectrum was derived by removal of the tone spike and fairing over the spectrum. The spectra were then plotted as the SPL falloff from the peak (BPF) level against the one-third octave band center frequency (f_c) normalized by the BPF ($f^* = f_c/BPF$). It was found that for $f^*<1$ all the spectra collapsed together fairly well. However, for $f^*>1$ the SPL fall off increased with the power setting. Hence, two separate spectra were defined, one each for approach and take-off power settings, based on the data shown in Figures 4.3-2 and -3. The two derived spectra are compared in Figure 4.3-4.

The only reliable spectra for the higher (take-off) power settings were obtained from Engine "C". A high broadband floor masked the CF6 spectrum, and the tones went well above 10 kHz for the TF34, resulting in very large air attenuations. The data used in the spectral analysis presented above were for BPF's in the 4 to 10 kHz one-third octave bands.

4.4 TURBINE NOISE DIRECTIVITY

The high broadband noise floors preclude the use of CF6 and Quiet Engine "A" data in formulating the directivity. However, these data can and were used to check the directivities derived with TF34 and Quiet Engine "C" data.

- QUIET ENGINE "C"
- TURBINE NOISE SPECTRA
- 150 FT.(45.7m) ARC
- 120°(2.09 rad) FROM INLET
- 1/3 OCTAVE BAND DATA
- CORRECTED TO STANDARD DAY

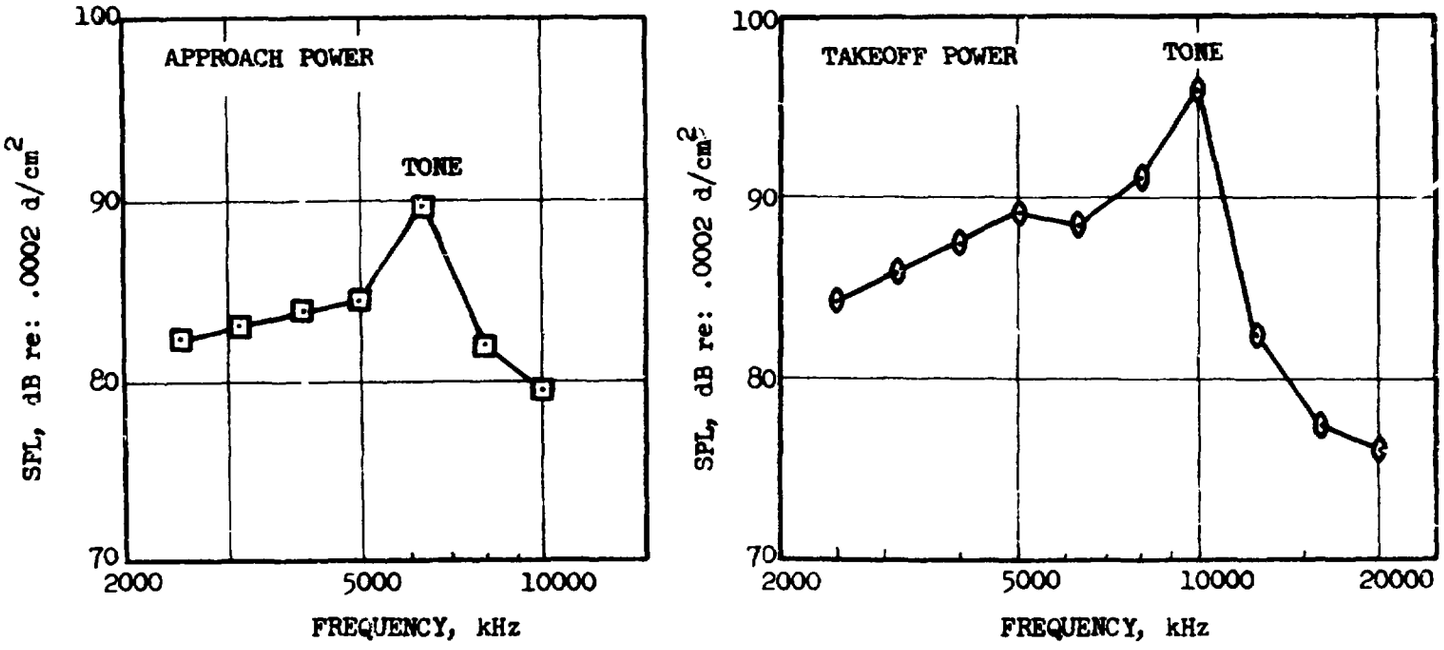

FIGURE 4.3-1 DERIVED TURBINE NOISE SPECTRA FOR QUIET ENGINE "C".

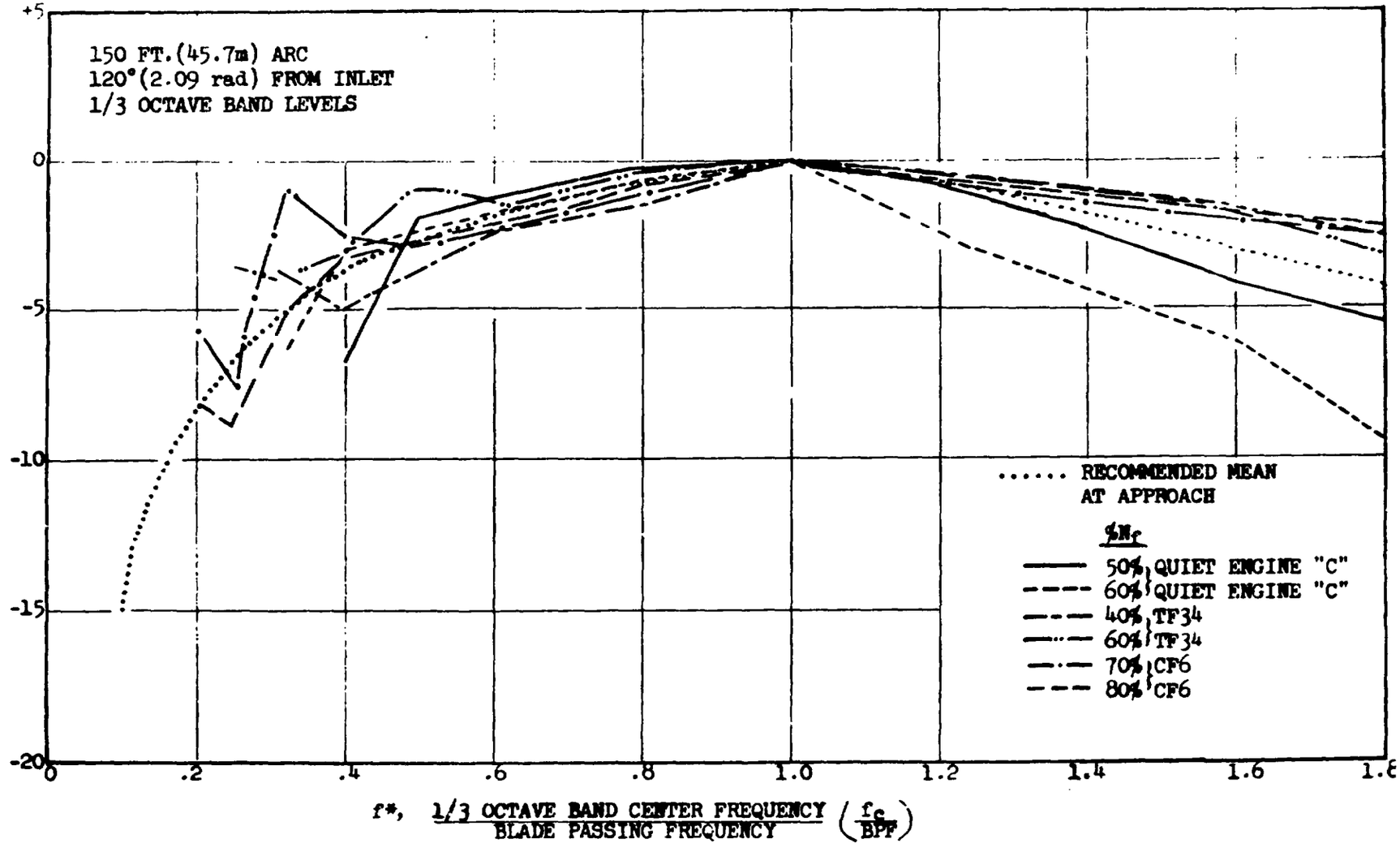

FIGURE 4.3-2 RECOMMENDED BROADBAND NOISE SPECTRUM FOR TURBINE NOISE (APPROACH POWER)

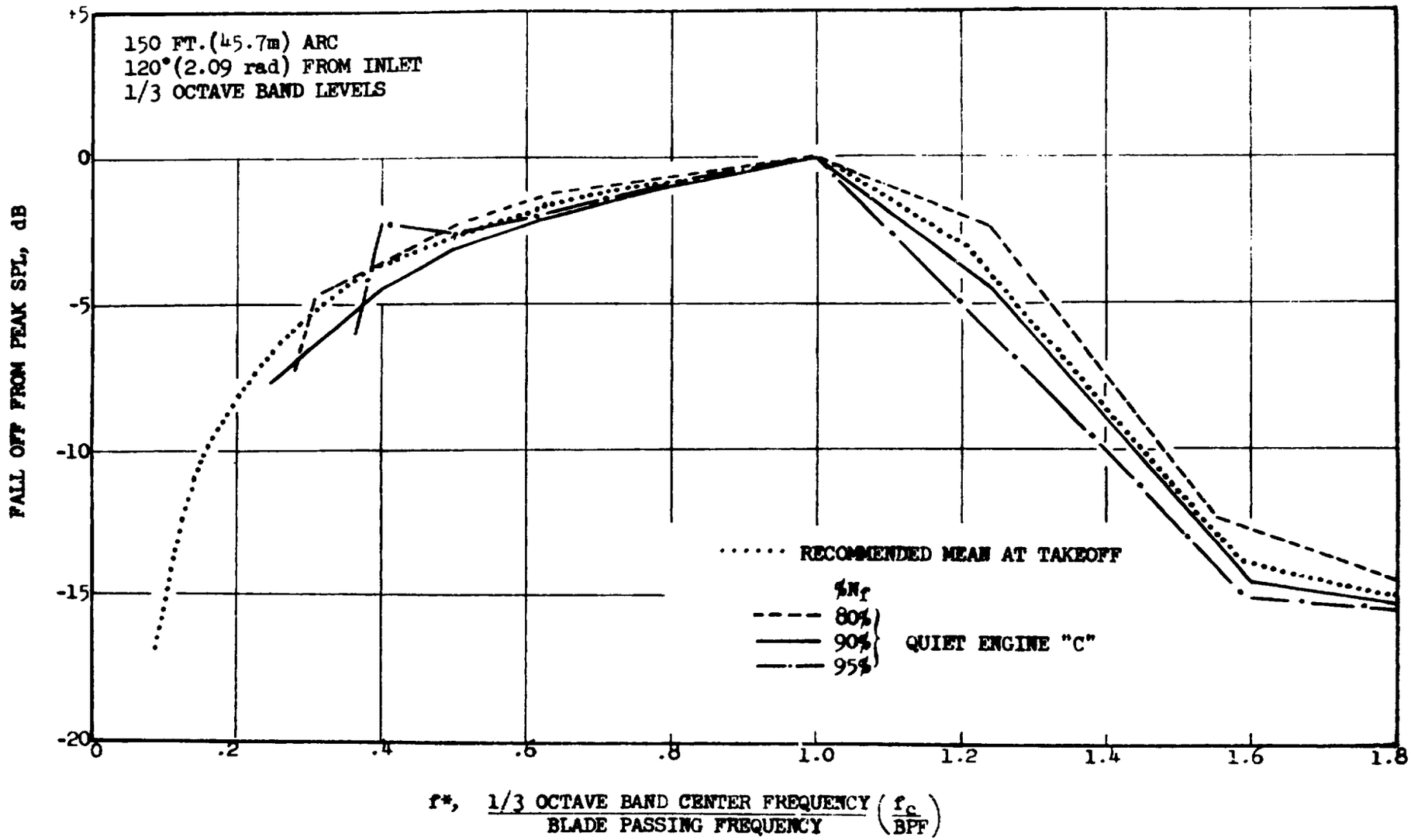

FIGURE 4.3-3 RECOMMENDED BROADBAND NOISE SPECTRUM FOR TURBINE NOISE (TAKEOFF POWER).

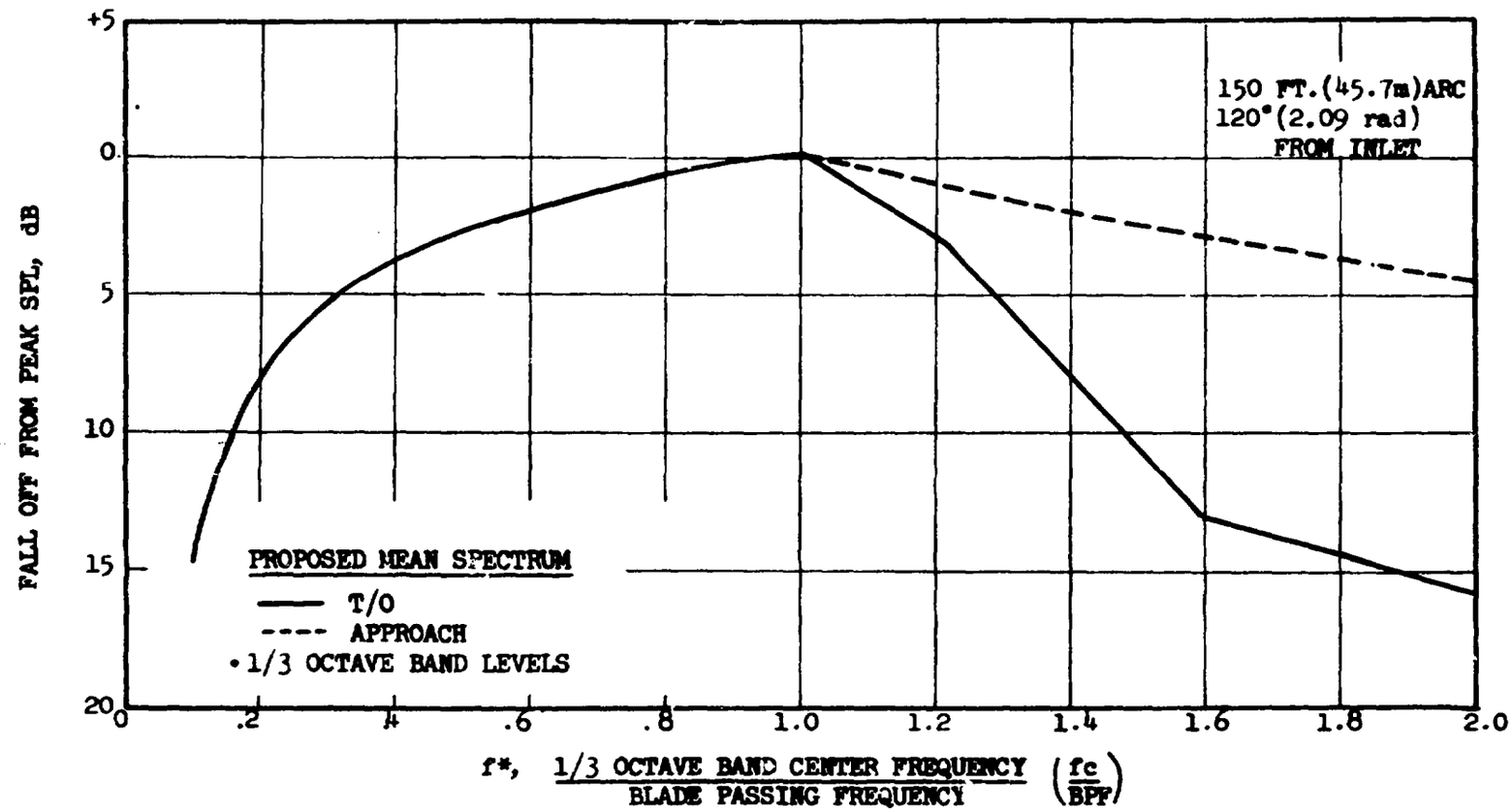

FIGURE 4.3-4 RECOMMENDED BROADBAND SPECTRUM FOR TURBINE NOISE.

Separate directivities were required for the "composite" noise (OASPL) and discrete frequency noise prediction. The directivity was defined for an arc in each case.

To determine the directivity for the turbine noise OASPL, the levels for a hardwall core nozzle configuration were normalized with respect to the peak angle OASPL and plotted as shown in Figure 4.4-1 for Quiet Engine "C". Data are presented for 50, 60, 70 and 80% design fan speeds (Nf), where turbine noise dominates the aft angles. The Figure shows the turbine noise to peak at 120° and to be discernible from 90° to 160° at the lower power settings (50 and 60% Nf). As the speed is increased, refraction theory would predict a shift of the peak from 120° towards 110°. Unfortunately, data were not recorded between 110 and 120°, only at the two discrete locations, and the velocity changes were apparently insufficient to cause the peak to shift all the way to 110°. However, the directivities plotted in Figure 4.4-1 would seem to indicate a small (less than 5°) shift in the peak from 120° to smaller angles as (1) the falloff between 120° and 110° decreases with increasing speed and (2) the falloff between 120° and the higher angles (130°, 140°) is seen to increase with speed initially before the trend is obscured by jet noise (at speeds above 80% N). A similar shift of the peak angle towards the sideline was observed by Smith and Bushell (Reference 4.1-1). Hence, separate directivities were provided for approach and take-off power settings, reflecting a small shift in peak angle. Mean directivities for approach and takeoff for TF34 and Quiet Engine "C" data are shown plotted in Figures 4.4-2 and -3, along with the recommended directivities.

Farfield data from the CF6 and Quiet Engine "A" appear to agree with the recommended directivities for the OASPL.

The directional array was found to be of considerable help in evaluating the directivity for discrete frequency noise. The accuracy of the array diminishes, however, with increasing frequency (normally restricted to 6.3 kHz or below) and the array could not be used for take-off power settings.

Typical array results are presented in Figures 4.4-4 and -5 for Quiet Engines "C" and "A", respectively, at approach power. The results were obtained with a 20 Hz filter. Turbine tone/jet stream interactions cause a frequency spread of the tone (Section 5 of Volume II) and, therefore, narrowband data must be used with some caution. One-third octave band data are preferable because it includes the tonal energy distributed into the sidebands by the interaction effect.

Figure 4.4-6 shows the directivity exhibited by the 1/3 octave band containing the dominant tone for the TF34 and Quiet Engines "A" and "C" at approach power settings. A high broadband floor seriously contaminates the Engine "A" data at all but the peak angle. The Engine "A" data are only plotted to define a limiting envelope and provide a check for Engine "C" and TF34 directivities. The mean of the TF34 and Engine "C" plots is presented in Figure 4.4-7 as the directivity for turbine discrete frequency noise at approach power settings.

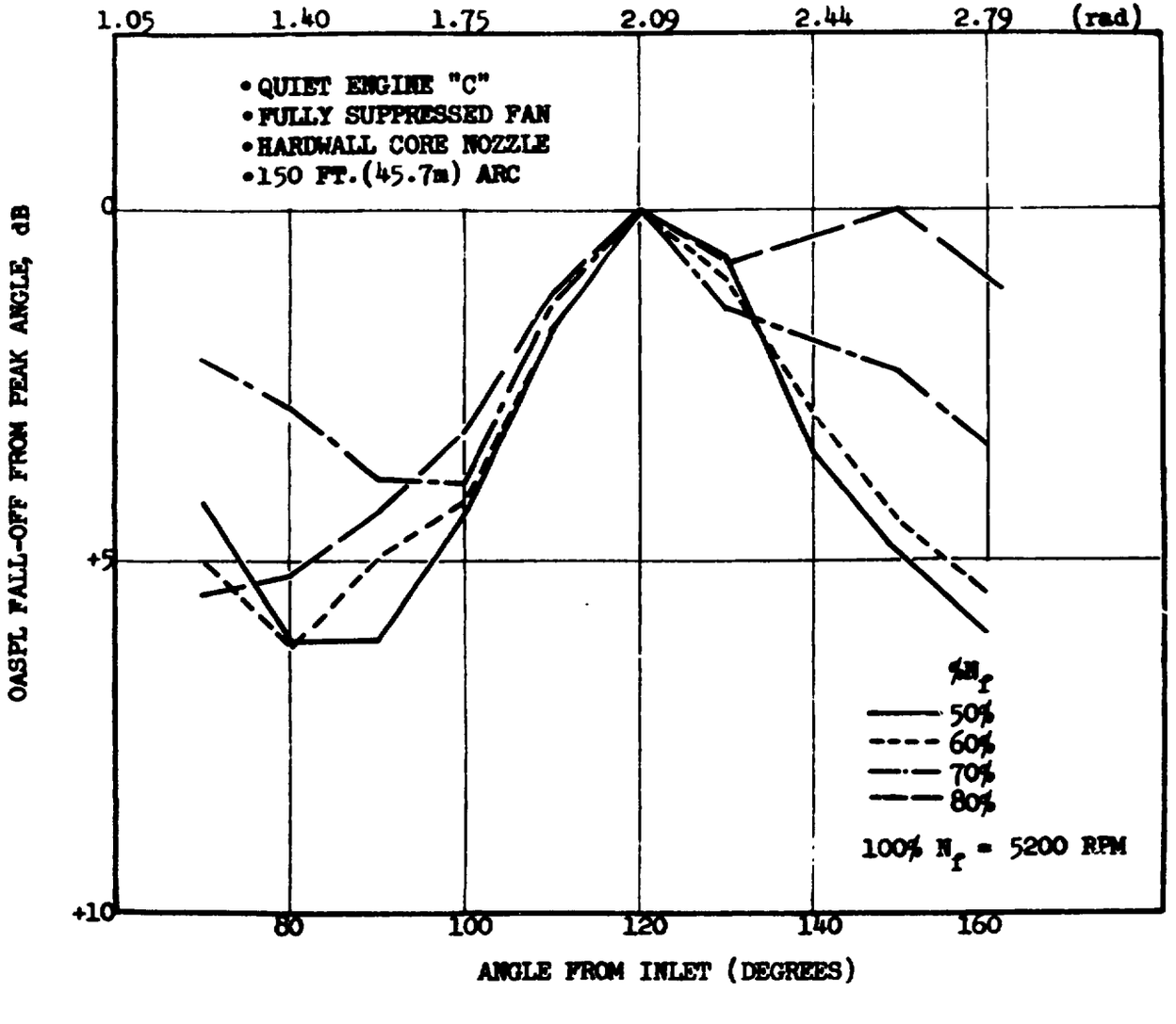

FIGURE 4.4-1 DIRECTIVITY FOR TURBINE NOISE (BROADBAND AND DISCRETE FREQUENCY).

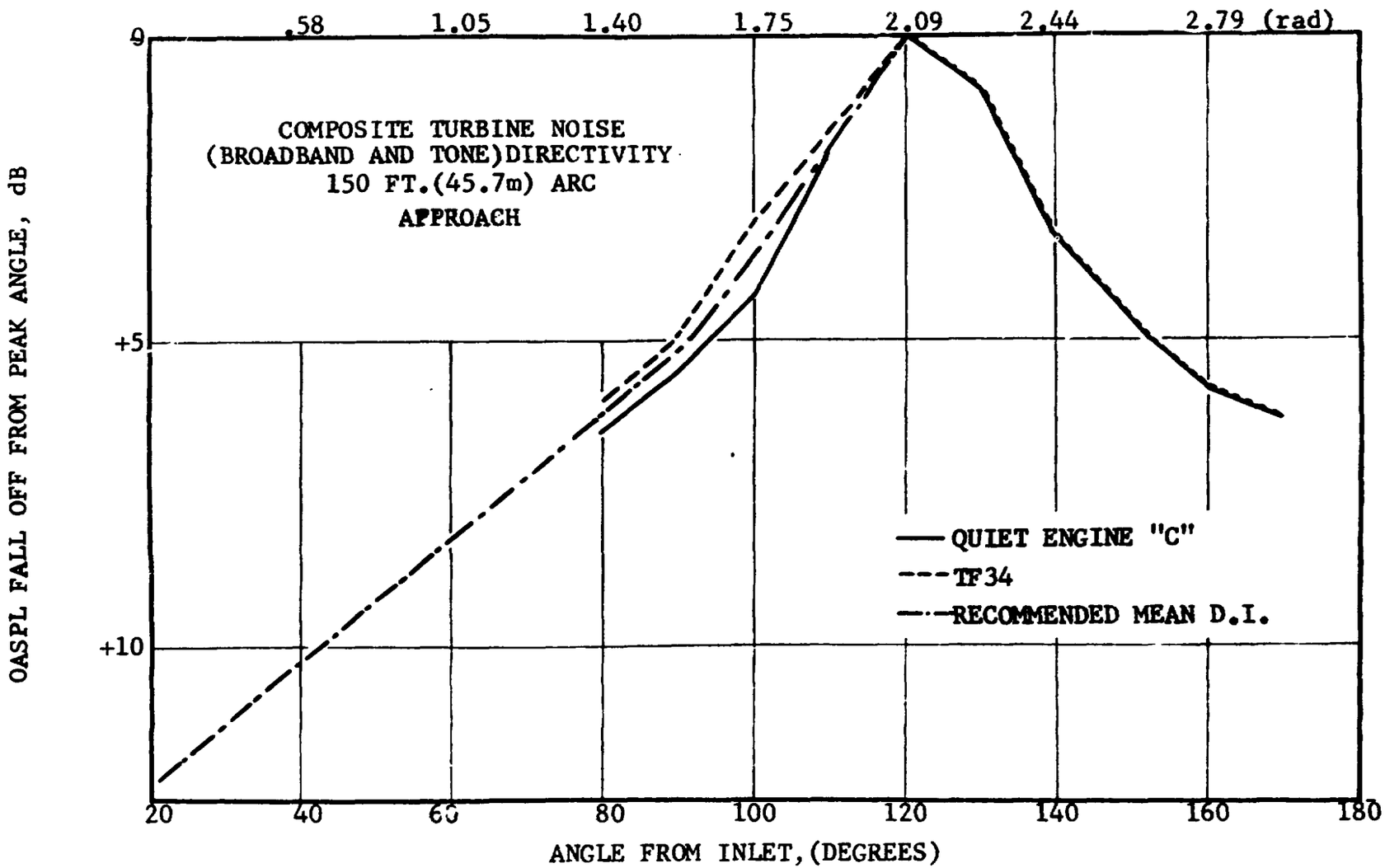

FIGURE 4.4-2 DIRECTIVITY FOR TURBINE NOISE (BROADBAND AND DISCRETE FREQUENCY) OASPL AT APPROACH POWER.

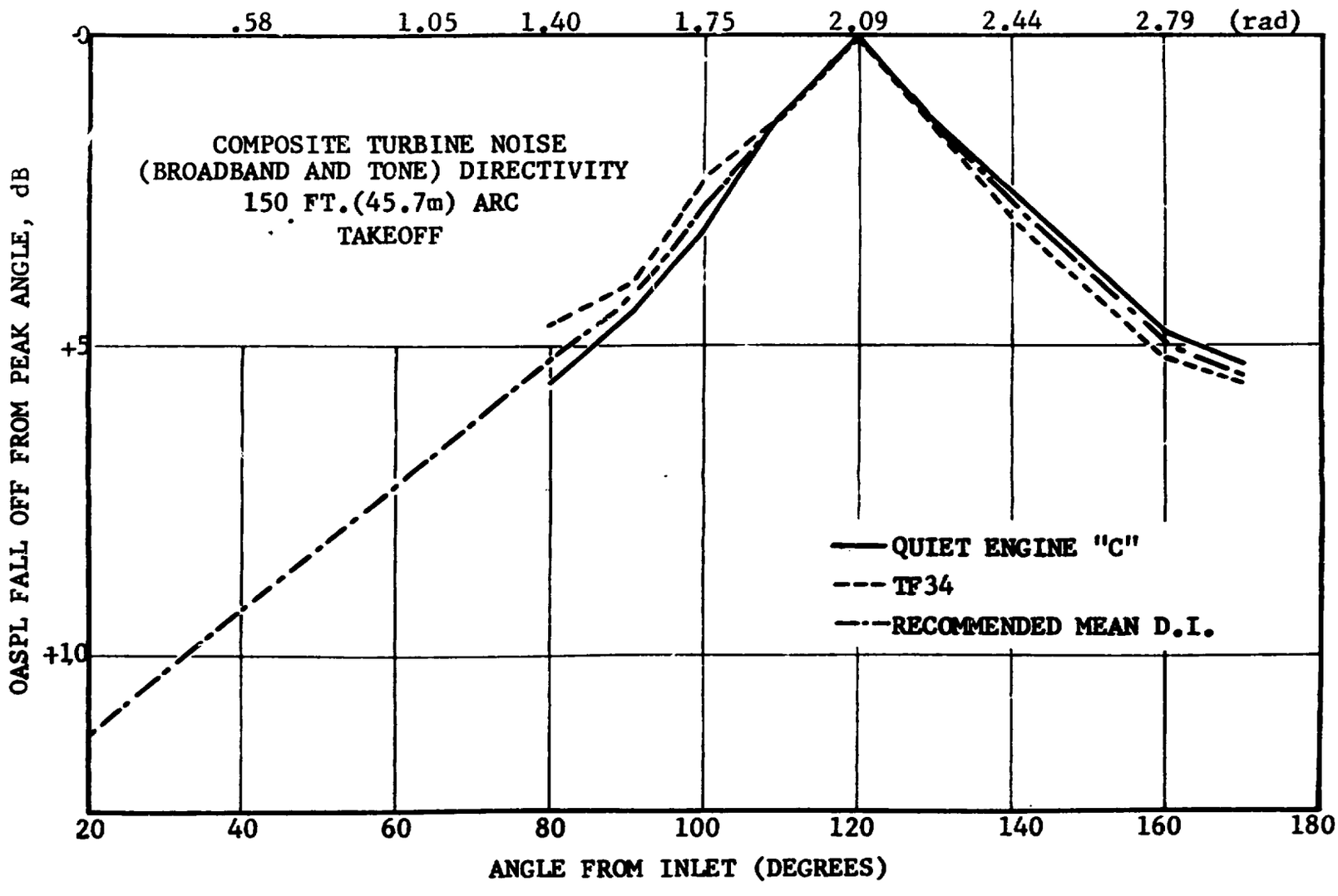

FIGURE 4.4-3 DIRECTIVITY FOR TURBINE NOISE (BROADBAND AND DISCRETE FREQUENCY) OASPL AT TAKEOFF POWER.

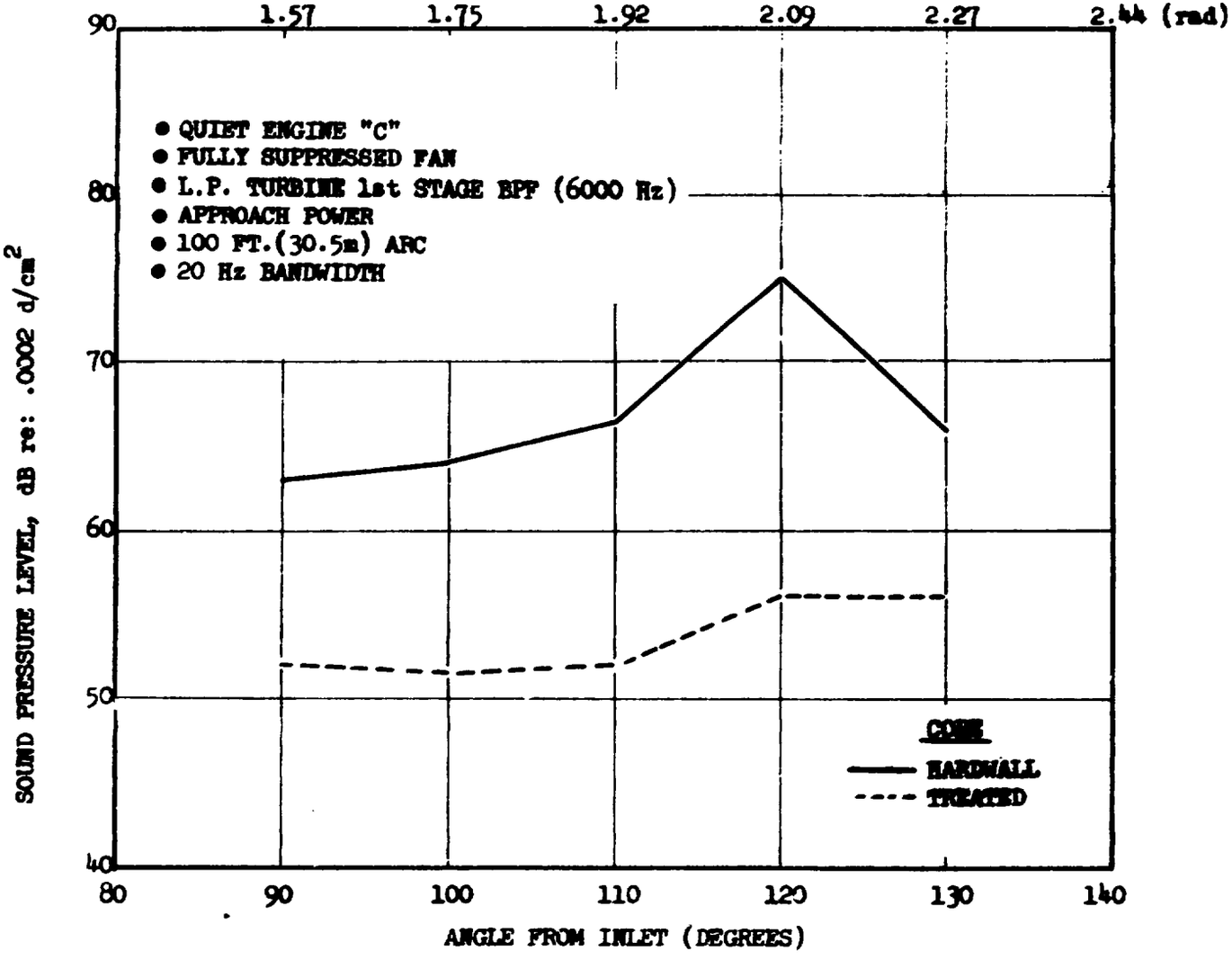

FIGURE 4.4-4 QUIET ENGINE "C" DIRECTIONAL ARRAY MEASURED TURBINE DIRECTIVITY.

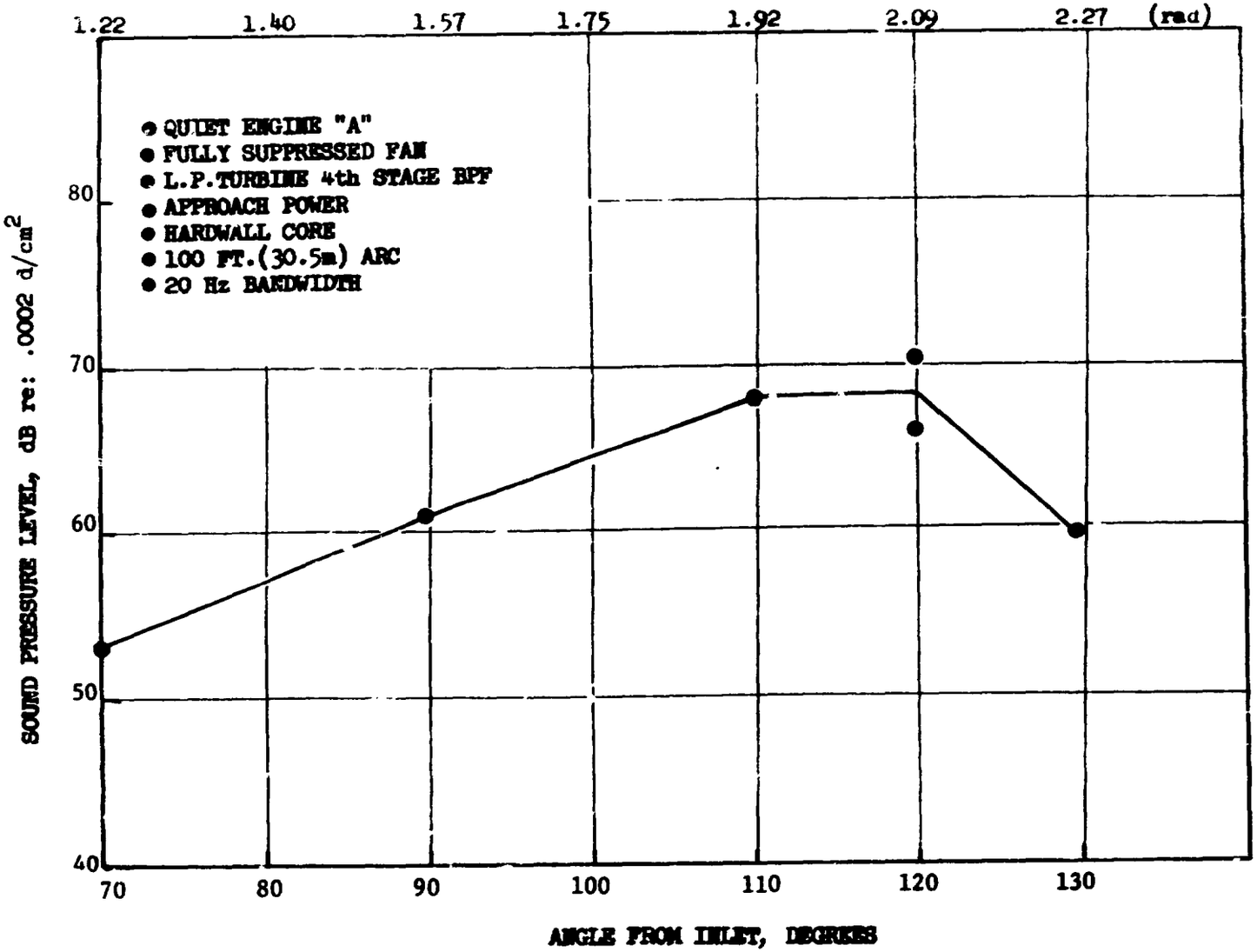

FIGURE 4.4-5 QUIET ENGINE "A" DIRECTIONAL ARRAY MEASURED TURBINE TONE DIRECTIVITY.

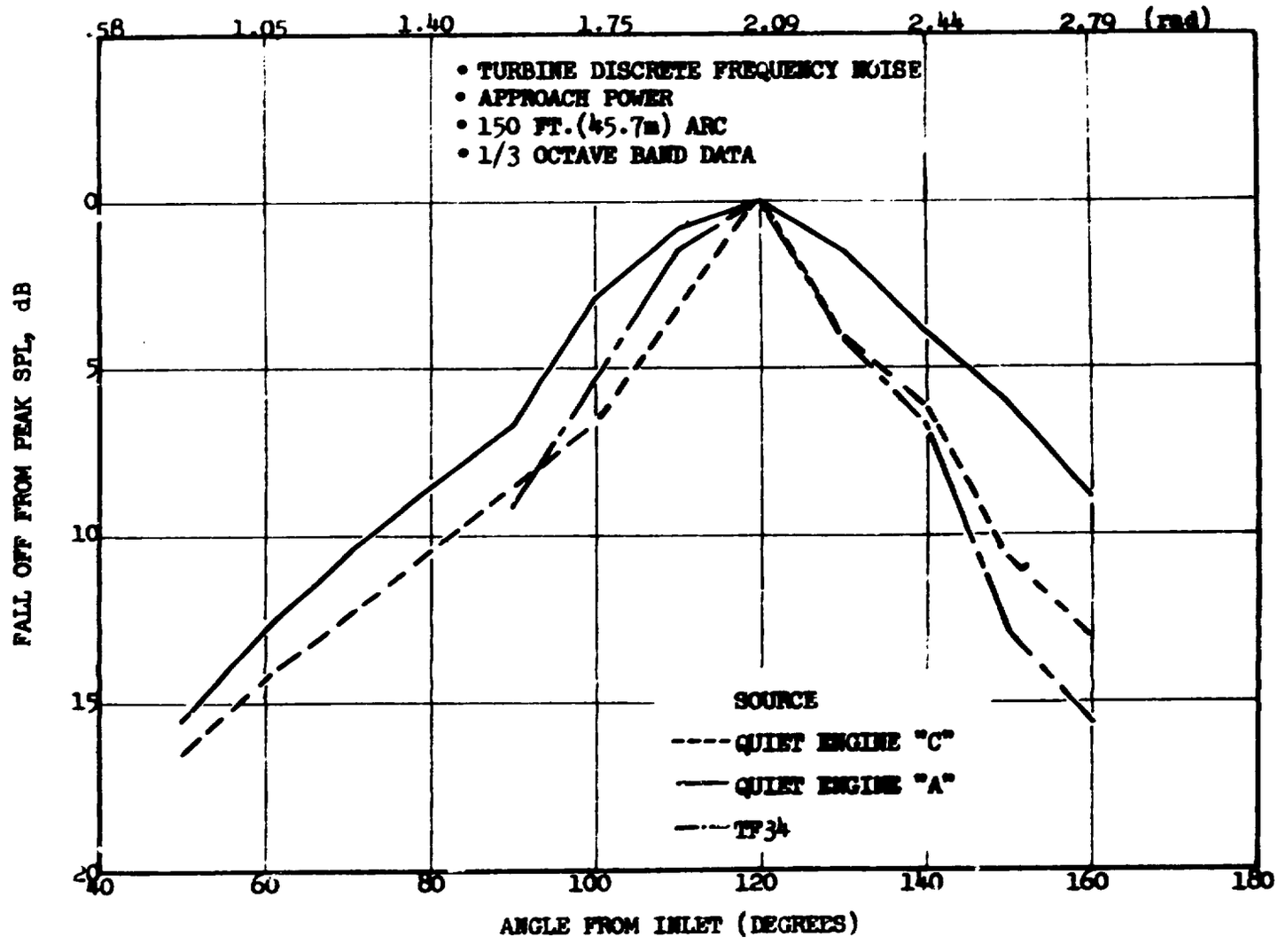

FIGURE 4.4-6 TURBINE TONE DIRECTIVITY AT APPROACH POWER - POLAR ARC.

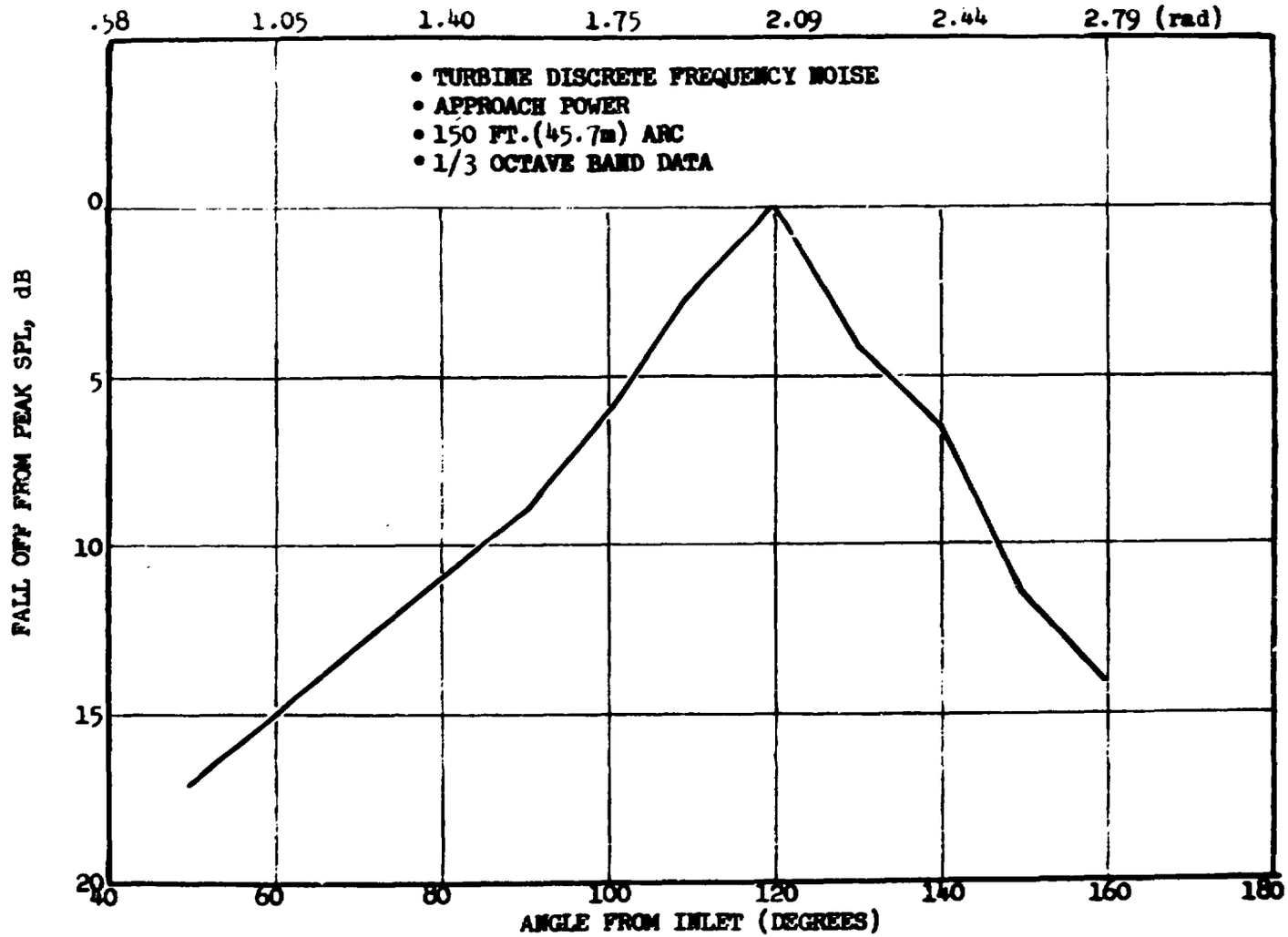

FIGURE 4.4-7 RECOMMENDED DIRECTIVITY FOR TURBINE TONE 1/3 OCTAVE BAND AT APPROACH - POLAR ARC.

The peak is assumed to shift to 115° at take-off power due to refraction effects as shown in Figure 4.4-8.

Appendix A shows how to generate a sideline directivity for a given frequency from a polar directivity by applying the inverse square law, air attentuation, and extra ground attenuation.

Directivities herein were derived from high bypass ratio engines, but experience indicates that a shift of the peak angle from 120° to 110° allows the results to be applied to turbojet engines with reasonable success.

4.5 ADDITIONS TO THE PREDICTION METHODS

The analytical prediction technique for turbine discrete frequency noise includes the effects of many geometric and aerodynamic parameters (see Table 4.5-1) and, therefore, no separate corrections are required for factors such as the temperature (density effect) or blade row axial spacing. Since the prediction provides a source PWL, however, it is necessary to account for blade row attenuation of noise generated upstream of the last blade row pair. Some analytical work has been reported in References 4.5-1 and 4.5-2 on sound transmission through blade rows, and early experience indicates that 10 dB attenuation per turbine stage is reasonable. An energy split of 6 dB to the rotor and 4 dB per nozzle row is suggested, based on the energy split assumed in fan/compressor noise work. Six dB per compressor stage is a commonly assumed value and the higher attenuation for turbine stages is considered to be due to larger turning and higher solidities.

The results of the correlations are expected to be applicable to various engine sizes, pressure ratios and wheel speeds. The turbofan engines used to derive them encompass a wide range of thrusts and operating parameters. A separate temperature correction is unnecessary since the inlet enthalpy (temperature) is used to nondimensionalize the correlating parameter.

A correction for the axial spacing between blade is necessary, however, The mean value of the axial spacing to upstream blade chord (s/ℓ) for the data used in the correlations is 0.5. Based on experience of two turbine tests with increased blade row spacing (Section 4.3 of Volume II), a 10 $\log_{10}$ (s/ℓ) correction is suggested for discrete frequency noise at values of s/ℓ other than 0.5. The effect on broadband noise is much lower and a 5 $\log_{10}$ (s/ℓ) correction is recommended. This effect is linear only over a limited (s/ℓ) range, roughly 0.4 to 1.5. It is suggested that the correction be doubled for (s/ℓ) less than 0.3. Separate corrections are believed unnecessary for blade numbers and solidity since these are somewhat constrained by turbine performance requirements and the effects are small.

Correlations have been provided for multistage, low pressure (fan) turbines. The predicted values should be reduced by 10 dB for a single-stage turbine because of reduced turbulence effects. (See the data of Reference 4.1-1 for a single-stage turbine. The prediction method based on these data underpredicted the noise levels for the two-stage Engine "C" fan turbine by some 10 dB as shown in Figures 4.1-4 and -5).

Table 4.5-1. Data Required for Turbine Discrete Frequency Noise Prediction.

Geometric	Aerodynamic
Blade Row Solidities*	Rotor Speed
Tip Radius	Static Pressure
Hub Radius	Static Temperature
Number of Blades Blade Trailing Edge Thickness	Relative and Absolute Air Angles Entering and Leaving Each Blade Row*
Number of Vanes	Section Profile Loss Coefficient*
Number of Spinning Lobes	
Harmonic Number (1 - Fundamental)	
Axial Spacing between Blade Rows*	

*Asterisked items are required at hub, midspan and tip radii

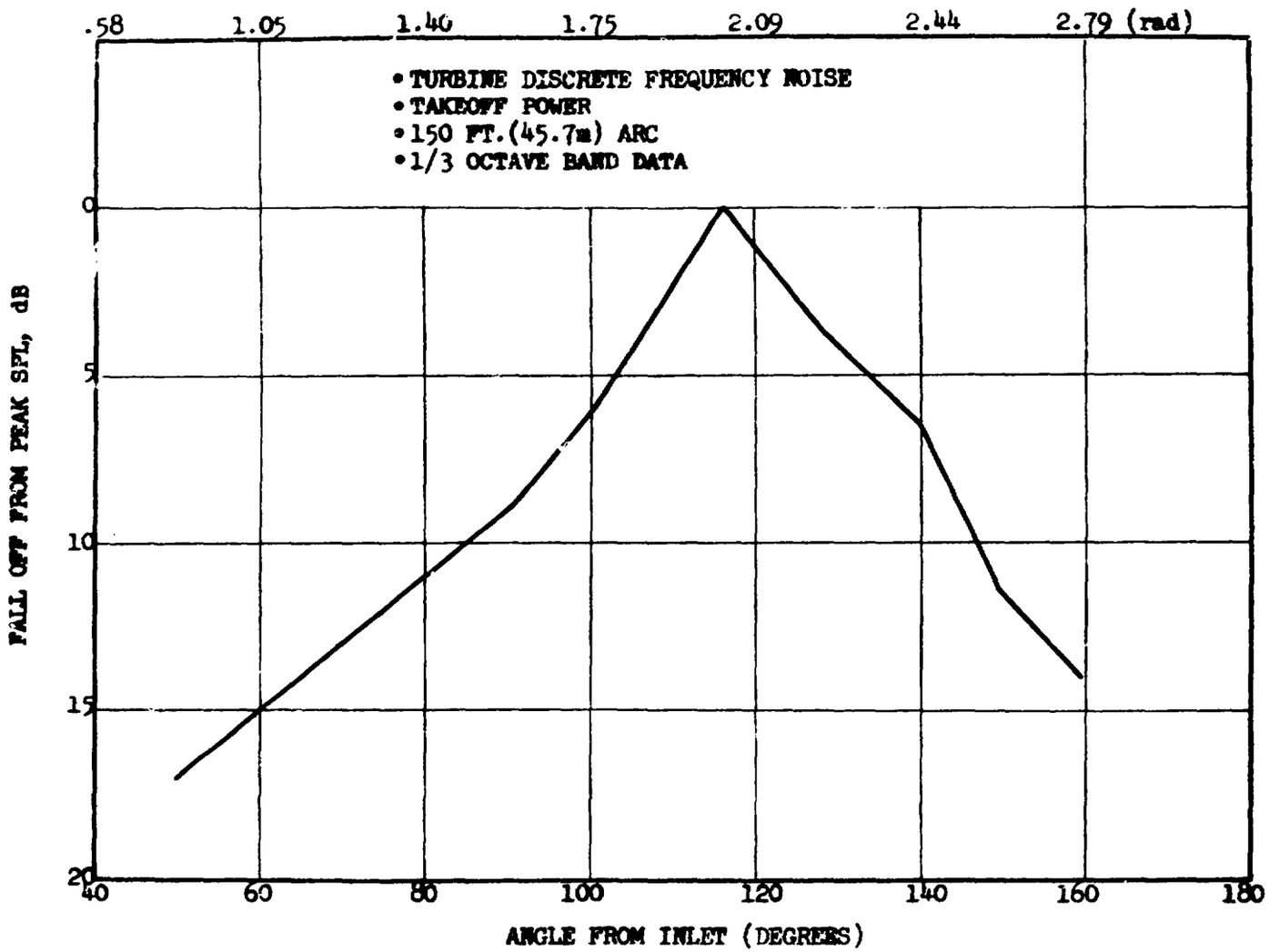

FIGURE 4.4-8 RECOMMENDED DIRECTIVITY FOR TURBINE TONE 1/3 OCTAVE BAND AT TAKEOFF - POLAR ARC.

4.6 SUMMARY - FLOW CHARTS

Three prediction methods have been presented to meet varied requirements:

(A) Preliminary design prediction method - provides quick, one-point estimates of the PNL at max angle for turbofans using information commonly available at an early design stage. The scope of the method is presented in Table 4.6-1 and a flow chart for implementation of the method in Figure 4.6-1. The OASPL which includes both the broadband and discrete frequency noise at the peak angle (normally 120°) and 200 ft. (60.96 m) sideline is computed, using the turbine overall pressure ratio, the blade tip speed of the last stage and the core nozzle exit area, through Equation (4.2.2-1):

$$\text{Peak OASPL} = 40 \log_{10} \left(\frac{\Delta T}{T}\right)_{\text{turbine}} - 20 \log_{10} U_T + 10 \log_{10} A + 164$$

$$\text{where} \quad \left(\frac{\Delta T}{T}\right)_{\text{turbine}} = 1 - \left(\frac{1}{2P_{P_{\text{turbine}}}}\right) \qquad (4.2.2\text{-}1)$$

The OASPL includes air and extra ground attenuation. The PNL is then computed using

$$\text{PNL} = \text{OASPL} + \delta \qquad (4.2.2.2)$$

where δ is provided as a function of the location of the dominant stage BPF in Figure (4.2.2-6). The dominant stage is generally the last or second-to-last stage (Section 4.2.2).

If desired, an estimate of the dominant stage tone SPL may be made at the peak angle and 200 ft (60.96 m) sideline using the turbine overall pressure ratio, blade tip speed and nozzle exit area through Equation (4.2.2-3):

$$\text{Peak SPL} = 40 \log_{10} \left(\frac{\Delta T}{T}\right)_{\text{turbine}} - 20 \log_{10} U_T + 10 \log_{10} A + 165 \qquad (4.2.2.3)$$

This SPL does notinclude air or extra ground attenuation.

The PNL at the peak angle appears to be controlled by the discrete frequency noise.

(B) Comprehensive prediction method - provides a complete turbine noise spectrum at each farfield location. The input requires a knowledge of the stage pressure ratios, the blade tip velocities, the blade relative velocities into the buckets, the percentage speed and the spacing between the blade rows.

Table 4.6-1. Preliminary Design Estimate, Method A.

- Semiempirical Relationship, Correlating Parameter - Turbine Ideal Work Extraction.
- Input

  Turbine Pressure Ratio
  Blade Tip Velocity (Last Stage)
  Core Nozzle
  Exit Area
  Tone BPF

- Output

  Peak OASPL & PNL at 200 ft (60.96 m) Sideline

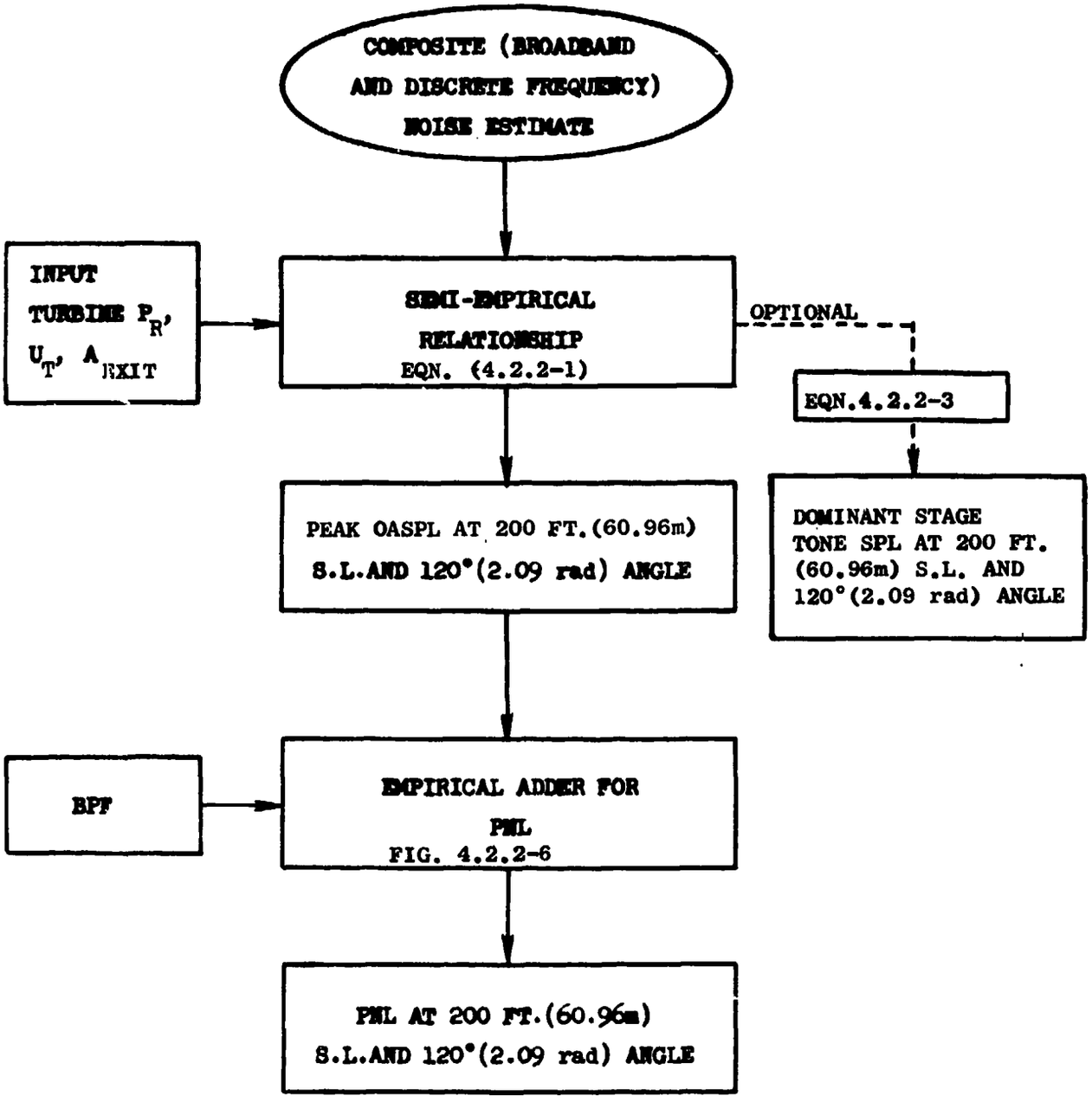

FIGURE 4.6-1 FLOW CHART FOR PRELIMINARY ESTIMATES OF TURBINE NOISE (METHOD A).

The scope of this method is provided in Table 4.6-2 and a flow chart for implementation in Figure 4.6-2.

The noise levels for each stage are computed separately and summed to give the turbine noise spectra.

The composite noise level (broadband plus discrete frequency noise) for any stage at the 200 ft (60.96 m) sideline peak angle is computed using the stage pressure ratio, tip blade relative velocity at inlet to the rotor and stage exit area through Equation (4.2.2-4).

The empirical directivity index presented in Figure 4.4-2 or Figure 4.4-3 is applied to determine the OASPL at angles other than the peak (which Figure depends on the power setting, approach or takeoff).

The directivities are provided for an arc because the tone frequency has significant effect on the sideline directivity due to varying air attenuation. It is suggested that the spectra be computed over an arc and then extrapolated to the sideline. Alternately, the arc directivities can be converted to sideline directivities for a given sideline distance using Appendix A.

The discrete frequency noise for each stage is then obtained from Equation (4.2.2-5) as a function of the pressure ratio, blade tip speed and exit area:

$$\text{Peak SPL} = 21\log_{10}\left(\frac{\Delta T}{T}\right)_{\text{stage}} - 20\log_{10}(U_T) + 10\log_{10}A + 161.5 \qquad (4.2.2\text{-}5)$$

The output SPL does not include the air and extra ground attenuations; these must be subtracted from the SPL to arrive at the farfield value.

The directivity of either Figure 4.4-7 or 4.4-8 (depending on the power setting) is imposed on the peak SPL to arrive at the SPL's at the other angles.

The discrete frequency SPL is logarithmically subtracted from the combined noise OASPL at each location to yield the broadband noise OASPL. The 1/3 octave band levels for the broadband noise may be derived by imposing the appropriate spectrum shape from Figure 4.3-4 (depending on the power setting). The tone SPL is added to the appropriate 1/3 octave band to give the complete spectrum for that one stage.

The levels so derived imply an axial spacing/upstream blade chord ratio of 0.5. For other values a correction of 10 log (s/ℓ) is recommended to be applied to the tone SPL and 5 $\log_{10}$ (s/ℓ) to the broadband OASPL, where s is the axial spacing and ℓ the upstream blade chord. For example, for s/ℓ = 1, 3 dB should be subtracted from the tone SPL and 1-1/2 dB from the broadband SPL. The spacing correction is linear over a small (s/ℓ) range only, roughly 0.4 to 1.5. For (s/ℓ) less than 0.3 it is advisable to double the corrections.

Table 4.6-2. Comprehensive Noise Estimate, Method B.

- Semiempirical Relationship, Correlating Parameter - Stage Ideal Work Extraction
- Input

  Stage Pressure Ratio
  Blade Tip Velocity and Relative Velocity Into Buckets
  Percentage Speed
  Blade Passing Frequency
  Spacing-to-Chord Ratios
  Exit Area

- Output

  1/3 Octave Band Spectrum at Each Angle Over a 150 ft (45.7 m) arc

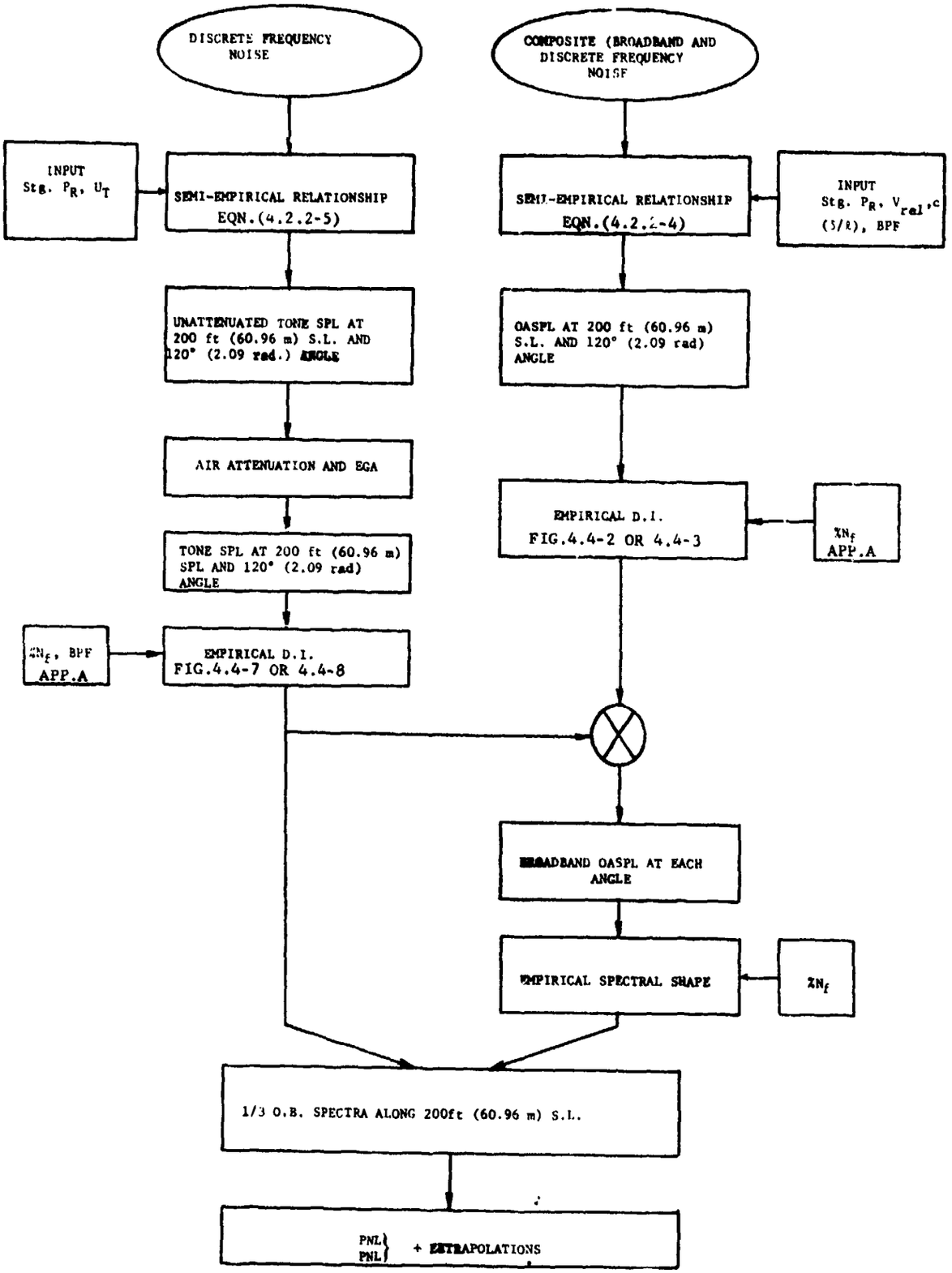

Figure 4.6-2 FLOW CHART FOR COMPREHENSIVE TURBINE NOISE PREDICTION PROCEDURE. (METHOD B)

The foregoing process supplies accurate representations of the spectra for either the last or second-to-last stage, which are normally the dominant stages in fan turbines. For stages other than these, blade row attenuation amounting to 10 dB/stage (6 dB per rotor and 4 dB per nozzle) should be imposed.

The process is repeated for each desired stage and the spectra summed to form the complete turbine noise spectrum.

(C) Analytical prediction of turbine discrete frequency noise - capable of evaluating effects of aeromechanical configuration variations on the noise generated. Implementation of this method requires knowledge of the blade geometry and the stage aerodynamics, and provides the source PWL for each blade pair. The scope of the analysis and the input required are given in Table 4.6-3. A flow chart is provided in Figure 4.6-3.

The analysis models the noise generated by viscous wakes from upstream blading impinging on a downstream blade row. The model includes a semiempirical description of the viscous wake and velocity defect, the unsteady circulation generated at the downstrear blade row by the velocity defect and couples this periodic disturbance into the duct acoustic modes [Equations (4.2.1-1) through (4.2.1-8)].

The analysis is capable of providing noise generation at design and off-design operating points. Cutoff is implicit in this analysis, because modes with imaginary wave-numbers will decay exponentially down the duct.

The prediction equations provided show that fan turbine noise reduction can be obtained through increased blade tip speed or reduced relative velocity incoming to the rotor for any required pressure ratio. At a given tip speed, decreased pressure ratio should result in reduction in the generated noise. This effect may be utilized by designing a front-loaded turbine with the last two stages lightly loaded. The noise generated by the earlier stages is highly attenuated by passage through the downstream stages.

Additional spacing between the blade rows has been shown to be a viable noise reduction technique for both high and low pressure turbines. The analysis for viscous wake interaction indicates that curtailment of the wake defect will also yield noise relief.

All of the foregoing are source noise reduction techniques. Turbine noise may also be controlled through utilization of propagation effects. Enhancement of the haystacking (Section 5) is one example. Pushing the BPF to higher frequencies, particularly over 10 kHz, is another technique. This not only results in larger air attenuation, but also pushes the tone beyond the annoyance rating range.

Table 4.6-3. Analytical Computation of Turbine Tone, Power Level.

- Noise Generation Mechanisms are Similar to Those for Fan/Compressor
- Viscous Wake Interaction is the Dominant Mechanism
- Modified Analytical Model Developed for Fan/Compressor Noise to Accommodate Turbine Blading:

  Thick, Highly Cambered Blades
  Trailing Edge Thickness
  Favorable Pressure Gradients

- Input

  Pressure
  Blade Relative Velocity
  Number of Vanes and Blades
  Turbine Size
  Axial Spacing
  Blade Geometry
    Chord
    Solidity
    Aspect Ratio
    Trailing Edge Thickness

- Output

  Tone PWL at Source

- Apply Blade Row Attenuation Per Stage
  -Tone PWL at Turbine Exit

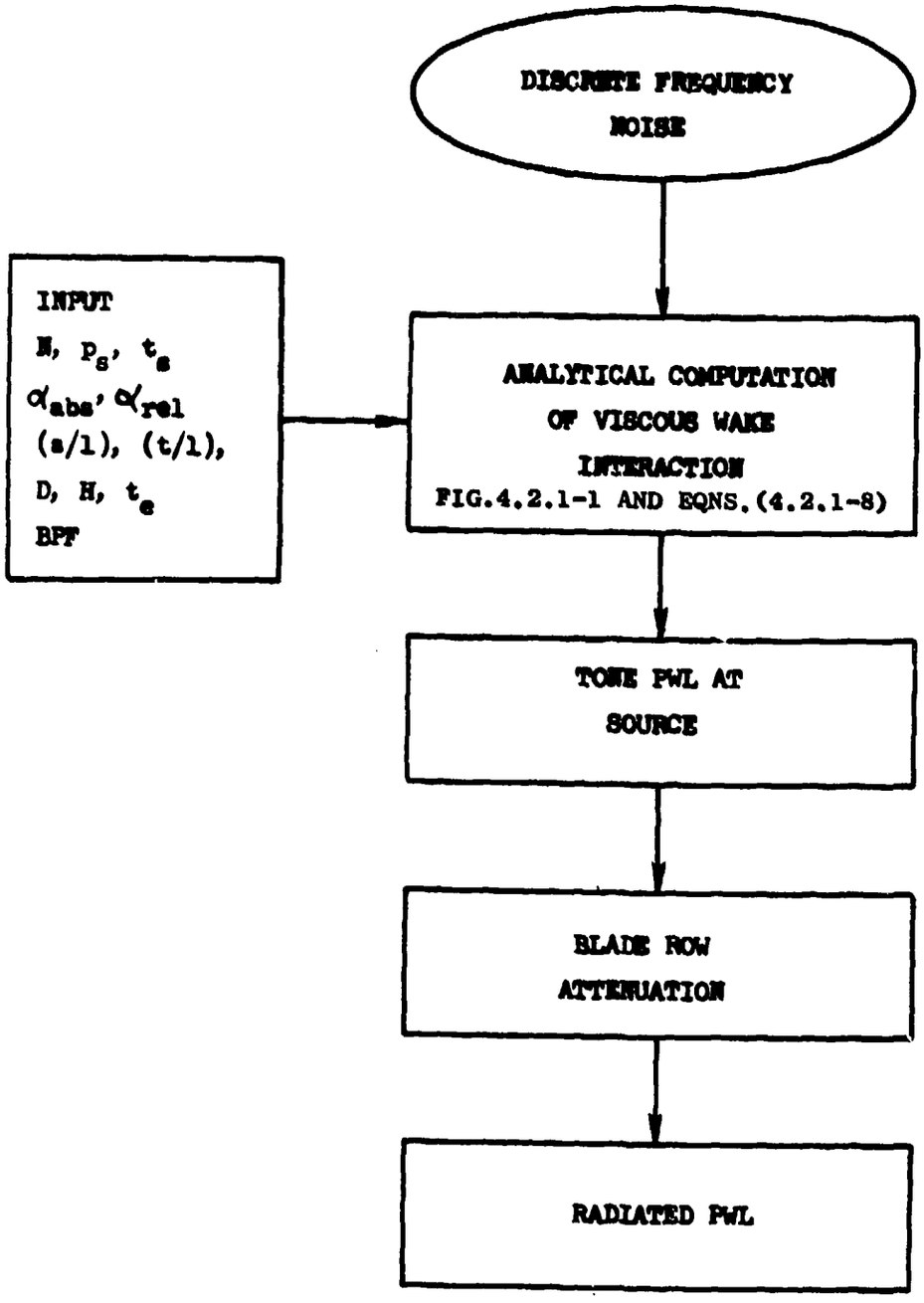

FIGURE 4.6-3 FLOW CHART FOR ANALYTICAL COMPUTATION OF TURBINE DISCRETE FREQUENCY NOISE (METHOD C).

References

4.1-1 Smith, M.J.T. and Bushell, K.W.; "Turbine Noise - Its Significance in the Civil Aircraft Noise Problem," ASME 69-WA/GT-12, 1969.

4.1-2 Smith, M.J.T. and House, M.E.; "Internally Generated Noise from Gas Turbine Engines, Measurement and Prediction," J. Eng. for Power. Trans. ASME, Series A, 89, April 1967.

4.1-3 Dunn, D.G. and Peart, N.A.; "Aircraft Noise Source and Contour Estimation," NASA CR-114649, July 1973.

4.2.1-1 "Fan/Compressor Noise Research, Volume 1," Final Report under DOT/FAA Contract FA68WA-1960, Project Number 550-001-01H, General Electric Company, December 1970, FAA Report FAA-RD-71-85, December 1971.

4.2.2-1 Benzakein, M.J. and Smith, E.B.; "Turbine Noise Generation and Suppression," ASME 73-WA/GT-7, 1973.

4.5-1 Mani, R. and Horvay, G.; "Sound Transmission Through Blade Rows," Report No. 69-C-104, General Electric R&D Center, Schenectady, N.Y., February 1969.

4.5-2 Kaji, S. and Okazaki, T.; "Propagation of Sound Waves Through a Blade Row, I. Analysis Based on the Semi-Actuator Disk Theory," J. Sound and Vibr. 11, part 3, 1970.

SECTION 5.0

INTERACTION NOISE

5.1 BACKGROUND

The interaction of a turbine tone with the fan/core jet stream turbulence results in a drop in the blade passing frequency (BPF) sound pressure level and a spread in the signal bandwidth, which is manifested as a haystack in the narrowband spectrum. Section 5 of Volume II qualitatively explains this shift in discrete frequency acoustic energy into sidebands through scattering of the coherent signal by turbulence cells in the jet mixing region(s). A simplified model shows that, as a coherent signal propagates through a region of turbulence, part of the incident acoustic energy is redistributed into a scattered wave by the turbulence cells. The time variation of turbulence seen by the incident wave produces a change in the frequency of the outgoing wave and results in a broadening of the acoustic signature. The nature of the broadening can be inferred from the form of the time autocorrelation functions of the amplitude and phase fluctuations. In particular, the frequency spread is determined by the correlation time of the turbulence eddies. The amplitude transformation is a strong function of the correlation length, of the eddies, and of the turbulence intensity.

Using a limiting case (a full ON/full OFF switching mechanism where the tone is completely cut off except for a brief time interval Δt), the frequency spread is given by:

$$(\Delta\omega)(\Delta t) \sim 1 \qquad (5.1\text{-}1)$$

where $\Delta\omega = 2\pi\ (\Delta f)$

and Δf = frequency spread over which the signal stays within 6 dB of the maximum value.

The results of the turbulence cell scattering analysis [Volume II, Equations (5.3.3-15) and (-17)] indicate that, at low Mach numbers, the important determinants of the interaction effects include:

- The intensity of the incident tone, $[|A_o^2|/\rho c]$.
- The size of the eddies in the mixing zone, ℓ_c.
- The Mach number of the turbulent velocity fluctuations downstream of the nozzle exhaust plane where the tones propagate out to the surrounding air, M_t.

The following become significant parameters [Volume II, Equations (5.3.3-13) and -14)] when the compressibility and density perturbations imposed by the turbulence cells cannot be ignored:

- The frequency of the incident tone, $\omega_o/2\pi$.

- The difference between the eddy and freestream density and compressibility. Loosely interpreted, this would be a function of the difference between the fan and core stream temperatures.

The section below develops an empirical correlation using the above parameters to define interaction effects.

5.2 EMPIRICAL CORRELATION FOR INTERACTION EFFECTS

5.2.1 Introduction

The haystacking phenomenon involves both a reduction in the BPF SPL and a frequency spread (see the narrowband data in Figure 5.2.1-1). If energy is conserved during the modulation process as is assumed, there must exist a functional relationship between the reduction and the spread which may be defined empirically and which should result in:

- A correlation between δ, the SPL drop at the blade passing frequency location, and various aerodynamic and engine geometry parameters.

- A measure of frequency spread as a function of δ.

5.2.2 Amplitude Modulation

A δ was defined for purposes of the correlation study as the difference between the pure, unattenuated (discrete frequency) SPL and the modulated peak SPL, as shown in Figure 5.2.1-1. Since the modulation mechanism involved (turbulence scattering) merely results in a redistribution of the tonal energy into sidebands, the unattenuated tone SPL may be approximated by the SPL for the 1/3 octave band containing the BPF. This assumption is supported by the agreement which exists between the turbine tone PWL's in the core nozzle (as determined from narrowband spectra obtained from internal probes) and the farfield PWL's for the 1/3 octave bands containing the tones. The farfield PWL's were determined for Quiet Engines "A" and "C" and for the CF6 in Volume II (Section 5.3.2). δ is defined as:

δ = 1/3 O.B. SPL-Haystack Peak SPL (20 Hz bandwidth) (5.2.2-1)

Acoustic data from Quiet Engine "C" (nominal and coplanar configurations) and from the TF34 were compiled for this study. Only those data points were utilized where the tone (or haystack) clearly dominated the 1/3 octave band SPL.

Figure 5.2.2-1 shows δ as a function of the power setting. The increase of δ with speed is as expected. The data for the three configurations appear to fall on three parallel lines. The major difference between the two Engine

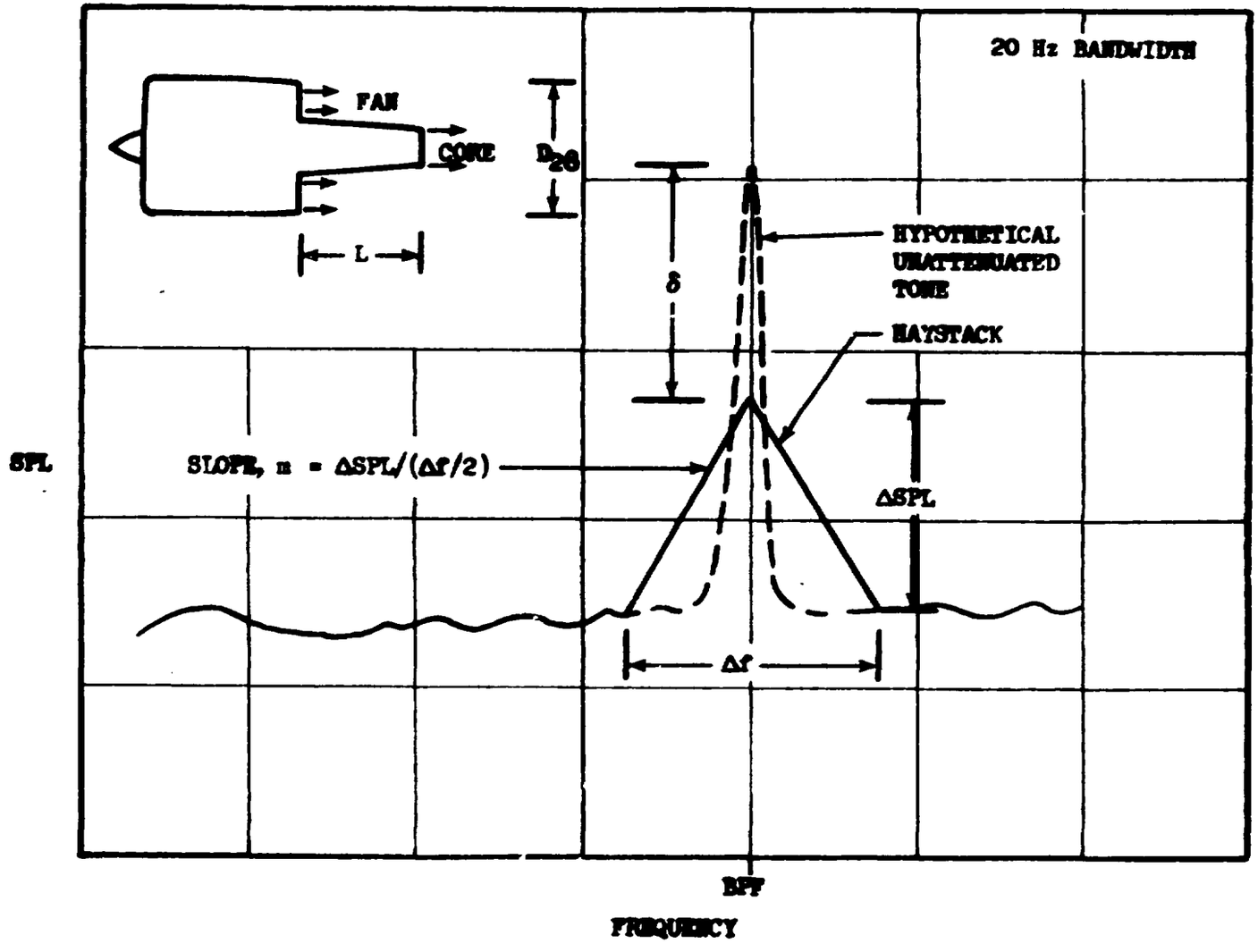

FIGURE 5.2.1-1 DEFINITION OF INTERACTION EFFECTS.

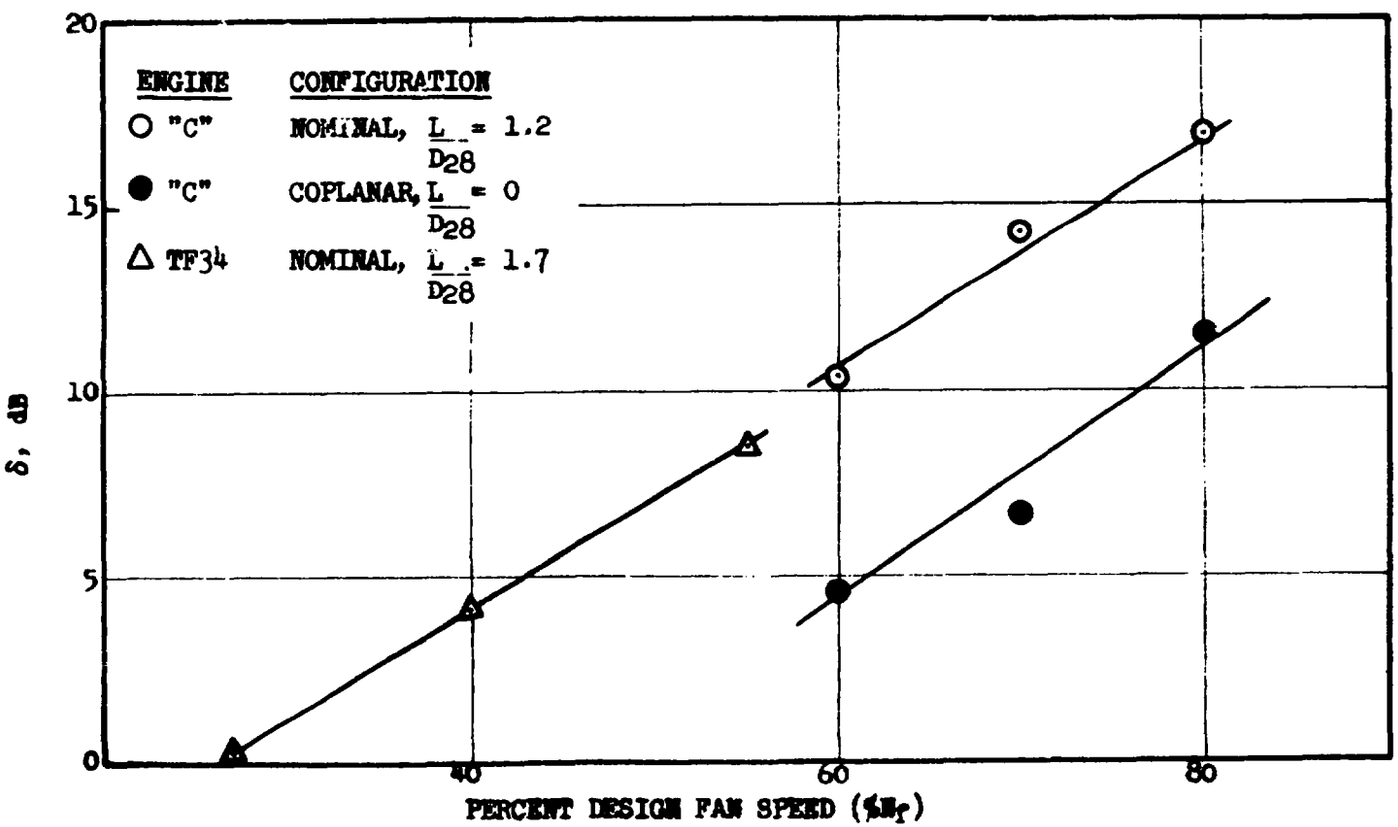

FIGURE 5.2.2-1 AMPLITUDE MODULATION AS A FUNCTION OF SPEED SETTING.

"C" configurations is the relative location of the fan and core nozzle exhaust planes. This suggests using the distance (L) between the two exhaust planes as a normalizing parameter. Figure 5.2.2-2 shows that a 20 log $(1 + L/D_{28})$ factor collapses the Engine "C" data. Here, the fan nozzle outer diameter (D_{28}) is used to nondimensionalize L (thereby providing a size correction). The correction is in agreement with the analysis of Volume II, Section 5.3.3, and the results of Ho and Kovasznay (Reference 5.2.2-1) which indicate that the thickness of the turbulence zone and the turbulence intensity at the tone propagation point are important determinants of the tone modulation. Both the turbulence thickness and the intensity encountered by the turbine tone are strong functions of L/D_{28}.

The linear relationship between δ and % N_f is somewhat misleading. The percent speed setting encompasses a multitude of other parameters, and a similar relationship would be encountered for a number of other quantities. The problem is to identify the independent parameter(s).

Per the analysis of Section 5.3.3, Volume II, the turbulence velocity (and therefore the jet velocity) is seen to influence the scattering. The fan and core jet velocities, the relative velocities, and the velocity ratio were examined and it was found that a data collapse could be achieved with the fan exhaust velocity as the correlating parameter (Figure 5.2.2-3). The correlating line is approximately given by:

$$\delta = 40 \log_{10}\left(\frac{V_{28}}{100}\right) + 20 \log_{10}\left(1 + \frac{L}{D_{28}}\right) - 25, \text{ dB} \qquad (5.2.2\text{-}2)$$

where V_{28} is the fan exhaust velocity in ft/sec.

Equation (5.2.2-2) is applicable for positive values of δ only. Because of the narrow frequency range used and the limited data, it was impossible to separate out the tone frequency dependence.

5.2.3 Frequency Spread

Haystacks in farfield narrowband spectra can normally be approximated by a triangle, as shown in Figure 5.2.3-1. The slope of the sides provides a convenient measure of the frequency spread (Figure 5.2.1-1). The slope (m) is defined as:

$$m = \frac{\Delta SPL}{(\Delta f/2)} \qquad (5.2.3\text{-}1)$$

where Δf is the frequency spread suffered by the tone and ΔSPL represents the haystack amplitude, as seen in a 20 Hz bandwidth spectrum.

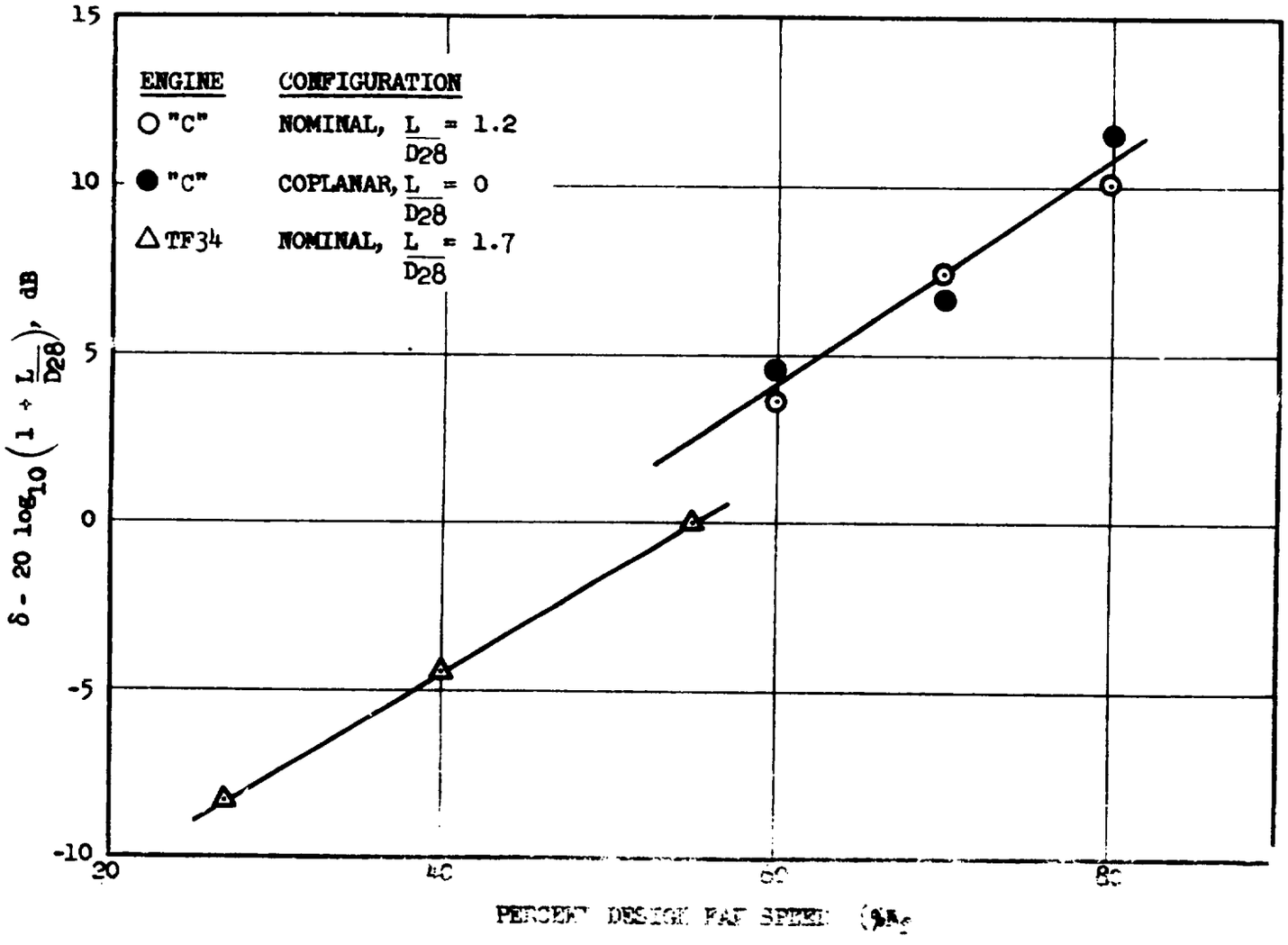

FIGURE 5.2.2-2 EFFECT OF RELATIVE LOCATION OF FAN AND CORE NOZZLE EXHAUST PLANES ON TONE AMPLITUDE LOSS.

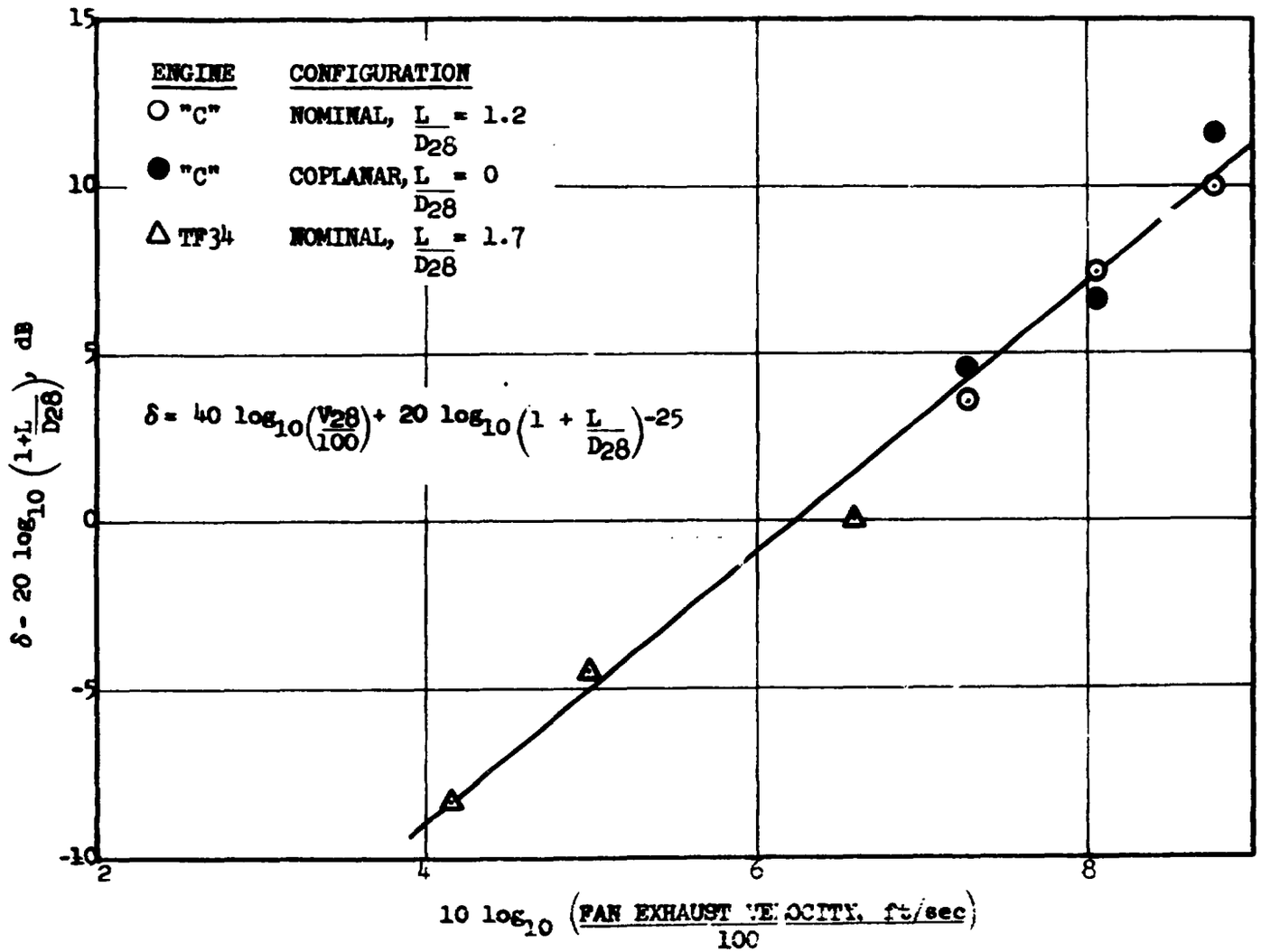

FIGURE 5.2.2-3 CORRELATION FOR INTERACTION EFFECTS.

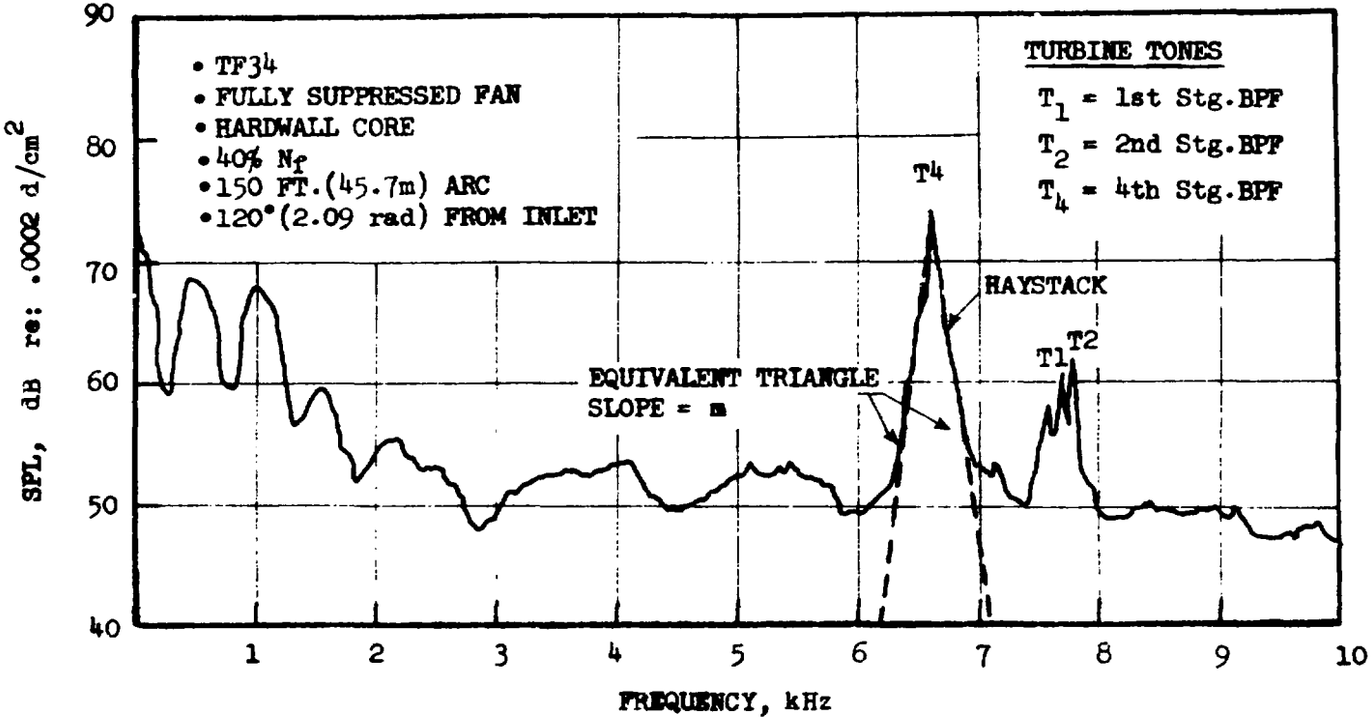

FIGURE 5.2.3-1 APPROXIMATION OF A HAYSTACK BY A TRIANGLE IN ORDER TO DETERMINE THE FREQUENCY SPREAD.

The interaction mechanism apparently does not involve amplification, but merely involves redistribution of the discrete frequency acoustic energy into adjacent bands (see Section 5.3 of Volume II). Conservation of energy therefore implies a unique relationship between the frequency spread and the amplitude drop, regardless of the engine configuration. This relationship is demonstrated by Figure 5.2.3-2 in which 10 log (1/m) is plotted against δ for the TF34 and for both Engine "C" configurations. The rough correlation line shown in Figure 5.2.3-2 may be expressed as:

$$10 \log_{10} (1/m) = .85 (\delta) + 8.4 \qquad (5.2.3\text{-}2a)$$

$$\text{or} \quad (1/m) = 6.92 \times 10^{.085(\delta)} \qquad (5.2.3\text{-}2b)$$

Analysis (Volume II, Section 5.3) does indicate a frequency dependence, therefore it is suggested that a 20 log f correction (increasing haystacking with frequency) be used with Equation (5.2.2-2) till data to the contrary become available. This f^2 dependence falls out of the classical works of Tatarski and others.

5.3 SUMMARY - FLOW CHARTS

Turbine tones propagating through the jet stream turbulence regions suffer frequency and amplitude modulation resulting in a decrease in the discrete frequency amplitude along with a spread in the signal bandwidth. This phenomenon has been termed "haystacking". A correlation was derived to predict the extent of the scattering at the max angle (120°) using available high bypass engine data. The prediction method formulation is outlined in Table 5.3-1 and a flow chart for estimating the interaction effects is given in Figure 5.3-1.

A haystack is modeled as a triangle on a 20 Hz bandwidth spectral basis (Figure 5.2.1-1). The modulated tone is described by a loss (δ) in the amplitude and a change in the slope (m) of the triangular sides.

The amplitude loss (δ) is obtained from Equation (5.2.2-1) as a function of the fan jet velocity and the relative location of the fan and core nozzle exhaust planes:

$$\delta = 40 \log_{10} \left(\frac{V_{28}}{100}\right) + 20 \log_{10} \left(1 + \frac{L}{D_{28}}\right) - 25 \text{ (dB)} \qquad (5.2.2\text{-}2)$$

(V_{28} = ft/sec)

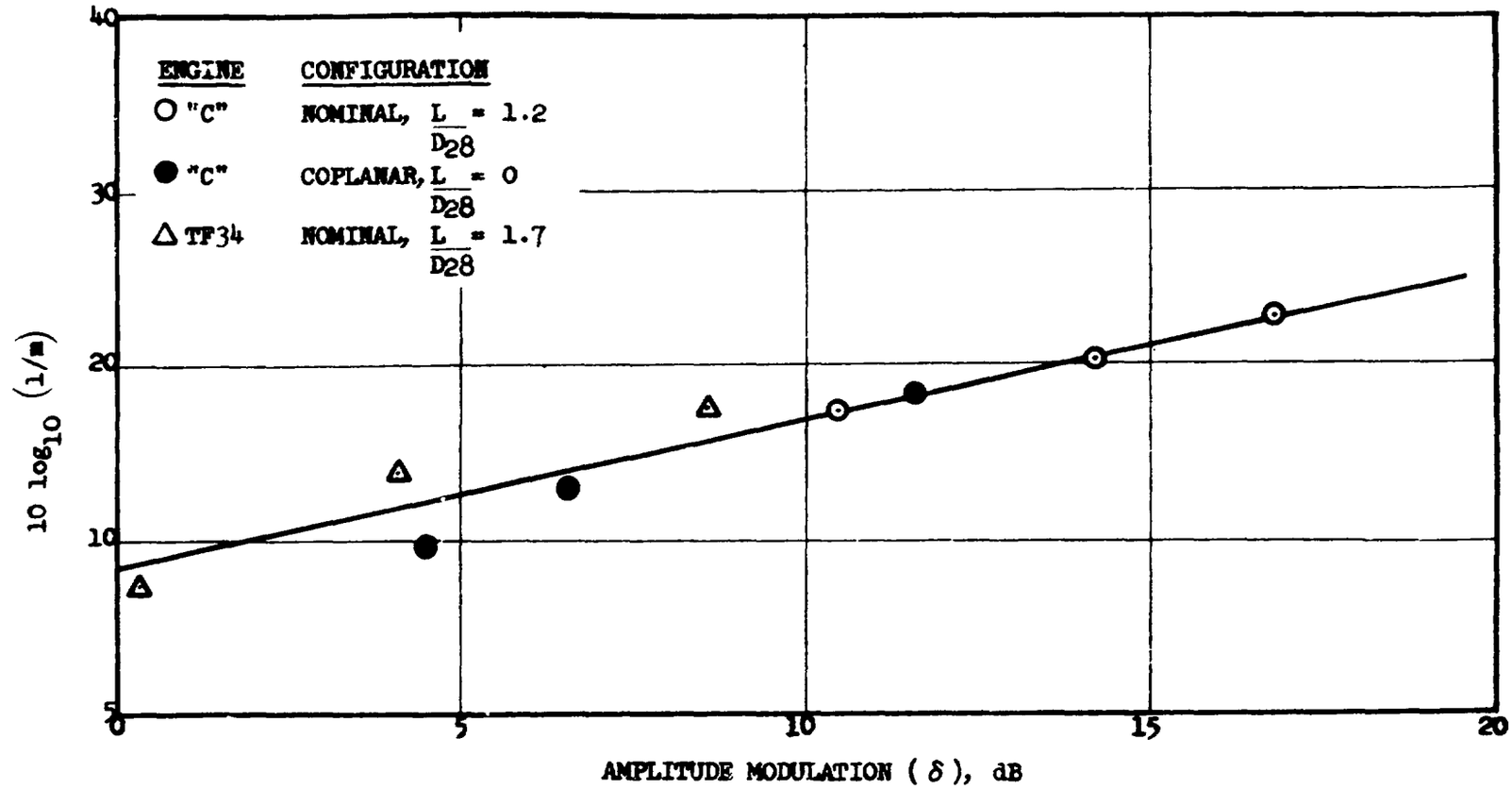

FIGURE 5.2.3-2 RELATIONSHIP BETWEEN FREQUENCY SPREAD AND TONE AMPLITUDE LOSS.

Table 5.3-1. Prediction of Interaction Effects.

- Semiempirical Relationships. Correlating Parameter is the Fan Exhaust Velocity

- INPUT

  Fan Exhaust Velocity

  Distance Between Fan and Core Nozzle Exhaust Planes

  Outer Diameter of Fan Nozzle

- OUTPUT

  Tone Amplitude Loss

  Frequency Spread

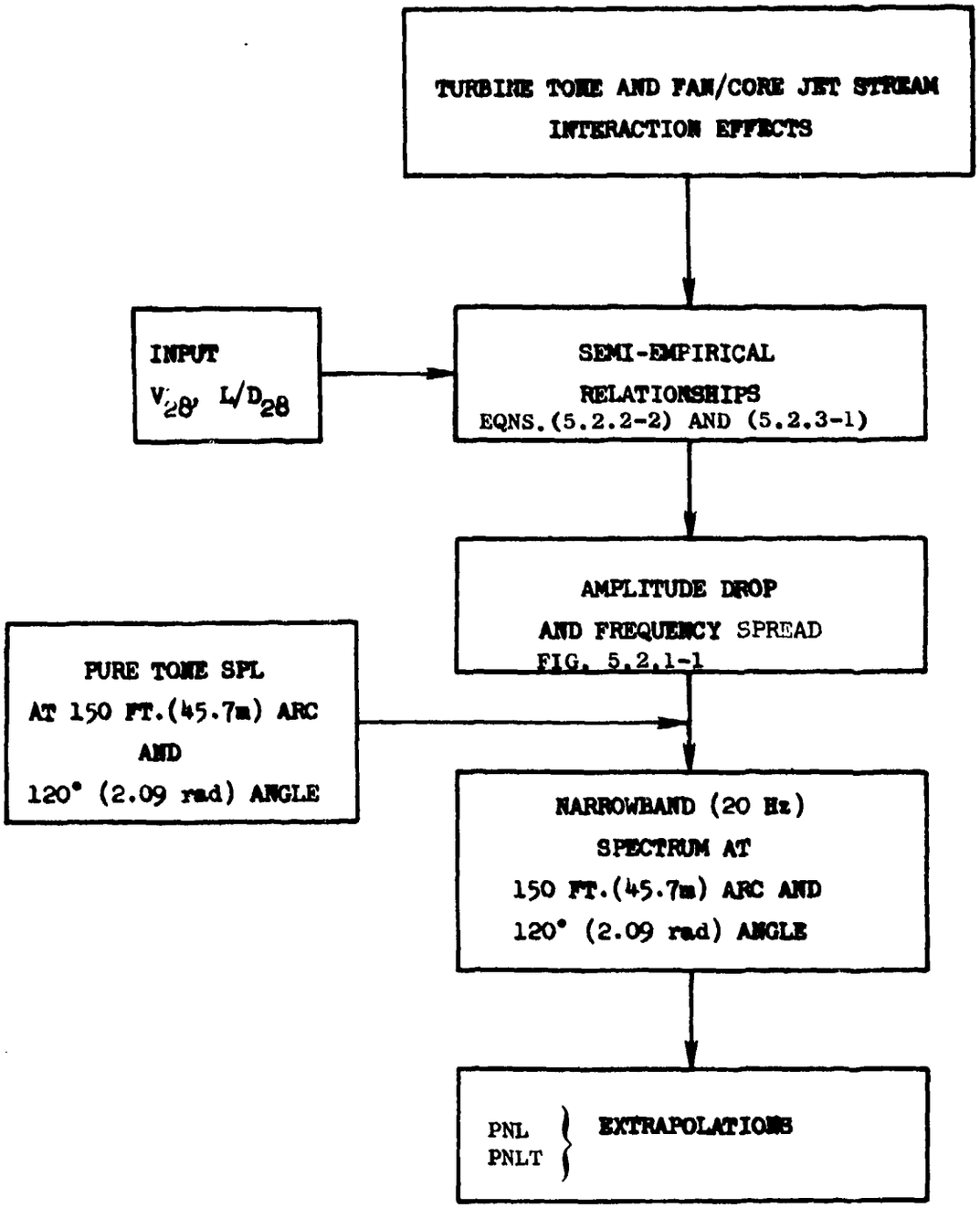

FIGURE 5.3-1 FLOW CHART FOR ESTIMATING TURBINE TONE INTERACTION EFFECTS.

In addition, a frequency correction may be added through 20 log f for very high frequencies (>10k Hz). The f^2 variation is indicated by analysis.

The slope (m) of the haystack triangle is computed from Equation (5.2.3-2b) as a function of δ:

$$(1/m) = 6.92 \times 10^{0.085\delta} \qquad (5.2.3\text{-}2b)$$

Example:

Given:

V_{28} = 600 ft/sec

L/D_{28} = 1.0

Predicted 5000 Hz tone = 80 dB

Calculate:

$$\delta = 40 \log_{10}\left(\frac{600}{100}\right) + 20 \log_{10}(2) - 25 \qquad \text{(Equation 5.2.2-2)}$$

$$= 12.1 \text{ dB}$$

$$1/m = 6.92 \times 10^{(.085 \times 12.1)} \qquad \text{(Equation 5.2.3-2b)}$$

$$= 73.91$$

$$\frac{\Delta f/2}{\Delta SPL} = 73.91 \qquad \text{(Equation 5.2.3-1)}$$

the observed 20 Hz bandwidth SPL at 5000 Hz would be 67.9 dB and the frequency spread at a location 6 dB below this would be given by:

$$\Delta f = 2 \times 6 \times 73.91$$

$$= 889 \text{ Hz}$$

The turbine noise prediction method of Section 4 includes the above haystacking prediction method and provides a means of identifying the propagation effects for unusual configurations such as coplanar exhausts and diverted fan flows.

The correlating equation suggests that the amount of haystacking may be minimized by cutting down on the distance between fan and core exhaust planes and by decreasing the fan velocity. These two parameters determine

the thickness of the mixing region and the extent of turbulence encountered by the turbine tone propagating out of the core nozzle.

The analysis of Volume II indicates that the phenomenon is frequency dependent and that the modulation increases with frequency. The Volume II analysis also shows that the haystacking increases with the eddy correlation length, ℓ_c.

Haystacking provides a means of reducing the PNL, and therefore the effect may be desirable.

References

5.2.2-1 Ho, C., and Kovasznay, L.S.G.; "Acoustic Wave Propagation Through a Two-Dimensional Turbulent Jet", Interagency Symposium on University Research in Transportation Noise, Volume I, Stanford University, Stanford, California (March 1973).

SECTION 6.0

OBSTRUCTION NOISE

6.1 BACKGROUND

Struts, pylons, flameholders and sensing probes are some examples of typical obstructions thay may exist in the flowpath of jet engines. Flow of air over these bodies generates acoustic radiation. Obstruction noise can be controlled by proper design of the struts. Typical acoustic data from engines with struts having blunt shapes and streamlined shapes are presented in Volume I. An extensive series of model tests was conducted to measure the influence of various geometric and aerodynamic parameters on the overall acoustic power level and the power level spectrum (Volume II, Section 6.0). An empirical method was formulated to predict the overall power level and the one-third octave band power level spectrum for obstructions placed in smooth uniform flow. Details of the prediction model are given below.

6.2 PREDICTION METHOD

6.2.1 Overall Power Level

The overall acoustic power level radiated by strut-shaped bodies placed in low turbulence flow is given by

$$OAPWL = 10 \log_{10}(\ell \cdot t_{max} \cdot h \cdot \bar{U}_o^5) + 4 \log_{10} C_D + 16.8, \quad \text{db re } 10^{-13} \text{ watt} \qquad (6.2.1\text{-}1)$$

where

ℓ = chord, ft

t_{max} = maximum thickness, ft

h = span, ft

$\bar{U}_o$ = Upstream mean axial velocity, ft/sec

C_D = profile drag coefficient

This formulation is valid for angles of attack in the range of 0° to 15°, Reynolds numbers in the range 3×10^5 to 1×10^6 and smooth, low turbulence flows.

6.2.2 One-Third Octave Band Power Level Spectrum

The one-third octave band power level spectrum is presented in a normalized form in Figure 6.2.2-1. A normalized 1/3 OB PWL is defined as

$$PWL_N = PWL_{1/3\ OB} - OAPWL_{calculated} \qquad (6.2.2\text{-}1)$$

This is plotted in Figure 6.2.2-1 versus a thickness-based Strouhal number defined as

$$f^* = \frac{f\delta}{U_o} \qquad (6.2.2\text{-}2)$$

where δ = maximum thickness, inches

f = frequency, Hz

The spectrum for any specific condition may be obtained as follows:

(i) Calculate OAPWL from Equation (6.2.1-1)

(ii) For each 1/3 OB frequency of interest, calculate $f^* = \frac{f\delta}{U_o}$

(iii) Read PWL_N from Figure 6.2.2-1 corresponding to f*

(iv) Obtain the 1/3 OB PWL at the chosen f as

$$PWL_{1/3\ OB} = PWL_N + OAPWL$$

(Note that t_{max} is in feet and δ is in inches)

6.3 COMPARISON WITH AVAILABLE DATA

The OAPWL calculated by using the correlation of Equation (6.2.1-1) is shown plotted in Figure 6.3-1 versus the measured OAPWL for eight configurations tested at $\alpha° = 0$. The correlation was derived from the measured data. The line drawn at 45° to either axis indicates that the correlation collapses the data very well. Data obtained in two other tests are listed below and are plotted as the solid symbols on Figure 6.3-1.

(a) Hayden et al., References 6.3-1 and 6.3-2
NACA 0012 Airfoil
chord = 6", wetted span = 16", δ = 0.72", $\bar{U}_o$ = 100 fps, C_D = 0.007, $\alpha° = 4$
Measured OAPWL = 94.7 dB re 10^{-13} Watt
OAPWL calculated by the proposed model = 94.5 dB re 10^{-13} Watt
This is plotted as the solid square in Figure 6.3-1.

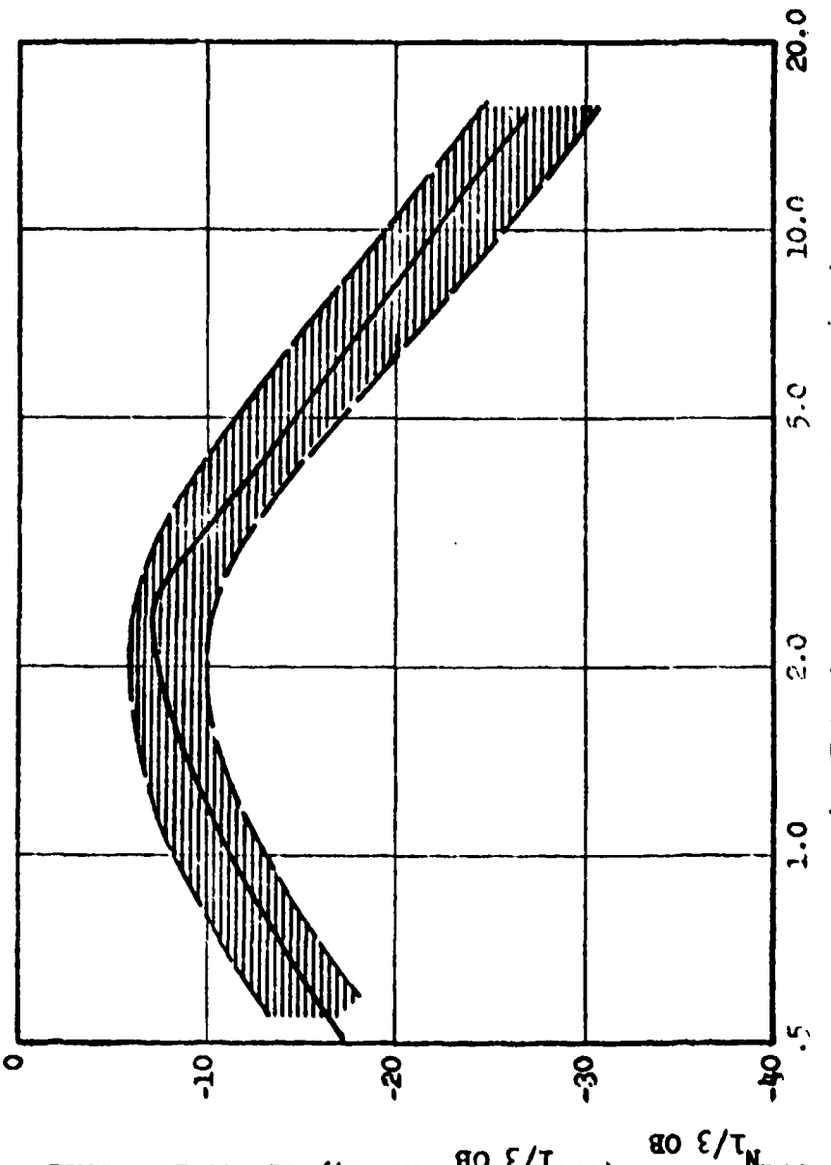

FIGURE 5.2.2-1 NORMALIZED SPECTRUM OF OBSTRUCTION NOISE

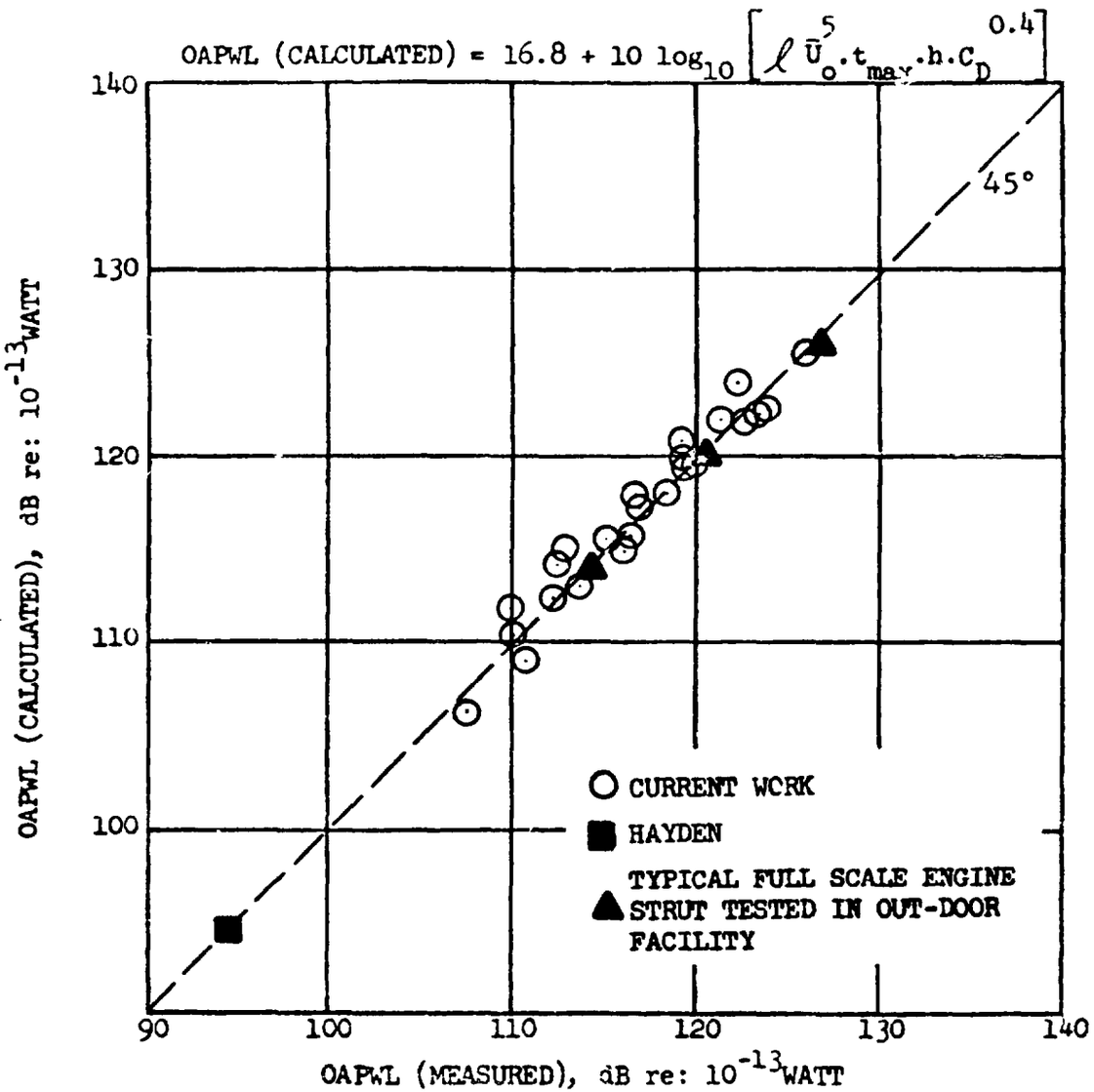

FIGURE 6.3-1 COMPARISON BETWEEN CALCULATED AND MEASURED OVERALL POWER LEVELS. $a^0 = 0$, ALL CONFIGURATIONS, M = 0.30, 0.40, 0.45.

(b) Typical Full-Scale Engine Strut Noise Test - GE

Comparison of the calculated OAPWL with data measured from tests on a typical full-scale engine strut also indicates excellent agreement. These tests were conducted in a different test facility from that in which the data used to arrive at the correlation were obtained. Acoustic measurements were made by means of microphones located on a 25 ft arc at angles of 20°, 30°, 40°, 50°, 60°, 70°, 80°, and 90° relative to the duct exit axis. (The current core engine tests were conducted in a semireverberent room.) The significant parameters are listed below:

Elliptical Section:

δ = 0.73", ℓ = 1.74", h = 4", $\alpha°$ = 0

C_D = 0.15 (Reference 6.3-3)

$\bar{U}_o$ (fps)	OAPWL calculated (dB)	OAPWL measured (dB)
335	114.3	114.5
445	120.2	120.8
588	126.6	126.8

These data are shown in Figure 6.3-1 as solid triangles. Figure 6.3-1 thus collapses data obtained from three entirely independent sources under different test conditions.

6.4 SUMMARY - FLOW CHART

A method is presented to predict the overall power levels and 1/3 octave band power level spectra for acoustic radiation from struts placed in a smooth, uniform flow. The parameters required for the prediction are the mean upstream axial flow velocity and the strut chord, maximum thickness, wetted span and profile drag coefficient. A flow chart is provided in Figure 6.4-1. The method is based on a correlation of data from a series of model tests in a free jet. The formulation is valid for angle of attack below 15°, a Reynolds number range (based on the chord) of 3×10^5 to 1×10^6, and smooth, nonturbulent flows.

To apply the method, the OAPWL is computed from Equation (6.2.1-1):

$$OAPWL = 10 \log_{10} (\ell . t_{max} \; h . \bar{U}_o^5) + 4 \log_{10} C_D + 16.8 \qquad (6.2.1\text{-}1)$$

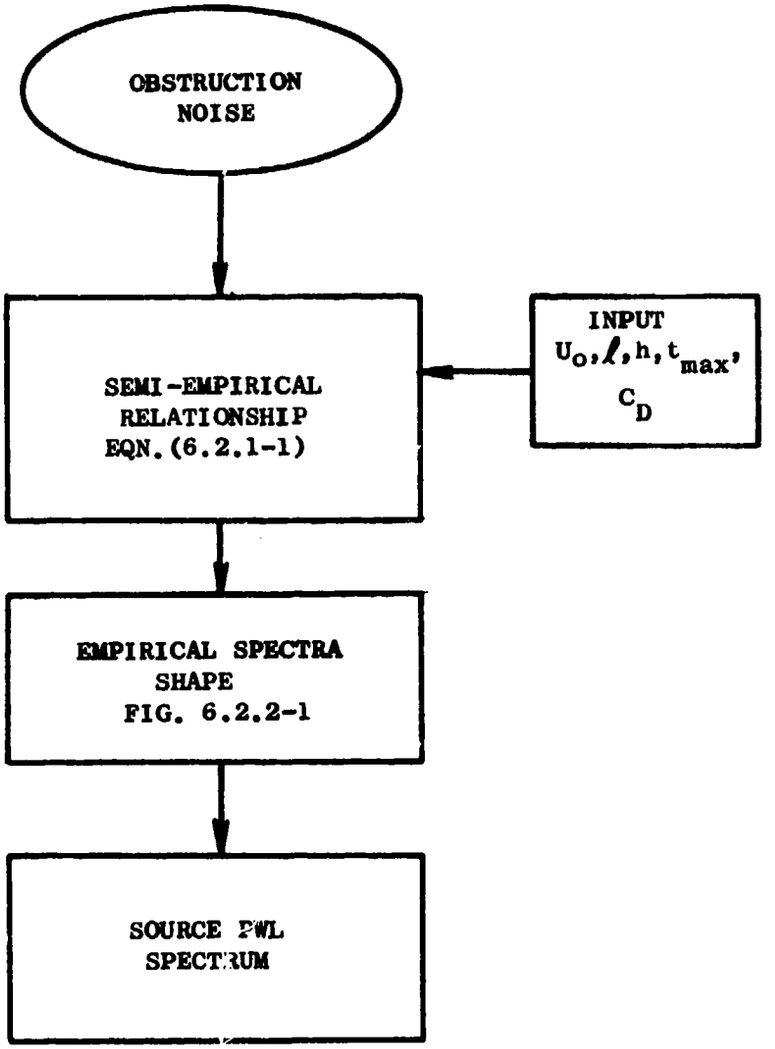

FIGURE 6.4-1 FLOW CHART FOR ESTIMATING OBSTRUCTION NOISE.

The power level spectrum is then obtained using

$$PWL_{1/3\ OB} = OAPWL + PWL_N \qquad (6.4\text{-}1)$$

where PWL_N is given by Figure 6.2.2-1 for each 1/3 octave band as a function of the Strouhal number (based on the max thickness).

This prediction method shows excellent agreement with acoustic data from other obstruction noise tests.

Several noise reduction techniques are provided by the prediction equation. The largest effect is obtained by reduction of the inflow velocity, amounting to a 50 log effect. Decrease in the strut size would also afford noise relief, for example, through a drop in the chord or max thickness. Finally, it can be seen that aerodynamic faring to reduce the profile drag coefficient will reduce the noise generated. For example, merely rounding the corners of a rectangular strut can drop the drag coefficient five fold, which provides 3 dB of suppression.

References

6.3-1 Hayden, Richard W.; "Noise from Interaction of Flow with Rigid Surfaces: A Review of Current Status of Prediction Techniques", Bolt, Beranek and Newman Report No. 227b.

6.3-2 Hersh, Alan S. and Hayden, Richard W.; "Aerodynamic Sound Radiation from Lifting Surfaces with and without Leading-Edge Serrations", NASA CR-114370.

6.3-3 Hoerner, Sighard F.; Fluid Dynamic Drag, Published by Author, 1965.

SECTION 7.0

CASING RADIATION

7.1 INTRODUCTION

The effect of casing radiation on overall engine noise is examined in Section 2.2.6 of Volume I. Under certain circumstances, casing radiation is concluded to have a measurable effect on the engine noise spectrum. Section 7 of Volume II explores the various engine configuration and structural properties, which have an effect on the degree of casing radiation, to expect from a turbomachinery component.

Casing radiation is determined by evaluating the component source noise and applying the casing transmission characteristics contained in Section 7.3 of Volume II. It is not often practical in the engine preliminary design stage, however, to address casing radiation in such detail. With the preliminary evaluation concept in mind, this section therefore contains a less detailed, more practical core engine casing radiation noise prediction procedure.

7.2 DERIVATION OF THE SOURCE SPECTRUM

The J79 data previously examined in Volume II were used to develop this source spectum prediction method. Acoustic data taken with casing and nearfield microphones were used in the correlation (Figure 7.2-1). Nearfield microphone #21 (Figure 7.2-1) was selected to compute the core acoustic radiation through the casing in order to minimize contamination from residual inlet and exhaust noise. Data for the 90% and 100% speed points were obtained from 40 Hz narrowband plots and summed to provide 1/3 octave band levels shown in Figure 7.2-2.

The two spectra were then collapsed by means of the following correlation:

$$SPL^* = SPL - 10 \log_{10} \dot{W} - 60 \log_{10} U_T$$

or

$$SPL = SPL^* + 10 \log_{10} \dot{W} + 60 \log_{10} U_T \qquad (7.2\text{-}1)$$

where SPL = Value measured by microphone #21, dB re .0002 d/cm^2 @ 8 ft (2.4 m) from the engine casing

$\dot{W}$ = Core flow, lb/sec

U_T = Tip speed of compressor first stage, ft/sec

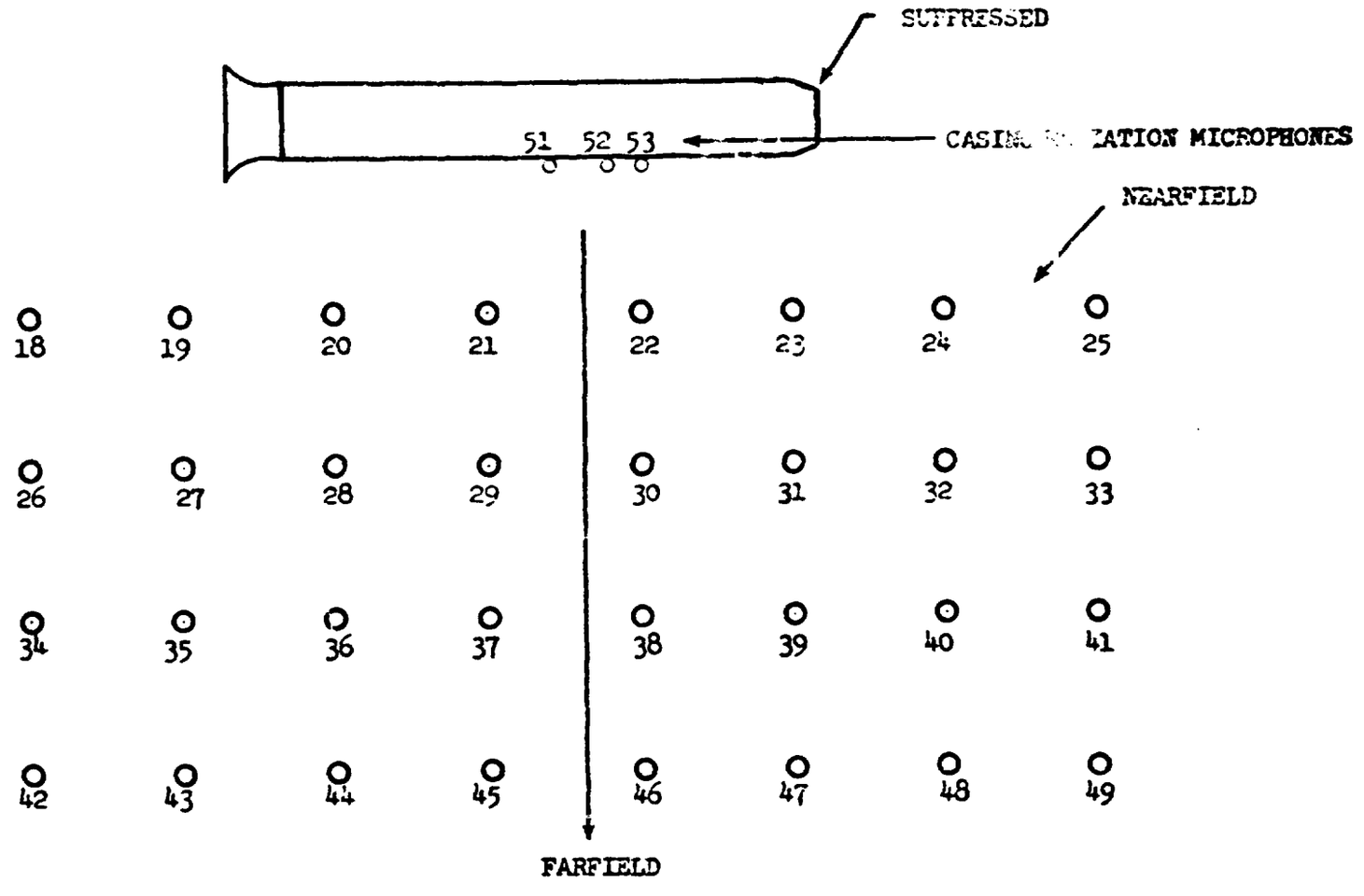

FIGURE 7.2-1 NEARFIELD MICROPHONE ARRANGEMENT FOR J79 TESTS.

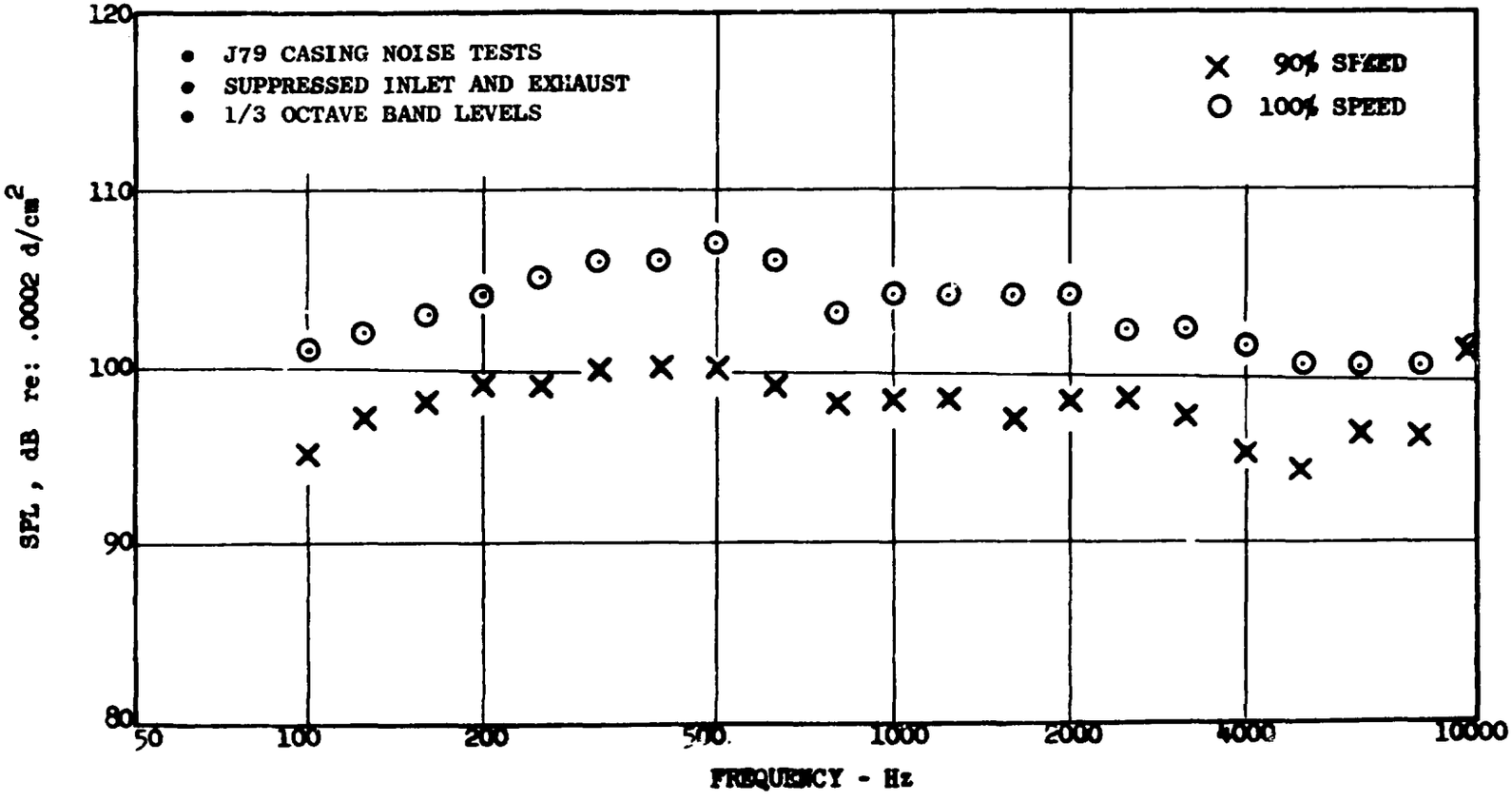

FIGURE 7.2-2 COMPARISON OF NEARFIELD SPECTRA AT TWO SPEEDS- 8 FT.(2.44m) FROM CORE (MICROPHONE #21).

Figure 7.2-3 shows that this normalization is effective in collapsing the J79 spectra.

This spectrum is unique to the J79 engine, but the effect of the casing may be removed by applying the formulae of Section 7.3 of Volume II. A normalized spectrum is then obtained:

$$SPL = K_f + 10 \log_{10} \dot{W} + 60 \log_{10} \left(\frac{U_T}{100} \right) \qquad (7.2\text{-}2)$$

where K_f is given in Table 7.2-1.

Equation (7.2-2) and Table 7.2-1 thus represent a "no casing" source spectrum. In order to obtain the external spectrum, the casing transmission characteristics for the particular engine under study should be applied. The equations of Section 7.3, Volume II, provide these characteristics. Equation (7.2-3) would then be written as

$$SPL = K_f + 10 \log_{10} \dot{W} + 60 \log_{10} \left(\frac{U_T}{100} \right) - TL \qquad (7.2\text{-}3)$$

where TL is the casing transmission loss.

A predicted spectrum is compared to data from a highly suppressed TF34 engine whose fan casing had been wrapped with foam and a lead blanket as a check on the above casing radiated noise estimate (Figure 7.2-4). The agreement is good except for the fan blade passing frequency.

7.3 SUMMARY - FLOW CHART

A preliminary design prediction method is presented for the casing noise spectrum of an engine when little is known about the constituent noise sources. Figure 7.3-1 provides a flow chart for implementing this method which was derived from a correlation of J79 data, using the blade tip speed for the compressor as the correlating parameter. A "no casing" source spectrum (K_f) at 8 ft and 90° is provided in Table 7.2-1. The level of the entire spectrum is adjusted for the compressor tip speed and weight flow through Equation (7.2-2):

$$SPL = K_f + 10 \log_{10} \dot{W} + 60 \log_{10} \left(\frac{U_T}{100} \right) \qquad (7.2\text{-}2)$$

The transmission loss (TL) is computed for the engine casing in question to provide the casing radiation noise at 8 ft and 90°. This spectrum may be extrapolated to any farfield distance using the inverse square law and the appropriate air and ground attenuations.

When the engine cycle has been defined, the casing radiated noise is estimated by first predicting the individual component source noise levels and applying the casing transmission characteristics contained in Section 7.3 of Volume II.

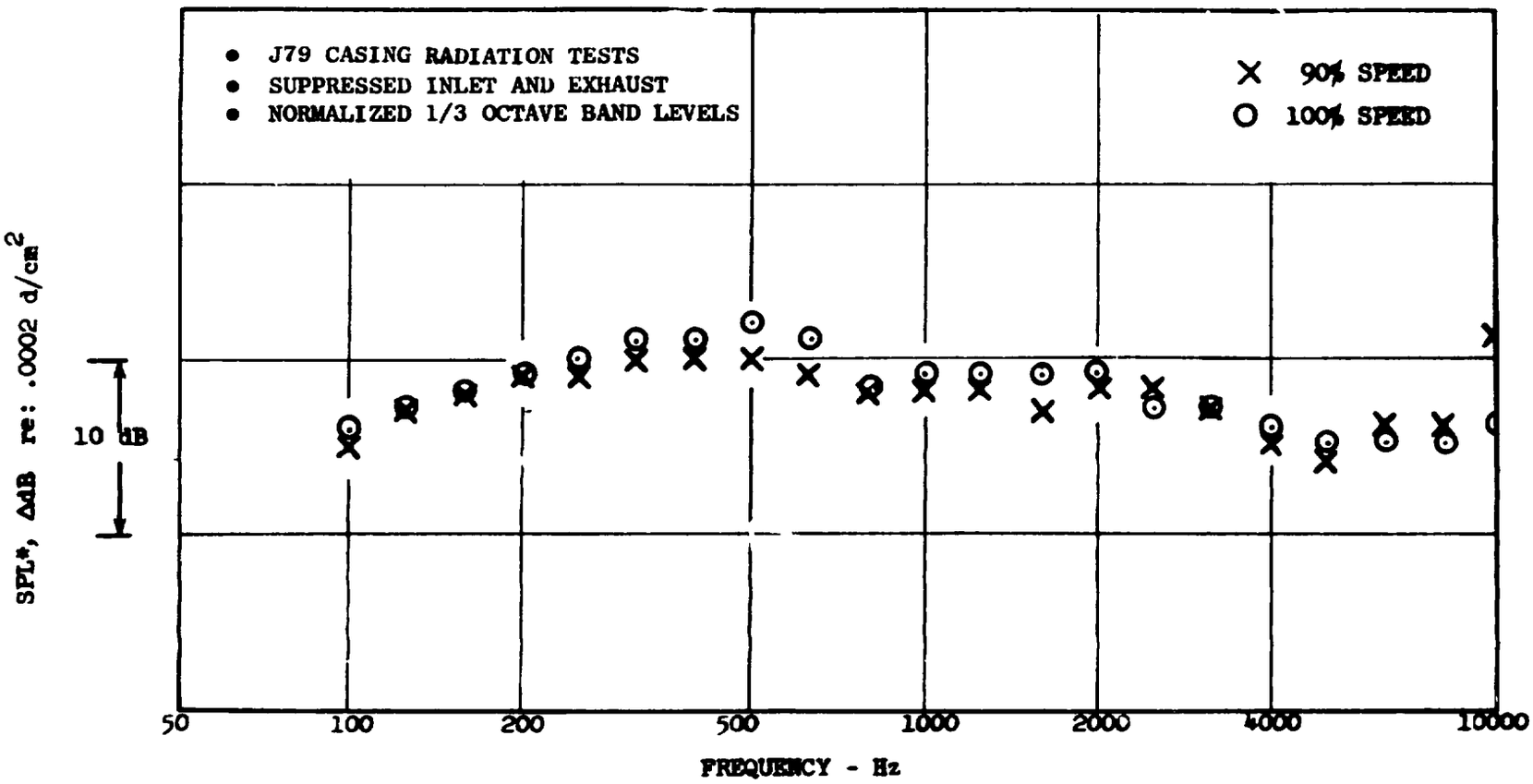

FIGURE 7.2-3 NEARFIELD SPL CORRECTED FOR FLOW AND TIP SPEED.

Table 7.2-1. Casing Radiation Source Correction Factors for Use With Equation 7.2-3.

K_f @ 8 ft SL @ 90°

Hz	K_f	Hz	K_f
100	16	1000	19
125	18	1200	19
160	19	1600	19
200	20	2000	19
250	21	2500	18
315	21	3150	18
400	21	4000	17
500	22	5000	16
630	21	6300	16
800	19	8000	16
1000	19	10000	19

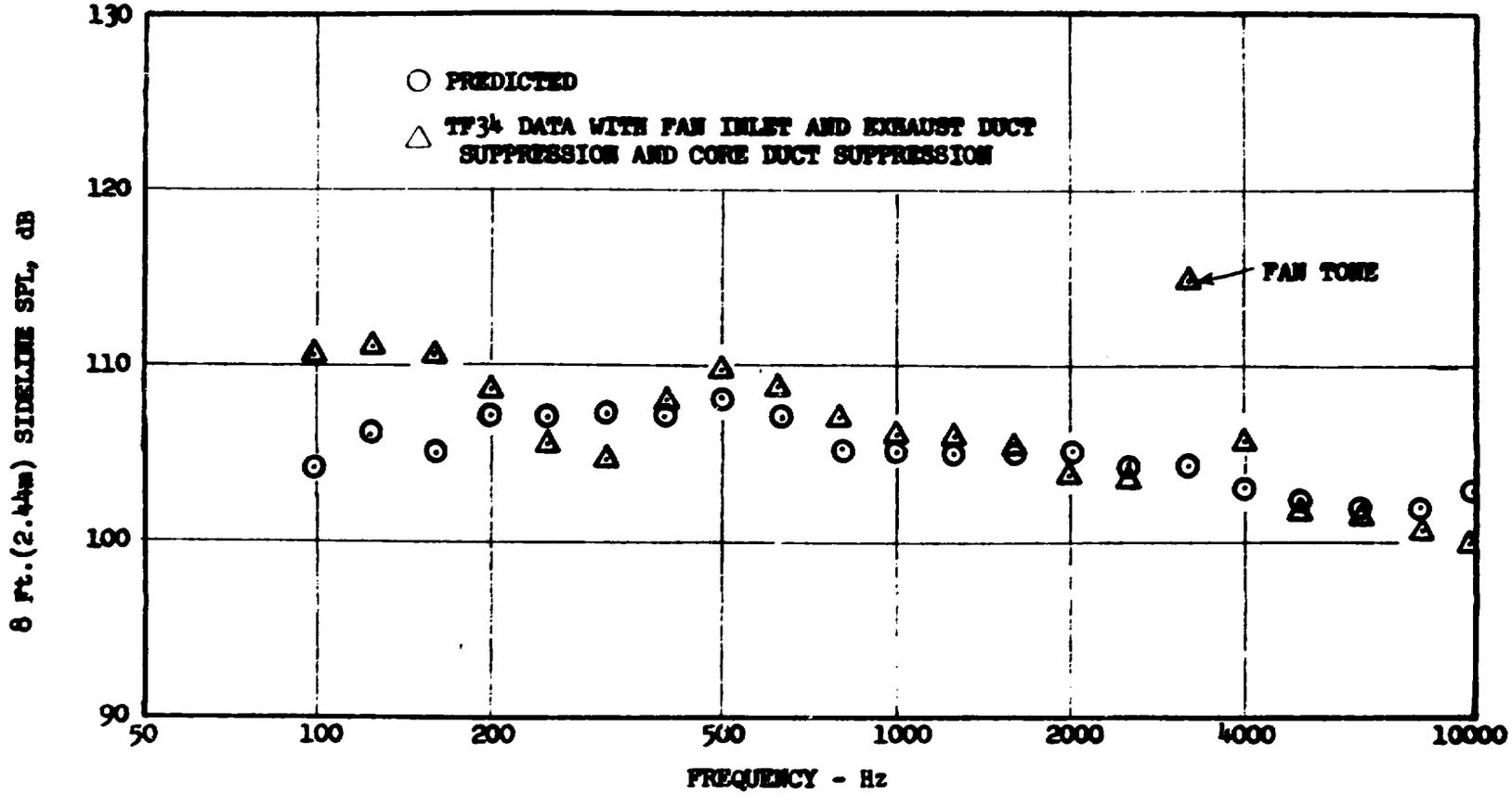

FIGURE 7.2-4 TF34 CASING RADIATION PREDICTION COMPARED TO DATA.

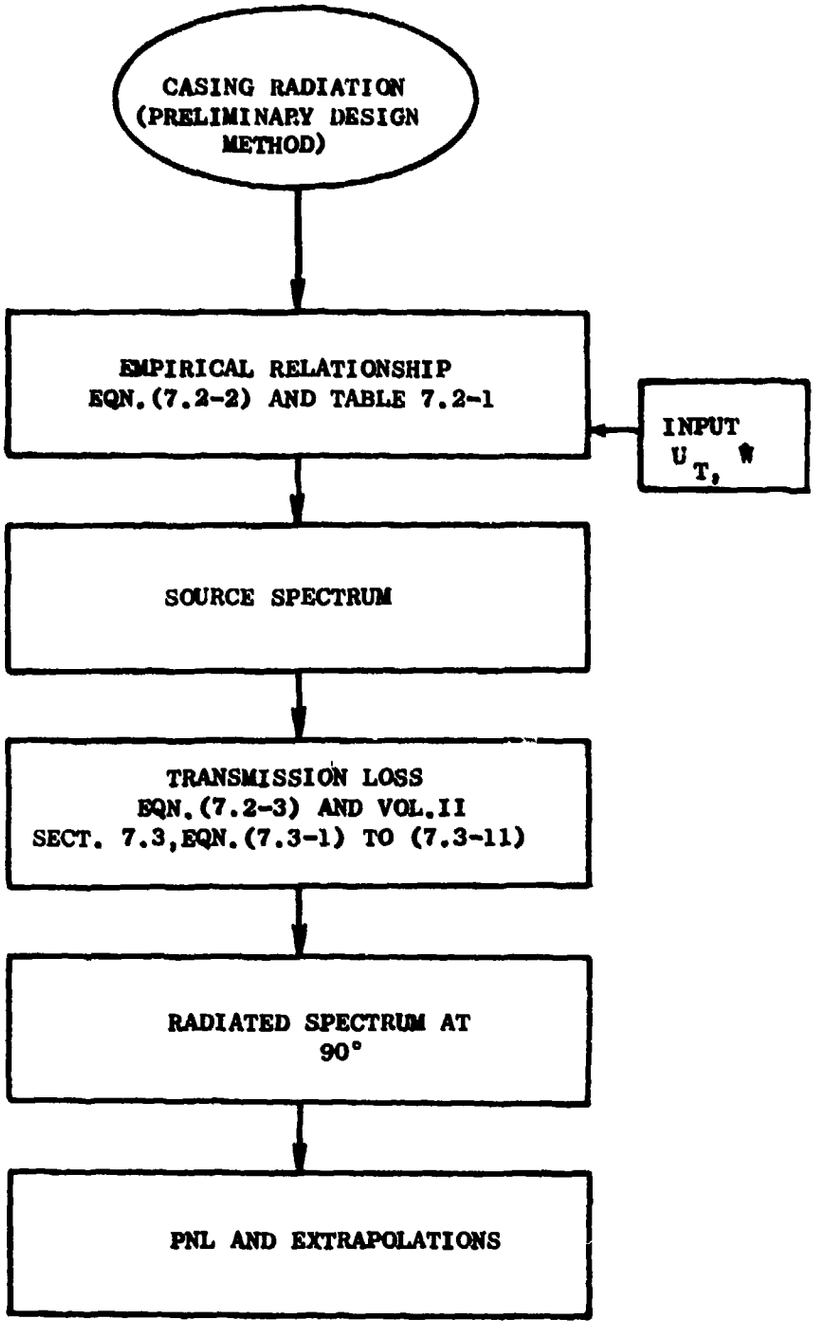

FIGURE 7.3-1 FLOW CHART FOR ESTIMATING RADIATION.

Casing radiation may be reduced by any means that increases the transmission loss. This may be accomplished, for example, through increased casing thickness, visco-elastic wraps or manipulation of the engine casing to obtain high ring and critical frequencies. As explained in Volume II, the transmission efficiency increases at and above the critical and the ring frequencies.

SECTION 8.0

EPNL ESTIMATES OF CORE ENGINE NOISE

8.1 BACKGROUND

The purpose of this section is to provide the EPNL noise estimates for the core engine alone for an aircraft powered by typical turbofan engines. Included are the spectral characteristics of the major core engine noise constituents. Further, the impact of implementing the core engine suppression techniques identified during this program on the core engine EPNL's are also shown.

8.2 CORE ENGINE NOISE

The core engine noise spectra were predicted for a 4-engine aircraft powered by "typical" bypass ratio = 4 engines using the methods provided in this volume. The spectra at the front max (nominally 60°) and aft max angles are shown in Figure 8.2-1 at approach power and 8.2-2 at takeoff power. The corresponding component perceived noise levels (in the form of PNLT's) are provided in bar chart form in Figures 8.2-3 and -4, along with the EPNL's for the core engine alone. The jet noise spectra include simulated flight (relative velocity, Dynamic and Doppler) effects, while the remaining core engine sources include only Dynamic and Doppler effects. The relative velocity corrections imposed on the jet noise are conservative estimates obtained in part by comparison of static and flight data. The jet, combuster and turbine were all contributors to the approach levels, but the aft angle (120°) PNLT was totally dominated by turbine noise. Interaction (Haystacking) effects are included in the turbine noise estimate. The EPNL for the unsuppressed core engine fell about 4.6 EPNdB below FAR36.

At takeoff power, the jet was by far the dominant noise source and turbine noise could not be discerned. At this power setting, the core engine EPNL fell about 4 EPNdB below FAR36.

8.3 APPLICATION OF CORE ENGINE SUPPRESSORS

Core engine technology suppressors were applied to the core engine spectra by assuming the benefits of the following:

- An 18 lobe suppressor nozzle on the core exhaust
- A deep cavity resonator in the core
- Blade row spacing in the low pressure turbine.

The suppressions were applied as follows. Table B3 (Appendix B) was used to define the jet noise suppression at takeoff, giving 2.5 PNdB suppression at the maximum aft angle - 120°. The suppressor tests (Section

- CORE ENGINE NOISE - BR=4 TURBOFAN
- 4 ENGINES; 770000 lb (349580 kg) TOGW
- APPROACH POWER - 40% F_n
- 370 ft (113m) alt., 0.25 M_n

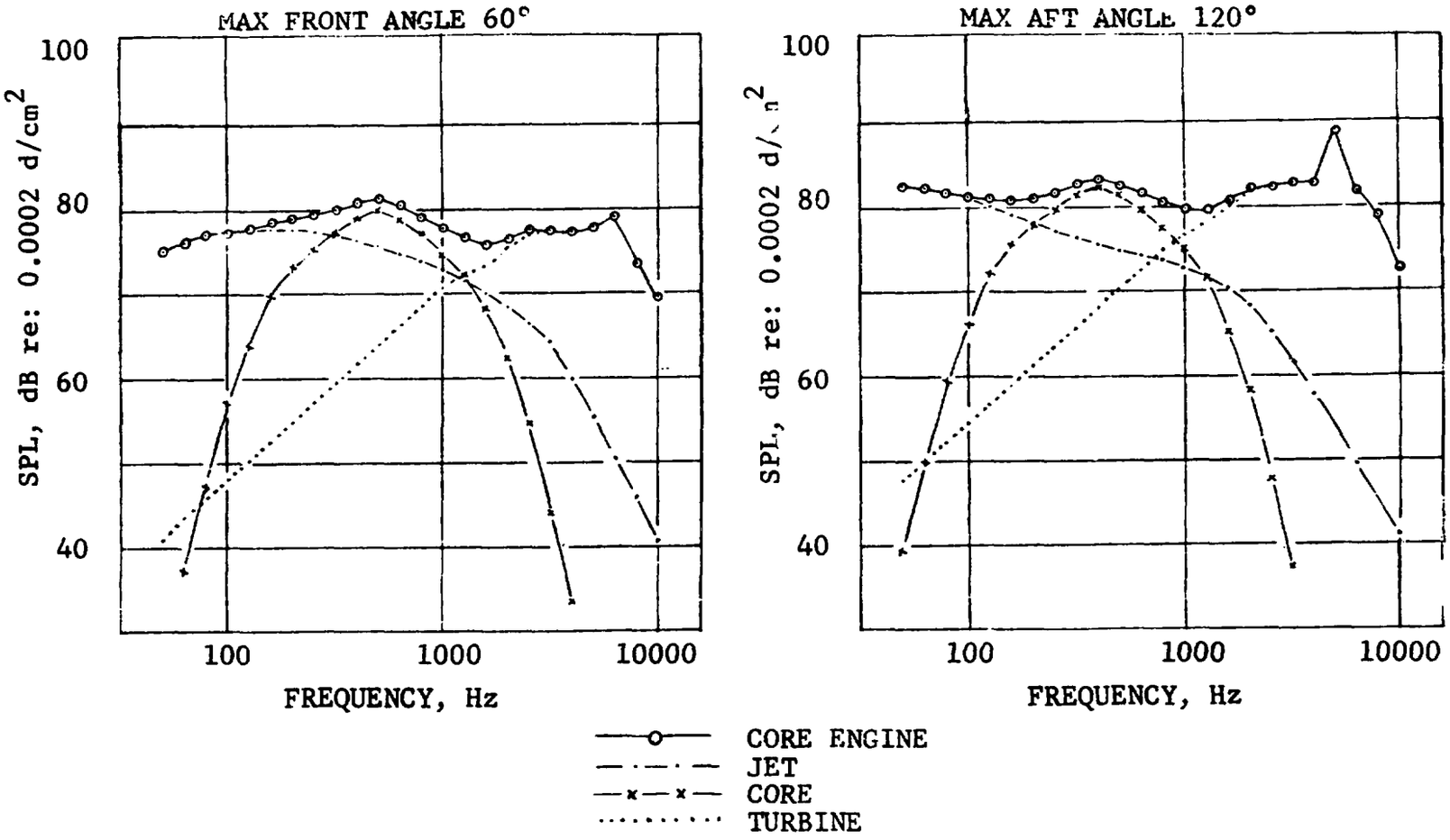

FIGURE 8.2-1 SPECTRAL MAKE-UP OF CORE ENGINE NOISE AT APPROACH

- CORE ENGINE NOISE - BPR=4 TURBOFAN
- 4 ENGINES; 770000 lb (349580 kg) TOGW
- TAKEOFF POWER - 100% F_n
- 1000 ft (305m) alt., 0.3 M_n

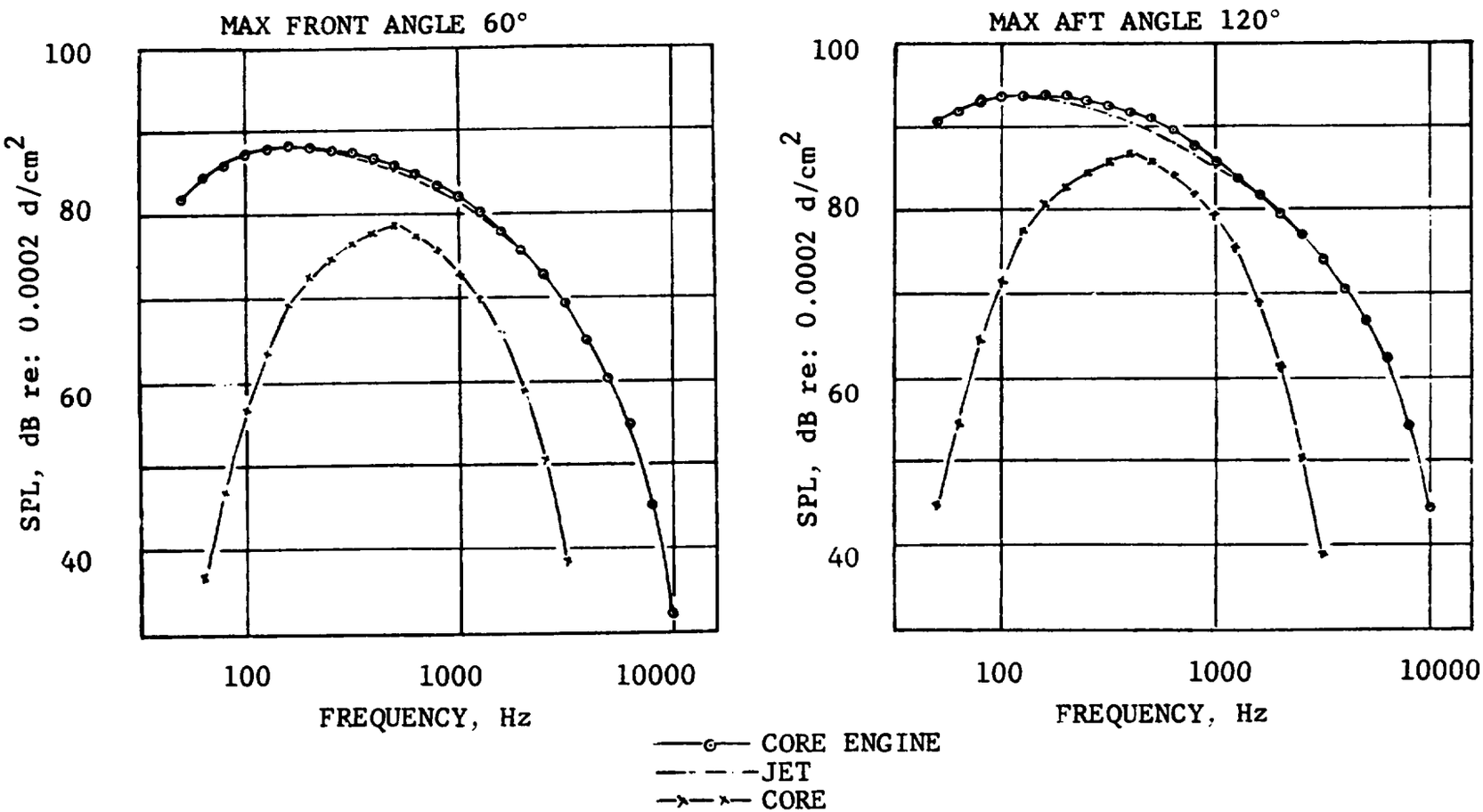

FIGURE 8.2-2 SPECTRAL MAKE-UP OF CORE ENGINE NOISE AT TAKEOFF

- CORE ENGINE NOISE - BR=4 TURBOFAN
- 4 ENGINES; 770000 lb (349580 kg) TOGW
- APPROACH POWER - 40% F_n
- 370 ft (113m) alt., 0.25 M_n

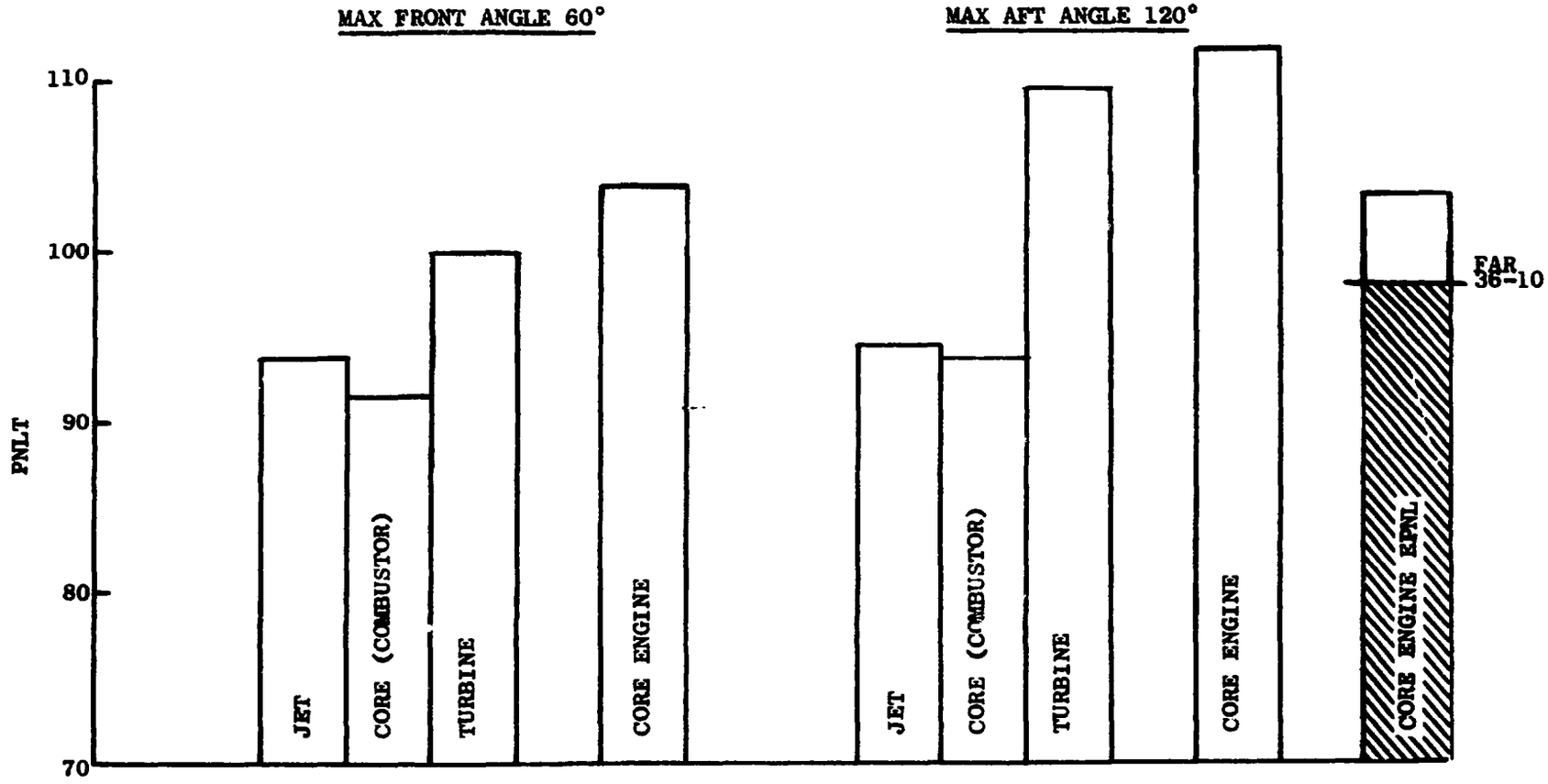

FIGURE 8.2-3 CORE ENGINE NOISE CONSTITUENT BREAKOUT AT APPROACH

- CORE ENGINE NOISE - BR=4 TURBOFAN
- 4 ENGINES; 770000 lb (349580 kg) TOGW
- TAKEOFF POWER - 100% F_n
- 1000 ft (305m) alt., 0.3 M_n

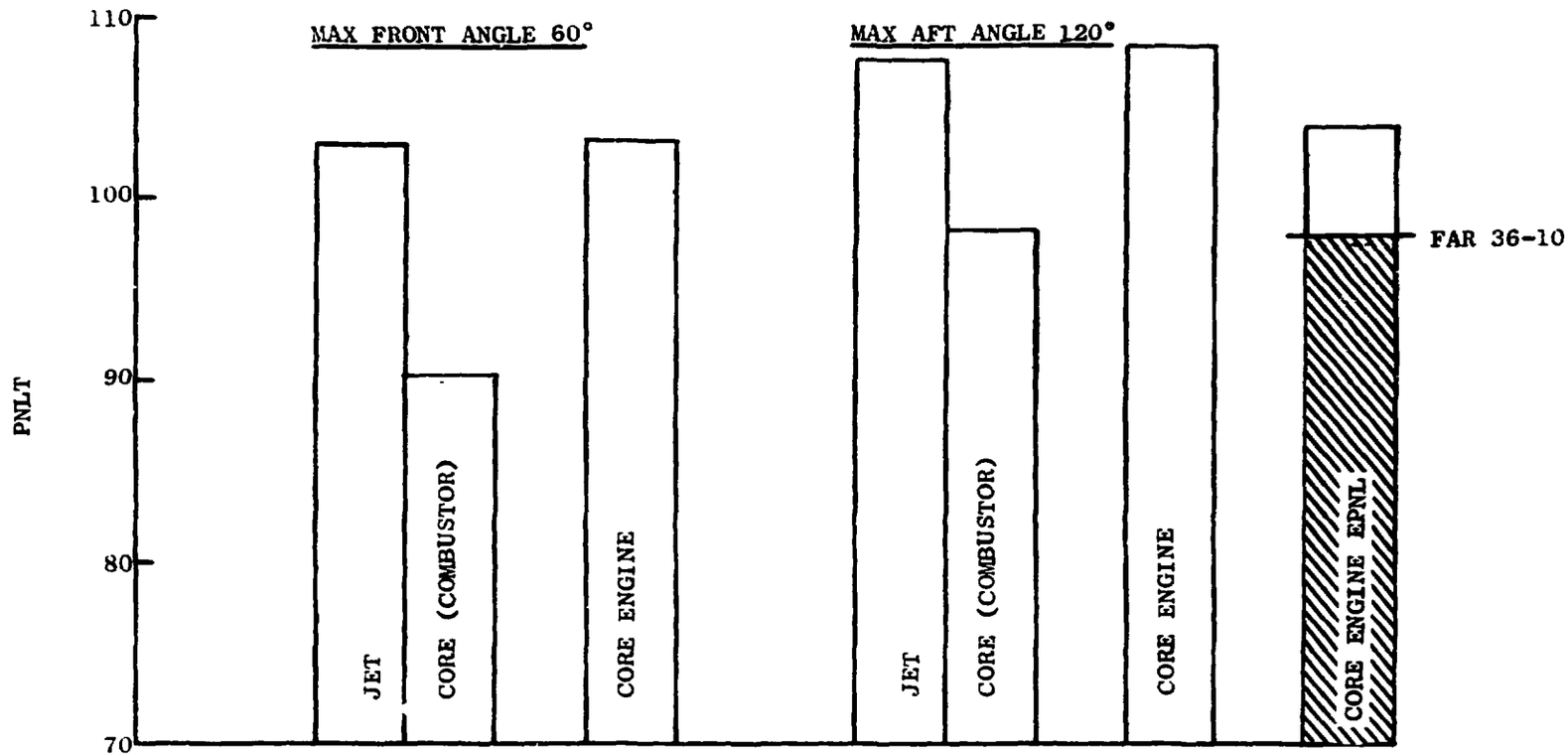

FIGURE 8.2-4 CORE ENGINE NOISE CONSTITUENT BREAKOUT AT TAKEOFF

2.4, Volume II) indicated negligible effects on the PNL at approach. It was assumed that the static results would be realized in-flight. The deep-cavity resonator was assumed to be peaked at 400 Hz and the suppression spectrum indicated by the component tests (Section 8.4, Volume II) was applied to the core noise. The suppression resulting was 9.2 PNdB at takeoff and 8.8 PNdB at approach for the max aft angles. Finally, spacing was introduced in the turbine and the spectrum suppressed as indicated by the results of Section 4.3, Volume II. The turbine noise reduction obtained through spacing was 5.5 PNdB at the max aft angle at approach.

The resultant spectra are shown in Figures 8.3-1 and -2, respectively. The corresponding PNL's and estimated EPNL's are provided in Figures 8.3-3 and -4. The core engine noise is still 0.9 EPNdB above FAR36-10 at approach and 3.3 EPNdB at takeoff. However, the noise relief obtained is significant. It should be noted that turbine noise attenuation due to acoustic treatment in the core was not assumed. Hence, even further core engine noise reduction could be obtained at approach power by including separate high frequency acoustic treatment in the core or by designing this capability into the low frequency combustor noise treatment. For example, if 3 PNdB worth of turbine suppression were obtained through treatment in the core nozzle (requiring only a small treated area), the approach power EPNL for the core engine noise would be 1.4 EPNdB below FAR36-10.

8.4 SUMMARY

The core engine noise levels for a high bypass turbofan were predicted and shown to be significant with reference to FAR36 levels. In particular, the turbine at approach and the jet at takeoff were the major contributors to the noise.

Application of core engine suppressors results in substantial noise relief, but still leaves the core engine slightly above FAR36-10. The results are summarized in Table 8.4-1.

The suppressor concepts identified in this program may not be directly applicable to engines because of constraints of size and weight and associated performance penalties. For example, the 18 lobe suppressor would obviously result in some drag loss-the amount remains to be defined, while the existing deep cavity combustor noise suppressor could hardly be accommodated within a flight worthy engine, and the spaced turbine would add to the weight. Also, the inflight effects remain to be demonstrated, particularly on the 18 lobe jet suppressor.

- CORE ENGINE NOISE - BR=4 TURBOFAN
- 4 ENGINES; 770000 lb (349580 kg) TOGW
- APPROACH POWER - 40% F_n
- 370 ft (113m) alt., 0.25 M_n

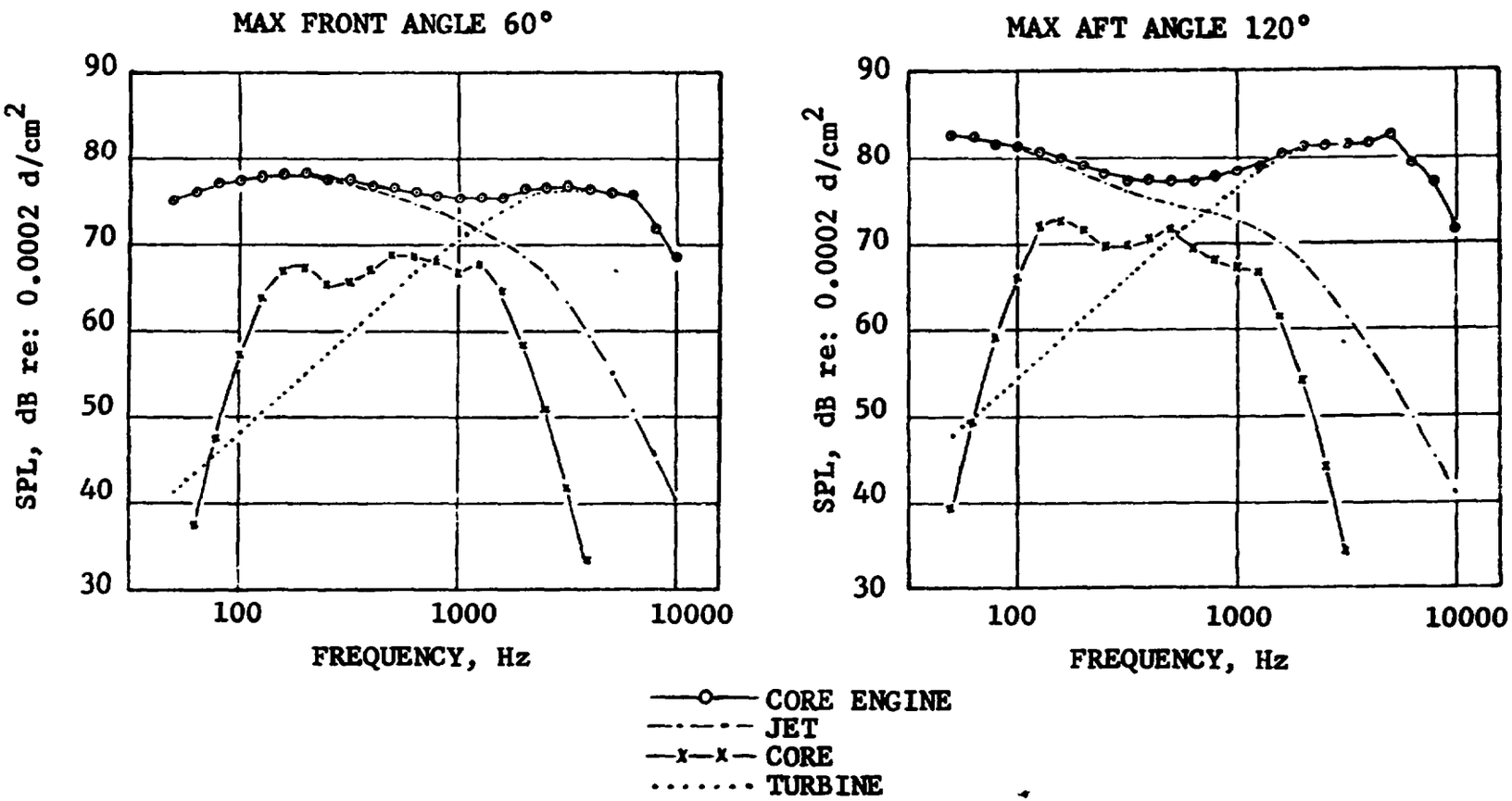

FIGURE 8.3-1 SPECTRAL MAKE-UP OF CORE ENGINE NOISE AT APPROACH WITH SUPPRESSED JET, COMBUSTOR AND TURBINE

- CORE ENGINE NOISE - BR=4 TURBOFAN
- 4 ENGINES; 770000 lb (349580 kg) TOGW
- TAKEOFF POWER - 100% F_n
- 1000 ft (305m) alt., 0.3 M_n

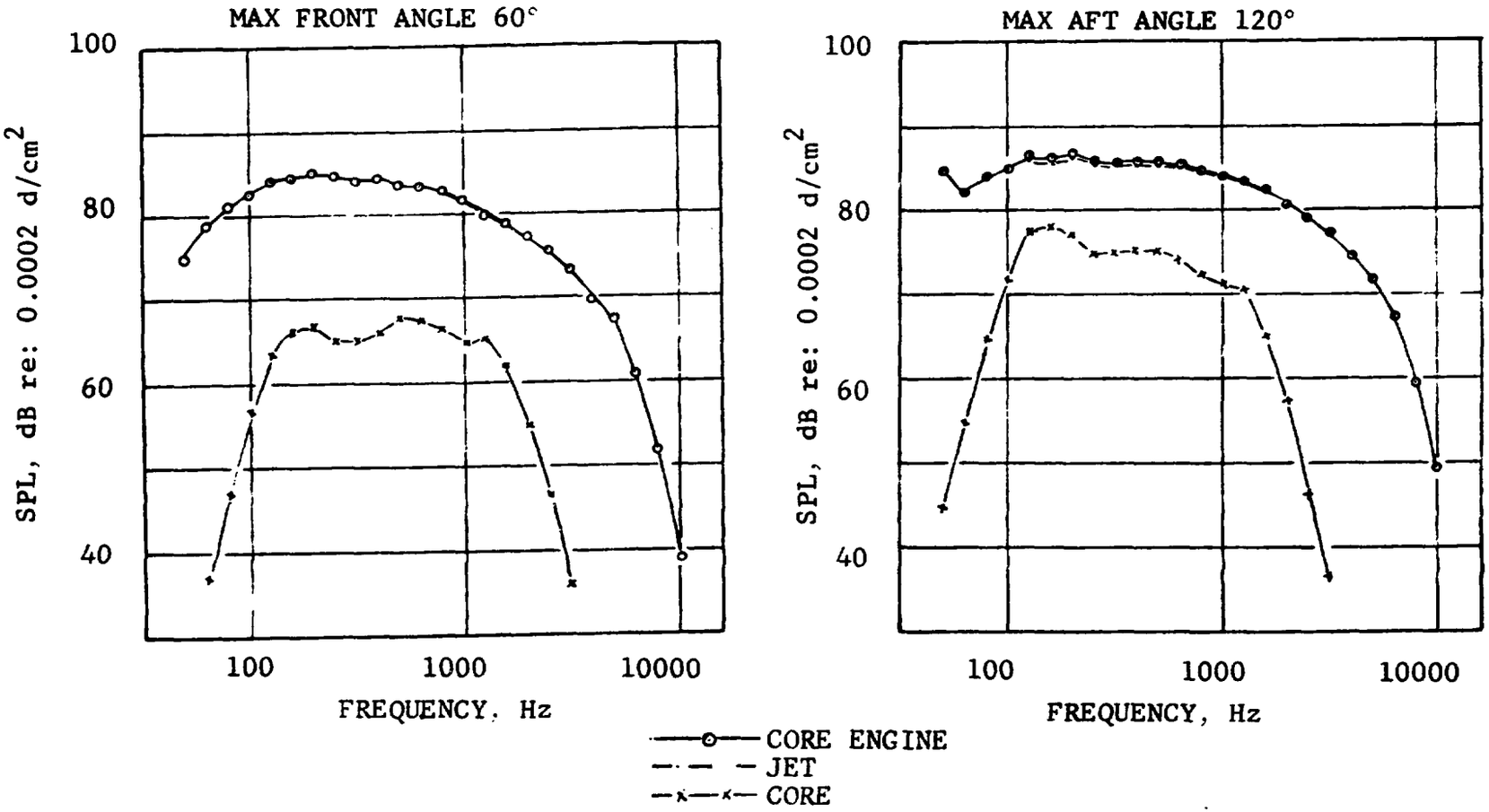

FIGURE 8.3-2 SPECTRAL MAKE-UP OF CORE ENGINE NOISE AT TAKEOFF WITH SUPPRESSED JET, COMBUSTOR AND TURBINE

- CORE ENGINE NOISE - BR=4 TURBOFAN
- 4 ENGINES; 770000 lb (349580 kg) TOGW
- APPROACH POWER - 40% F_n
- 370 ft (113m) alt., 0.25 M_n

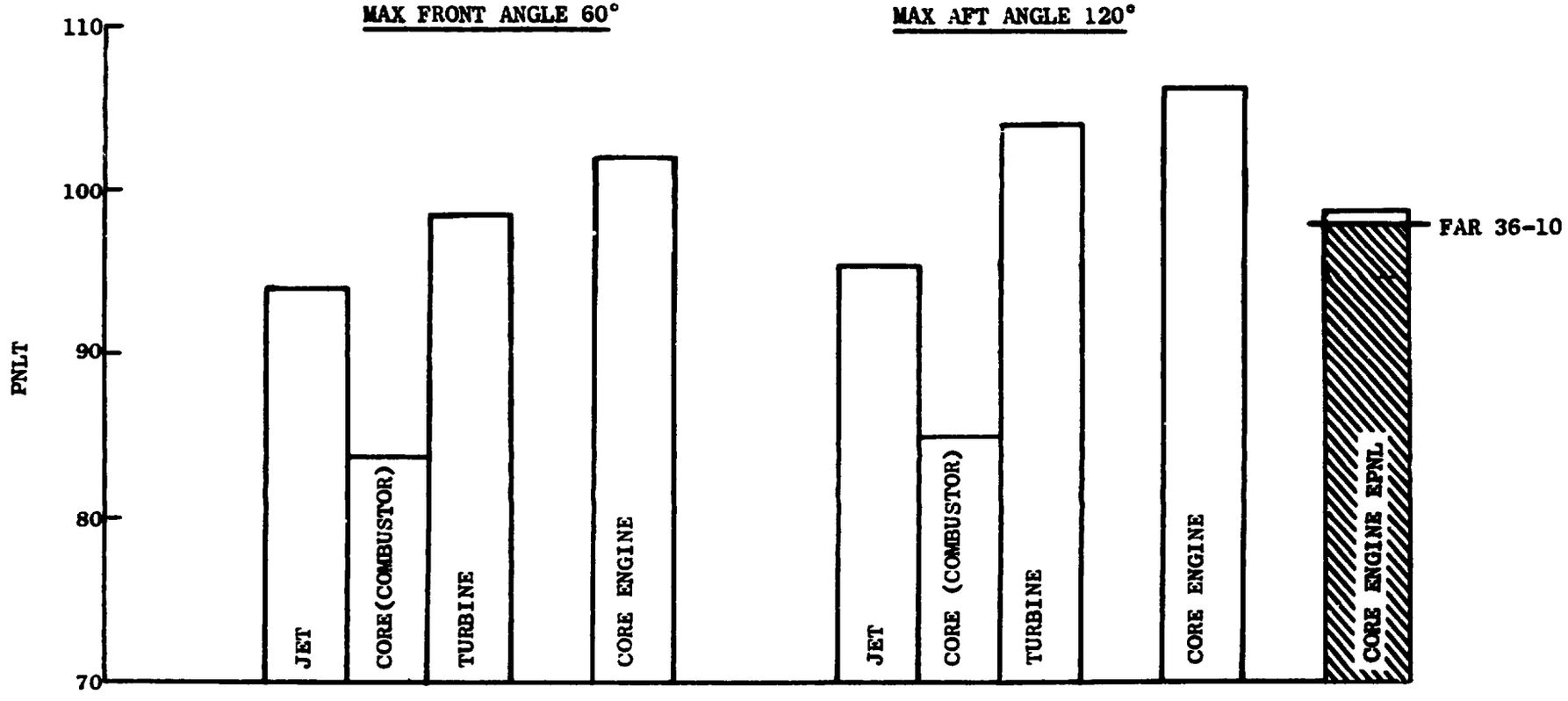

FIGURE 8.3-3 CONSTITUENT BREAKOUT AT APPROACH WITH SUPPRESSED JET, COMBUSTOR AND TURBINE

- CORE ENGINE NOISE - BR=4 TURBOFAN
- 4 ENGINES; 770000 lb (349580 kg) TOGW
- TAKEOFF POWER - 100% F_n
- 1000 ft (305m) alt., 0.3 M_n

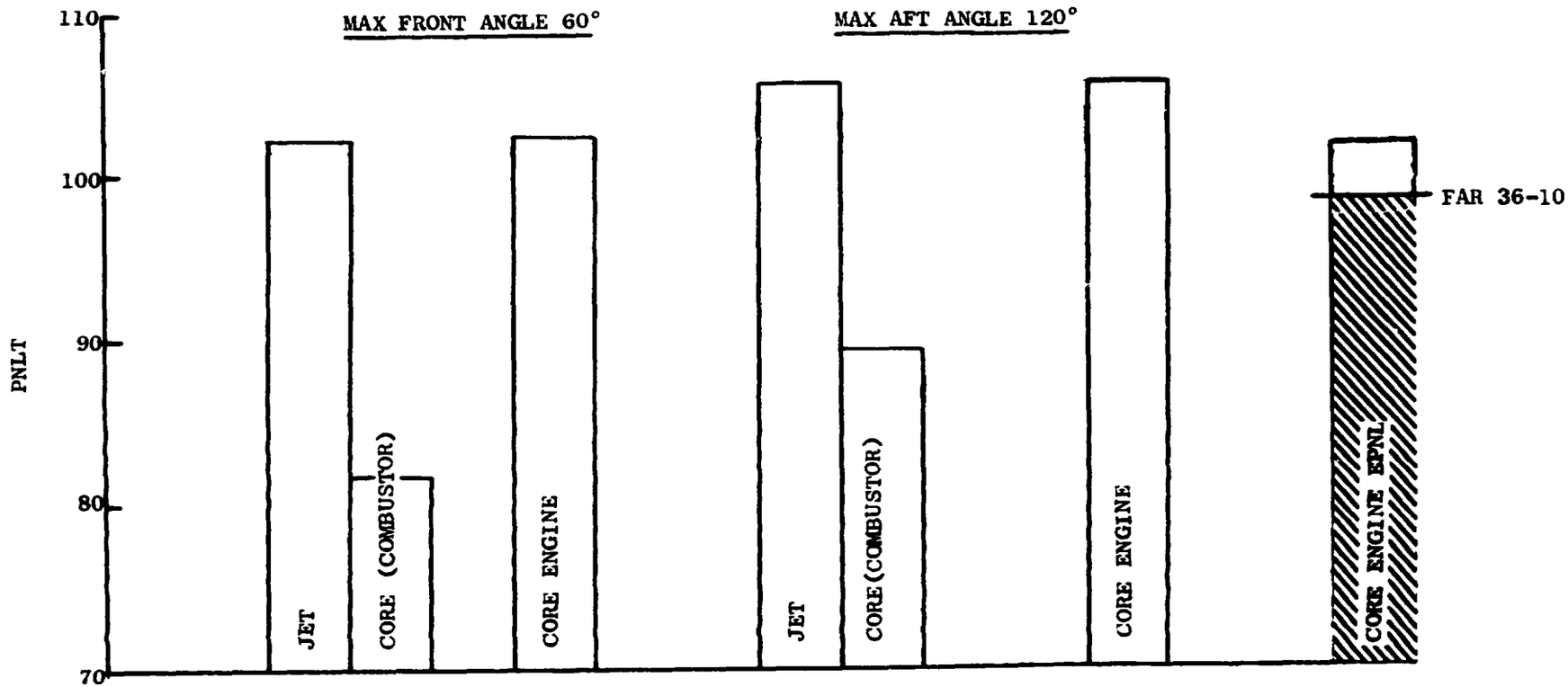

FIGURE 8.3-4 CONSTITUENT BREAKOUT AT TAKEOFF WITH SUPPRESSED JET, COMBUSTOR AND TURBINE

Table 8.4-1

BR = 4 CORE ENGINE NOISE LEVELS

- 4 Engines; TOGW = 770,000 lb (349580 kg)
- Takeoff 100% F_n, 1000 Ft (305 m) Alt.,.3M_n
- Approach 40% F_n, 370 Ft (113 m) Alt., .25M_n
- Core Engine Noise - Jet, Combustor (Core) and Turbine
  Does Not Include Fan or Airframe Noise

CORE ENGINE EPNL (EPNdB)

	Takeoff Power		Approach Power*	
	Absolute Level	Relative To FAR36	Absolute Level	Relative To FAR36
Without Suppression	104	-4	103.4	-4.6
With Suppression*	101.3	-6.7	98.9	-9.1

* Jet suppressor, low frequency treatment, turbine spacing; does not include high frequency treatment.

APPENDIX A

EXTRAPOLATION OF DIRECTIVITY ALONG AN ARC TO A SIDELINE

Assume that the arc directivity is provided as $DI_R(\theta)$, where θ is the angle from inlet. DI is defined as:

$$DI(\theta) = \text{Peak SPL} - SPL(\theta)$$
$$\text{or} \quad DI(\theta) = SPL(120°) - SPL(\theta) \tag{A-1}$$

The subscripts R and SL denote arc and sideline values. Referring to Figure A-1, the SPL at any sideline location can be found from the corresponding arc SPL:

$$SPL_{SL}(\theta) = SPL_R(\theta) - 20 \log_{10}\left(\frac{r(\theta)}{R}\right) + \alpha(R)-\alpha(r) + EGA(R)-EGA(r) \tag{A-2}$$

where $r(\theta)$ = distance from engine to the sideline location
R = arc radius
α = air attenuation
EGA = extra ground attenuation

Note that α and EGA are functions of the atmospheric conditions and frequency, but while α varies linearly with distance, the EGA does not.

For example, taking the directivity to bbe falloff from max aft angle (120°), the directivity along the sideline is given by:

$$DI_{SL}(\theta) = SPL_{SL}(120°) - SPL_{SL}(\theta)$$

$$= SPL_R(120°) - SPL_R(\theta)$$

$$-\left[20 \log_{10}\left(\frac{r(120°)}{R}\right) - 20 \log_{10}\left(\frac{r(\theta)}{R}\right)\right]$$

$$+ \alpha(R) - \alpha(R) + EGA(R) - EGA(R)$$
$$-\{\alpha\, r(120°)] - \alpha[r(\theta)]\}$$
$$-\{EGA[r(120°)] - EGA[r(\theta)]\}$$

$$\text{or } DI_{SL}(\theta) = DI_R(\theta) - 20 \log_{10}\left(\frac{r(120°)}{r(\theta)}\right) - \{\alpha[r(120°)] - \alpha[r(\theta)]\}$$

$$-\{EGA[r(120°)] - EGA[r(\theta)]\}$$

$$\text{or } DI_{SL}(\theta) = DI_R(\theta) - 20 \log_{10}\left(\frac{\sin\theta}{.866}\right) - \{\alpha(1.155L) - \alpha(L/\sin\theta)\}$$

$$-\{EGA(1.155L) - EGA(L/\sin\theta)\} \tag{A-3}$$

where L is the sideline distance.

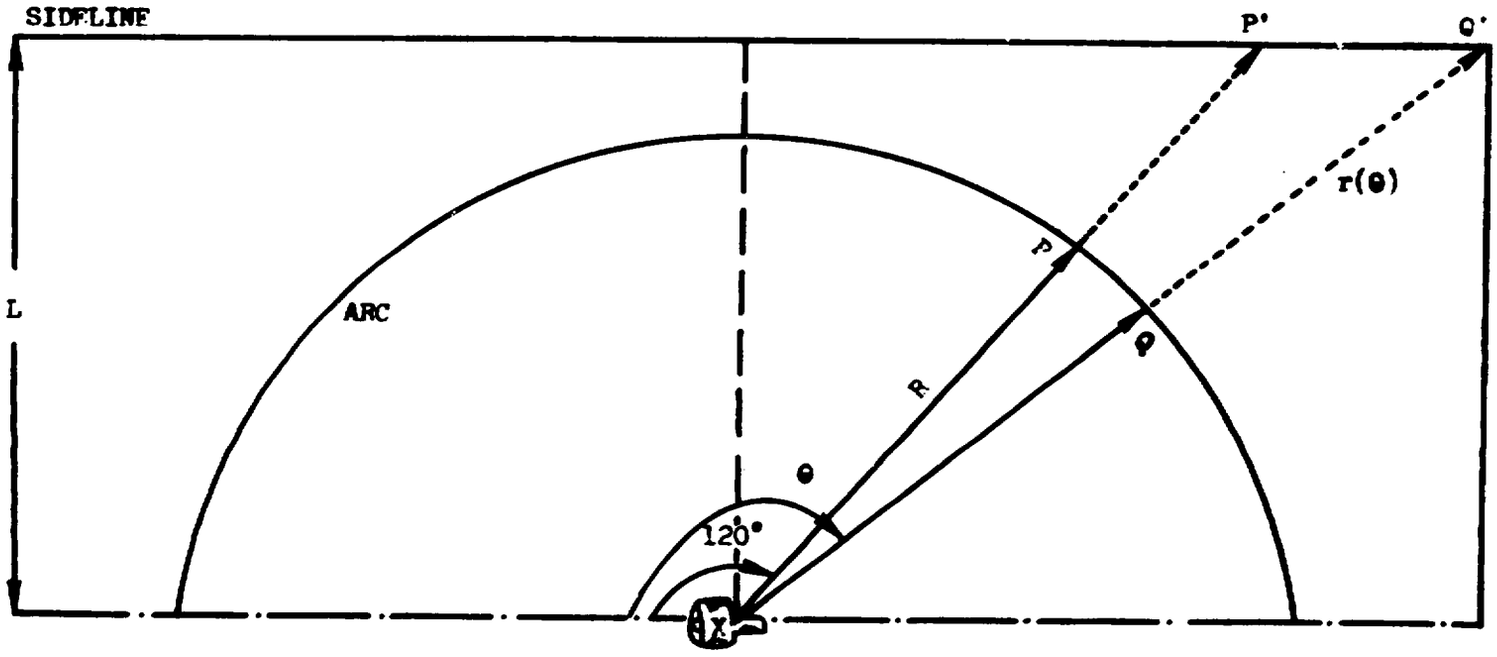

FIGURE A-1 CONVERSION OF POLAR DIRECTIVITY TO SIDELINE.

APPENDIX B

Sound Pressure Level Differences Between
Unsuppressed and Suppressed Coaxial Jet Systems

TABLE B1

18 LOBE CAPPED CORE SUPPRESSOR, $\frac{V_f}{V_c} = 0.6$

Δ SPL = $COANN_{UNSUPP}$ - $COANN_{SUPP}$ AT 320 ft (97.6 m.) ARC FOR BASELINE I

	Angles From Inlet						
Frequency	30	60	90	120	140	150	160
50	5	4	4	5	7	7	8
63	5	5	4	6	8	8	9
80	5	5	4	6	9	9	9
100	5	4	4	6	9	9	9
125	5	4	3	6	9	9	8
160	5	4	3	6	9	9	8
200	4	3	3	5	8	8	7
250	4	3	2	5	7	7	7
315	3	3	2	4	5	6	6
400	3	2	2	3	3	4	5
500	3	2	1	2	2	3	4
630	2	1	1	1	1	2	4
800	2	1	0	0	1	2	3
1000	1	0	0	-1	0	1	3
1250	1	-1	0	-2	0	1	3
1600	0	-1	-1	-3	-1	0	3
2000	-1	-2	-2	-3	-1	0	3
2500	-1	-3	-2	-3	-1	0	3
3150	-2	-3	-3	-4	-1	0	3
4000	-2	-4	-4	-4	-1	0	3
5000	-3	-4	-4	-4	0	1	3
6300	-4	-4	-5	-4	0	1	3
8000	-4	-5	-5	-3	1	2	3
10000	-5	-5	-5	-3	2	3	3

TABLE B2

18 LOBE CAPPED CORE SUPPRESSOR, $\frac{V_f}{V_c} = 0.5$

Δ SPL = $COANN_{UNSUPP} - COANN_{SUPP}$ AT 320 ft (97.6 m.) ARC FOR BASELINE I

	Angles From Inlet						
Frequency	30	60	90	120	140	150	160
50	6	5	3	5	10	10	10
63	7	5	4	7	12	12	12
80	7	6	5	8	13	13	13
100	8	6	5	8	13	13	14
125	8	6	5	8	13	14	15
160	8	6	5	8	13	14	16
200	7	5	5	8	12	13	15
250	7	5	4	7	11	12	13
315	6	4	3	6	9		10
400	6	4	2	5	6		7
500	5	3	1	4	4	4	4
630	4	2	0	2	3		2
800	3	1	-1	0	2	2	2
1000	2	0	-2	-2	2		1
1250	0	0	-2	-3	1	1	1
1600	-1	-2	-3	-4	1	1	1
2000	-2	-2	-3	-4	1	1	1
2500	-3	-3	-3	-5	1		2
3150	-4	-4	-3	-5	1		2
4000	-5	-4	-3	-6	1	2	3
5000	-6	-4	-3	-6	2	3	4
6300	-6	-5	-3	-6	2	3	5
8000	-6	-5	-3	-6	2	3	5
10000	-6	-5	-3	-6	3	4	6

TABLE B3

18 LOBE CAPPED CORE SUPPRESSOR, $\frac{V_f}{V_c} = 0.6$

Δ SPL = $COANN_{UNSUPP} - COANN_{SUPP}$ AT 320 ft (97.6 m.) ARC FOR BASELINE II

	Angle From Inlet					
Frequency	30	60	90	120	140	150
50	6	7	7	6	10	11
63	6	6	6	10	11	12
80	6	5	5	9	11	12
100	7	5	5	9	11	12
125	6	4	4	8	11	12
160	5	4	4	8	10	10
200	4	3	3	7	9	9
250	4	3	3	7	8	8
315	3	3	3	6	6	7
400	3	2	2	5	5	6
500	3	2	2	4	4	5
630	2	1	1	3	3	4
800	2	0	1	2	3	3
1000	1	0	1	1	3	3
1250	1	0	0	0	2	3
1600	0	-1	-1	-1	2	3
2000	-1	-2	-2	-1	2	3
2500	-2	-3	-4	-2	1	3
3150	-3	-4	-5	-3	1	3
4000	-4	-5	-5	-4	-1	2
5000	-5	-6	-6	-4	-1	2
6300	-6	-6	-7	-5	0	2
8000	-6	-7	-7	-5	0	2
10000	-7	-7	-7	-5	1	3